UNIVERSITÉ DU LUXEMBOURG

PhD-FSTM-2023-071
The Faculty of Science, Technology and Medicine

DISSERTATION

Defence held on 18/09/2023 in Esch-sur Alzette, Luxembourg

to obtain the degree of

DOCTEUR DE L'UNIVERSITÉ DU LUXEMBOURG

EN BIOLOGIE

by

Axel Jonathan CHEMLA
Born on July 31, 1995 in Courcouronnes (France)

FUNCTIONAL CHARACTERIZATION OF NEURODEGENERATION IN CELLULAR AND MOUSE MODELS OF PARKINSON'S DISEASE CARRYING PATHOGENIC VARIANTS IN THE *RHOT1* GENE ENCODING MIRO1

Dissertation defence committee

Dr. Rejko Krüger, dissertation supervisor
Professor, Université du Luxembourg, Esch-sur-Alzette, Luxembourg

Dr Alexander Skupin, Chair
Associate Professor, Université du Luxembourg, Esch-sur-Alzette, Luxembourg

Dr Julia Fitzgerald, Vice-Chair
Junior group leader, Hertie Institute for Medical Brain Research, Tübingen, Germany

Dr Enza Maria Valente
Professor, University of Pavia, Pavia, Italy

Dr Olga Corti,
Directeur de recherche, Inserm, Institut du Cerveau, Paris, France

PARK-QC DTU (PRIDE17/12244779/PARK-QC).

Affidavit

I hereby confirm that the PhD thesis entitled “FUNCTIONAL CHARACTERIZATION OF NEURODEGENERATION IN CELLULAR AND MOUSE MODELS OF PARKINSON’S DISEASE CARRYING PATHOGENIC VARIANTS IN THE *RHOT1* GENE ENCODING MIRO1” has been written independently and without any other sources than cited. All necessary ethical approvals have been obtained in accordance with the “Règlement grand-ducal du 11 janvier 2013 relatif à la protection des animaux utilisés à des fins scientifiques” adapted from and in line with the European Directive 2010/63/EU.w (on the use of clinical samples and on the Care and Use of laboratory animals, where applicable). The Luxembourgish National Research Ethics Committee (CNER) provided ethical approval for the following project: “Disease modelling of Parkinson’s disease using patient-derived fibroblasts and induced pluripotent stem cells” (DiMo-PD, CNER #201411/05).

Luxembourg, August 11, 2023 _____

Axel Chemla

Acknowledgements

This PhD has been a life-changing experience, significantly changing the scientist, and the person I was several years ago. Achieving it would not have been possible without people who provided support and help throughout the years. I express my greatest gratitude to all of you.

First, I would like to thank Prof. Dr. Rejko Krüger for allowing me to join his Translational Neuroscience group. Thank you for your advice and supervision. Your love for research, hard-working spirit, and what you have done for PD patients worldwide and especially in Luxembourg is a great source of inspiration. Being in your team, having the possibility to be closer to patients, and interact with clinical researchers, was an honor. Being allowed to teach Master's students in your course every year was also an aspect of this PhD I loved.

Thank you, Assoc. Prof. Alex Skupin for accepting to be the President of my PhD committee, and for the simple, albeit impactful sentence you said during that time we casually spoke at LCSB and that I always kept in mind since (cf page 8).

I would also like to thank the other members of my PhD defense jury, Prof. Dr Enza Maria Valente, Dr Olga Corti, Dr. Julia Fitzgerald who accepted to be vice President of the Jury,, Prof. Dr. Lena Burbulla, for accepting to evaluate my thesis, investing your time in this important part of my journey.

Thank you, Prof. Dr Anne Grünewald, for being a member of my yearly thesis evaluation committee (CET) and your suggestions.

Thank you, Prof. Dr. Jens Schwamborn, for your advice as the third member of my CET committee. Thank you also for the collaboration on Miro1 modelling in midbrain organoids. This significantly helped in many ways.

I am also immensely grateful to Dr. Giuseppe Arena, who co-supervised me after my first year of PhD. Your insights helped to shape the project, always with valuable input. Your motivation and will to include me in other projects were especially important to me during the last years. Above all, the fact that you are here, as you once said, "to do good science, not sloppy science", and seeing you demonstrate this resolve through your everyday work was amazing, and especially inspiring.

Dr Cláudia Saraiva, a heartfelt thank you. You are a great, utterly motivated researcher. I thoroughly enjoyed working with you, our Miro1-related discussions, and overall, that you were among the very few people working on Miro1 and PD. You helped immensely.

A special thanks goes to the original Miro1 enthusiast, Dr. Dajana Großmann. Your love for Miro1 is admirable.

Of course, I will not forget Dr. Clara Berenguer-Escuder, the second member of the Miro1 team when I started this PhD. I respect your dedication and tenacity. Your supervision in the lab at the beginning, even though you were a busy PhD student at that time, helped a lot.

Paul, I deeply appreciated working with a person as passionate and competent as you. The time we spent setting up microscopy assays, and new methods, even when it was not successful, was one of the moments that made this PhD enjoyable.

And now, to the world's best "mouse-icist": Pierre. Working with you was great. Your expertise exceeded my expectation back when you first started helping me with the Miro1 mouse project. Keep your passion, as well as your awesome taste in music.

To my peers within Rejko's group, thank you. Borja, for our conversations, and your great spirit, "go big or go home" mentality, your clever ideas, and jokes. Vyron, for the scientific discussions, and the Rockhall concerts we sometimes met at. Ibo, for teaching me everything regarding iPSCs. Pete, for your advice, cheerfulness, and our discussions about everything, including non-PD related science. It was great meeting you again at AD/PD this year. To Sinthu and Laure, for helping each other and keeping ourselves motivated, for your help with understanding genetics, or neuropsychology, "we can do it". To Armelle, you are a great person, among the few that truly helped me keep my hopes up at work during though times and I'm glad we met, and to have you as a friend. To Vera, like Armelle, meeting you was one of the highlights of these years. I'm glad to have you as a friend, keep your hopes up, you will make it.
To the ones who joined recently, Yahya, even though we did not speak much, I did enjoy our short conversations, and thank you for always being here to help with PCR and agarose gel related questions. To Alex, it was nice having you as a colleague, going for lunch breaks, and that you also have the will to understand and sometimes challenge what you are asked to do; don't lose this. And of course, everyone else within or outside the Translational Neuroscience team, LCSB, LIH, everywhere.

Manuel, your proactiveness and work put into setting up the Science4Everyone series, allowing me and other to speak about our subject of expertise or scientific subjects we enjoy to a lay audience. This was of paramount importance in staying motivated during tough lockdown and post lockdown, covid times.
Last, but not least, Sofia and Bianca, thank you for your help and efficiency with all my questions regarding administrative tasks. To Shayan, from the office of doctoral studies, for always answering my many questions quickly and efficiently since day one.
Of course, research is never possible without funding, so I would like to thank the funding bodies that allowed me to perform research since I started this PhD, especially the FNR.

To my former supervisors, Yann Decker, Walter Schulz-Schaeffer, Maxime Lehmann, Uli Mueller, Samuel Liégeois, Valérie Dufour, thank you. Each one of you contributed to my development as a scientist. To Mr. François, my middle school “Sciences de la Vie et de la Terre“ teacher, who further fed my passion for biology.

To Gilles Macagno, whose books “Une histoire de la vie, 4 milliards d’années”, “Génétique, Génétoc“, and “Mille milliards de cellules” were gifted to me by my parents at the beginning of elementary school and shaped my love for Science and Biology.

To “les petits confinés”, and the future game nights we will do. To the other board games enthusiasts. To Cynthia, for our friendship, your support and advice since we met. To Plümli for singing, swooshing, roaring, interfering, as well as playing with me, and pecking me.

To Lara, without whom I would not have made it. A special thank you for your mental, scientific, and overall support during these years, and for everything else.

To my family, parents, and sister. Thank you for your unconditional and unceasing support for my career and life. Thank you for believing in me, and understanding the substantial amount of work invested, and sacrifices done during the recent years. Knowing that you will always be on my side is something I deeply appreciate. Mom, Dad, I love you, thank you for everything.

Last but not least, I want to thank me. I want to thank me for believing in me. I want to thank me for doing all this hard work. I want to thank me for having no days off. I want to thank me for never quitting. I want to thank me for trying to do more right than wrong. And I want to thank me for just being me at all times (adapted from Snoop Dogg, Walk of Fame ceremony, 2018).

"Deeds will not be less valiant because they are unpraised. "
"All we have to decide is what to do with the time that is given to us. "
"There is nothing like looking, if you want to find something. You certainly usually find something, if you look, but it is not always quite the something you were after."
J.R.R Tolkien

"A PhD is a lot of stress. But only pressure makes diamonds."
Assoc. Prof. Dr. Alexander Skupin.

Table of contents

Contents

Abbreviations

6-OHDA	6-hydroxydopamine
Ac-CoA	acetyl coenzyme A
ALDH1A1	aldehyde deshydrogenase 1
AD	Alzheimer's disease
ADP	Adenosine diphosphate
APP	amyloid precursor protein
ATP	Adenosine Triphosphate
BAPTA	1,2-bis (o-aminophenoxy) ethane-N, N, N′, N'-tetraacetic acid
BBB	blood brain barrier
BSA	Bovine serum albumin
CCCP	Carbonyl cyanide m-chlorophenyl hydrazone
CL	Cardiolipin
ctrl	control
DA	dopaminergic (neurons)
DEGs	differentially expressed genes
DMEM	Dulbecco's modified Eagle's medium
DMSO	Dimethylsulfoxide
DNA	desoxyribonucleic acid
Drp1	Dynamin 1 like dependent protein
EF (hand)	helix E-loop-helix F region
ER	Endoplasmic Reticulum
ETC	Electron Transport Chain
FBS	Fetal Bovine Serum
FCCP	Carbonyl cyanide 4-(trifluoromethoxy)phenylhydrazone
GBA	Glucosylceramidase Beta 1
GC-MS	gaz chromatography-mass spectrometry
GDNF	Glial cell line-derived neurotrophic factor
GO	gene ontology
GTP	Guanosine triphosphate
H2O2	hydrogen peroxide
IDH	NAD+ isocitrate deshydrogenase
iPD	idiopathic/sporadic PD
IP/RT-QuIC	immunoprecipitation-based real-time quaking-induced conversion
iPSCs	induced-Pluripotent Stem Cells
KI	knock-in
KO	knock-out
LC-MS	liquid chromatography-mass spectrometry
LoF	Loss of function
LRRK2	Leucine Rich Repeat Kinase 2
L / R / T CC	L / R / T type calcium channels
MAPT	Microtubule associated protein Tau
MCU	Mitochondrial Calcium Uniporter
MDVs	Mitochondrial-derived vesicles
MERCs	Mitochondrial-ER Contact Sites
MIB	mitochondria isolation buffer
MICOS	mitochondrial contact site and cristae organizing complex

Miro1	Mitochondrial Rho GTPase 1
MO	Midbrain organoids
mtDNA	Mitochondrial DNA
MiST	Mitochondria shape transition
MMP	Mitochondrial Membrane Potential
MPTP	1-methyl-4-phenyl-1,2,3,6-tetrahydropyridine
mRNA	messenger RNA
mt-RNR2	Mitochondrially encoded 16S RNA / Humanin
MTG	Mitotracker Green
NAD	nicotinamide adénine dinucléotide
NADP	NAD phosphate
nDAns	nigrostriatal dopaminergic neurons
NLRP3	NOD Like Receptor family pyrin domain containing 3
OGDH	oxoglutarate deshydrogenase
PARKIN	Parkin RBR E3 Ubiquitin Protein Ligase
PARK7	Parkinsonism Associated Deglycase, DJ-1
PBS	phosphate buffered saline
PD	Parkinson's disease
PDH	pyruvate deshydrogenase
PINK1	PTEN Induced Kinase 1
PTM	post translational modification
RBD	REM sleep behavior disorder
REM	rapid eye movement
RHOT1	Ras Homolog family member T1
ROS	Reactive Oxygen Species
sc-RNAseq	single-cell-ribonucleic acid sequencing
SNCA	synuclein alpha
SNpc	Substantia Nigra pars compacta
SDS	Sodium Dodecylsulfate
SPLICS	split Green Fluorescent Protein-based contact sites sensors
T2D	Type 2 diabetes
TCA	tricarboxylic acid cycle
TMRE	Tetramethylrhodamine Methyl Ester
TnTs	Tunneling nanotubes
TUNEL	Terminal deoxynucleotidyl transferase dUTP nick end labeling
WIMF	Wounding-induced mitochondrial fragmentation
WT	Wild-type

List of publications which are part and not part of the thesis

Manuscript I

Generation of two induced pluripotent stem cell lines and the corresponding isogenic controls from Parkinson's disease patients carrying the heterozygous mutations c.1290A > G (p.T351A) or c.2067A > G (p.T610A) in the *RHOT1* gene encoding Miro1.

Axel Chemla, Giuseppe Arena, Cláudia Saraiva, Clara Berenguer-Escuder, Dajana Grossmann, Anne Grünewald, Christine Klein, Phillip Seibler, Jens C. Schwamborn, Rejko Krüger

Status: Published in *Stem Cell Research* 25.03.2023

Manuscript II

Generation of two induced pluripotent stem cell lines and the corresponding isogenic controls from Parkinson's disease patients carrying the heterozygous mutations c.815G > A (p.R272Q) or c.1348C > T (p.R450C) in the *RHOT1* gene encoding Miro1.

Axel Chemla, Giuseppe Arena, Gizem Onal, Jonas Walter, Clara Berenguer-Escuder, Dajana Grossmann, Anne Grünewald, , Jens C. Schwamborn, Rejko Krüger

Status: Published in *Stem Cell Research* 14.06.2023

Manuscript III

Parkinson's disease related Miro1 mutation induces mitochondrial dysfunction and loss of dopaminergic neurons *in vitro* and *in vivo*

Axel Chemla, Giuseppe Arena, Ginevra Sacripanti, Kyriaki Barmpa, Alise Zagare, Pierre Garcia, Paul Antony, Jochen Ohnmacht, Alexandre Baron, Jaqueline Jung, Anne Marie Marzesko, Manuel Buttini, Thorsten Schmidt, Anne Grünewald, Jens C.Schwamborn, Rejko Krüger, Cláudia Saraiva

Status: Under review at *Nature Communications*

Review, not part of the thesis (see Appendix I):

The Emerging Role of *RHOT1*/Miro1 in the Pathogenesis of Parkinson's Disease

Dajana Grossmann, Clara Berenguer-Escuder, Axel Chemla, Giuseppe Arena, and Rejko Krüger

Status: Published in *Frontiers in Neurology* 15.09.2020

Abstract

Parkinson's disease (PD) is the fastest growing neurological disorder, and the first most common neurodegenerative movement disorder, with patient number expected to double in 2040 (Dorsey et al., 2018b). While most PD cases are sporadic, approximately 10% of patients develop PD due to genetic causes.

Interestingly, many of these PD causing genes are related to mitochondrial function, which is in line with the main pathological hallmark of PD, namely the selective death of the dopaminergic (DA) neurons in the Substantia Nigra Pars Compacta (SNpc) of the brain. Indeed, DA neurons heavily rely on adenosine triphosphate (ATP) production via mitochondrial oxidative phosphorylation, to sustain their pace-making activity.

The last few years saw an increasing interest in the Mitochondrial Rho GTPase 1 (Miro1) protein, a mitochondria-anchored cytosolic calcium sensor involved in the regulation of mitochondria-ER contact sites (MERCs), mitochondrial transport, and mitophagy.

Our team previously demonstrated in fibroblasts that four different Miro1 mutations found in PD patients pathologically affected calcium homeostasis, mitochondrial quality control, and MERCs formation (Berenguer-Escuder et al., 2019a; Grossmann et al., 2019a).

Moreover, Miro1 p.R272Q mutant induced-pluripotent stem cells (iPSCs)-derived neurons, display a significant impairment of cytosolic calcium handling compared to age/gender matched controls, similarly to fibroblast from this patient (Berenguer-Escuder et al., 2020a). This phenotype was accompanied by MERCs levels dysregulation as well as mitophagy and autophagy impairment, supporting the role of Miro1 as a rare genetic risk factor for PD (Berenguer-Escuder et al., 2020a).

Moreover, recent studies revealed a pathological retention of Miro1 upon mitophagy induction, thus delaying mitophagy in cells from genetic PD as well as in a significant proportion of sporadic PD patients (Hsieh et al., 2016a, 2019a; Shaltouki et al., 2018a).

In this thesis, we first generated and characterized iPSCs and isogenic controls lines from the four aforementioned PD patients.

We then explored the pathogenic effect of the Miro1 p.R272Q mutation in three different models, namely iPSC-derived neurons, midbrain organoids (MO), and Miro1 p.R285Q knock-in (KI) mice.

We first confirmed the exacerbated sensitivity to calcium stress *in vitro* in neurons, and unveiled that it was also accompanied by mitochondrial bioenergetics impairment (lower ATP levels) and elevated reactive oxygen species (ROS) production in both 2D and 3D models, finally resulting in DA neurons death in MO.

This was accompanied by elevated *SNCA* mRNA expression in both models, as well as higher α-synuclein protein amounts in neurons, which was already found in post-mortem samples from PD patients (Shaltouki et al., 2018a). Lastly, our mouse model displayed significant neuronal loss in its SNpc, as well as impaired motor learning, recapitulating two PD signs found in patients.

Taken together, these results support the involvement of Miro1 in PD pathogenesis, and highlights the potential of Miro1 variants to be used as novel, promising models for PD *in vitro* and *in vivo*.

Aims/Objectives

As growing evidence points towards an important role of Miro1 in PD pathogenesis, and knowing the importance of Miro1 for preserving mitochondrial health, we investigated whether the p.R272Q Miro1 mutation would affect calcium dynamics, mitochondrial bioenergetics and function, as well as its effect on DA neurons health *in vitro*. To date, this is the first study assessing the involvement of Miro1 variants in the pathogenesis of PD using three different models: 2D iPSC-derived neurons and 3D midbrain organoids *in vitro*, as well as Miro1 p.R285Q KI mice *in vivo*.

Moreover, the use of gene-corrected, isogenic controls allowed us to assign significant effects not only to the genetic background but to the point mutation, while comparison to age/gender matched control line allowed us to use Miro1 to model “typical” PD. The second part of this project aimed at finding out whether the aforementioned Miro1 mutation could affect PD pathogenesis in our mouse model, and seeing whether the Miro1 p.R285Q mice could be used as a PD model.

The objectives of the study were the following:

- Generation and characterization of PD patient-derived iPSCs, including isogenic controls

- *In vitro* characterization of the impact of the p.R272Q Miro1 variant on mitochondrial function and bioenergetics

- *In vivo* characterization of PD-related phenotypes in the ortholog p.R285Q mutant Miro1 mouse

- Assessment of the involvement of Miro1 variants in PD pathogenesis

- Assessment of the possibility to use Miro1 variants to model PD

Synopsis

I Introduction:

I.I Parkinson's disease:

Parkinson's disease (PD) is the fastest growing neurological disease in terms of mortality, disability and prevalence, and is the most common neurodegenerative disorder after Alzheimer's disease (Dorsey et al., 2018a; Feigin et al., 2017; GBD 2015 Disease and Injury Incidence and Prevalence Collaborators, 2016; Mhyre et al., 2012). In 20 years, predictions claim that the number of individuals with PD will reach 12 million, shifting places with Alzheimer's disease (AD) as the most common neurodegenerative disease (Dorsey et al., 2018a). More than 10 million people suffer from PD worldwide, affecting around 1% of the 60 years old population, increasing to more than 5% in people older than 80 (Reeve et al., 2014). On top of the increased risks of developing PD with aging, its incidence is more frequent in men compared to women (3:2), adding sex to the many factors involved in the disease etiology (Kalia and Lang, 2015).

PD main feature is dopamine deficiency due to degeneration of dopaminergic neurons in the Substantia Nigra pars compacta (SNpc). Following diagnosis, patients usually live up to 16 years (Kalia and Lang, 2015). Clinically, diagnosis is based on bradykinesia, resting tremor, rigidity and postural instability (Jankovic, 2008), while it is only possible to confirm the diagnosis after the patient's death, when seeing the presence of Lewy bodies in the patient's brain. However, some PD cases do not present Lewy bodies, such as loss of function (LoF) PARKIN, mostly, as well as in a few LRKK2 G2019S carriers (Gaig et al., 2009; Johansen et al., 2018).

Up to now, the current therapies for PD are only able to treat symptoms, disability, and prolong life expectancy, but cannot stop the neurodegenerative process (Shulman et al., 2011). It is important to note that motor symptoms, on which diagnosis is based, appear at a disease stage where already more than 50% of the dopaminergic neurons in the SNpc are lost (Kia et al., 2021). However, PD is also characterized by non-motor symptoms, such as sleep disorders, hyposmia, and constipation that can manifest up to 20 years before the motor symptoms (Hawkes, 2008; Hely et al., 2005). Autonomic dysfunction like incontinence and psychiatric complications like depression, hallucinations and dementia are among the other non-motor symptoms of PD that appear at later disease stages, most likely due to the extension of the pathology outside of the basal ganglia (Chaudhuri and Schapira, 2009;

Langston, 2006). These non-motor symptoms are deemed more invalidating by patients, and do not respond to dopamine replacement therapy.
PD's etiology is complex, including genetic and environmental factors. This urges the need to further dissect the underlying molecular alterations, and stratify patients in order to develop personalized therapy, or, even better, preventive medicine for patient that have higher risks to develop PD, for example patients affected by rapid eye movement (REM)-sleep behavior disorder (RBD) (Barasa et al., 2021; de Lau and Breteler, 2006).

Historically, the impact of the environment on PD development emerged 40 years ago, when the opioid 1-methyl-4-phenyl-1,2,3,6-tetrahydropyridine (MPTP), a precursor of the toxin MPP+, was found to cause PD like symptoms in drug addicts, leading to dopaminergic neurons death in the SNpc. This effect was later confirmed in the brain of non-human primates (Langston et al., 1984, 1983). This enabled scientists to study PD by using a MPTP induced model, and helped to investigate mitochondria-linked phenotypes of the disease, due to MPP+ being an inhibitor of this organelle's function (Ramsay et al., 1987, 1986).

Beyond the many sporadic and the rare chemical-induced cases of PD, genetic background and variation between individuals is estimated to account for around 25% of the risk of developing PD (Goldman et al., 2019; Keller et al., 2012; Nalls et al., 2019).
The different genetic variants associated with PD differ in terms of frequency and penetrance, and, interestingly, comprise many genes associated to mitochondria, allowing us to grade them, on top of the commonly used effect size and allele frequency, according to their effect on mitochondrial function, instead of only their effect size (Day and Mullin, 2021; Larsen et al., 2018) (Figure 1, from (Larsen et al., 2018)). One can also include other variants in genes found in PD patients, such as Ras Homolog family member T1 (*RHOT1*), a major player in mitochondrial health, of which four different mutations were found in PD patients via exome sequencing, without any other known PD-related variants (Berenguer-Escuder et al., 2019a, 2020a; Grossmann et al., 2019a). Many genes and loci have been associated with PD, and historically numbered "PARK", in order of discovery. However, due to this nomenclature leading to loci referring to the same gene (e.g synuclein alpha (*SNCA*) being PARK1 and PARK4), the current recommendations are to use the gene name instead of "PARK" and number (Day and Mullin, 2021; Marras et al., 2016) (Table 1).
Among the many genes involved in PD, *SNCA*, the gene encoding α-synuclein was the first "PARK" loci identified. α-synuclein, among lipids and other components, is the main unit of Lewy bodies (Fujiwara et al., 2002a; Spillantini et al., 1997).

Mutations found in PD patients, namely *SNCA*-A53T and *SNCA*-A30P increase the capacity of α-synuclein to form toxic oligomers, and later fibrils, preventing their proper disposal by the proteasome or lysosome (Krüger et al., 1998; Polymeropoulos et al., 1997; Riederer et al., 2019).

As previously mentioned, a rather small percentage of PD cases are due to identified genetic variants. However, these familial cases of PD can immensely help us deciphering the molecular mechanisms underlying PD pathogenesis, and better understand what lies behind the development of sporadic PD.

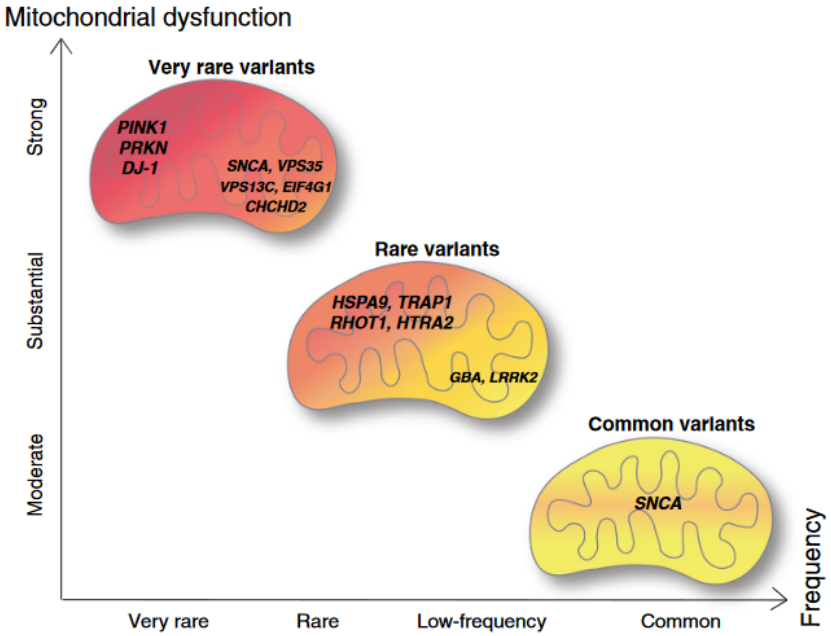

Fig. 1 Graded risk concept for genes related to mitochondrial dysfunction in Parkinson disease. Severity of mitochondrial dysfunction is represented in a gradient from *red* (strong mitochondrial dysfunction) to *yellow* (moderate mitochondrial dysfunction). Figure adapted from Manolio et al. 2009

Figure 1: Distribution of genes related to PD, according to their effect on mitochondrial dysfunction, and frequency in the population (From Larsen et al. 2018, use authorized by Creative Commons Attribution 4.0 International License).

I.II Models of Parkinson's disease:

Models of PD are diverse and can first be divided into two classes. Chemically induced PD, such as the MPTP mouse and primate (as *in vivo* examples), briefly mentioned in the previous chapter, and genetic models of PD. The latter category includes yeast and animal models, as well as *in vitro* models such as cell lines, primary cultures, and lastly, patient-derived cultures. Among these multiple models, patient-derived cells are the highest standard to date for the *in vitro* study of PD, allowing the identification of disease biomarkers, link genetic factors to specific disease mechanisms, and study the complex biochemical and molecular pathways involved in PD.

A major breakthrough in biological models was made thanks to the discovery of Yamanaka, allowing us to reprogram cells that can easily be obtained from patients, such as skin fibroblasts, into iPSCs. This stems from the ectopic expression (which is now one of the many methods of reprogramming) of c-myc, Klf4, Oct4, and Sox2 genes, also known as Yamanaka factors, in both human and mouse embryonic fibroblasts (Takahashi et al., 2007; Takahashi and Yamanaka, 2006).

This allowed researchers to study PD in relevant cell types from tissues that would otherwise be inaccessible such as neurons, by differentiating patient-derived iPSCs. Moreover, iPSCs possess the same genetic background of patients from which biopsies were taken, allowing researchers to study the important contribution of the individual genetic landscape, which could be considered as the main benefit of iPSC-derived models when studying complex diseases with a genetic component, like PD.

This can be achieved by using isogenic lines, either by correcting the mutation in cells with the patient background, or by inserting the mutation of interest into cells from a healthy control.

	Gene (HGNC Approved Name)	Alternative Gene Names	Inheritance	Pathogenicity	PD Phenotype	Function
High penetrance	*SNCA*	*PARK1, PARK4, NCAP*	AD	Pathogenic	Early-onset	Uncertain (encodes α-synuclein)
	VPS35	*PARK17, MEM3*	AD	Pathogenic	Typical	Retromer and endosomal trafficking
	PINK1	*PARK6*	AR	Pathogenic	Early-onset	Mitochondrial
	PARK7	*DJ-1*	AR	Pathogenic	Early-onset	
	PRKN	*PARK2, PARKIN*	AR	Pathogenic	Early-onset	
	PLA2G6	*PARK14, IPLA2*	AR	Pathogenic	Early-onset, atypical	Cell membrane
	ATP13A2	*PARK9*	AR	Pathogenic	Early-onset, atypical	Lysosomal
	FBXO7	*PARK15, FBX7*	AR	Pathogenic	Early-onset, atypical	Mitochondrial
	POLG	*POLG1, POLGA*	AD	Pathogenic	Early-onset, atypical	Mitochondrial DNA maintenance
	DNAJC6	*PARK19, DJC6*	AR	Likely pathogenic	Early-onset	Synaptic vesicle formation and trafficking
	DNAJC13	*PARK21, RME8*	AD	Conflicting reports	Typical	
	TMEM230	*C20ORF30*	AD	Conflicting reports	Typical	
	SYNJ1	*PARK20*	AR	Pathogenic	Early-onset, atypical	
	VPS13C	*PARK23*	AR	Pathogenic	Early-onset	Mitochondrial
	CHCHD2	-	AD	Pathogenic	Typical	Uncertain
	DCTN1	-	AD	Pathogenic	Atypical	Microtubule
Variable penetrance	*LRRK2*	*PARK8, DARDARIN*	AD	Pathogenic	Typical	Lysosomal, mitochondrial, microtubule
	GBA	*GBA1*	AD	Pathogenic	Typical	Lysosomal
Associated with PD but unlikely to be pathogenic	*HTRA2*	-	AD	Uncertain/likely benign	-	Mitochondrial
	UCHL1	*PARK5*	AD	Uncertain/likely benign	-	Ubiquitin-proteasome
	GIGYF2	*PARK11*	AD	Uncertain/likely benign	-	Uncertain
	EIF4G1	-	AD	Benign	-	mRNA translation
	LRP10	*LRP9*	AD [1]	Uncertain	-	Uncertain

[1] AD = autosomal dominant, AR = autosomal recessive, HNGC = HUGO Gene Nomenclature Committee.

Table 1: Monogenic variants associated to Parkinson's disease (from Day et al. 2021, use authorized by Creative Commons Attribution 4.0 International License).

In the context of PD, it is of particular interest to differentiate iPSCs into midbrain dopaminergic neurons. iPSCs-derived neurons are now a widely used model in PD. For example, the study of homozygous DJ-1 mutations showed that it caused increased mitochondrial damage, leading to dopamine oxidation (Burbulla et al., 2017). As expected, iPSC-derived neurons from PD patients with a triplication in the SNCA gene revealed that there was twice more α-synuclein in patient neurons than in controls (Byers et al., 2011). Excessive α-synuclein accumulation, increased intracellular dopamine levels as well as disruption of mitochondrial morphology were found in iPSC-derived neurons from PINK1 patients (Chung et al., 2016).

As a last example, neurons from LRRK2-G2019S patients have a higher amount of damaged mitochondrial DNA (Sanders et al., 2014). While iPSC-derived neurons have significantly improved our understanding of the disease, these are not the only cell type affected. Indeed, astrocytes and microglia also play an important role in PD, and protocols also exist to generate iPSC-derived models of these two cell types (Haenseler et al., 2017; Li et al., 2018). Although co-culture models have been developed, they are still far from the real situation, in which cell types develop in the brain all together. The first iPSCs-derived models that come close to this are organoids, 3D models, so called “mini brains” in neuroscience research (while they can also be used to model other organs) (Corsini and Knoblich, 2022). Of particular interest for us are MO, that, on top of midbrain dopaminergic neurons, also contain astrocytes and oligodendrocytes, and are similar to fetal midbrain at the transcriptomic level (Monzel et al., 2017a; Nickels et al., 2020; Zagare et al., 2021a).

Lastly, *in vivo* models of PD are also widely used to better understand the disease complexity: non-human primates, mice and rats, fishes, C. elegans, and drosophila. Starting with neurotoxic models, the 6-hydroxydopamine model (6-OHDA) and MPTP models have been used for decades. Even if 6-OHDA cannot cross the blood brain barrier (BBB) and has to be injected into the brain, whereas MPTP can be given systematically as it crosses the BBB, both drugs do lead to dopaminergic neuron loss and allow the modelling of some specific aspects of PD (Blesa et al., 2016b). More pathophysiologically relevant animal models of PD were developed, taking advantage of the accumulated knowledge on genetic causes of PD. Unfortunately, many of these models do not display the characteristic dopaminergic neuron loss in the substantia nigra found in PD patients (Blesa et al., 2016b). This includes transgenic mice with knocked-out or overexpression of *SNCA*, Leucine Rich Repeat Kinase 2 (*LRRK2*) G2019S, PTEN Induced Kinase 1 (*PINK1*) or Parkin RBR E3 Ubiquitin Protein Ligase (*PARKIN*) knock-out (KO) (Chesselet et al., 2008; Gispert et al., 2009; Matthew S. Goldberg et al., 2003; Hinkle et al., 2012).

Interestingly, a PARK7 (Parkinsonism Associated Deglycase, DJ-1) KO mouse model loses its SNpc dopaminergic neurons already at a young age, and also displays mild behavioral impairments (Rousseaux et al., 2012). To conclude, it is important to note the limitations of both models: toxin-induced PD models do not model chronic, progressive neurodegeneration, while genetic models often do not fully represent PD as seen in human, especially DA neuron loss in the SNpc. The heterogeneity of the efficiency in modelling PD depending on the model used exacerbates the need for studies using multiple models, which was one of the aims of this PhD thesis.

I.III Mitochondria in PD:

Mitochondria, known as the cell's powerhouses by non-scientists, are dynamic organelles capable of dividing and fusing depending on cellular needs and possible impairments they might face. Fission of mitochondria isolates damaged subparts to be degraded, while fusion serves as a way to dilute damages, avoiding degradation by cellular quality control systems (Friedman and Nunnari, 2014; Van Laar and Berman, 2009). Their main role is producing adenosine triphosphate (ATP) via oxidative phosphorylation, but they are also involved in cell growth, differentiation and neuronal development by providing the aforementioned energy source, as well as apoptosis, regulation of intracellular calcium and lipid metabolism (Beckervordersandforth et al., 2017; Grünewald et al., 2019; Karbowski and Youle, 2003; McBride et al., 2006). As mentioned earlier and depicted in Figure 1, many genes related to PD encode for proteins that regulate mitochondrial function or even localize in mitochondria (Larsen et al., 2018). Dopaminergic neurons are especially vulnerable to mitochondrial impairment due to their high energy demand that is required to sustain their pace-making activity (Grossmann and Krüger, 2020; Saxton and Hollenbeck, 2012; Yellen, 2018). Moreover, reactive quinones, a byproduct of the oxidation of dopamine, disrupt protein degradation, mitochondrial function, and promote the development of α-synuclein protofibrils (Segura-Aguilar et al., 2014).

Dopaminergic neurons are also highly susceptible to ROS and oxidative stress (Dias et al., 2013). Under physiological conditions, ROS are a byproduct of the electron transport chain (ETC) activity. Briefly, electrons go through complexes I, III and IV, and allow proper functioning of ATP synthase, complex V of the ETC, which is responsible for the conversion of adenosine diphosphate (ADP) to ATP using the proton-motive force (Fernie et al., 2004). Throughout this process, ROS are produced mainly at complexes I and III (Zhao et al., 2019). More precisely, ROS are produced at two sites of complex I: the Flavin mononucleotide site (IF) and ubiquinone binding site (IQ) sites (Brand, 2010).

Electrons from NADH reduce the IF site, and when electrons leak from the reduced Flavin mononucleotide, they react with oxygen, leading to superoxide production (Brand, 2010; Nolfi-Donegan et al., 2020). ROS can also arise from the IQ site of complex I during reverse electron transport, when ubiquinol is oxidized and driven back to the IF site to produce NADH from NAD^+ (Scialò et al., 2017; Wong et al., 2017). Lastly, electrons produced by complex I (or II) are used to reduce ubiquinone to ubiquinol, which is then oxidized by complex III, allowing, *in fine*, the entrance of protons into the intermembrane space via sequential transfer of electrons to the cytochrome c. This sequential transfer, leaving only one electron on complex III while the other one goes to cytochrome c can lead to ROS production due to the interaction of the electron left within complex III with O2 (Nolfi-Donegan et al., 2020). Normally, glutathione neutralizes (reduces) ROS produced by the ETC. Other ROS managing proteins such as DJ-1 can also quench ROS and increase glutathione levels as well as activate pathways involved in antioxidant response (Dias et al., 2013).

It is known that among the many cellular hallmarks of PD, accumulation of ROS exacerbates mitochondrial dysfunctions, lowering the mitochondria's capacity to produce ATP, disturbing proper functioning of protein degradation systems, which, for example, will prevent proper degradation of intracellular α-synuclein (Bentea et al., 2017; Chung et al., 2003). Moreover, increased mitochondrial ROS induce oxidative stress and damages DNA, mitochondrial DNA (mtDNA), proteins as well as other cellular components, lowering further the cell's capacity to produce ATP (Ebrahimi-Fakhari et al., 2012; Luo et al., 2015). The evidence for a role of mtDNA damage in PD was found by studying brains from idiopathic PD which presented more mitochondrial DNA deletions than controls (Grünewald et al., 2016). Moreover, dysfunctional ETC complexes (subunits of complexes I and III encoded by mtDNA) can arise from mtDNA mutation induced by ROS (Franco-Iborra et al., 2016).

The intrinsic properties of pace-making dopaminergic neurons are based on an L-type, voltage dependent calcium channel. This creates an important influx of calcium into the cell that need to be buffered by consuming ATP, further increasing the already high need for ATP of dopaminergic neurons (Surmeier and Schumacker, 2013). The main organelles involved in calcium buffering are the mitochondria, thanks to the mitochondrial calcium uniporter (MCU), a channel found at the inner mitochondrial membrane (Rizzuto et al., 2012). Interestingly, the MCU is regulated by Miro1 (Niescier et al., 2018, 2013). Moreover, calcium entry into the mitochondria upregulates the activity of several enzymes involved in the tricarboxylic acid cycle (TCA cycle) and ATP production (Rizzuto et al., 2012). Furthermore, the driving force of the ETC, the mitochondrial membrane potential (MMP), is also involved in the mitochondrial uptake of calcium (Fernie et al., 2004; Rizzuto et al., 2012; Stock et al., 1999).

The importance of calcium and MMP regulation can be illustrated with the use of staurosporine. This compound overburdens the mitochondria with calcium, over activating the ETC and oxidative phosphorylation; this is accompanied by mitochondrial hyperpolarization, finally inducing the release of cytochrome c and apoptosis initiation (Kruman and Mattson, 1999; Poppe et al., 2001; Vander Heiden et al., 1997). Taken together, this highlights the important role of calcium dysregulation in PD pathogenesis, and makes impaired calcium homeostasis one of the cellular hallmarks of PD (Figure 2) (Paul M. A. Antony et al., 2013).

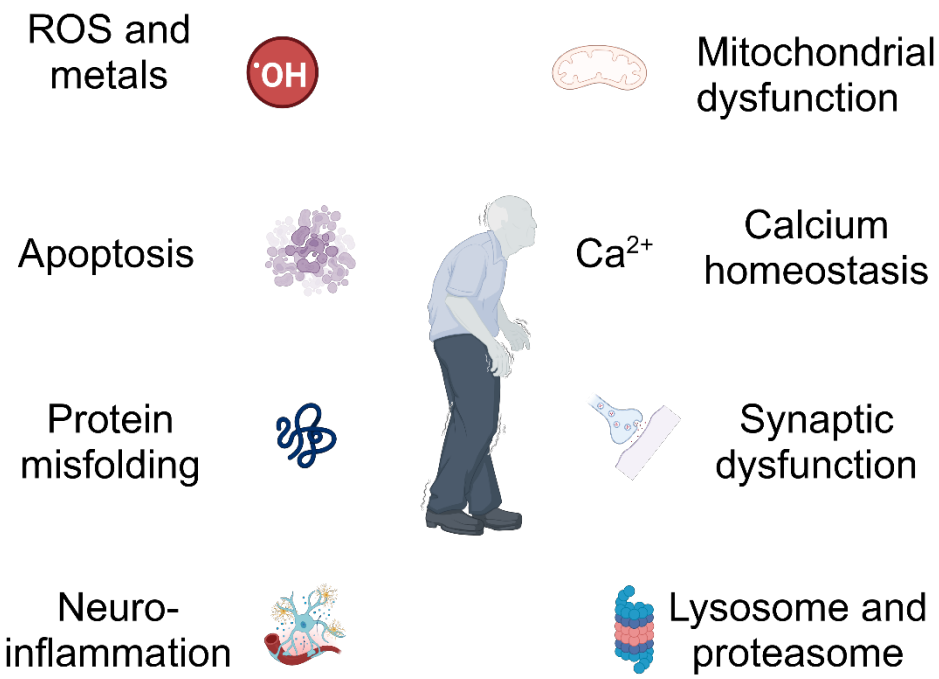

Figure 2: Cellular hallmarks of Parkinson's disease (created with BioRender.com, adapted from Antony et al. 2013).

I.IV Miro1 in PD:

The *RHOT1* gene, located on the chromosome 17, encodes the protein Miro1, a Guanosine Triphosphate-(GTP)ase whose first described role was being an adaptor for calcium-dependent mitochondrial transport (Chang et al., 2011; MacAskill et al., 2009a; Wang and Schwarz, 2009). At the structural level, Miro1 is made of an N- and C-terminal GTP binding motif, exclusive to the Miro1 proteins, whereas it lacks the typical Rho insert usually found in RHO GTPases (Colicelli, 2004; Smith et al., 2019; Vlahou et al., 2011). The GTP binding motifs are connected to two calcium sensing EF hands domains by linker regions (Klosowiak et al., 2013). Interestingly, these two domains of Miro1 do not have the exact same role. Indeed, while the N-terminal GTPase domain is involved in bidirectional mitochondrial transport, the C-terminal GTPase domain of Miro1 seems to be either involved in retrograde transport only or it does not play a role at all in mitochondrial transport (Babic et al., 2015; Guo et al., 2005; MacAskill et al., 2009a). In contrast, the Miro1 C-terminal GTPase domain interacts with and stabilizes the protein's EF (helix E-loop-helix F) region hands, thus is more closely involved in Miro1 calcium binding capacity instead of mitochondrial transport (Klosowiak et al., 2013; Saotome et al., 2008). Miro1 also contains two canonical EF hands, linked to non-canonical or "hidden" EF hands by ligand-mimicking domains (Klosowiak et al., 2013). Lastly, Miro1 is hooked to the outer mitochondrial membrane by its C-terminal transmembrane domain (Klosowiak et al., 2013; MacAskill et al., 2009a).

Another Miro GTPase exists in mammals, encoded by the gene *RHOT2*, with a 60% peptide sequence homology: Miro2 (Grossmann et al., 2020a). Interestingly, *RHOT2* gene expression was found to be decreased in the SNpc of PD patients, while protein network analysis showed Miro2 interaction with PINK1 and PARKIN (Saeed, 2018), but until now, a direct implication of Miro2 in PD has not been demonstrated. Curiously, PARKIN ubiquitinates Miro1 more efficiently and faster than Miro2 (Klosowiak et al., 2016a). Moreover, Miro1 seems to be rather associated with neurodegeneration (Panchal and Tiwari, 2021), but also cancer (Zhuang et al., 2023), while Miro2 has been associated with prostate cancer progression (Furnish et al., 2022) as well as invasion and migration of colon cancer cells (Zhuang et al., 2023). Although no associations were found between *RHOT1*, *RHOT2* and PD by the International Parkinson's Disease Genetics Consortium, the fact that their analysis was based on whole genome sequencing explain their inability to find rare, PD-associated RHOT variants (Periñán et al., 2020). Whole exome sequencing recently allowed the identification of *RHOT2* as a potential PD associated gene (Gialluisi et al., 2021). Moreover, while Miro2-KO mice are viable and fertile, Miro1-KO animals die a few minutes after birth (López-Doménech et al., 2016a). The fact that Miro2 is not able to compensate for the loss of Miro1 suggests that the two proteins do not have the exact same roles (López-

Doménech et al., 2016a). Moreover, KO Miro1 in mouse brains led to the death of upper motor neurons, (López-Doménech et al., 2016a; Nguyen et al., 2014) a study from which we can remember two points: Miro2 is not able to rescue a neuron specific Miro1 loss, and Miro1 KO might affect preferentially neurons with long processes, which suggests that DA neurons might also be especially vulnerable to Miro1 disruptions or mutations due to their long axons. Additional studies are needed to decipher the differences between Miro1 and Miro2, as Miro2 is not always able to compensate for Miro1 dependent defects (Grossmann et al., 2020a).

Over the last years, our group identified four PD patients carrying distinct heterozygous mutations in the *RHOT1* gene encoding Miro1, without any other known mutation in established PD causing genes (Berenguer-Escuder et al., 2019a, 2020a; Grossmann et al., 2019a). The p.R272Q mutation is located in the ligand mimicking domain of the N-terminal EF hand, p.T351A in the C-terminal EF hand, p.R450C in the C-terminal GTPase, while the p.T610A mutation is located close to the transmembrane domain (Grossmann and Krüger, 2020) (Figure 3). We first guessed that based on the position, the different mutations would affect to a higher or lesser extent calcium binding and homeostasis, mitochondrial transport and/or other mechanisms linked to Miro1 such as mitophagy (Berenguer-Escuder et al., 2019a, 2020a; Grossmann et al., 2019a).

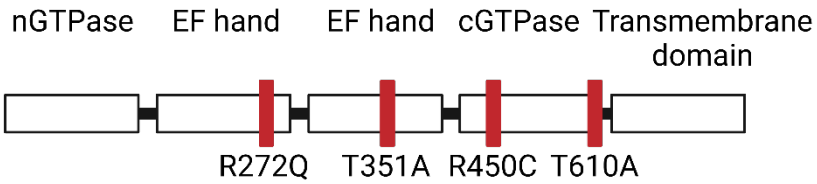

Figure 3 Schematic representation of Miro1 protein structure, showing the four identified mutation identified in PD patients

Miro1 is the adaptor protein between the mitochondria and the transport machinery, allowing mitochondrial movement on the cytoskeleton highway, and, through sensing calcium, also responsible for mitochondrial arrest after detaching from the transport machinery. It is also known as a regulatory component of the so-called mitochondria/ER contact sites (MERCs), which are involved in many mechanisms such as calcium and lipid exchange, and initiation of autophagy.

Lastly, Miro1 is involved in mitophagy, since, if it is not degraded, damaged mitochondria stay anchored to the cytoskeleton, and cannot be engulfed by the autophagosome and disposed of by mitophagy (Grossmann and Krüger, 2020).

Now, going more into details, one can describe the mitophagy process via its known PD-related proteins, the PINK1/PARKIN pathway. When mitochondria are damaged, their MMP drops significantly, letting PINK1 accumulate on the outer mitochondrial membrane. PINK1 will then start to phosphorylate several ubiquitinated proteins, leading to PARKIN activation which will provide more ubiquitin residues. Accumulation of phospho-ubiquitinated mitochondrial proteins at the surface of the mitochondria will, *in fine*, trigger the autophagosome enveloping the damaged mitochondria, to then fuse with a lysosome and degrade it (Bayne and Trempe, 2019). Miro1 is a target of PARKIN, and after being ubiquitinated, can be degraded by the proteasome (Grossmann and Krüger, 2020).

On top of the association of Miro1 with the PD-related proteins PINK1 and PARKIN, its removal from damaged mitochondria, paramount for proper management of ROS and healthy neurons, has been even more strongly associated with PD over the last years (Grossmann and Krüger, 2020). The team of Prof. Xinnan Wang at the Stanford University showed, first in cells from PD patients with LRRK2 G2019S or A53T α-synuclein mutation, that both proteins were associated with Miro1 and that their pathogenic mutations led to a delay in Miro1 detachment and proteasomal degradation, preventing mitophagy to happen and leading to a detrimental accumulation of damaged mitochondria both in fibroblasts and iPSC-derived neurons. Interestingly, this seems not to be the only mechanism responsible for delayed mitophagy, since this phenotype was also found in sporadic PD patients and was even happening in more than 90% of idiopathic PD patients fibroblasts. Moreover, using a compound to trigger Miro1 degradation rescued neurodegeneration both in iPSC-derived neurons carrying the A53T SNCA mutation or from a sporadic PD patient, as well as in three well established PD drosophila models (LRRK2 G2019S, A53T SNCA, and PINK1 null) (Hsieh et al., 2016a, 2019a; Shaltouki et al., 2018a).

Interestingly, this is reminiscent of an earlier study done in 2009 by Liu and colleagues using Drosophila, in which Miro1 overexpression resulted in DA neurons death, supposedly due to delayed mitophagy caused by overabundant amounts of Miro1 (Liu et al., 2012). Two years later; deletion of PINK1 in drosophila was shown to stabilize Miro1, resulting in neuronal death (Tsai et al., 2014a) .

From the former studies, the Miro1 retention phenotype and impairment of mitophagy, even though the underlying mechanisms are not fully understood, seems to be robust. In our published studies in fibroblasts from the four PD patients with heterozygous Miro1 mutations, we indeed found mitophagy alterations.

However, while the p.R272Q and p.R450C mutant fibroblasts displayed higher mitophagy levels than controls, the p.T351A and p.T610A rather displayed a reduced mitophagy process (Berenguer-Escuder et al., 2019a; Grossmann et al., 2019a). Interestingly, in Miro1 p.R272Q iPSC-derived neurons, mitophagy was reduced, in contrast to what we saw in fibroblasts (Berenguer-Escuder et al., 2020a). This could be explained by the high ATP need of dopaminergic neurons, who would try to keep even slightly damaged mitochondria as they cannot rely on glycolysis alone. Degeneration could also happen as a consequence of reduced mitophagy, and accumulation of dysfunctional mitochondria. Another possibility could be that, instead of clearing entire mitochondria via mitophagy, a more fine-tuned mechanism would be involved: Mitochondrial-derived vesicles (MDVs). Mitochondrial stress and PARKIN activation trigger the formation of MDVs (McLelland et al., 2014), which contain damaged mitochondrial proteins, leading to their incorporation into peroxisomes or late endosomes (Sugiura et al., 2014), which could result in insufficient removal of damaged mitochondrial parts in DA neurons requiring complete mitophagy. Additionally, a conditional KO of Miro1 in neurons led to mitophagy disruption and activation of the integrated stress response, as shown in a study using mouse embryonic fibroblasts, primary mouse neurons, and histology from conditional Miro1 KO mice (López-Doménech et al., 2021). Moreover, this study revealed the Miro1 ubiquitination was required for proper mitophagy progression, as using a modified Miro1 protein with arginine in place of sites that were thought to be lysine targeted for ubiquitination within the *PINK1/PARKIN* mediated mitophagy process. Interestingly; many of the sites targeted within this construct are close to the N-terminal EF hand of Miro1 (namely K153, K182, K187, K194), which is the EF hand where the p.R272Q Miro1 mutation takes place in our PD patient. One could therefore wonder whether the p.R272Q mutation affects not only calcium sensing based on the point mutation position (as briefly mentioned on page 25 and related to Figure 3), but could also have an impact on Miro1 structure and induce conformational stress, preventing access to these lysine residues and their ubiquitination, which could give an additional explanation for the impaired mitophagy phenotype found in Miro1 p.R272Q DA neurons by Berenguer and colleagues (Berenguer-Escuder et al., 2020a).

Mitophagy is tightly related to another role of Miro1, which is the regulation of MERCs. In particular, “wide” MERCs, characterized by a space between mitochondria and ER of around 30nm, are known to play a role in mitophagy (Cieri et al., 2018; McLelland et al., 2018). In fact, it is at this level that PARKIN ubiquitinates the outer mitochondrial membrane proteins of damaged mitochondria, allowing their detachment from the ER and mitophagy initiation (Berenguer-Escuder et al., 2019a; Grossmann et al., 2019a).

In accordance with this, our previous studies demonstrated that Miro1 mutant fibroblasts with the p.T351A and p.T610A mutation, characterized by a reduced amount of “wide” MERCs, were unable to properly start autophagy and mitophagy upon CCCP treatment, which could come from the lower amount of wide MERCs not providing enough material for the formation of the autophagosome membrane (Berenguer-Escuder et al., 2019a). On the other hand, wide MERCs were unaffected in p.R450C and p.R272Q fibroblasts, which allowed proper initiation of mitophagy (Berenguer-Escuder et al., 2019a). Impaired mitophagy and MERCs seem to be a shared feature in PD, given that several studies proved the involvement of PD-related proteins in these mechanisms. For example, α-synuclein was found in MERCs from mouse and human tissues, while PINK1, PARKIN, and LRRK2 are also involved in MERCs (Grossmann et al., 2020a; Guardia-Laguarta et al., 2014). Interestingly, there were more MERCs in our Miro1 p.R272Q iPSC-derived neurons, but no increase in mitophagy, indicating that the p.R272Q Miro1 mutation could affect the function of MERCs (Berenguer-Escuder et al., 2020a). This could be caused by the fact that the p.R272Q mutation is located in Miro1 EF hand, and thus, could affect calcium sensing, which is required for mitochondria detachment. In neurons, the increased number of MERCs, supposedly caused by mutant p.R272Q Miro1, preventing the mitochondria to detach from the ER would hinder proper induction of mitophagy. However, this was seen when looking at total MERCs number in neurons, not subtypes such as wide MERCs. Further investigation of Miro1’s role in MERCs regulation, whether its activity, protein levels, or specific mutation can differentially affect MERCs subtypes and function could help better understand specific PD phenotypes in the future.

Miro1 is a major protein responsible for regulating calcium homeostasis in the mitochondria, as well as mitochondrial transport and arrest, as mitochondrial arrest and detachment from the transport machinery is triggered by increased cytosolic calcium levels sensed by Miro1. This protein has a high calcium binding affinity, and binds it when cytosolic calcium levels rise (Koshiba et al., 2011; Nemani et al., 2018; Saotome et al., 2008; Wang and Schwarz, 2009). Moreover, it is known that the speed at which mitochondria move throughout the cytoskeleton is not only controlled by intracellular, but also intramitochondrial calcium levels (Chang et al., 2011). Studies in drosophila revealed that Miro1 helps calcium entry from the ER to the mitochondria (Lee et al., 2016). The precise mechanism was revealed 5 years ago, when the N-terminal part of the MCU was found to go through the mitochondrial intermembrane space (while the MCU is located at the inner mitochondrial membrane), and directly interacts with Miro1. Thus, calcium sensed by Miro1 is then entering the mitochondria via a Miro1-MCU interaction (Niescier et al., 2018). Calcium entry into the mitochondria, besides its use as a buffer in case of too high cytosolic calcium levels, is paramount for energy production

(Jouaville et al., 1999; McCormack et al., 1990).

The importance of Miro1 calcium related activity in regulating ATP production was proved in drosophila and yeast, either by expressing a LoF variant of Miro1, or knocking out the gene in yeast. This led to a decrease in ATP production in both cases, which was seen concomitantly with a reduced entrance of calcium into the mitochondria (Lee et al., 2016; Vlahou et al., 2011). We also provided more insight into the importance of Miro1 in maintaining calcium homeostasis by using our Miro1 mutant lines in former publications. In fibroblasts, we used thapsigargin, which prevents the use of the ER for calcium buffering, leading to an increase of cytosolic calcium levels, and more importantly, forcing the cell to rely on non-ER buffering mechanisms, so to rely on mitochondria. Calcium buffering was significantly less efficient in Miro1 mutant patient-derived fibroblasts. Adding Ru360, a MCU inhibitor, to the thapsigargin-treated cells reduced the calcium buffering capacity of control lines at a similar extent to that observed in Miro1 mutant fibroblasts. This proved that calcium buffering was dysfunctional in Miro1 mutant fibroblasts, and that, when ER cannot be used for buffering, the cell relies mostly on mitochondria (Berenguer-Escuder et al., 2019a; Grossmann et al., 2019a). The importance of Miro1 in the regulation of calcium handling was also confirmed in cell types more relevant to neurodegenerative diseases. Disruption of Miro1 EF hand in primary rat astrocytes, or overexpression of Miro1 in fly's primary neurons both led to a dysregulation of calcium homeostasis (Jackson and Robinson, 2015; Lee et al., 2016).

Miro1 is also involved in another mechanism linked to calcium and mitophagy, which is the mitochondria shape transition (MiST) (Nemani et al., 2018). This mechanism is independent of Dynamin 1 like protein 1 (Drp1), MMP or ROS, and is required before mitophagy initiation (Nemani et al., 2018). Findings obtained by our team in Miro1 p.R272Q mutant neurons revealed that mitochondrial fragmentation was higher in mutant neurons, most likely due to their incapacity to deal with calcium stress (Berenguer-Escuder et al., 2020a). In summary, the previously published research on Miro1 and calcium, its impact of ATP production and calcium dependent MiST strengthens its links with PD. Interestingly, research done on Caenorhabditis elegans, revealed the role of Miro1 on the so-called wounding-induced mitochondrial fragmentation (WIMF), participating to tissue repair after wounding (Fu et al., 2020). In this paper, researchers discovered WIMF, a process similar to MiST, as it is also a Miro1-calcium dependent, Drp1 independent mitochondrial fragmentation process, although significantly faster (happening in seconds for WIMF, while MiST takes minutes) (Fu et al., 2020). Interestingly, overexpression of Miro1 in a rat model of secondary brain injury following intracerebral hemorrhage led to increased mitochondrial transport, as well as reduction of edema, lower cognitive impairment and less neuronal death (B. Li et al., 2021).

Although Berenguer and colleagues already investigated MiST in Miro1 p.R272Q mutant neurons compared to age/gender matched controls, it would still be worth investigating it in our isogenic pair, as well as WIMF by focusing on a faster frame of observation (seconds) and, perhaps, also perform wounding, or wound healing studies with our Miro1 p.R285Q KI model to decipher the extent to which this EF hand variant of Miro1 also affects healing in the context of acute stress, in opposition to chronic, neurodegenerative diseases such as PD. Knowing that mitochondria from Miro1 p.R272Q DA neurons move at a slower pace (Berenguer-Escuder et al., 2020a), one could expect that this particular mutation would impair WIMF and healing after acute injury.

One last role of Miro1 to discuss in more details in this thesis is its involvement in mitochondrial transport. Miro1 role as a linker between the mitochondria and motor proteins for transport along the cytoskeleton has been extensively documented (Grossmann and Krüger, 2020). As mentioned earlier, the involvement of Miro1 in the regulation of mitochondrial transport relies on its calcium sensing properties, as upon sensing elevated cytosolic calcium levels, Miro1 will induce, while its GTPases domains, mainly the N-terminal are involved in mitochondrial movement in either anterograde or retrograde direction. We already know that modifications in Miro1 affect mitochondrial movement and placement in mouse and rat neurons and glial cells (López-Doménech et al., 2016a; MacAskill et al., 2009b; Stephen et al., 2015) The regulation of mitochondrial transport by Miro1 is of particular interest in the context of neurodegenerative diseases such as PD, since dopaminergic neurons require a tightly controlled distribution of their mitochondria to provide enough ATP to support their pace-making activity and maintain the integrity of their long, unmyelinated axonal arborization (Course and Wang, 2016; Haddad and Nakamura, 2016; Matsuda et al., 2009). Moreover, the anterograde transport of mitochondria from the soma to synapses to provide ATP and manage calcium levels is essential in cells and subcellular compartments with high energetic needs such as neurons and synapses (Course and Wang, 2016). On the other hand, retrograde mitochondrial transport is also of utmost importance for neuronal wellbeing, by allowing damaged mitochondria to go back to the soma, where they are degraded by the lysosomes (Course and Wang, 2016; LaMonte et al., 2002). Studies in drosophila first demonstrated the importance of Miro1 in anterograde transport in neurons toward synapses (Guo et al., 2005). Removing Miro1 in drosophila reduced mitochondrial transport in both directions, while the N-terminal GTPase domain was shown to be crucial for axonal and dendritic mitochondrial transport (Babic et al., 2015; Russo et al., 2009). Moreover, neuronal survival was decreased in flies with a LoF mutation in Miro1 EF hand, likely due to impairment in Miro1 mediated mitochondrial placement (Wang and Schwarz, 2009). Knocking out Miro1 in mice reduced the number of mitochondria in dendrites,

decreased dendritic complexity and increased neurodegeneration (López-Doménech et al., 2016a). Later, Kalinski and colleagues unraveled another aspect of Miro1 related modulation of mitochondrial transport in primary neurons from rats, showing that deacetylation of the N-terminal GTPase domain of Miro1 by histone deacetylase 6 was involved in inhibition of mitochondrial transport and the axonal growth cone (Kalinski et al., 2019). Acetylation of Miro1 at lysine 105 decreased its sensitivity to calcium and helped with axon growth (Kalinski et al., 2019). As the p.R272Q mutation is located in one of Miro1 EF hands, and might therefore decrease mutant Miro1 calcium sensitivity, one could also investigate this process in Miro1 p.R272Q ipsc-derived DA neurons, but also in primary neurons from the Miro1 p.R285Q KI mice.

Lastly, it is important to keep in mind that the dynamic of mitochondrial transport does not only depend on Miro1 GTPases domains and calcium sensing activity, but also on the motor proteins to which Miro1 binds. Thus, if the complex is made with kinesin, anterograde transport will happen, while a complex including dynein is responsible for retrograde transport (Hirokawa et al., 1998; Morlino et al., 2014; Wang and Schwarz, 2009). The proteins in between Miro1 and kinesin/dynein also play an important role: TRAK1 mediates the bidirectional transport of axonal mitochondria while transport along dendrites is mediated by TRAK2 (Kay et al., 2018; van Spronsen et al., 2013).

The last years saw a rising interest toward Miro1 implication in neurodegeneration, especially related to PD. Miro1 has even been proposed as a possible PD biomarker, and compounds aimed at inducing Miro1 degradation to allow proper functioning of the mitophagy machinery and rescue neurodegeneration have been developed (Hsieh et al., 2019a). However, until today, only our group managed to identify PD patients with mutations in Miro1. In this study, we first reprogrammed available fibroblasts from the four Miro1 mutant carriers into iPSCs, followed by correction of each mutation by CRISPR/Cas9-mediated gene editing (Figure 3 and Table 2) (Miro1 p.T351A and p.T610A, manuscript I; Miro1 p.R272Q and p.R450C, manuscript II). Finally, we explored the functional consequences of Miro1 p.R272Q mutation in iPSC-derived midbrain neurons and MO, and investigated the impact of Miro1 deficiency *in vivo* using a Miro1 R285Q (KI) mouse model, ortholog to the p.R272Q human mutation (manuscript III).

Table 2 Information about the four Miro1 mutant carriers

Gender	Female	Male	Female	Male
Age of onset	70	60	50	40
Age at biopsy	78	65	54	45
Mutation	R272Q	T351A	R450C	T610A

II Discussion

The involvement of Miro1 in PD pathogenesis became more and more evident over the last few years, mainly due to the Miro1 retention phenotype observed in fibroblasts and iPSC-derived neurons from both familial (e.g LRRK2, α-synuclein(Hsieh et al., 2016a; Shaltouki et al., 2018a)) and sporadic PD patients, which finally results in delayed mitophagy and neurodegeneration (Hsieh et al., 2019a). These findings significantly multiplied the interest for Miro1 as a potential biomarker, and early clinical trials using the Miro1 retention phenotype as a way to measure efficiency of potential therapeutic compounds are currently ongoing by the company AcureX Biosciences. The team from Prof.Xinnan Wang (co-founder, advisor, and shareolder of AcureX) at Standford University developed a peripheral blood mononuclear cells (PBMC)-based, Miro1 drug responsive assay for the detection of PD, which enabled them to screen compounds that would rescue PD-associated impairments by looking at the restoration proper degradation of Miro1 ("Acurex Biosciences to Present Early Clinical Results Supporting its Novel Parkinson's Disease Biomarkers at a Michael J. Fox Foundation Biomarkers Workshop," 2023; Bharat et al., 2022b). Moreover, studies in fibroblasts and iPSC-derived neurons from PD patients, as well as in drosophila PD models showed that promoting Miro1 degradation rescued neurodegeneration (Hsieh et al., 2016a, 2019a; Shaltouki et al., 2018a).

We previously identified four PD patients with heterozygous Miro1 mutations (p.T351A, p.T610A, p.R450C and p.R272Q), and first demonstrated in fibroblasts that these Miro1 variants were involved in PD-relevant molecular mechanism such as disruption of calcium homeostasis, MERCs, as well as mitophagy and autophagy (Berenguer-Escuder et al., 2019a; Grossmann et al., 2019a). We then also demonstrated the calcium related issues, MERCs, and mitophagy/autophagy impairments in iPSC-derived Miro1 p.R272Q mutant neurons (Berenguer-Escuder et al., 2020a).

However, this work was done using only age/gender-matched controls. Therefore, we need to better dissect the molecular and cellular alterations caused by Miro1 variants by comparing the mutants to isogenic, gene-corrected lines, which would allow us to confidently demonstrate that phenotypes are caused by the Miro1 variant itself.

Thus, the overall objective of this thesis was to investigate the contribution of Miro1 variants in PD pathogenesis. To allow future researchers to investigate the impact of Miro1 rare variants on neurodegeneration, we first generated iPSCs and gene corrected lines from our previously characterized fibroblasts (Manuscripts I and II).

In particular, the generation of gene-corrected isogenic controls will be crucial to distinguish between Miro1-specific effects and alterations potentially linked to the genetic background of these patients (Manuscript I and II).
Moreover, we provided strong evidence supporting the involvement of one rare Miro1 variant (i.e p.R272Q) in PD pathogenesis using both, isogenic iPSC-derived neuronal cultures and MO, as well as a KI mouse model expressing mutant Miro1 (Manuscript III).

II.I The Miro1 p.R272Q disrupts calcium homeostasis and mitochondrial bioenergetics:

First, Miro1 p.R272Q mutant neurons presented a reduced ability to deal with calcium stress induced by ionomycin, a calcium ionophore that increases intracellular calcium concentration by facilitating its transport across the plasma membrane. In particular, iPSC-derived neurons displayed a significantly higher sensitivity to calcium stress compared to an age/gender-matched control, confirming our previous study (Berenguer-Escuder et al., 2020a), but also compared to their isogenic counterpart (Manuscript III, Figure 2 G). Interestingly, disrupted calcium homeostasis was identified in drosophila with a *PINK1* LoF or the LRRK2 G2019 mutation, associated with mitochondrial defects and death of dopaminergic neurons, with Miro1 being a central player in this mechanism (Lee et al., 2018). More precisely, in the aforementioned study, calcium regulation and homeostasis were influenced by MERCs, which are strengthened in *PINK1* loss-of-function mutant DA neurons from flies, leading to the elevation of mitochondrial calcium levels, resulting in neuronal death. In the same study, overexpressing Miro1 replicated the effect of *PINK1* loss-of-function, while knockdown of Miro1 rescued harmful *PINK1* loss of function phenotypes (Lee et al., 2018). This is especially interesting when compared to our former study, where Berenguer-Escuder and colleagues demonstrated that Miro1 p.R272Q iPSC-derived DA neurons had more MERCs than age and gender-matched controls (Berenguer-Escuder et al., 2020a). Further investigation in our in vitro and in vivo model is needed to dissect the implication of mutant Miro1 in the regulation of MERCs and their role in calcium homeostasis, and more precisely, intra mitochondrial calcium.

The disruption of calcium homeostasis in Miro1 p.R272Q iPSC-derived DA neurons is also in line with a study on primary rat astrocytes overexpressing calcium insensitive, mutant Miro1 EF-hand. After stimulation with ATP, calcium levels were significantly increased compared to control astrocytes (Stephen et al., 2015).

This led the authors to conclude that disruption of Miro1 EF hands impairs intracellular calcium regulation, culminating in increased vulnerability to excessive calcium levels. Furthermore, disruption of Miro1 EF hands in a drosophila model significantly reduced calcium influx into the mitochondria (Chang et al., 2011).
Our study also gives another argument in favor of the influence of patient genetic background, as a study in which the p.R272Q Miro1 mutation was inserted into cells from a healthy donor showed only a mild impact of the point mutation on calcium homeostasis under stress, compared to the healthy donor with no mutation inserted (Schwarz et al., 2022a).

In our study, the isogenic control, with the patient background and the p.R272Q Miro1 mutation corrected, showed an elevation of intracellular calcium under stress that, although it was significantly lower compared to PD-R272Q neurons, was also significantly higher than the age and gender matched control line (Manuscript III, Figure 2, panel G). In other experiments, isogenic and wt control behaved similarly (e.g ROS measurement, Manuscript III, Figure 2, panel E), indicating that genetic background can exacerbate, or alleviate, some of the PD associated phenotypes linked to the Miro1 p.R272Q mutation. As mentioned in the introduction, Miro1 regulates calcium uptake into the mitochondria via its interaction with the MCU, thus controlling the activity of several key TCA cycle enzymes, including NAD+ isocitrate deshydrogenase (IDH), pyruvate deshydrogenase (PDH), oxoglutarate deshydrogenase (OGDH) and the complex V of the ETC ATP synthase (Figure 4). In line with this notion, our findings obtained in iPSC-derived 2D neurons and 3D MO carrying the Miro1 p.R272Q mutation revealed a dramatic alteration of mitochondrial respiration compared to both, isogenic and age/gender-matched healthy controls (Manuscript III, Figure 3, panels A and D). As expected, ATP-linked oxygen consumption rates (OCR) were also reduced in mutant cells, as well as the intracellular ATP levels. Further reinforcing an impairment of mitochondrial bioenergetics due to the Miro1 p.R272Q mutation, we also showed that forcing Miro1 p.R272Q fibroblasts to produce ATP via their mitochondria – by replacing glucose with galactose in their culture media – led to the same alterations observed in iPSC-derived neurons and MO (Appendix II and Manuscript III, Figure 3 panels A and D). Reduction of ATP production was also seen in flies expressing a LoF Miro1 mutation, as mentioned in the introduction (Lee et al., 2016). The essential role of mitochondrial calcium homeostasis in the maintenance of dopaminergic neurons electrophysiological properties is also confirmed by a recent study showing that mitochondrial calcium uptake via the MCU enhanced pyramidal neurons firing activity and metabolism (Groten and MacVicar, 2022).

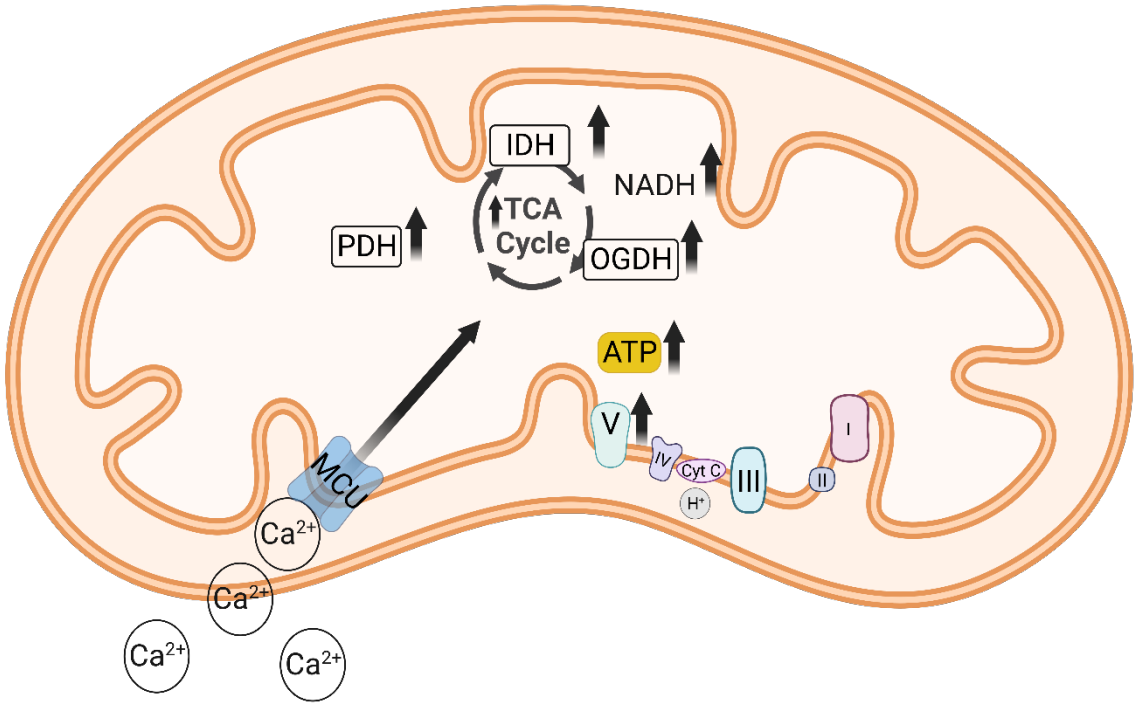

Figure 4 Upregulation of key TCA and cellular bioenergetics enzymes via entry of calcium into the mitochondria (Created with BioRender.com).

II.II Bioenergetics and calcium impairments are accompanied by disruption in ROS management, and metabolic reprogramming:

Impairment in mitochondrial bioenergetics and increased oxidative stress observed in Miro1 p.R272Q mutants are consistent with multiple studies presenting alteration of mitochondrial respiration and metabolism in iPSC-derived neurons from LRRK2 (Howlett et al., 2017; Schwab et al., 2017), SNCA (Barbuti et al., 2020), PINK1 (Bus et al., 2020), DJ-1 (Burbulla et al., 2017) and GBA mutation carriers (Tran et al., 2020). Similarly, impaired mitophagy/autophagy observed in our Miro1 models (Berenguer-Escuder et al., 2020a) – recapitulating a phenotype previously seen in PARKIN, LRRK2, SNCA and PINK1 mutants (Tran et al., 2020) – leads to the toxic accumulation of dysfunctional organelles and misfolded/aggregated proteins, including α-synuclein (see next section page 38: “II.III Miro1 p.R272Q and α-synuclein:”). Another parallel can be made with A30P and A53T α-synuclein iPSC-derived neurons, which also display higher ROS levels and mitochondrial bioenergetics impairments (Barbuti et al., 2020; Ryan et al., 2013)

By looking deeper into possible metabolic alterations linked to the Miro1 p.R272Q mutation, we found a significant decrease of intracellular nicotinamide adenine dinucleotides (NAD, NADH, NADP and NADPH), as well as pyruvate, and NAD and FAD in MO (Manuscript III, Figure 3, panel B, E, F).

Miro1 mutant iPSC-derived neurons seem to rely not only on pyruvate but also on glycine and glutamate (more abundantly taken up from the extracellular medium compared to isogenic controls) (Manuscript III, Figure 3, panel F). One could speculate that these are compensatory strategies mutant cells put into place to deal with impaired oxidative phosphorylation and increased ROS levels, providing additional substrates to the TCA cycle (i.e Ac-CoA and alpha-ketoglutarate, from pyruvate and glutamate, respectively) and to the scavenging machinery (i.e glutathione, from glutamate and glycine) (Figure 5). Additionally, the elevated release of lactate could indicate that pyruvate is also used to replenish NAD stocks, whose reaction byproduct is lactate.

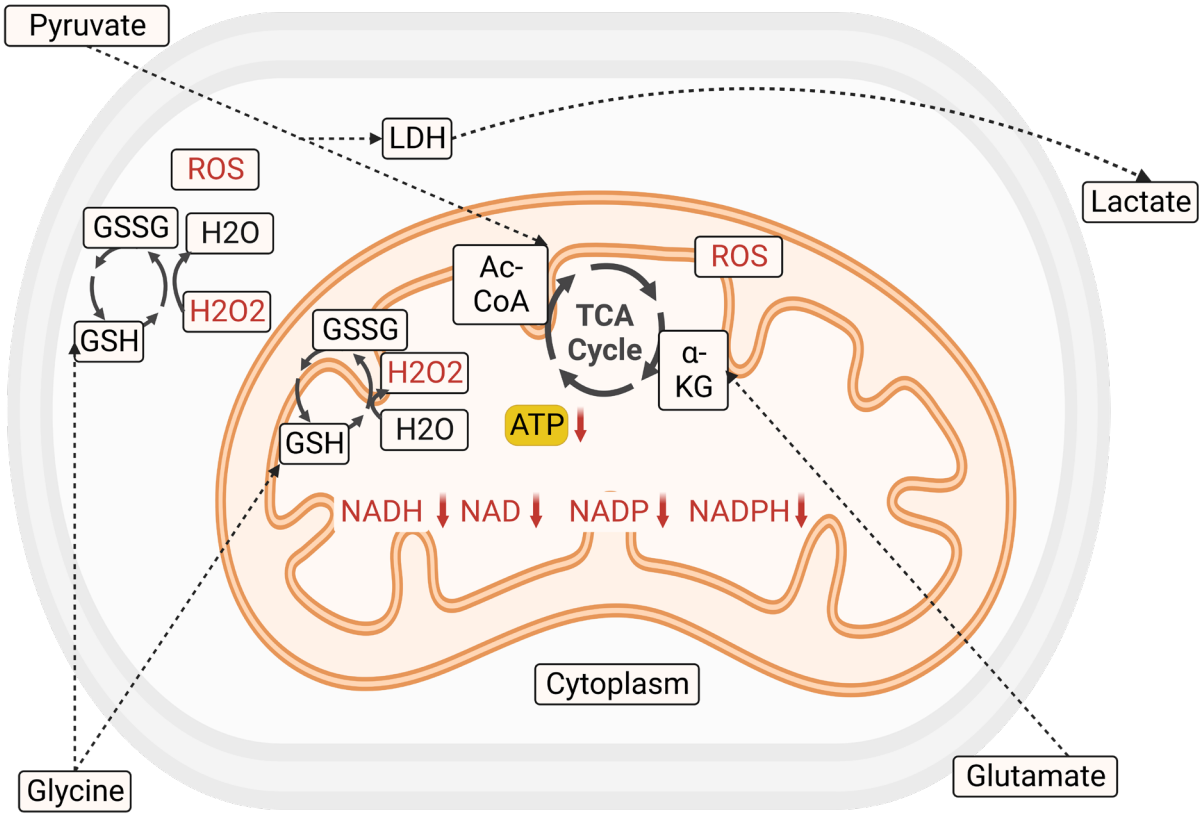

Figure 5 Increased uptake of pyruvate, glycine and glutamate in PD-R272Q Miro1 neurons. Illustration of possible use of the aforementioned metabolites, which could serve as fuel for the TCA cycle and antioxidant mechanisms. Created with BioRender.com.

It is worth noting that Miro1 mutations could also lead to increased ROS levels by disrupting peroxisomal function. Indeed, these organelles play a crucial role not only in controlling lipid metabolism, but also in counteracting oxidative stress (Jo et al., 2020). As a consequence, when peroxisomes are damaged, hydrogen peroxide (H2O2) is released into the cytosol thus increasing oxidative stress (Jo et al., 2020). Interestingly, Miro1 was found in peroxisomes of fibroblast cell lines (Costello et al., 2017), where it seems to be involved in their transport (Castro et al., 2018), and also affects their size, number and dynamics (Castro and Schrader, 2018, 2018; Covill-Cooke et al., 2020). Follow-up studies focusing on the biological significance of this Miro1-peroxisome interaction are needed, and would be especially interesting not only in neurons, but also in immune cells, as peroxisomes have been shown to be involved in innate immunity (Dixit et al., 2010).
Moreover, as peroxisomes are tightly associated with lipid metabolism, one could speculate that Miro1 could also play a role in metabolic diseases, including type 2 diabetes (T2D). Of note, an increased risk of developing PD has been reported for diabetic patients (Sabari et al., 2023). Sijun Yang and colleagues published several articles on the subject.

First, in 2015, they showed in rat pancreatic beta cells that increased calcium levels led to Miro1 detachment from the mitochondria, resulting in activation of the NLRP3 inflammasome, impaired insulin secretion, and apoptotic cell death under high-fat and high-glucose diet (Gao et al., 2015). They then found that Miro1 ablation in pancreatic islets using the widely used RIP-Cre mouse model led to obesity, a phenotype possibly linked to reduced mitophagy, increased ROS, over-activation of the integrated stress response and induction of NOD Like Receptor family pyrin domain containing 3 (NLRP3)(Chen et al., 2017; Li et al., 2020). More recently, using mouse models of T2D, differentiated adipocytes from a mouse embryonic fibroblast cell line, and primary hepatocytes, they revealed that macrophages derived-exosomes contained high levels of micro RNA-27-3p, which acted as a Miro1 repressor, resulting in mitophagy impairments, NLRP3 activation and insulin resistance in both their *in vivo* and *in vitro* models, while inactivation of micro RNA-27-3p prevented T2D in high fat diet fed mice (Li et al., 2023).
Mitochondrial dysfunction, together with endoplasmic reticulum stress and chronic inflammation, is a shared feature between PD and T2D (Santiago and Potashkin, 2013). In light of the fundamental role of Miro1 in regulating mitochondrial dynamics and quality control, understanding the molecular mechanisms underlying neurodegeneration in PD patients carrying Miro1 pathogenic variants could also shed light on common targets playing a role also in diabetes.

Another subject that deserves to be mentioned relates to the interaction between Miro1 and the inner mitochondrial membrane protein MIC60, which is a structural component of the mitochondrial contact site and cristae organizing complex (MICOS). Li and colleagues found that drosophila MIC60 gets oxidized by the ROS produced by the ETC and, in this form, its association with Miro1 is increased (L. Li et al., 2021a; Wasilewski and Chacinska, 2021a). More precisely, a conformational transition of dMIC60 triggered by oxidation of its cysteine residues promotes stable binding to dMiro resulting in its accumulation (Wasilewski and Chacinska, 2021a).

Interestingly, a significant reduction of cristae number was observed in iPSC-derived neurons from a healthy donor upon insertion of the Miro1 p.R272Q mutation (Schwarz et al., 2022a). Further investigations in patient-derived models are needed to assess whether mutations in Miro1 could influence the interaction with MIC60 and the activity of MICOS, finally impinging on mitochondrial cristae organization and ETC function.

II.III Miro1 p.R272Q and α-synuclein:

Strikingly, *SNCA* and *RHOT1* mRNAs were upregulated in Miro1 p.R272Q MO compared to both, age/gender-matched controls and isogenic gene-corrected lines (Manuscript III, Figure 4, panel A). Similar results were observed in Miro1 mutant 2D neurons lines (Manuscript III, Figure 4, panel C).
Here, we also demonstrated that upregulation of *SNCA* transcript effectively led to higher α-synuclein protein levels in comparison to the isogenic control (Manuscript III, Figure 4, panel D). This fits with the observation made by Shaltouki and colleagues, describing an upregulation of both α-synuclein and Miro1 in postmortem PD brains (Shaltouki et al., 2018a).

However, α-synuclein protein levels were not different when compared to the WT control (Manuscript III, Figure 4, panel C), which further strengthens the importance of genetic background in PD, as well as indicating that different individuals do not have the same thresholds at which α-synuclein has deleterious effects. For instance, iPSC-derived neurons from a PD patient carrying the heterozygous N370S mutation in the Glucosylceramidase beta 1 (GBA) gene did not display higher levels of α-synuclein when compared to a WT control line, while comparing them to an isogenic control revealed a significantly higher protein amount (Schöndorf et al., 2014).

A recent study using A53T *SNCA* iPSC-derived neurons revealed that mutant α-synuclein accumulated at mitochondrial membranes domains defined by the presence of cardiolipin (CL), a component of the inner mitochondrial membrane known to be exposed on the mitochondrial surface upon stress conditions (Choi et al., 2022). The interaction with CL accelerates A53T α-synuclein oligomerization and leads to increased ROS levels, creating a self-sustained loop in which oligomeric α-synuclein would exacerbate ROS production, while ROS themselves enhance the oligomerization of α-synuclein (Choi et al., 2022). While it was not demonstrated in the previous study, Scott D. Ryan and colleagues found that CL accumulates at the outer mitochondrial membrane, and that binding of WT α-synuclein to OMM CL containing vesicles is normally inhibited by LC3, and vice versa. However, in the case of mutant *SNCA* A53T, this inhibition of LC3-CL binding does not take place, and could explain the increased mitophagic rate in these iPSC-derived neurons (Ryan et al., 2018). These observations are in line with our findings in Miro1 p.R272Q neurons showing a positive correlation between α-synuclein accumulation, mitochondrial dysfunction and elevated ROS levels (Manuscript III). Analysis of CL (and α-synuclein) sub-mitochondrial localization in our Miro1 mutant models may provide a molecular link underlying the accumulation of α-synuclein we observed in Miro1 p.R272Q neurons.

Of note, another study showed that Lewy bodies present in the SNpc of PD brains contained dysfunctional mitochondria as well as pS129 α-synuclein, a phosphorylated form which favors oligomerization (Shahmoradian et al., 2019). The higher abundance of pS129 α-synuclein in the striatum of homozygous Miro1 p.R285Q mice also gives an additional information to helps decipher and strengthen the importance of Miro1 role in PD pathogenesis (Manuscript III, Figure 6, panel F). The presence of pS129 α-synuclein in SNCA A53T overexpressing mice was also demonstrated (Yoon et al., 2022). Moreover, intrastriatal injection of pS129 α-synuclein led to increased α-synuclein aggregation, SNpc neuron loss, striatal dopamine depletion and impaired motor coordination (Karampetsou et al., 2017). Using a mouse model overexpressing wt human α-synuclein, (which displays motor impairments but no loss of DA neurons) while reducing phosphorylation of pS129 α-synuclein improved motor performance (Lee et al., 2011a), providing a potential link between α-synuclein and the behavioral deficits we observed in female Miro1 p.R285Q mice.

While pS129 is the main post translational modification (PTM) found in dementia with Lewy bodies (Anderson et al., 2006), another PTM could be investigated in the context of Miro1 mutations, i.e nitrated tyrosine, as nitration has been previously linked with oxidative stress (Sonustun et al., 2022).

In particular, α-synuclein nY39 was found in pathological inclusions of brains from idiopathic PD patients, and it also favors protein oligomerization (Brembati et al., 2023; Sonustun et al., 2022). Lastly, cleaved form of α-synuclein would also be worth investigating. Indeed, our preliminary findings revealed the presence of a fast-migrating protein compatible with cleaved α-synuclein, the expression of which was significantly more abundant in the Miro1 p.R272Q Miro1 neurons compared to both isogenic and age/gender-matched controls (Appendix III, corresponding to Manuscript III, figure 4, panel D). Firstly, as we used an antibody targeting the α-synuclein NAC domain, using different antibodies targeting either the N- or the C-terminal of the protein would help to understand if this protein fragment corresponds to cleaved α-synuclein. Another way to confirm the presence of cleaved α-synuclein would be by investigating the activity of enzymes responsible for α-synuclein processing, such as calpain. Indeed, cleavage of α-synuclein by calpain results in β sheet conformation, as well as increased aggregation (Dufty et al., 2007). However, many truncated forms of α-synuclein exist, and several conflicting studies study their presence, structure, and impact (Sorrentino and Giasson, 2020), which prevents us to describe a precise mechanism without doing more in-depth analysis of which cleaved form of α-synuclein is present in the Miro1 p.R272Q mutant neurons. Interestingly, given the calcium issues seen in Miro1 p.R272Q mutant cells (Manuscript III, Figure 2, panel G), one could speculate that the increase in intracellular calcium could increase calpain activity, resulting in higher generation of this cleaved form, that is known to facilitate the formation of aggregated α-synuclein (Diepenbroek et al., 2014; Nath et al., 2011). More precisely regarding the results of these studies, mice overexpressing A30P α-synuclein and deficient for the calpain specific inhibitor calpastatin had higher calpain activity, accompanied by increased cleaved and aggregated α-synuclein. Additionally, primary neurons exposed to the PD associated herbicide Paraquat saw a shift in their monomer to tetramer ratio toward monomers, that were subsequently cleaved by calpain activation, resulting in the production of toxic oligomers (Nuber and Selkoe, 2023). Lastly, calcium binding to the NAC domain of α-synuclein leads to its exposure, promoting further the formation of aggregates (Han et al., 2018a). As all four Miro1 mutant lines share a disturbed calcium balance phenotype (Berenguer-Escuder et al., 2020a, 2019a; Grossmann et al., 2019a), it would be especially promising to also investigate α-synuclein and its different forms or post translational modifications within the p.R450C, p.T351A, and p.T610A lines. Additionally, one could also investigate potential calcium management defects, as well as α-synuclein cleavage/aggregation in the Miro1 p.R285Q mice.

Interestingly, α-synuclein also interferes with autophagosome formation, maturation, autophagosome-lysosome fusion, as well as lysosomal function, leading to its own accumulation within malfunctioning lysosomes, creating a self-sustaining pathological feedback loop (Leandrou et al., 2019a).

This is in line with our previous findings comparing Miro1 p.R272Q with Ctrl DA neurons, which revealed reduced baseline levels of Rab9a GTPase, as well as enlarged lysosomes, which suggest possible impairments of lysosomal maturation (Berenguer-Escuder et al., 2020a). While the exact link between Miro1 and lysosomes has not been deciphered yet, one can speculate that Miro1 being a regulatory subunit of Mitochondria-ER contact sites, it would also be involved in mitochondria lysosomes contact sites regulation, thus affection lysosomal function.

II.IV Miro1 and intercellular communication

The ability of Miro1 to interact both with components of the cytoskeleton and with mitochondrial-derived vesicles (König et al., 2021) suggests a potential role in regulating intercellular communication via tunneling nanotubes (TNTs) and exosomes (EVs), respectively. Miro1 is known as a regulator of intercellular mitochondrial donation, as its knockdown impaired mitochondrial transfer (Ahmad et al., 2014). This was also seen in a cardiomyopathy model, where high levels of Miro1 increased mitochondrial transfer, as well as preserving mitochondrial respiration and ATP production in mouse cardiomyocites (Zhang et al., 2016). Tseng and colleagues recently demonstrated that oxidative stress in neurons triggers inflammation and increases Miro1 expression, which then boosts mitochondrial motility from mesenchymal stem cells to neurons, improving neuronal survival and mitochondrial respiration (Tseng et al., 2021). Lastly, overexpressing Miro1 in mesenchymal stem cells was shown to promote TNTs formation and mitochondrial transfer in astrocytes (Babenko et al., 2018). Additionally, co-culture of primary cortical neurons and astrocytes from Long Evans rats along treatment with cisplatin, an anti-cancer chemotherapy, with neurotoxic side effects, revealed that treated neurons received healthy mitochondria from astrocytes, improving their survival as well as MMP, bioenergetics, and calcium dynamics (English et al., 2020). Accordingly, siRNA mediated knockdown on Miro1 in astrocytes significantly decreased mitochondrial transfer from astrocytes to neurons, preventing rescue of calcium, MMP, and bioenergetics related, cisplatin-induced defects, giving another clue towards the understanding and implications of Miro1 in mitochondrial transfer and maintenance of neuronal health (English et al., 2020). Moreover, this also hints at the potentially beneficial effect of Miro1 modulation in other contexts than neurodegeneration, as in this case, it could help counteract neurotoxic side effect of chemotherapy.

Of particular interest for our study, not only mitochondria can be exchanged through TNTs, but also α-synuclein, as demonstrated in microglia (Scheiblich et al., 2021). Existing literature has already reported the intercellular transfer of α-synuclein through both TNTs and EVs, a mechanism likely implicated in neuroinflammation and spreading of PD pathology (Emmanouilidou et al., 2010). Interestingly, our transcriptome data obtained in Miro1 p.R272Q neurons revealed not only the significant α-synuclein upregulation already discussed above (II.III, Manuscript III, Figure 4, and Appendix III) but also a clear signature related to secretory and exocytic vesicles, with most genes found to be significantly upregulated (Manuscript III, Figure 1, Panel F, and data not shown). Confirming the upregulation of exosome-related genes at both RNA and protein level and measuring α-synuclein protein levels within Miro1 p.R272Q-derived exosomes is currently under investigation. Mechanistically, increased exosome secretion could be linked to the impairment of mitophagy we observed in 2D neurons from the Miro1 p.R272Q patient (Berenguer-Escuder et al., 2020a). In fact, it has been previously shown that downregulation of PARKIN, which is a major effector of the mitophagic process, significantly increased EV release (Song et al., 2016).

II.V Miro1 and dopaminergic loss

As the characteristic feature of PD is death of dopaminergic neurons, we finally investigated tyrosine hydroxylase (TH) expression in Miro1 mutant MO. Strikingly, not only TH levels were significantly reduced, but also DA neurons fragmentation index and dopaminergic complexity (Manuscript III, Figure 5, panels A and B), considered early signs of neurodegeneration and already observed in other PD models such as A30P SNCA iPSC-derived neurons (Barbuti et al., 2020), were severely impaired. Terminal deoxynucleotidyl transferase dUTP nick end labeling (TUNEL) assay in 20 days (data not shown) and 30 days old neurons indicated an age dependent dopaminergic loss, with neuronal apoptosis being significantly detectable from 30 days onward (Manuscript III, Figure 5, panel E). This also correlates with the dopaminergic neuron loss in the Miro1 mutant KI mice (Manuscript III, Figure 6, panel D).

II.VI Pathological retention of Miro1 p.R272Q in native fibroblasts:

Wang and colleagues reported in PD patients with α-synuclein or LRKK2 mutations, as well as in sporadic PD, that Miro1 removal from the mitochondria and its degradation were significantly delayed compared to controls, while reducing Miro1 levels alleviated symptoms of neurodegeneration (Hsieh et al., 2016a, 2019a; Shaltouki et al., 2018a).

It is worth noting that this Miro1 retention phenotype was always observed in the context of wild-type Miro1, therefore we still need to elucidate how distinct PD-associated variants in Miro1 behave in regard to this retention phenotype. To this end, we first analyzed Miro1 protein levels in the mitochondrial fraction of native skin fibroblasts isolated from PD patients carrying either the p.R272Q or the p.R450C mutation in Miro1 (Appendix number IV). Strikingly, upon mitophagy induction by CCCP treatment, the two cell lines displayed a very different Miro1 degradation pattern, with a robust 80% reduction of Miro1 levels in the p.R450C carrier (similar to those previously reported for healthy cells) and a slight 30% decrease in the p.R272Q mutant fibroblasts (Appendix number IV). Given the different position of the mutation one could speculate that the Miro1 retention phenotype is heavily dependent on calcium, which could explain why the fibroblasts with the Miro1 p.R450C mutation do not display it. However, both EF hands and GTPase domain of Miro1 are in close proximity (Klosowiak et al., 2013), which led us to think that both domains played a significant role in Miro1 calcium related functions (Grossmann et al., 2019a). Additionally, in light of the Miro1 retention phenotype being only present in the p.R272Q mutation carrier, although both mutation impacted calcium response (Grossmann et al., 2019a), the p.R450C mutation within Miro1 does not seem to disrupt calcium sensing to the point of preventing Miro1 detachment from the mitochondria. Investigating the Miro1 retention phenotype in the fibroblasts with the p.T351A and p.T610A would help in understanding the reason underlying this PD specific Miro1 degradation defect. At first glance, since these two other Miro1 mutation also disrupt calcium homeostasis in fibroblasts (Berenguer-Escuder et al., 2020a), we could expect to see retention of Miro1, especially for the p.T351A mutant fibroblasts, as the mutation is located in one of Miro1 EF hand, although it is not the same as for the p.R272Q mutation. It would be more difficult to predict whether the p.T610A mutation, located in Miro1 transmembrane domain, would lead to increased Miro1 retention, as *in silico* prediction of the variant impact were contradictory, predicting a stabilizing or destabilizing effect depending on the analysis approach used (Grossmann et al., 2019a). We also extended the analysis to primary skin fibroblasts from healthy controls and iPD patients previously stratified according to different degree of mitochondrial risk as defined by polygenic risk scores for common variants in nuclear-encoded mitochondrial genes regulating oxidative phosphorylation (OXPHOS-PRS, Appendix V) (Arena et al., 2023). Different from what we expected based on existing literature (Hsieh et al., 2019a), the Miro1 retention phenotype was very fluctuating across individuals, even among cell lines belonging to the same group (Appendix V). Precisely, individuals from the control group displayed a reduction of Miro1 after CCCP treatment that went from 80%, clear degradation, while another control individual only displayed a degradation of Miro1 of 30-40% (ctrl4). On the other hand, iPD fibroblasts displayed a negligible, 10% (iPD1) to 50% reduction of Miro1 levels after CCCP

treatment. Additional investigation, possibly adopting the same technical procedure used by Xinnan Wang's group, is needed before drawing definitive conclusions. Of note, pathological Miro1 retention has been also observed in prodromal PD, including individuals with hyposmia or with rapid eye movement sleep behavior disorder (RBD) (Nguyen et al., 2021a). Unfortunately, only 6 individuals with hyposmia or RBD have been assessed in this study, thus requiring validation experiments in larger cohorts.

Our preliminary observations in Miro1 p.R272Q fibroblasts (Appendix V) seem to confirm the Miro1 retention phenotype for this mutant, which also fits with the impaired mitophagy observed in iPSC-derived MO. In the future, the same analyses could be extended to the Miro1 R285Q KI mouse model, to investigate the potential usage of Miro1 as a PD biomarker. In this regard, the Acurex Biosciences company based in California recently suggested the possibility to assess Miro1 levels also in PBMCs ("Acurex Biosciences to Present Early Clinical Results Supporting its Novel Parkinson's Disease Biomarkers at a Michael J. Fox Foundation Biomarkers Workshop," 2023), which would make Miro1 a reliable blood-based biomarker to test novel PD therapies, as Hsieh and colleagues demonstrated that Miro1 removal alleviated neurodegeneration (Hsieh et al., 2019a). Therefore, one could test the effectiveness of potential PD drugs by measuring Miro1 removal and degradation following addition of therapeutic candidates.
Finally, Bharat and colleagues also demonstrated that Miro1 degradation was disrupted in fibroblasts from patients with mutations in the microtubule associate protein Tau (MAPT) gene (Bharat et al., 2021). This extends the role of Miro1 towards other neurodegenerative diseases, tauopathies, such as Alzheimer's disease, progressive supranuclear palsy, frontal temporal lobar neurodegeneration, and parkinsonism (Bharat et al., 2021).

II.VII Miro1 variant as a PD model *in vivo*:

The last but not least part of this project aimed at exploring the consequences of Miro1 deficiency *in vivo*. To this end, we generated a Miro1 R285Q KI mouse model, which is the ortholog of the human p.R272Q Miro1 mutation studied *in vitro* (Manuscript III; Figure 6, panel A). Genetic animal models of PD are known to rarely recapitulate the disease phenotypes clinician see in humans (Blesa et al., 2016b). Strikingly, the Miro1 R285Q mouse displayed a significant decrease of dopaminergic neurons in the SNpc of 15 months old animals (Manuscript III; Figure 6, panel D), increased phospho-S129 α-synuclein (Manuscript III; Figure 6, panel E) as well as impaired motor learning (Manuscript III; Figure 6, panels H and E), which are major hallmarks of PD in human patients (Paul M. A. Antony et al., 2013).

Interestingly, this also brings our model closer to an already published study (mentioned in the introduction), in which expression of LoF mutations in the EF hands of dMiro1 led to neuronal death (Wang and Schwarz, 2009).

However, we did not see a clear reduction of dopamine levels (Manuscript III; Supplementary Figure 7, panel F), likely due to the low precision of our method; in fact, we used a slice of striatum instead of proceeding with a microdissection approach. Alternatively, this could also be explained by possible compensatory mechanisms from remaining neurons overproducing dopamine (Zigmond et al., 2002).

The presence of mutant Miro1 affected the mouse ability to learn new motor tasks, which is indicative of impaired anterograde procedural memory. Interestingly, this phenotype was observed in both heterozygous (R285Q/+) and homozygous (R285Q/R285Q) 15 months old mice, but it reached statistical significance only in females (Manuscript III; Figure 6, panel H). One should first keep in mind that the mutation was found at the heterozygous state in the PD patient, and more importantly, that it was found in a woman (Grossmann et al., 2019a). Therefore, the potentially stronger effect seen in female mice could be further investigated in regard to sex specific gene expression or hormonal regulation, even though in human, PD incidence is higher in men (Kalia and Lang, 2015). Recently, using a rat model of early, pre-motor stage of PD, Conner and colleagues found that lower androgen levels protected male rats against memory-related impairments caused by 6-OHDA lesions (Conner et al., 2020), which does not correspond to our study, comprised mostly of female mice. On the other hand, lower levels of autophagy are generally found in women, and could contribute to the higher prevalence of Alzheimer's disease in women (Congdon, 2018). Although we did not investigate *in vivo* consequences of Miro1 variants on autophagy, we previously published that autophagy flux (as well as mitophagy) was blocked in Miro1 p.R272Q iPSC-derived neurons derived from the female patient (Berenguer-Escuder et al., 2020a).

Regarding the presence of statistical difference only in female mice for the Rotarod test (Manuscript III; Figure 6, panel H and I), it is important to note that weight has a significant impact on rotarod performance, and that the weight of male mice could interfere with their performance. Moreover, the low number of male mice available for assessment of neurodegeneration in the SNpc might also explain the absence of differences (Manuscript III; Figure 6, panel D and Supplementary Figure 7, panel G). Relevant for neurodegeneration in PD, impaired motor learning was previously reported in mice where expression of the aldehyde deshydrogenase 1 (ALDH1A1) gene – encoding a key enzyme in dopamine metabolism (Cai et al., 2014; Liu et al., 2014; Marchitti et al., 2007) – was specifically ablated in nigrostriatal dopaminergic neurons (nDANs) (Wu et al., 2019).

Of note, ALDH1A1+ nDAN-ablated mice performed at a similar level than WT mice on the first trial, but then failed to improve their performance during the course of rotarod test, suggesting an impaired acquisition of skilled movements(Wu et al., 2019). Similarly, injection of antisense oligonucleotides targeting synaptotagmin, a regulator of calcium-dependent exocytosis and endocytosis, disrupted dopamine release in the rat striatum and prevented the retainment of motor skills previously learned (Akita et al., 2006).
Conversely, Miro1 R285Q mice perform worse than controls on the first trial (Manuscript III; Figure 6, panel H), but they are able to improve their performance with training (Manuscript III; Figure 6, panel I). This phenotype is clearly indicative of dysfunctional anterograde procedural memory, which controls the learning of new motor tasks. Impaired performance during the first rotarod trial, but not during following ones was also seen in transgenic ataxia mice (Boy et al., 2009a). Similar observations have been made on humans by Frith, whose cohort of PD patients displayed worse performance than healthy people in learning new motor tasks, but motor skills improved over time and trials repetition (Frith et al., 1986a). Later on, many other studies, compiled in a meta-analysis, confirmed the impairment of implicit learning in PD patients (Richard J. Siegert et al., 2006).

In summary, our study asserts the importance of rare Miro1 variants as drivers for neurodegeneration in PD. Future studies could expand on the functional impairments we mainly demonstrated *in vitro* (e.g *in vivo* assessment of calcium homeostasis and electrophysiology), thus paving the way for therapeutic interventions based on e.g calcium channels targeted drugs or compounds promoting Miro1 degradation to counteract its pathological retention. Moreover, Miro1 implication in other disease, or disease-relevant cell types appears as a promising area to study in the near future.

III Materials and methods

iPSCs generation, culture, and characterization: See Manuscripts I and II

Neuronal and organoids culture and experiments, mouse model generation and characterization: See Manuscript III

For Appendix III, methods can be found in Manuscript III, in the part “Dopaminergic neurons Western blotting”.

Additional methods corresponding to Appendices II, IV, and V

Fibroblasts culture:

Dermal skin biopsies were obtained from the lower back arm of PD patients and controls. Prior to the skin biopsy, informed written consent was obtained from each patient enrolled in the study. The informed consent was approved by the Ethics Committee of the Medical Faculty and the University Hospital Tübingen, Germany and the Research Ethics Board of the University of Lübeck, Germany. Additionally, dermal fibroblasts from sporadic PD patients and healthy controls were collected in Luxembourg as a part of the NCER-PD study. Once thawed, all fibroblasts were grown in Dulbecco’s modified Eagle’s medium (DMEM) containing 4.5g/L D-glucose, 2mM L-Glutamine, 10% FBS, 1% Pen-Strep (Thermo Fischer Scientific, Braunschweig, Germany), and maintained in a 37°C, 5% CO_2 incubator with humidified atmosphere. DMEM medium was changed every two days. Additionally, once the fibroblasts have reached at least 80% confluency, as confirmed by microscopy, a cell splitting protocol was initiated. Briefly, cell culture medium was aspirated from the dish using a sterile autoclaved glass pipette followed by two subsequent washes in phosphate buffered saline (PBS). 1ml of trypsin 0.25% was added to each dish followed by incubation at 37 °C during 5 minutes. Cells were removed from the incubator and the dish was gently smacked until cells were no longer adherent to the wall. Trypsin was diluted at least 4-5 times by adding warm complete medium. Cells were plated in new dishes containing warm complete medium. Cells were regularly tested for mycoplasma contamination using the Plasmo Test TM detection kit.

Carbonyl cyanide *m*-chlorophenyl hydrazone (CCCP) treatment:

To trigger mitochondrial depolarization, fibroblasts were treated overnight with CCCP, at a concentration of 40 µM. Dimethyl sulfoxide (DMSO) was used as vehicle. After overnight treatment, the drug-containing medium was aspirated and DMSO- and CCCP-treated cells were washed in phosphate-buffered saline (PBS) twice, followed by a 5-minutes incubation with trypsin 0.25%. Cells were resuspended in medium (DMEM 10% FBS 1% P/S) and centrifuged at 300g during 3 minutes. Cell pellets were resuspended in 1ml PBS and centrifuged again during 5 minutes at 300g. PBS-containing supernatant was aspirated, and cell pellets were stored frozen at -80 °C.

Protein extraction and Western blotting:

Fibroblasts were lysed in 1% sodium dodecylsulfate (SDS) with complete protease inhibitor (Roche, Mannheim, Germany) and then boiled at 95°C for 5 minutes. Cells lysates were then sonicated at 4°C (5 cycles, 30 seconds on, 30 seconds off). Proteins were quantified using the Pierce™ BCA Protein assay kit (Thermo Scientific). Sodium dodecyl sulfate polyacrylamide gel electrophoresis (SDS-PAGE) was performed using 4-12% Bis-Tris 10-well precast gels. Gels were transferred onto nitrocellulose membranes, followed by overnight incubation with 5% bovine serum albumin (BSA) blocking solution (in TBS-T) to prevent non-specific binding of the antibodies. Western Blot analysis was completed using antibodies against Miro1 (E117773) (Sigma Aldrich, Munich, Germany, ref. no. HPA010687, rabbit secondary antibody) and β-actin (8H10D10) (ref. no. 3700S, Cell Signaling, mouse secondary antibody) that served as a loading control. Protein bands were detected by applying ECL™ Prime Western Blotting (Amersham) detection reagent to the membranes, and images were acquired via the STELLA imaging system (raytest Isotopenmessgeräte GmBh, Straubenhardt, Germany). Western Blot membranes were visually analysed by Image J software (Wayne Rasband; National Institute of Health, USA) and further assessed by densitometry.

Mitochondria isolation:

Isolation of functional mitochondria from CCCP- and DMSO-treated fibroblasts was performed as previously described (Frezza et al., 2007; Moore, 2020). Briefly, cells were resuspended in mitochondria isolation buffer (MIB, 0.1M Tris-MOPS, 0.1M EGTA/Tris, 1M sucrose, sterile water) and then lysed using a motor-driven homogenizer operating at 1600 rpm (20 strokes). An aliquot of the resulting extract was used as whole cell lysate. The remaining lysate was centrifuged at 600g during 10 minutes at 4°C to remove any contaminants coming from the nuclear fraction and then centrifuged again at 10000g for 10 minutes at 4°C to pellet mitochondria.

The mitochondrial fraction was washed once in MIB, and finally resuspended in 1% SDS Lysis buffer and boiled at 95°C for 5 minutes. The supernatant resulting from the high-speed centrifugation, containing cytosoluble proteins, was centrifuged again at 10000g for 10 minutes at 4°C to remove potential contamination from the mitochondrial fraction. All fractions were stored at -80°C until SDS-PAGE protocol initiation. Samples always remained on ice during the entire manipulation. The resulting fractions (cytosolic, mitochondrial) were examined by Western Blotting. The mitochondrial markers used were rabbit polyclonal antibody against *RHOT1*/Miro1 (E117773) (Sigma Aldrich, Munich, Germany, ref. no. HPA010687, rabbit secondary antibody), mouse polyclonal antibody against voltage-dependent anion channel 1 (VDAC1) (N152B/23) (Millipore, ref. no. MABN504, mouse secondary antibody), rabbit polyclonal antibody against Heat Shock Protein 60 (Hsp60) (D307) (Cell Signaling, ref. no. 4870S, rabbit secondary antibody) and rabbit polyclonal antibody against Translocase Of Outer Mitochondrial Membrane 20 (Tom20) (Santa Cruz Biotechnology, ref. no. FL-145, rabbit secondary antibody). Mouse polyclonal antibody against β-actin (8H10D10) (Cell Signaling, ref. no. 3700S) served as cytosolic protein marker.

Analysis of oxygen consumption rate in fibroblasts cultivated either in glucose- or galactose-based medium:

The experiment was performed as described in Manuscript III for iPSC-derived neurons, except that two different media were used, one containing glucose, the other galactose at 25mM concentration, and that FCCP concentration was 2μM.

IV Results

IV.I Manuscript I

Generation of two induced pluripotent stem cell lines and the corresponding isogenic controls from Parkinson's disease patients carrying the heterozygous mutations c.1290A > G (p.T351A) or c.2067A > G (p.T610A) in the *RHOT1* gene encoding Miro1

Chemla et al. 2023.

Status:

Published in Stem Cell Research
25.03.2023

Description of contribution:
I wrote the manuscript, prepared the figures, and performed the experiments on iPSC lines to complete the quality control performed by the Stem Cell Medicine Gene Editing Facility at the Murdoch Children's Research Institute, Australia. I made the experiments for panels A, F and G.

Our team previously provided a comprehensive functional characterization of fibroblasts from PD patients carrying the Miro1 mutations p.T351A and p.T610A, located in the C-terminal EF-hand and close to the transmembrane domain, respectively (Berenguer-Escuder et al., 2019a). In brief, cells from the aforementioned Miro1 mutant patients showed increased sensitivity to calcium stress, lower number of MERCs containing Miro1, and impaired LC3-dependent autophagy with compensation by Rab9-dependent autophagy (Berenguer-Escuder et al., 2019a). However, to this date, these mutations have not been studied in a cell type more relevant to PD. In this paper, we described the generation of iPSCs from the p.T351A and p.T610A Miro1 mutant fibroblasts. Episomal reprogramming was done on the fibroblasts to generate iPSCs, followed by correction of the mutations using CRISPR/Cas9-mediated gene editing. The resulting iPSCs lost the reprogramming vectors as expected, properly expressed stemness factors, and could differentiate into the three germ layers.

The generation of this model will allow future researchers to answer several questions:

In another Miro1 mutant line, i.e the cells carrying the p.R272Q mutation, not all phenotypes observed in fibroblasts have been also confirmed in iPSC-derived neurons. p.R272Q fibroblasts had increased mitophagy, alternative autophagy, and reduced MERCs amount, while neurons had opposite phenotypes (Berenguer-Escuder et al., 2020a; Grossmann et al., 2019a). However, calcium buffering and response to calcium stress were impaired both in fibroblasts and iPSC-derived neurons (Berenguer-Escuder et al., 2020a; Grossmann et al., 2019a). First, differentiating iPSCs into midbrain dopaminergic neurons will indicate whether phenotypes found in fibroblasts are the same in neurons. Moreover, investigating the impact of a Miro1 mutation located, like the p.R272Q, in an EF-hand (p.T351A), could provide insight on the role of the first EF-hand (p.R272Q) of Miro1 compared to the second one (p.T351A), or if the two mutations have similar impact on PD pathogenesis. Regarding the p.T610A mutation, its location within the transmembrane domain is also intriguing, as it could disrupt Miro1 anchoring onto the mitochondrial membrane. Investigating how a possible disruption of Miro1 anchoring to the outer mitochondrial membrane would relate to PD and whether it prevents its proper degradation is in line with the pathological stabilization of Miro1 seen in α-synuclein, LRRK2, and sporadic PD patients (Hsieh et al., 2016a, 2019a; Shaltouki et al., 2018a).

Stem Cell Research 69 (2023) 103085

Contents lists available at ScienceDirect

Stem Cell Research

journal homepage: www.elsevier.com/locate/scr

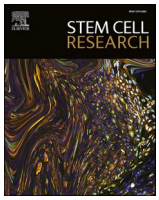

Lab Resource: Genetically-Modified Multiple Cell Lines

Generation of two induced pluripotent stem cell lines and the corresponding isogenic controls from Parkinson's disease patients carrying the heterozygous mutations c.1290A > G (p.T351A) or c.2067A > G (p.T610A) in the RHOT1 gene encoding Miro1

Axel Chemla [a], Giuseppe Arena [a,*], Claudia Saraiva [b], Clara Berenguer-Escuder [a], Dajana Grossmann [a,c], Anne Grünewald [d,e], Christine Klein [d], Philip Seibler [d], Jens C. Schwamborn [b], Rejko Krüger [a,f,g,*]

[a] Translational Neuroscience, Luxembourg Centre for Systems Biomedicine (LCSB), University of Luxembourg, Luxembourg
[b] Developmental and Cellular Biology, Luxembourg Centre for Systems Biomedicine (LCSB), University of Luxembourg, Luxembourg
[c] Translational Neurodegeneration Section "Albrecht-Kossel", Department of Neurology, University Medical Center Rostock, University of Rostock, Rostock, Germany
[d] Institute of Neurogenetics, University of Lübeck, Lübeck, Germany
[e] Molecular and Functional Neurobiology, Luxembourg Centre for Systems Biomedicine (LCSB), University of Luxembourg, Luxembourg
[f] Transversal Translational Medicine, Luxembourg Institute of Health (LIH), Luxembourg
[g] Parkinson Research Clinic, Centre Hospitalier de Luxembourg (CHL), Luxembourg

A B S T R A C T

Primary skin fibroblasts from two Parkinson's disease (PD) patients carrying distinct heterozygous mutations in the *RHOT1* gene encoding Miro1, namely c.1290A > G (Miro1 p.T351A) and c.2067A > G (Miro1 p.T610A), were converted into induced pluripotent stem cells (iPSCs) by episomal reprogramming. The corresponding isogenic gene-corrected lines have been generated using CRISPR/Cas9 technology. Here, we provide a comprehensive characterization and quality assurance of both isogenic pairs, which will be used to study Miro1-related molecular mechanisms underlying neurodegeneration in iPSC-derived neuronal models (e.g., midbrain dopaminergic neurons and astrocytes).

1. Resource table

Unique stem cell line identifier	1. LCSBi011A 2. LCSBi011A-1 3. LCSBi012A 4. LCSB012A-1
Alternative name(s) of stem cell line	1. RHOT1_T351A_clone1_PD 2. RHOT1_T351A_clone25.2_IsogenicControl 3. RHOT1_T610A_clone6_PD 4. RHOT1_T610A_clone62.19.37_IsogenicControl
Institution	*Luxembourg Centre for Systems Biomedicine (LCSB), University of Luxembourg, Luxembourg*
Contact information of the reported cell line distributor	*Prof. Rejko Krüger; rejko.krueger@uni.lu*
Type of cell line	*iPSCs*
Origin	*Human*

(*continued on next column*)

(*continued*)

Additional origin info *(applicable for human ESC or iPSC)*	1. Age at biopsy: 65 years *Sex: male Ethnicity: European White* 2. As in 1. 3. Age at biopsy: 45 years *Sex: male Ethnicity: European White* 4. As in 3.
Cell Source	*Dermal fibroblasts*
Method of reprogramming	*Electroporation of episomal reprogramming vectors*
Clonality	*Clonal*
Evidence of the reprogramming transgene loss (including genomic copy if applicable)	*Loss of reprogramming plasmids was confirmed by PCR*
The cell culture system used	*iPSCs were maintained under feeder-free conditions, on Matrigel-coated wells, in presence of Essential 8™ (E8) medium*

(*continued on next page*)

* Corresponding authors.
E-mail addresses: giuseppe.arena@uni.lu (G. Arena), Rejko.Krueger@lih.lu (R. Krüger).

https://doi.org/10.1016/j.scr.2023.103085
Received 27 February 2023; Received in revised form 21 March 2023; Accepted 24 March 2023
Available online 25 March 2023

(*continued*)

Type of the Genetic Modification	*Spontaneous point mutation (LCSBi011A and LCSBi012A)* *Gene correction (LCSBi011A-1 and LCSB012A-1)*
Associated disease	*Parkinson disease (OMIM #168600)*
Gene/locus	*RHOT1 (17q11.2), Gene ID: 55288, NM_001033568.2*
Method of modification/ user-customisable nuclease (UCN) used, the resource used for design optimisation	*CRISPR/Cas9*
User-customisable nuclease (UCN) delivery method	*Electroporation*
All double-stranded DNA genetic material molecules introduced into the cells	*Episomal reprogramming vectors, sgRNA plasmids, repair template plasmid*
Analysis of the nuclease-targeted allele status	*Sanger Sequencing of the targeted alleles*
Method of the off-target nuclease activity prediction and surveillance	*The "CRISPR-Cas9 guide RNA design checker" tool (from Integrated DNA Technology, Inc.) was used to assess on– and off-target potential of selected* guide RNA *sequences*
Descriptive name of the transgene	*N/A*
Eukaryotic selective agent resistance cassettes (including inducible, gene/cell type-specific)	*N/A*
Inducible/constitutive expression system details	*N/A*
Date archived/stock creation date	*01.12.2022*
Cell line repository/bank	*https://hpscreg.eu/cell-line/LCSBi011-A* *https://hpscreg.eu/cell-line/LCSBi011-A-1* *https://hpscreg.eu/cell-line/LCSBi012-A* *https://hpscreg.eu/cell-line/LCSBi012-A-1*
Ethical/GMO work approvals	*The Luxembourgish National Research Ethics Committee (CNER) provided ethical approval for the following project: "Disease modelling of Parkinson's disease using patient-derived fibroblasts and induced pluripotent stem cells" (DiMo-PD, CNER #201411/05).*
Addgene/public access repository recombinant DNA sources' disclaimers (if applicable)	*pEP4 E02S ET2K (Addgene #20927)* *pEP4 E02S EN2L (Addgene #20922)* *pEP4 E02S EM2K (Addgene #20923)* *pSimple-miR302/367 (Addgene #98748)* *pSMART-sgRNA (Sp) plasmid (Addgene #80427)* *pSMART HC Kan (Addgene #178883)*

2. Resource utility

We recently provided evidence supporting the involvement of heterozygous mutations in the *RHOT1* gene encoding Miro1 in PD pathogenesis (Berenguer-Escuder et al., 2019, 2020; Grossmann et al., 2019; Grossmann et al., 2020). Here, we reported generation of iPSC lines from PD patients carrying two distinct *RHOT1* mutations that will be used, together with the corresponding gene-corrected lines, for phenotypic analysis and *in vitro* disease modeling.

3. Resource details

To generate the parental iPSC lines (i.e., *LCSBi011A* and *LCSBi012A*), primary skin fibroblasts were obtained from two PD patients carrying the *RHOT1* heterozygous mutations c.1290A > G (Miro1 p.T351A) and c.2067A > G (Miro1 p.T610A), which are located in the second EF-hand (EF2) and in the transmembrane (TMD) protein domain, respectively (Berenguer-Escuder et al., 2019). Clonal iPSC populations were derived following electroporation of episomal reprogramming vectors into patient fibroblasts. Individual iPSC colonies (clone 1 for Miro1 p.T351A, clone 6 for Miro1 p.T610A) were identified by morphology, isolated and expanded (Fig. 1A, left panels). Loss of reprogramming vectors was confirmed by PCR analysis using primers specific to the AmpR gene (Fig. 1B). Isogenic controls (i.e., *LCSBi011A-1 and LCSBi012A-1)* were generated by introducing gene editing factors into the aforementioned iPSC clones. Briefly, iPSCs were co-transfected with the specific sgRNA (Table 2), the Cas9 mRNA and a repair template comprising homology arms flanking the target site (Table 2, Supplementary Figs. 1 and 2). Gene-edited iPSCs were identified by PCR using allele-specific primers flanking the intended correction (Fig. 1C). The resulting amplicons were Sanger sequenced to confirm the successful gene editing and the absence of indel mutations. For the Miro1 p.T351A gene correction, a single iPSC colony (clone 25) showing a substantial proportion of edited cells was subjected to subcloning to obtain a pure culture of gene-corrected cells. Individual colonies were again isolated, expanded and screened by PCR and Sanger sequencing. One subclone (clone 25.2) showed the complete loss of the c.1290A > G mutation and gain of the synonymous changes (Fig. 1D, left panel). For the gene editing of Miro1 p.T610A, the sequencing analysis initially revealed not only the successful correction of the c.2067A > G mutation, but also the presence of an indel mutation in the wild-type allele of all clones screened, namely a 1 bp insertion (T) at the expected Cas9 cutting site. We therefore selected a single c.2067A > G gene-corrected colony (clone 62) and performed a second round of gene editing to correct the insertion in the second allele. The transfection was realized as described above, but using an alternative sgRNA that specifically recognizes the insertion mutation (Table 2). A colony (clone 62.19) containing a significant proportion of corrected iPSCs (identified by PCR) was further selected for subcloning to attain a pure population of gene-edited cells. Individual colonies were again isolated, expanded and screened. One subclone (clone 62.19.37) showed complete loss of both, the Miro1 c.2067A > G mutation and the 1 bp insertion, along with homozygous gain of the synonymous changes (Fig. 1D, right panel). Miro1 T351A_25.2 and T610A_62.19.37 corrected clones both displayed a typical iPSC colony morphology (Fig. 1A, right panels). Patient-derived and gene-edited clones were then expanded and subjected to further characterization. They all expressed different stemness markers, as demonstrated by both FACS analysis (Fig. 1E) and immunofluorescence (Fig. 1F). Pluripotency capacity was also confirmed by their ability to differentiate into the three germ layers (Fig. 1G). SNP array analysis excluded the presence of aneuploidies in all clones (Supplementary Fig. 3). Genetic identity between patient-derived iPSCs and the corresponding gene-edited clones was confirmed by SNPduo comparative assessment (Supplementary Fig. 4). Finally, all clones were free from mycoplasma contamination (Supplementary Fig. 5).

4. Materials and methods

4.1. Cell culture and reprogramming

PD patient-derived fibroblasts were grown in DMEM medium containing 4.5 g/L D-glucose, 10% FBS and 1% Pen/Strep (Thermo Fisher Scientific, Braunschweig, Germany) at 37 °C 5% CO_2. For iPSC generation, episomal vectors expressing reprogramming factors were introduced into fibroblasts by electroporation, using the Neon transfection system (1400 V, 20 ms, 2 pulses). Transfected cells were plated on Matrigel-coated wells in Essential 8 (E8) medium (Thermo Fisher Scientific) supplemented with 10 μM ROCK inhibitor, Y-27632 (Tocris). Medium changes were performed every day (without Y-27632) and individual iPSC colonies were isolated and expanded in E8 medium. Newly established iPSC lines were maintained in E8 medium (daily feeding) and passaged (1:4–1:6) every 3–4 days with 0.5 mM EDTA in PBS (Thermo Fisher Scientific). Bright field images confirmed the typical iPSC colony morphology for all lines (Fig. 1A).

4.2. Reprogramming vector analysis

Loss of reprogramming vectors was confirmed by PCR using primers specific to the AmpR gene (Table 2), which is present in all plasmids

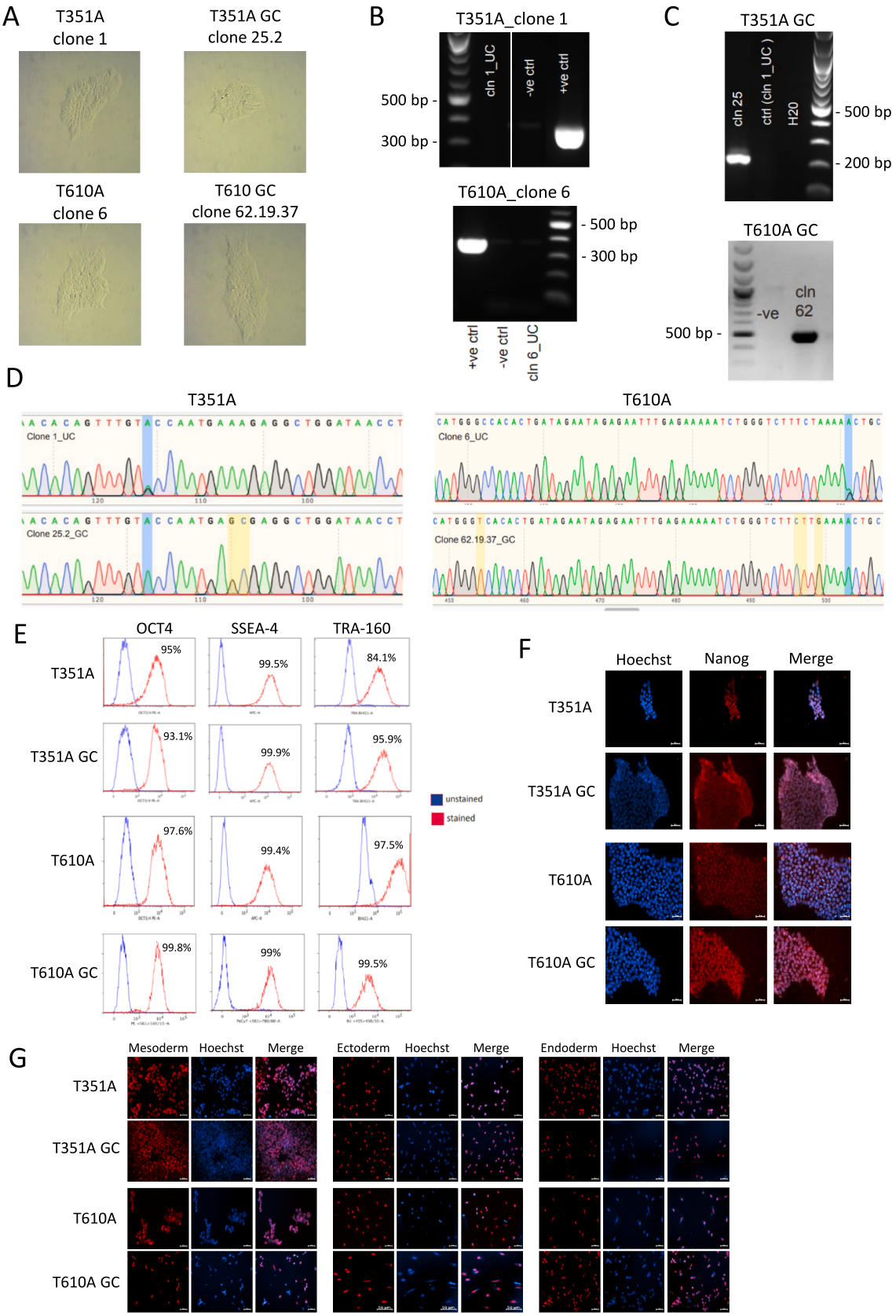
A
T351A clone 1
T351A GC clone 25.2
T610A clone 6
T610 GC clone 62.19.37
B
T351A_clone 1
500 bp -
300 bp -
cln 1_UC
-ve ctrl
+ve ctrl
T610A_clone 6
- 500 bp
- 300 bp
+ve ctrl
-ve ctrl
cln 6_UC
C
T351A GC
cln 25
ctrl (cln 1_UC)
H20
- 500 bp
- 200 bp
T610A GC
500 bp -
-ve
cln 62
D
T351A
Clone 1_UC
Clone 25.2_GC
T610A
Clone 6_UC
Clone 62.19.37_GC
E
OCT4
SSEA-4
TRA-160
T351A
95%
99.5%
84.1%
T351A GC
93.1%
99.9%
95.9%
T610A
97.6%
99.4%
97.5%
T610A GC
99.8%
99%
99.5%
unstained
stained
F
Hoechst
Nanog
Merge
T351A
T351A GC
T610A
T610A GC
G
Mesoderm
Hoechst
Merge
Ectoderm
Hoechst
Merge
Endoderm
Hoechst
Merge
T351A
T351A GC
T610A
T610A GC

Fig. 1.

Table 1
Characterization and validation.

Classification (optional italicized)	Test	Result	Data
Morphology	Photography	*Typical iPSC morphology*	Fig. 1 *panel A*
Pluripotency status evidence for the described cell line	Qualitative analysis *(i.e. Immunocytochemistry, western blotting)*	*All clones display a robust nuclear staining of the stemness marker Nanog*	Fig. 1 *panel F*
	Flow cytometry	*All clones are positive for the pluripotency markers OCT4, SSEA-4 and Tra1-60*	Fig. 1 *panel E*
Karyotype	SNP array Illumina Infinium GSA-24 v3.0, 0.50 Mb	*No aneuploidies detected Arr(X,Y)x1,(1–22)x2 for all clones*	*Supplementary Fig. 3*
Genotyping for the desired genomic alteration/allelic status of the gene of interest	PCR across the edited site or targeted allele-specific PCR	*Successful correction of the intended mutations*	Fig. 1 *panel C*
	Evaluation of the – (homo-/hetero-/hemi-) zygous status of introduced genomic alteration(s)	*N/A*	*N/A*
	Transgene-specific PCR (when applicable)	*N/A*	*N/A*
Verification of the absence of random plasmid integration events	PCR	*Loss of reprogramming vectors confirmed*	Fig. 1 *panel B*
Parental and modified cell line genetic identity evidence	SNPduo analysis of SNP array	*Identical genotypes between parental and gene edited lines*	*Supplementary Fig. 4*
Mutagenesis/genetic modification outcome analysis	Sanger Sequencing	*Confirmation of the homozygous corrections of the intended mutations*	Fig. 1 *panel D*
	PCR-based analyses	*N/A*	*N/A*
	Southern Blot or WGS; western blotting (for knock-outs, KOs)	*N/A*	*N/A*
Off-target nuclease activity analysis	PCR across top 5/10 predicted top likely off-target sites, whole genome/exome sequencing*[*Optional but highly-recommended if Cas editing is used*]*	*N/A*	*N/A*
Specific pathogen-free status	Mycoplasma	*Negative for mycoplasma contamination*	*Supplementary Fig. 5*
Multilineage differentiation potential	Directed differentiation	*Ability of all clones to differentiate into the three germ layers*	Fig. 1 *panel G*
Donor screening (OPTIONAL)	HIV 1 + 2 Hepatitis B, Hepatitis C	*N/A*	*N/A*
Genotype – additional histocompatibility info (OPTIONAL)	Blood group genotyping	*N/A*	*N/A*
	HLA tissue typing	*N/A*	*N/A*

encoding reprogramming factors. Briefly, 250 ng of gDNA from each iPSC clone (after >5 passages) was used in the PCR analysis (performed over 30 cycles). gDNA extracted from vector-free iPSCs was used as a negative control (-ve ctrl), whereas 1 ng of reprogramming plasmid was used as a positive control (+ve ctrl). An expected band of 350 bp was observed for both Miro1 p.T351A (cln 1_UC) and Miro1 p.T610A (cln 6_UC) uncorrected clones (Fig. 1B). Ladder: 1 kb plus DNA ladder (NEB).

4.3. Gene editing

Isogenic lines were generated by CRISPR/Cas9-mediated gene editing (Supplementary Figs. 1 and 2). Briefly, iPSCs were co-transfected with the Cas9-geminin mRNA, the pSMART-sgRNA (Sp) plasmid (encoding a guide RNA specific for either Miro1 p.T351A or Miro1 p.T610A) and a repair template incorporating the mutation and synonymous base changes that facilitate PCR screening and prevent Cas9-mediated re-cutting (Table 2). The repair template consisted of a single-stranded oligodeoxynucleotide (ssODN) for the correction of Miro1 p.T351A (Supplementary Fig. 1, Table 2), whereas it was cloned into the minimal pSMART HC Kan plasmid for the correction of Miro1 p.T610A (Supplementary Fig. 2, Table 2). The "CRISPR-Cas9 guide RNA design checker" tool (from Integrated DNA Technology, Inc.) was used to assess on– and off-target potential of the selected guide RNA sequences. Gene-editing factors were introduced into a single iPSC clone using the Neon transfection system (1100 V, 30 ms, 1 pulse). Electroporated cells were plated on Matrigel-coated wells in E8 medium supplemented with 10 μM ROCK inhibitor. The next day, the medium was switched to E8 without ROCK inhibitor, and changed every other day. Individual colonies were isolated and expanded in E8 medium. Subcloning was performed by dissociating the cells with TryPLE (Thermo Fisher Scientific), followed by plating at low density in E8 medium supplemented with Y-27632 (which was removed after 24 h).

4.4. Allele-specific PCR and Sanger sequencing

gDNA was extracted using the DNeasy Blood and Tissue kit (Qiagen) according to the manufacturer's instructions. Gene-edited iPSC clones were identified by PCR using specific primers recognizing the corrected alleles (Table 2). Expected bands of 213 bp and 502 bp respectively, were observed for Miro1 p.T351A (cln 25_GC) and Miro1 p.T610A (cln 62_GC) gene-corrected clones (Fig. 1C). Uncorrected Miro1 p.T351A (cln1_UC) and Miro1 p.T610A (cln1_UC, -ve) iPSC clones were used as negative controls (Fig. 1C). PCR amplicons generated with primers flanking the intended correction (Table 2) were Sanger sequenced to confirm the successful gene editing and the absence of indel mutations. Location of the uncorrected and gene-corrected mutations is highlighted in blue; homozygous incorporations of synonymous changes in the gene-edited clones are highlighted in yellow (Fig. 1D).

4.5. Pluripotency assays

Expression of stemness markers was evaluated by both FACS analysis and immunocytochemistry (ICC). For FACS, iPSCs were harvested with TrypLE and stained with the following antibodies: TRA-1-60 BV421 and SSEA4-AF647 were incubated in PBS + 2% FBS; OCT3/4 PE staining was performed on cells pre-treated with the Foxp3 fixation/permeabilisation buffer (Thermo Fisher Scientific, Cat No. 00-5523-00). Cells were analyzed using a FACSaria x-20 flow cytometer, with unstained iPSCs used as a gating control (Fig. 1E).

For the ICC, iPSCs were plated on Matrigel-coated coverslips and fixed in PBS + 4% PFA for 15 min. Cells were then permeabilized and blocked for 1 h in PBS supplemented with 10% goat serum, 2% BSA and 0.4% Triton-X 100, followed by overnight incubation at 4 °C with the Nanog antibody (Table 2), diluted in 1% goat serum, 0.2% BSA and 0.1% Triton-X 100. The following day, cells were washed in PBS and

Table 2
Reagent details.

Antibodies and stains used for immunocytochemistry/flow-cytometry			
	Antibody	Dilution	Company Cat # and RRID
Pluripotency Markers (FACS)	*TRA-1–60 BV421*	*As per manufacturer's specification*	*BD Biosciences, Cat No. 562711; RRID: AB_2737738*
Pluripotency Markers (FACS)	*SSEA4 AF647*		*BD Biosciences, Cat No. 330408; RRID: AB_1089200*
Pluripotency Markers (FACS)	*OCT3/4 PE*		*BD Biosciences, Cat No. 560186; RRID: AB_1645331*
Pluripotency Markers (ICC)	*Rabbit anti Nanog*	*1:500*	*Abcam, Cat #: ab21624; RRID: AB_446437*
Secondary antibody	*Alexa Fluor 568 Goat anti-Rabbit IgG (H + L)*	*1:1000*	*Invitrogen, Cat #: A11036; RRID: AB_143011*
Mesoderm Marker	*Goat anti Brachyury*	*1:500*	*Human Pluripotent Stem Cell Functional Identification Kit (R&D Systems, Cat No. SC027B)*
Endoderm Marker	*Goat anti SOX-17*	*1:500*	
Ectoderm Marker	*Goat anti OTX2*	*1:500*	
Secondary antibody	*Alexa Fluor 647 Donkey anti Goat IgG (H + L)*	*1:1000*	*Invitrogen, Cat No. A21447; RRID: AB_141844*
Site-specific nuclease			
Nuclease information	*Cas9-geminin*	*In vitro transcribed mRNA*	
Delivery method	*Electroporation*	*Neon transfection system (1100 V, 30 ms, 1 pulse)*	
Selection/enrichment strategy	*Any*	*Any*	
Primers and Oligonucleotides used in this study			
	Target	Forward/Reverse primer (5′-3′)	
Primers for verification loss of reprogramming vectors	*AmpR cassette*	*CAGTCTATTAATTGTTGCCGGG/GCTATGTGGCGCGGTATTAT*	
sgRNA Miro1 c.1290A > G mutation	*RHOT1 exon 13*	*CAGTTTGTGCCAATGAAAGA*	
sgRNA Miro1 c.2067A > G mutation	*RHOT1 exon 19*	*AATTCTCTATTCTATCAGTG*	
Miro1 c.1290A > G ssODN repair template	*RHOT1 exon 13*	*GCCAGATGTGAATAACACAGTTTGTACCAATGAGCGAGGCTGGATAACCTACCAGGGATTCCTT*	
Miro1 c.2067A > G repair template (plasmid)	*RHOT1 exon 19*	*AGACATGGGTCACACTGATAGAATAGAGAATTTGAGAAAAATCTGGGTCTTCTTGAAAACTGCT*	
sgRNA for correction indel mutation iPSCs Miro1 c.2067A > G GC	*1 bp insertion (T) at the Cas9 cut site*	*ATTCTCTATTCTATCAAGTG*	
Screening PCR Miro1 c.1290A > G gene-corrected clones	*RHOT1 exon 13*	*CACAGTTTGTACCAATGAGC/CATCTTAGAGATATCAGCAGC*	
Screening PCR Miro1 c.2067A > G gene-corrected clones	*RHOT1 exon 19*	*GAGAAAAATCTGGGTCTTCTTG/GCTACTAAGTCTCTGCCAGC*	
Sanger sequencing Miro1 c.1290A > G gene-corrected clones	*RHOT1 exon 13*	*GCTTTGTCACCTGATGAGC/CATCTTAGAGATATCAGCAGC*	
Sanger sequencing Miro1 c.2067A > G gene-corrected clones	*RHOT1 exon 19*	*CAAGCACATAACTGTGGTCATC/GCTACTAAGTCTCTGCCAGC*	

incubated with the corresponding secondary antibody for 1 h (Table 2). Finally, nuclei were stained with Hoechst and images acquired using a Zeiss AxioObserverZ1 microscope (Carl Zeiss Microimaging GmBH). Scale bar = 50 μm (Fig. 1F).

4.6. Three germ layer differentiation

iPSCs were plated on Matrigel-coated coverslips two days before the *in vitro* differentiation procedure started. The Human Pluripotent Stem Cell Functional Identification Kit (R&D Systems, Cat No. SC027B) was used to verify iPSCs capacity to differentiate into the three germ layers. Immunocytochemistry of the ectodermal marker OTX2, the mesodermal marker Brachyury and the endodermal marker SOX17 was performed. Images were acquired using a Zeiss AxioObserverZ1 microscope, scale bar = 50 μm (Fig. 1G).

4.7. Karyotyping and genetic identity

Genomic DNA was isolated from iPSCs and analyzed (Victorian Clinical Genetics Service, Murdoch Children's Research Institute, Australia) using an Illumina Infinium CoreExome-24 v1.1 SNP array (Supplementary Fig. 3). Genetic identity between gene-edited and parental lines was assessed by SNPduo analysis (https://pevsnerlab.kennedykrieger.org/SNPduo/) of the SNP array (Supplementary Fig. 4).

4.8. Mycoplasma analysis

iPSCs were submitted to Cerberus Sciences (https://www.cerberus.net.au/submission) for mycoplasma testing and confirmed all negative (Supplementary Fig. 5).

Declaration of Competing Interest

The authors declare that they have no known competing financial interests or personal relationships that could have appeared to influence the work reported in this paper.

Acknowledgements

AC is supported by the Luxembourg Fonds National de Recherche (FNR) within the framework of the PARK-QC DTU (PRIDE17/12244779/PARK-QC). Work of GA is supported by the FNR, grant number C21/BM/15850547/PINK1-DiaPDs. Work of AG was supported by the FNR within the ATTRACT program (Model-IPD, FNR9631103). RK obtained funding from the FNR PEARL Excellence Programme [FNR/P13/6682797], the Michael J. Fox Foundation, and the European Union's Horizon2020 research and innovation program (WIDESPREAD; CENTRE-PD; grant agreement no. 692320). In addition, RK, AG and GA were supported by the FNR CORE grant MiRisk-PD (C17/BM/11676395). CS is supported by the FNR CORE program C19/BM/13535609.

We thank the Stem Cell Medicine Gene Editing Facility at the Murdoch Children's Research Institute (The Royal Children's Hospital, Parkville, Victoria 3052 Australia) for the reprogramming and gene editing procedures. A special thanks to Sara Howden and Alison Graham for the regular feedback and support. We also thank the Victorian Clinical Genetics Services (VCGS, The Royal Children's Hospital, Parkville, Victoria 3052 Australia) for the assistance with the SNP array analyses.

Appendix A. Supplementary data

Supplementary data to this article can be found online at https://doi.org/10.1016/j.scr.2023.103085.

References

Berenguer-Escuder, C., Grossmann, D., Massart, F., Antony, P., Burbulla, L.F., Glaab, E., et al., 2019. Variants in Miro1 cause alterations of ER-mitochondria contact sites in fibroblasts from Parkinson's disease patients. J. Clin. Med. 8, 2226. https://doi.org/10.3390/jcm8122226.

Berenguer-Escuder, C., Grossmann, D., Antony, P., Arena, G., Wasner, K., Massart, F., Jarazo, J., Walter, J., Schwamborn, J.C., Grünewald, A., Krüger, R., 2020. Impaired mitochondrial-endoplasmic reticulum interaction and mitophagy in Miro1-mutant neurons in Parkinson's disease. Hum. Mol. Genet. 29 (8), 1353–1364. https://doi.org/10.1093/hmg/ddaa066.

Grossmann, D., Berenguer-Escuder, C., Bellet, M.E., Scheibner, D., Bohler, J., Massart, F., Rapaport, D., Skupin, A., Fouquier d'Hérouël, A., Sharma, M., Ghelfi, J., Raković, A., Lichtner, P., Antony, P., Glaab, E., May, P., Dimmer, K.S., Fitzgerald, J.C., Grünewald, A., Krüger, R., 2019. Mutations in RHOT1 disrupt endoplasmic reticulum-mitochondria contact sites interfering with calcium homeostasis and mitochondrial dynamics in Parkinson's disease. Antioxid. Redox Signal. 31 (16), 1213–1234. https://doi.org/10.1089/ars.2018.7718.

Grossmann, D., Berenguer-Escuder, C., Chemla, A., Arena, G., Kruger, R., 2020. The Emerging Role of RHOT1/Miro1 in the Pathogenesis of Parkinson's Disease. Front. Neurol. 11, 587. https://doi.org/10.3389/fneur.2020.00587.

IV.II Manuscript II

Generation of two induced pluripotent stem cell lines and the corresponding isogenic controls from Parkinson's disease patients carrying the heterozygous mutations c.815G>A (p.R272Q) or c.1348C>T (p.R450C) in the *RHOT1* gene encoding Miro1.

Chemla et al. 2023

Status:
Published in Stem Cell Research

Description of contribution:
I wrote the manuscript, made all the figures, and performed characterization experiments in panels A, C, D and E.

This manuscript refers to the generation of iPSC lines with the p.R272Q and p.R450C mutations and corresponding gene corrected, isogenic control lines. Briefly, iPSCs were generated using RNA based (p.R272Q) and episomal (p.R450C) reprogramming. The point mutations were then corrected via CRISPR/Cas9. The resulting iPSCs lost the reprogramming vectors as expected, properly expressed stemness factors, and could differentiate into the three germ layers.

In two of our previous publications, we characterized the effect of both variants in fibroblasts from the patients (Grossmann et al., 2019a). We observed disrupted capacity to maintain calcium homeostasis in the patient cells, reduced number of MERCs, increased LC3-independent autophagy, and reduced ATP levels (Grossmann et al., 2019a). IPSC-derived neurons were then generated from the p.R272Q Miro1 fibroblasts, and had higher number of MERCs, decreased mitophagy flux, and decreased Rab9 dependent autophagy, while they still displayed an increased sensitivity to calcium stress (Berenguer-Escuder et al., 2020a). However, the former study was done by comparing Miro1 p.R272Q mutant neurons to age and gender matched controls. This presented the Miro1 p.R272Q and healthy control as a model to investigate PD regardless of potential PD-favoring genetic background. By generating an isogenic pair, we now also have a model to investigate the point mutation effect in the same genetic background. Moreover, this isogenic pair will allow us to decipher the contribution of the point mutation to the robust calcium phenotype, found in our four Miro1 mutants, both in fibroblasts and p.R272Q iPSC-derived neurons. Using iPSC-derived neurons from the Miro1 p.R450C patient and its isogenic pair could also help us to understand the role of the C-terminal GTPase domain of Miro1 in mitochondrial transport and calcium regulation.

Stem Cell Research 71 (2023) 103145

Contents lists available at ScienceDirect

Stem Cell Research

journal homepage: www.elsevier.com/locate/scr

Lab Resource: Genetically-Modified Multiple Cell Lines

Generation of two induced pluripotent stem cell lines and the corresponding isogenic controls from Parkinson's disease patients carrying the heterozygous mutations c.815G > A (p.R272Q) or c.1348C > T (p.R450C) in the RHOT1 gene encoding Miro1

Axel Chemla [a], Giuseppe Arena [a,*], Gizem Onal [b,c,d], Jonas Walter [e,1], Clara Berenguer-Escuder [a], Dajana Grossmann [a,f], Anne Grünewald [g,h], Jens C. Schwamborn [e], Rejko Krüger [a,i,j,*]

[a] Translational Neuroscience, Luxembourg Centre for Systems Biomedicine (LCSB), University of Luxembourg, Luxembourg
[b] Department of Physiology, Anatomy and Genetics, University of Oxford, UK
[c] Kavli Institute for Nanoscience Discovery, University of Oxford, UK
[d] Department of Medical Biology, Faculty of Medicine, Balikesir University, Turkey
[e] Developmental and Cellular Biology, Luxembourg Centre for Systems Biomedicine (LCSB), University of Luxembourg, Luxembourg
[f] Translational Neurodegeneration Section "Albrecht-Kossel", Department of Neurology, University Medical Center Rostock, University of Rostock, Rostock, Germany
[g] Molecular and Functional Neurobiology, Luxembourg Centre for Systems Biomedicine (LCSB), University of Luxembourg, Luxembourg
[h] Institute of Neurogenetics, University of Lübeck, Lübeck, Germany
[i] Centre Hospitalier de Luxembourg, Luxembourg
[j] Transversal Translational Medicine, Luxembourg Institute of Health (LIH), Luxembourg

A B S T R A C T

Fibroblasts from two Parkinson's disease (PD) patients carrying either the heterozygous mutation c.815G > A (Miro1 p.R272Q) or c.1348C > T (Miro1 p.R450C) in the RHOT1 gene, were converted into induced pluripotent stem cells (iPSCs) using RNA-based and episomal reprogramming, respectively. The corresponding isogenic gene-corrected lines have been generated using CRISPR/Cas9 technology. These two isogenic pairs will be used to study Miro1-related molecular mechanisms underlying neurodegeneration in relevant iPSC-derived neuronal models (e.g., midbrain dopaminergic neurons and astrocytes).

1. Resource table

Unique stem cell line identifier	*1. LCSBi009-A* *2. LCSBi009-A-1* *3. LCSBi010-A* *4. LCSBi010-A-1* *5. LCSBi010-A-2*
Alternative name(s) of stem cell line	*1. RHOT1_R272Q_clone1_PD* *2. RHOT1_R272Q_clone18_IsogenicControl* *3. RHOT1_R450C_clone5_PD* *4. RHOT1_R450C_clone6_IsogenicControl* *5. RHOT1_R450C_clone10_IsogenicControl*
Institution	*Luxembourg Centre for Systems Biomedicine (LCSB), University of Luxembourg, Luxembourg*
Contact information of the reported cell line distributor	*Prof. Rejko Krüger; rejko.krueger@uni.lu*
Type of cell line	*iPSCs*
Origin	*Human*
Additional origin info *(applicable for human ESC or iPSC)*	*1. Age at biopsy: 78 years* *Sex: female* *Ethnicity: European White* *2. As in 1.* *3. Age at biopsy: 54 years* *Sex: female* *Ethnicity: European White* *4. As in 3.* *5. As in 3*
Cell Source	*Dermal fibroblasts*

(continued on next column)
(continued)
(continued on next page)

* Corresponding authors at: Translational Neuroscience team, Luxembourg Centre for Systems Biomedicine (LCSB), University of Luxembourg, Campus Belval, 6 Avenue du Swing, L-4367 Esch-sur-Alzette, Luxembourg.
E-mail addresses: Giuseppe.Arena@uni.lu (G. Arena), Rejko.Krueger@lih.lu (R. Krüger).
[1] Current address: Department of Proteomics, The Novo Nordisk Foundation Center for Protein Research, Faculty of Health and Medical Sciences, University of Copenhagen, Blegdamsvej 3B, Copenhagen 2200, Denmark.

https://doi.org/10.1016/j.scr.2023.103145
Received 3 April 2023; Received in revised form 9 June 2023; Accepted 12 June 2023
Available online 14 June 2023

(*continued*)

Method of reprogramming	*RHOT1_R272Q: RNA transfection* *RHOT1_R450C: nucleofection of episomal reprogramming vectors*
Clonality	*Clonal*
Evidence of the reprogramming transgene loss (including genomic copy if applicable)	*Loss of episomal reprogramming vectors (RHOT1_R450C only)*
The cell culture system used	*iPSCs were maintained under feeder-free conditions, on Matrigel-coated wells, in presence of Essential 8™ (E8) medium*
Type of the Genetic Modification	*Spontaneous point mutation (LCSBi009-A and LCSBi010-A)* *Gene correction (LCSBi009-A-1, LCSBi010-A-1 and LCSBi010-A-2)*
Associated disease	*Parkinson disease (OMIM #168600)*
Gene/locus	*RHOT1 (17q11.2), Gene ID: 55,288*
Method of modification / user-customisable nuclease (UCN) used, the resource used for design optimisation	*CRISPR/Cas9*
User-customisable nuclease (UCN) delivery method	*Nucleofection*
All double-stranded DNA genetic material molecules introduced into the cells	*Yamanaka reprogramming vectors, SpCas9 plasmid*
Analysis of the nuclease-targeted allele status	*Sanger Sequencing of the targeted alleles*
Method of the off-target nuclease activity prediction and surveillance	*The Benchling CRISPR design tool was used to assess on– and off-target potential of selected* guide RNA *sequences*
Descriptive name of the transgene	*N/A*
Eukaryotic selective agent resistance cassettes	*N/A*

(*continued on next column*)

(*continued*)

(including inducible, gene/cell type-specific)	
Inducible/constitutive expression system details	*N/A*
Date archived/stock creation date	*01.12.2022*
Cell line repository/bank	https://hpscreg.eu/cell-line/LCSBi009-A https://hpscreg.eu/cell-line/LCSBi009-A-1 https://hpscreg.eu/cell-line/LCSBi010-A https://hpscreg.eu/cell-line/LCSBi010-A-1 https://hpscreg.eu/cell-line/LCSBi010-A-2
Ethical/GMO work approvals	*The Luxembourgish National Research Ethics Committee (CNER) provided ethical approval for the following project: "Disease modelling of Parkinson's disease using patient-derived fibroblasts and induced pluripotent stem cells" (DiMo-PD, CNER #201411/05).*
Addgene/public access repository recombinant DNA sources' disclaimers (if applicable)	*pCXLE-hUL (Addgene #27080), pCXLE-hSK (Addgene #27078), and pCXLE-hOct3/4 (Addgene #27076)*

2. Resource utility

We recently identified distinct PD patients carrying different heterozygous mutations in the *RHOT1* gene encoding Miro1 (Berenguer-Escuder et al., 2019, 2020; Grossmann et al., 2019; Grossmann et al., 2020). Here we report the generation of iPSCs – and the corresponding gene-corrected lines – from two carriers of different PD-associated Miro1 mutations, which can be used to investigate the impact of Miro1 deficiency on PD pathogenesis Table 1.

Table 1
Characterization and validation.

Classification (optional *italicized*)	**Test**	**Result**	**Data**
Morphology	Photography	Typical iPSC morphology	Fig. 1 panel A
Pluripotency status evidence for the described cell line	Immunocytochemistry	All iPSC clones display a nuclear localization of the pluripotency markers Nanog and Oct3/4	Fig. 1 panel C
	RT-qPCR	All iPSC clones express the pluripotency markers Nanog and Oct3/4	Fig. 1 panel D
Karyotype	-Illumina iScan S/N: N234 -Karyostat+	No aneuploidies detected	Supplementary Fig. 5
Genotyping for the desired genomic alteration/allelic status of the gene of interest	PCR across the edited site or targeted allele-specific PCR *[mandatory]*	Successful correction of the intended mutations Absence of large deletions in the region targeted by the gRNAs	Fig. 1 panel B Supplementary Fig. 4
	Evaluation of the - (homo-/hetero-/hemi-) zygous status of introduced genomic alteration(s)	*N/A*	*N/A*
	Transgene-specific PCR (when applicable)	*N/A*	*N/A*
Verification of the absence of random plasmid integration events	PCR/Southern *[mandatory]*	Loss of reprogramming vectors confirmed	Supplementary Fig. 1
Parental and modified cell line genetic identity evidence	STR analysis	Identical genotypes between parental and gene-edited lines	Supplementary Fig. 6
Mutagenesis / genetic modification outcome analysis	Sanger Sequencing	Confirmation of the homozygous corrections of the mutated alleles and absence of indel mutations	Fig. 1 panel B
	PCR-based analyses	*N/A*	*N/A*
	Southern Blot or WGS; western blotting (for knock-outs, KOs)	*N/A*	*N/A*
Off-target nuclease activity analysis	Targeted PCR and sequencing for the top 5 predicted off-targets located in genes *[*Optional but highly-recommended if Cas editing is used*]*	*N/A*	*N/A*
Specific pathogen-free status	Mycoplasma *[mandatory]*	Negative	Supplementary Fig. 7
Multilineage differentiation potential	Directed differentiation *[mandatory]*	Ability of all clones to differentiate into the three germ layers	Fig. 1 panel E
Donor screening (OPTIONAL)	HIV 1 + 2 Hepatitis B, Hepatitis C, HTLV 1 + 2	Negative	Supplementary Fig. 7
Genotype - additional histocompatibility info (OPTIONAL)	Blood group genotyping	N/A	N/A
	HLA tissue typing	N/A	N/A

3. Resource details

For the generation of parental iPSC lines (i.e., *LCSBi009-A* and *LCSBi010-A*), we reprogrammed fibroblasts of two PD patients carrying different *RHOT1* heterozygous mutations – the c.815G > A (p.R272Q) and the c.1348C > T (p.R450C) mutation – which are located in the first EF-hand (EF1) and in the C-terminal GTPase (cGTPase) domain of Miro1, respectively (Grossmann et al., 2019). Miro1 p.R272Q fibroblasts were reprogrammed into iPSCs using a virus-free and integration-free RNA-based approach, consisting in the transfection of a synthetic *in vitro* transcribed RNA replicon expressing the reprogramming factors in a single self-replicating polycistronic transcript. Miro1 p.R450C iPSCs

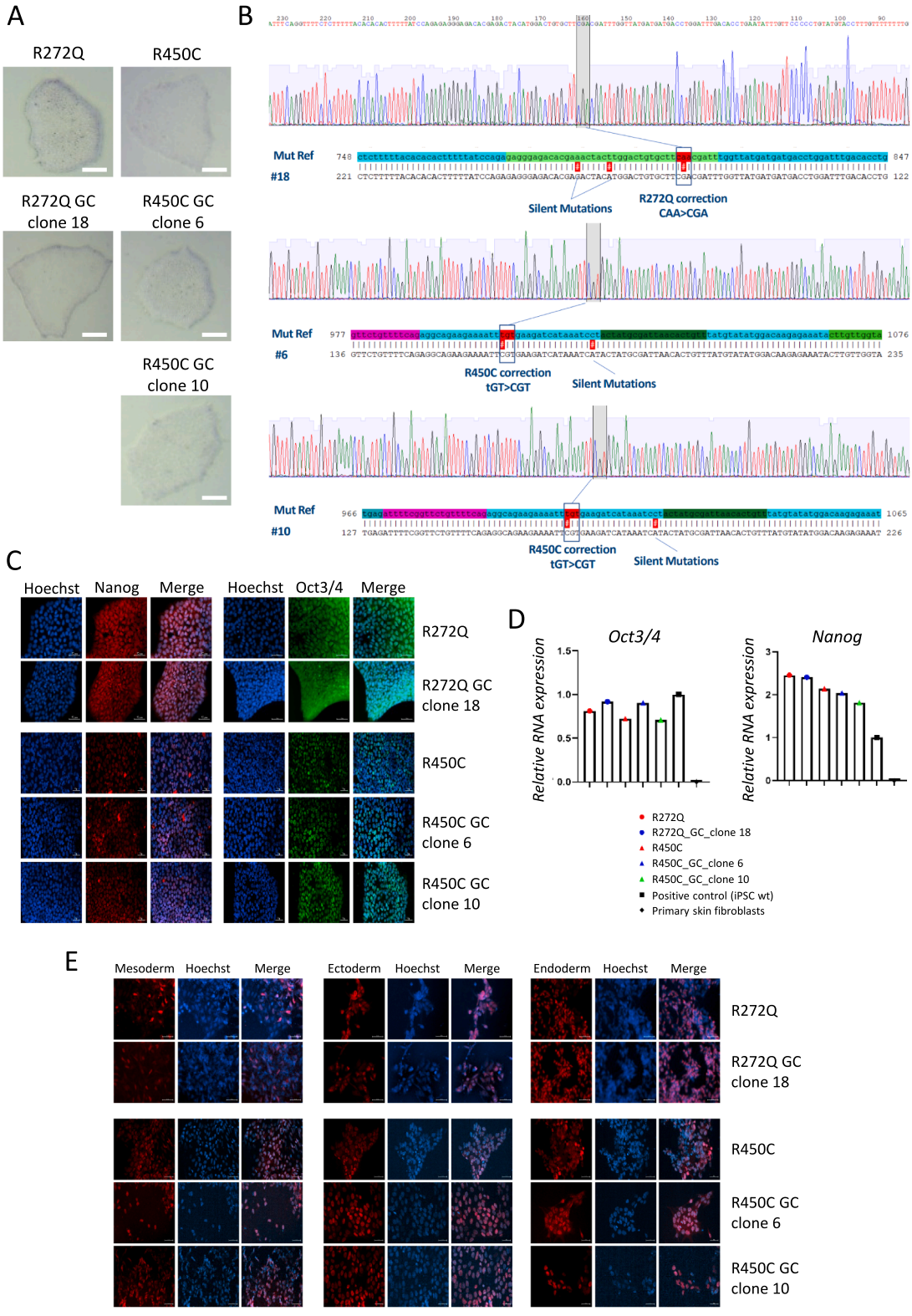

Fig. 1.

were established following electroporation of patient fibroblasts with episomal vectors expressing the four Yamanaka reprogramming factors. Clonal iPSC populations were identified by morphology, isolated and expanded (Fig. 1A, upper panels). The absence of plasmid integration in their genome was confirmed by PCR analysis (Supplementary Fig. 1). Isogenic, gene-corrected lines (i.e., *LCSBi009-A-1*, *LCSBi010-A-1* and *LCSBi010-A-2*) were generated by Axol Bioscience using a CRISPR/Cas9-mediated gene editing approach (Supplementary Figs. 2 and 3). For both Miro1 R272Q and Miro1 R450C gene correction, two distinct gRNAs targeting the intended mutation site were selected based on prior *in silico* analysis considering their distance from the target, predicted activity and off-target profile (Table 2). After testing their cutting efficiency in the corresponding parental iPSC lines, gRNAs of higher activity were chosen (C1917A-R272Q-g2 and C1917B-R450C-g1, respectively). Cas9-mediated re-cutting was prevented by introducing silent mutations in the gRNA binding sites present on the editing donor, consisting of a single-stranded oligodeoxynucleotide (ssODN) with homology arms flanking the target site (Table 2). Gene editing factors were introduced in the parental iPSC lines by nucleofection. Several iPSC colonies were screened by PCR and Sanger sequencing, confirming the successful corrections and the absence of indel mutations in one Miro1 p.R272Q (clone 18) and in two Miro1 p.R450C (clone 6 and 10) gene-edited clones (Table 2, Fig. 1B). qPCR analysis excluded the presence of large deletions in the region targeted by the respective gRNAs (Supplementary Fig. 4). The three gene-corrected lines, all displaying a typical iPSC morphology (Fig. 1A, lower panels), were then expanded and subjected to further characterization. Immunocytochemistry and RT-qPCR analyses confirmed that both patient-derived and gene-edited clones

Table 2
Reagent details.

Antibodies and stains used for immunocytochemistry/flow-cytometry			
	Antibody	**Dilution**	**Company Cat # and RRID**
Pluripotency Markers	*Rabbit anti Nanog*	*1:500*	*Abcam, Cat #: ab21624; RRID: AB_446437*
Pluripotency Markers	*Mouse anti Oct3/4*	*1:1000*	*Santa Cruz, Cat #: sc-5279; RRID: AB_628051*
Secondary antibody	*Alexa Fluor 488 Goat anti-Mouse IgG (H + L)*	*1.1000*	*Invitrogen, Cat #: A11029; RRID: AB_138404*
Secondary antibody	*Alexa Fluor 568 Goat anti-Rabbit IgG (H + L)*	*1:1000*	*Invitrogen, Cat #: A11036; RRID: AB_143011*
Mesoderm Marker	*Goat anti Brachyury*	*1:500*	*Human Pluripotent Stem Cell Functional Identification Kit (R&D Systems, Cat No.*
Endoderm Marker	*Goat anti SOX-17*	*1:500*	*SC027B)*
Ectoderm Marker	*Goat anti OTX2*	*1:500*	
Secondary antibody	*Alexa Fluor 647 Donkey anti Goat IgG (H + L)*	*1:1000*	*Invitrogen, Cat No. A21447; RRID: AB_141844*
Site-specific nuclease			
Nuclease information	*Nuclease type/version*	*SpCas9*	
Delivery method	*Nucleofection*	*Amaxa 4D*	
Selection/enrichment strategy	*Selection cassette(s), FACS*	*N/A*	
Primers and Oligonucleotides used in this study			
	Target	**Forward/Reverse primer (5′-3′)**	
Pluripotency Marker (RT-qPCR)	*OCT4-FAM*	*Hs00999632_g1 (Thermo Fisher Scientific)*	
Pluripotency Marker (RT-qPCR)	*NANOG-FAM*	*Hs02387400_g1 (Thermo Fisher Scientific)*	
Housekeeping gene (RT-qPCR)	*ACTB-VIC*	*Hs03023880_g1 (Thermo Fisher Scientific)*	
Potential random integration-detecting PCRs	*OriP fw*	*TTCCACGAGGGTAGTGAACC*	
Potential random integration-detecting PCRs	*OriP rv*	*TCGGGGGTGTTAGAGACAAC*	
gRNA Miro1 c.815G > A mutation	*RHOT1 exon 11*	*GAGGGAGACACGAAACTACT*	
gRNA Miro1 c.1348C > T mutation	*RHOT1 exon 16*	*ATTTTCGGTTCTGTTTTCAG*	
Miro1 c.815G > A ssODN repair template	*RHOT1 exon 11*	*GGAACAAATATTCAGGTGTCAAATCCAGGTCATCATCATAACC AAATCGTCGAAGCACAGTCCATGTAGTCTCGTGTCTCCCTCTCT GGATAAAAAGTGTGTGTAAAAAGAGAAAACCTGA*	
Miro1 c.1348C > T ssODN repair template	*RHOT1 exon 16*	*TCCATATACATAAACAGTGTTAATCGCATAGTAGGATTTATGA TCTTCACGAATTTTCTTCTGTCTCTGAAAACAGAACCGAAAAT CTCAATATCTGCAGTAACTAGTTTTCAA*	
Screening PCR Miro1 c.815G > A gene-corrected clones	*RHOT1 exon 11*	*GAGGCACAGTGAAGTTAATGAGATTG / CTTTAATCACAGCAATTTGGGAGGC*	
Screening PCR Miro1 c.1348C > T gene-corrected clones	*RHOT1 exon 16*	*ATGGTATAATGAAGATTGCCAGCAG / ACCACGCCTAGCCAAAAGAC*	
qPCR allelic status Miro1 c.815G > A gene-corrected clones	*RHOT1 intron 10*	*GGCCATTTCCTCTAGTGCTC / ATACGGATGCTAGCTTTGCATTG*	
qPCR allelic status Miro1 c.1348C > T gene-corrected clones	*RHOT1 intron 17*	*ACTTGTTGGTAAGAAATTCTGTGGC / CAGAAGTTCTACAGAGAGTCATTCA*	
Housekeeping gene (qPCR)	*GAPDH*	*TCTCCTGGAAGGGCTTCGTA / TAAGGCATGGCTGCAACTGA*	
Sanger sequencing Miro1 c.815G > A gene-corrected clones	*RHOT1 exon 11*	*GAGGCACAGTGAAGTTAATGAGATTG*	
Sanger sequencing Miro1 c.1348C > T gene-corrected clones	*RHOT1 exon 16*	*GAACAAATACATCTTTTATTTTAG*	

expressed the pluripotency markers OCT3/4 and Nanog (Fig. 1C and D). Moreover, they were all able to differentiate into the three germ layers (Fig. 1E). Finally, all iPSC lines displayed a normal karyotype (Supplementary Fig. 5), were genetically identical to the corresponding fibroblasts (Supplementary Fig. 6) and free of contamination by human pathogens (Supplementary Fig. 7).

4. Materials and methods

4.1. Cell culture and reprogramming

PD patient-derived fibroblasts were grown in DMEM medium containing 4.5 g/L D-glucose, 10% FBS and 1% Pen/Strep (Thermo Fisher Scientific). For the generation of Miro1 p.R272Q iPSCs, fibroblasts were reprogrammed using the Simplicon™ RNA Reprogramming Kit (Merck/EMD Millipore, Cat No. SCR550), according to the manufacturer's instructions. Briefly, cells were pre-treated with the B18R Protein (Millipore, Cat. No. GF156) to suppress the cellular interferon response, and then transfected with the VEE-OKS-iG RNA replicon expressing the reprogramming factors Oct4, Klf4, Sox2 and Glis1. To support iPSC induction, the TeSR™-E7™ reprogramming medium (STEMCELL Technologies, Cat No. 05914) was used until first iPSC colonies became visible; TeSR™-E7™ was then replaced by Essential 8 (E8) medium (Thermo Fisher Scientific). For the generation of Miro1 p.R450C iPSCs, episomal vectors expressing Yamanaka reprogramming factors, namely pCXLE-hUL (Addgene #27080), pCXLE-hSK (Addgene #27078) and pCXLE-hOct3/4 (Addgene #27076), were introduced into patient fibroblasts by electroporation, using the Amaxa Nucleofector II system (Lonza Bioscience) program B16. Transfected cells were plated on Matrigel-coated wells and fed every day with E8 medium. Undifferentiated iPSC colonies were identified by morphology, isolated and expanded; passages were performed every 3–4 days with 0.5 mM EDTA in PBS. Bright field images taken after expansion confirmed the typical iPSC colony morphology for all lines (Fig. 1A).

4.2. Reprogramming vector analysis

Loss of reprogramming vectors was confirmed by PCR using primers specific to the OriP region (Table 2, Supplementary Fig. 1), which is present in all plasmids encoding Yamanaka factors.

4.3. Gene editing

Gene-corrected iPSC lines were generated by Axol Bioscience using the CRISPR/Cas9 technology (Supplementary Fig. 2 and 3). Briefly, iPSCs were co-transfected with the SpCas9 plasmid, the specific gRNA and a single-stranded oligodeoxynucleotide (ssODN) repair template incorporating the corrected allele and also containing synonymous base changes that facilitate PCR screening and prevent Cas9-mediated re-cutting (Table 2, Supplementary Fig. 2 and 3). Cells were then plated on Matrigel-coated wells and fed with mTESR™1 (STEMCELL Technologies).

4.4. PCR and Sanger sequencing

Gene-edited iPSC clones were screened by PCR using the indicated primers (Table 2, Supplementary Fig. 4). PCR amplicons were then sequenced to confirm the successful gene editing and the absence of indel mutations (Table 2, Fig. 1B). Positive clones (clone 18 for Miro1 p.R272Q_GC, clones 6 and 10 for Miro1 p.R450C_GC) were finally expanded and gene correction further confirmed by PCR and sequencing. Location of the corrected alleles and silent mutations introduced are indicated by the hashtags highlighted in red (Fig. 1B).

4.5. Pluripotency assay

Expression of stemness markers was evaluated by both immunocytochemistry (ICC) and RT-qPCR analysis. For the ICC, iPSCs were plated on Matrigel-coated coverslips and fixed in PBS + 4% PFA for 15 min. Cells were then permeabilized and blocked for 1 h in PBS supplemented with 10% goat serum, 2% BSA and 0.4% Triton-X 100, followed by overnight incubation at 4 °C with Nanog and Oct3/4 primary antibodies (Table 2), diluted in 1% goat serum, 0.2% BSA and 0.1% Triton-X 100. The following day, cells were washed in PBS and incubated with the corresponding secondary antibodies (Table 2). Finally, nuclei were stained with Hoechst and images acquired using a Zeiss AxioObserverZ1 microscope (Carl Zeiss Microimaging GmBH). Scale bar = 50 μm (Fig. 1C).

For the RT-qPCR analysis, total RNA was extracted using the RNeasy Mini Kit (QIAGEN) and retrotranscribed using the Transcriptor High Fidelity cDNA Synthesis Kit (Roche). The resulting cDNAs were subjected to multiplex qPCR using the LightCycler® 480 Probes Master Kit (Roche) and the hydrolysis probes NANOG-FAM, OCT3/4-FAM and ACTB-VIC (Table 2). Relative RNA levels were expressed as fold change compared to a wild-type (wt) iPSC line that was used as positive control. cDNA obtained from primary skin fibroblasts was used as negative control (Fig. 1D).

4.6. Three germ layer differentiation

iPSCs were plated on Matrigel-coated coverslips two days before the *in vitro* differentiation procedure started. The Human Pluripotent Stem Cell Functional Identification Kit (R&D Systems, Cat No. SC027B) was used to verify iPSCs capacity to differentiate into the three germ layers. ICC of the ectodermal marker OTX2, the mesodermal marker Brachyury and the endodermal marker SOX17 was performed. Nuclei were stained with Hoechst and images were acquired using a Zeiss AxioObserverZ1 microscope. Scale bar = 50 μm (Fig. 1E).

4.7. Karyotyping and genetic identity

Genomic DNA was isolated from iPSCs and karyotype analysis was performed to exclude the presence of chromosomal aberrations. Karyotype of patient-derived iPSCs (Miro1 p.R272Q and p.R450C mutant lines) was assessed at Life&Brain Genomics (Bonn, Germany) using an Illumina iScan S/N: N234 array (Supplementary Fig. 5, upper panels). Karyotyping of gene-edited lines was performed by Life Technologies (Thermo Fisher Scientific, Madison, WI, USA) using a CytoScan HT-CMA 96F array for Karyostat + analysis (Supplementary Fig. 5, lower panels). Genetic identity between gene-edited and parental lines (both fibroblasts and mutant iPSCs) was confirmed by STR analysis (Cell Line Service, GmbH, Germany, Supplementary Fig. 6).

4.8. Human pathogens analysis

iPSCs were subjected to PCR analysis to exclude the presence of contamination by human pathogens, including Mycoplasma, Hepatitis, HIV and HTLV. All clones resulted negative (Supplementary Fig. 7).

Declaration of Competing Interest

The authors declare that they have no known competing financial interests or personal relationships that could have appeared to influence the work reported in this paper.

Acknowledgements

AC is supported by the Luxembourg Fonds National de Recherche (FNR) within the framework of the PARK-QC DTU (PRIDE17/12244779/PARK-QC). Work of GA is supported by the FNR, grant

number C21/BM/15850547/PINK1-DiaPDs. Work of AG was supported by the FNR within the ATTRACT program (Model-IPD, FNR9631103). RK obtained funding from the FNR PEARL Excellence Programme [FNR/P13/6682797], the Michael J. Fox Foundation, and the European Union's Horizon2020 research and innovation program (WIDESPREAD; CENTRE-PD; grant agreement no. 692320). In addition, RK, AG and GA were supported by the FNR CORE grant MiRisk-PD (C17/BM/11676395).

Appendix A. Supplementary data

Supplementary data to this article can be found online at https://doi.org/10.1016/j.scr.2023.103145.

References

Berenguer-Escuder, C., Grossmann, D., Massart, F., Antony, P., Burbulla, L.F., Glaab, E., Imhoff, S., Trinh, J., Seibler, P., Grünewald, A., Krüger, R., 2019. Variants in Miro1 cause alterations of ER-mitochondria contact sites in fibroblasts from Parkinson's disease patients. J. Clin. Med. 8 (12), 2226.

Berenguer-Escuder, C., Grossmann, D., Antony, P., Arena, G., Wasner, K., Massart, F., et al., 2020. Impaired mitochondrial-endoplasmic reticulum interaction and mitophagy in Miro1-mutant neurons in Parkinson's disease. Hum. Mol. Genet. 29, 1353–1364. https://doi.org/10.1093/hmg/ddaa066.

Grossmann, D., Berenguer-Escuder, C., Bellet, M.E., Scheibner, D., Bohler, J., Massart, F., Rapaport, D., Skupin, A., Fouquier d'Hérouël, A., Sharma, M., Ghelfi, J., Raković, A., Lichtner, P., Antony, P., Glaab, E., May, P., Dimmer, K.S., Fitzgerald, J.C., Grünewald, A., Krüger, R., 2019. Mutations in RHOT1 disrupt endoplasmic reticulum-mitochondria contact sites interfering with calcium homeostasis and mitochondrial dynamics in Parkinson's disease. Antioxid. Redox Signal. 31 (16), 1213–1234.

Grossmann, D., Berenguer-Escuder, C., Chemla, A., Arena, G., Kruger, R., 2020. The emerging role of RHOT1/Miro1 in the pathogenesis of Parkinson's disease. Front. Neurol. 11, 587. https://doi.org/10.3389/fneur.2020.00587.

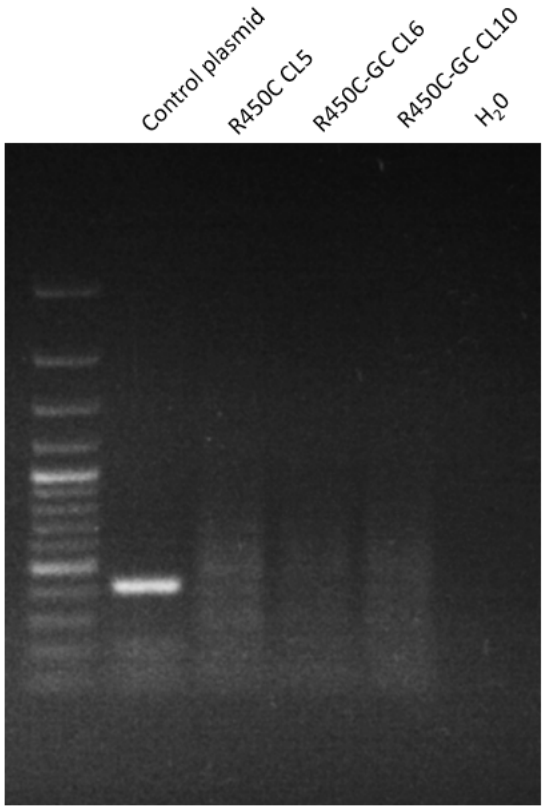

Supplementary Figure 1: Loss of reprogramming vectors in the RHOT1 R450C mutant and gene corrected iPSC lines. gDNA extracted from the indicated cell lines was subjected to PCR using the reprogramming vector specific OriP primers. The OCT4 plasmid was used as positive control for OriP amplification. PCR products were then resolved on agarose gel. Ladder: GeneRuler 100bp Plus.

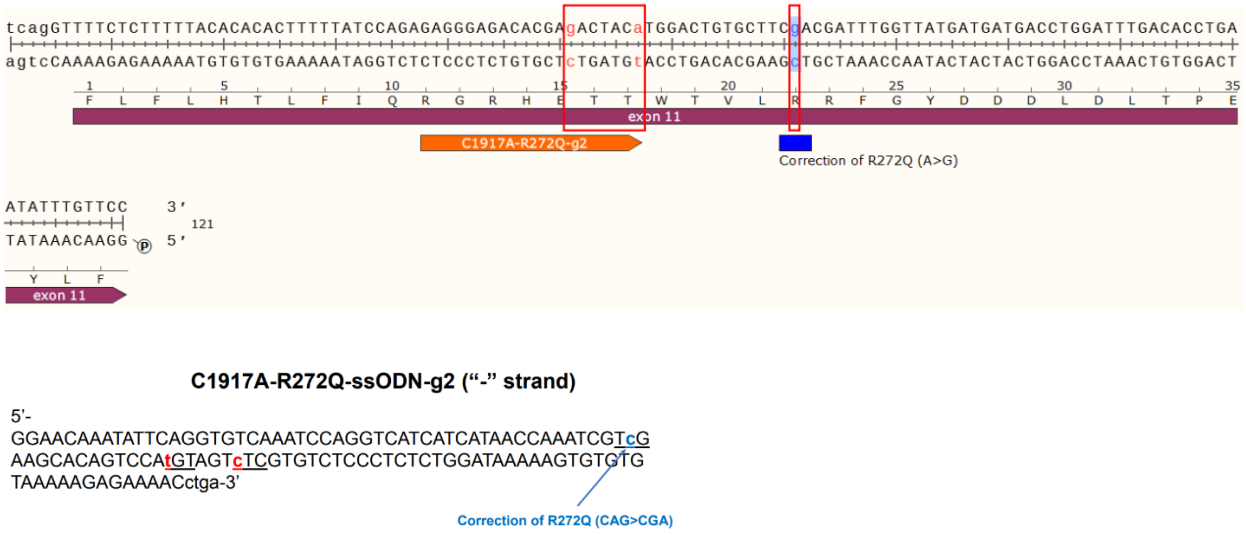

C1917A-R272Q-ssODN-g2 ("-" strand)

5'-
GGAACAAATATTCAGGTGTCAAATCCAGGTCATCATCATAACCAAATCGTcG
AAGCACAGTCCAtGTAGTcTCGTGTCTCCCTCTCTGGATAAAAAGTGTGTG
TAAAAAGAGAAAACctga-3'

Correction of R272Q (CAG>CGA)

Supplementary Figure 2: Schematic diagram of the targeting strategy for correction of the c.815G>A (p.R272Q) mutation in the exon 11 of RHOT1. Location of the patient-specific mutation is highlighted in blue; silent mutations, introduced to prevent Cas9-mediated re-cutting, are indicated in red. gRNA (C1917A-R272Q-g2) is highlighted in orange. Sequence of the ssODN repair template containing homology arms flanking the target site is also indicated.

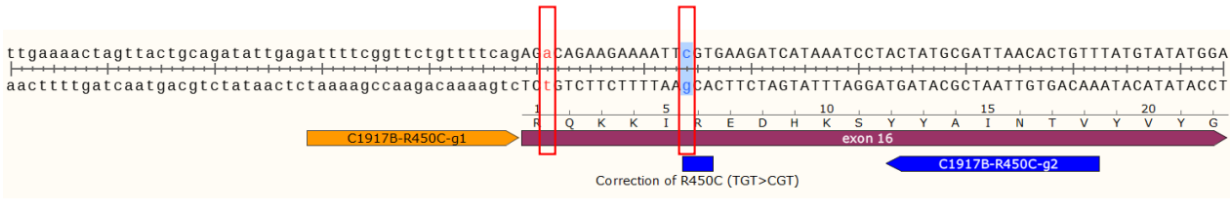

C1917B-R450C-ssODN-g1 ("-" strand)

5'-
TCCATATACATAAACAGTGTTAATCGCATAGTAGGATTTATGATCTTCACgA
ATTTTCTTCTGtCTctgaaaacagaaccgaaaatctcaatatctgcagtaactagttttcaa-3'

PAM

Correction of R450C (TGT>CGT)

Supplementary Figure 3: Schematic diagram of the targeting strategy for correction of the c.1348C>T (p.R450C) mutation in the exon 16 of RHOT1. Location of the patient-specific mutation is highlighted in blue; silent mutation, introduced to prevent Cas9-mediated re-cutting at the PAM site, is indicated in red. gRNA chosen (C1917B-R450C-g1) is highlighted in orange. Sequence of the ssODN repair template containing homology arms flanking the target site is also indicated.

Supplementary Figure 4: Genomic DNA was isolated from both Miro1 mutant (mut) and gene-corrected (GC) iPSC lines (either R272Q or R450C), followed by PCR amplification using primers recognizing the intronic regions adjacent to the corresponding gRNA target sites. GAPDH primers were used as reference for gene amplification.

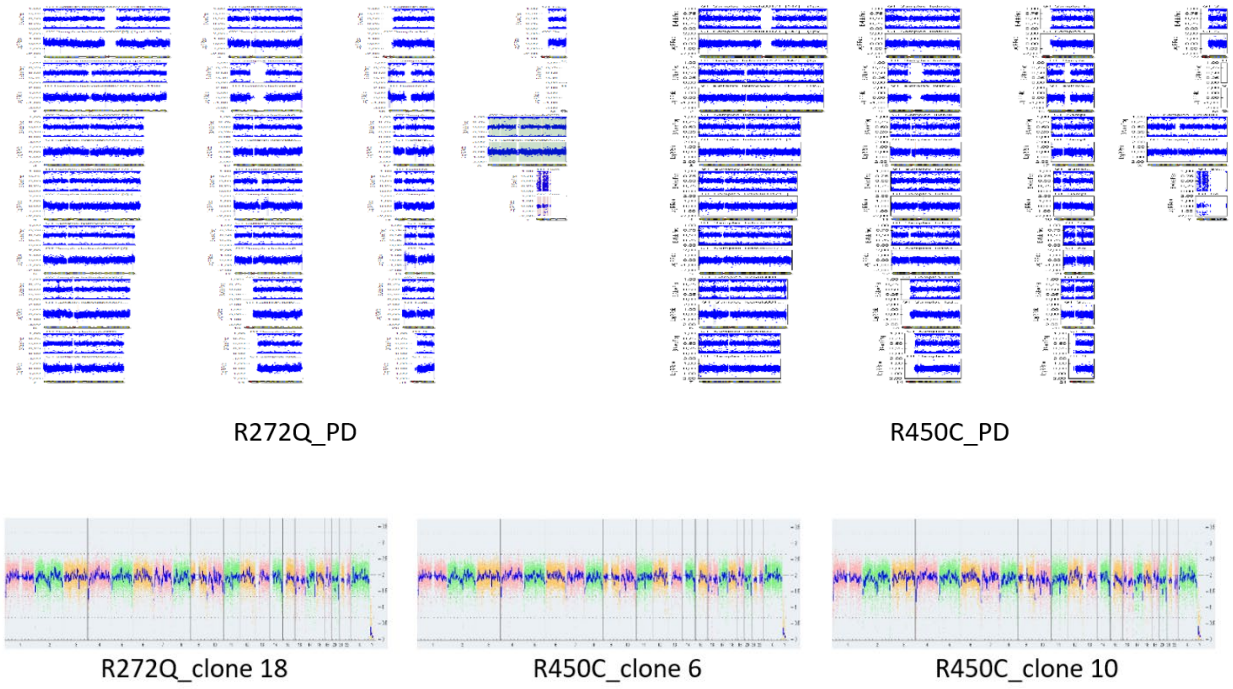

Supplementary Figure 5: PD patient-derived (R272Q_PD and R450C_PD) as well as gene-edited (R272Q_clone 18, R450C_clone 6 and R450C_clone 10) iPSCs were subjected to karyotype analysis using either an Illumina iScan S/N: N234 array (upper panels) or a CytoScan HT-CMA 96F array (lower panels).

R272Q_iPSC

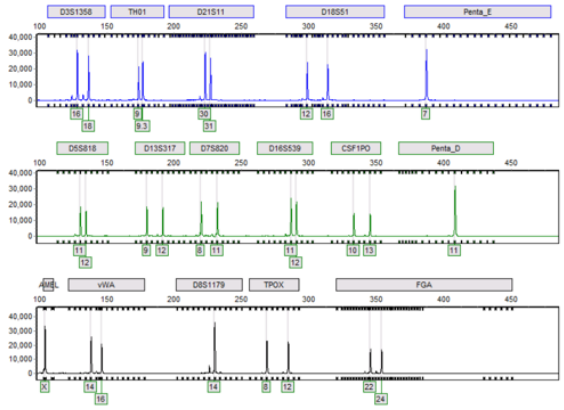

R272Q-GC_iPSC

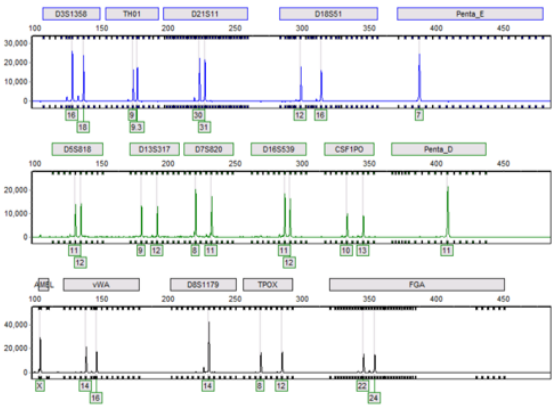

R272Q_fibroblast

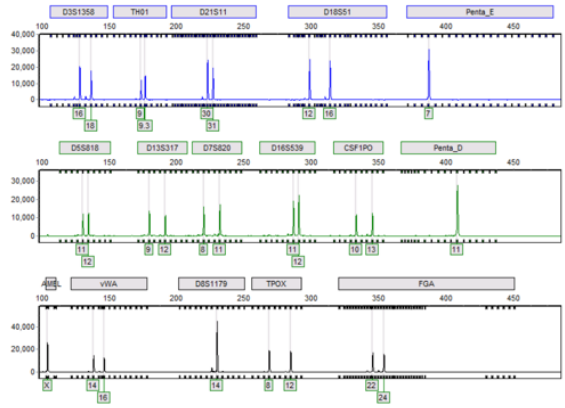

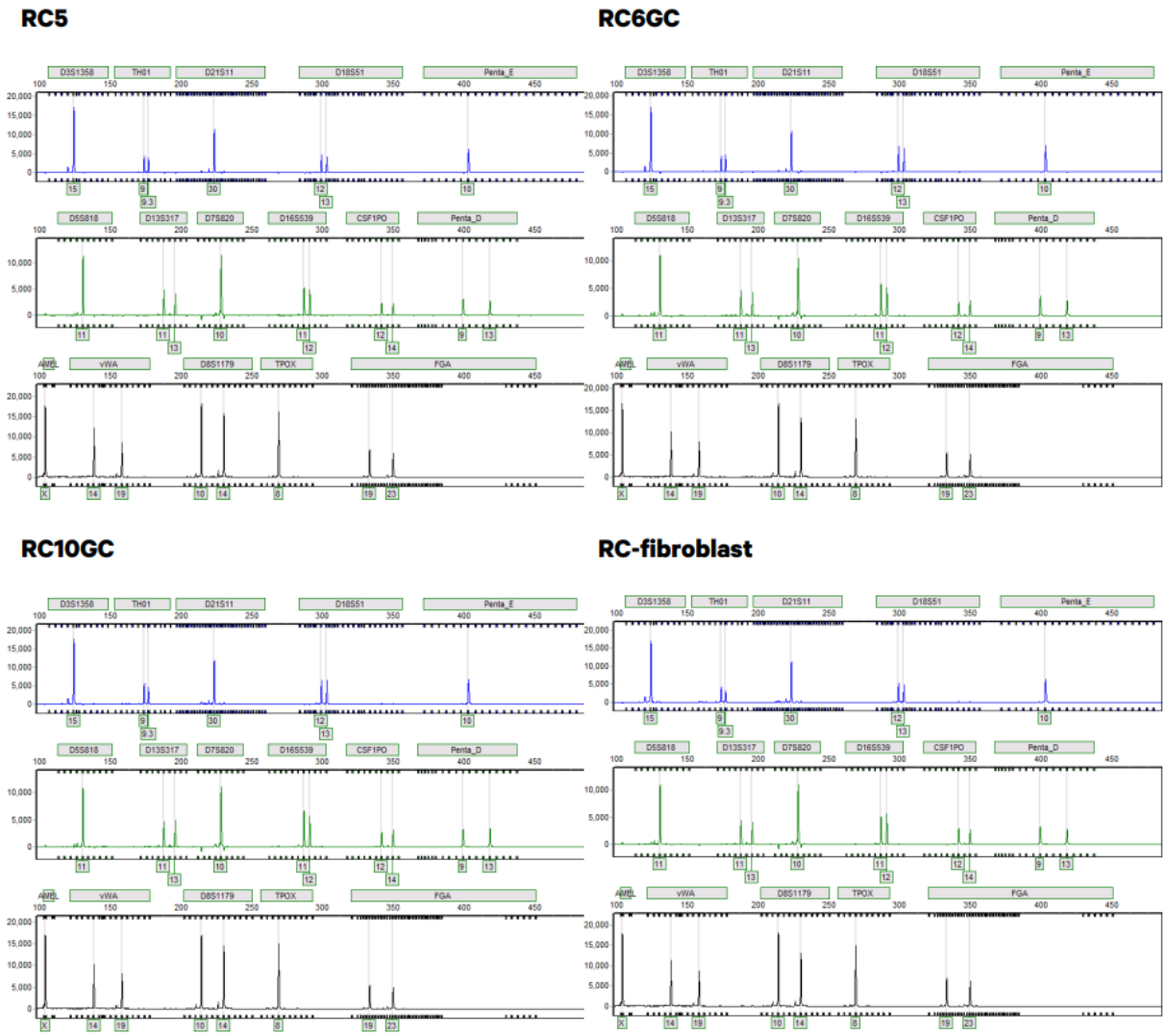

Supplementary Figure 6: Genetic identity analysis. Profiling of the cell lines was done using highly polymorphic short tandem repeat loci (STRs). STR loci were amplified using the PowerPlex® 16 HS System (Promega). Fragment analysis was done on an ABI3730xl (Life Technologies) and the resulting data were analyzed with GeneMarker HID software (Softgenetics).

PCR evaluation

cells	1	2
Hepatitis A	-	-
Hepatitis B	-	-
Hepatitis C	-	-
HIV1	-	-
HIV2	-	-
HTLV 1	-	-
HTLV 2	-	-
Mycoplasma sp.	-	-

Legend: + = positive - = negative id:id = pooled sample range id+id+id = non-range pooled sample NT or blank = no test performed

Supplementary Figure 7: Human pathogens analysis. R272Q (1) and R450C (2) lines were subjected to PCR analysis to exclude the presence of contamination by human pathogens, as indicated.

IV.III Manuscript III

Parkinson's disease-related Miro1 mutation causes mitochondrial dysfunction and loss of dopaminergic neurons *in vitro* and *in vivo*

Chemla et al. 2023

Description of contribution

This manuscript is the result of my PhD project on iPSC-derived neurons, and Miro1 R285Q KI mice. I designed and conducted the experiments, performed the data analysis, conceptualized the figures, and wrote the original draft of the manuscript. Rejko Krüger and Giuseppe Arena supervised and organized the project, conceptualized the experiments, supervised the experiments, and reviewed the manuscript. The organoid part of the project was done by Cláudia Saraiva, who also reviewed the manuscript. All experiments related to midbrain organoids derived from iPSCs were performed by her or other members of Jens Schwamborn's group. Behavioral experiments on mice were done by Jaqueline Jung, and Thorsten Schmidt supervised this part of the project. Matlab-based high content image analysis was done by Paul Antony.

More precisely:

Figure 1: Panel A was created by Cláudia Saraiva. Data for panels B, C, D were generated by Cláudia Saraiva, and analyzed by Kyriaki Barmpa and Alise Zagare. Data for panels E and F were generated by me and analysed by Jochen Ohnmacht.

Figure 2: Data for panels A, B, C, D were generated and analyzed by Cláudia Saraiva. Data for panels E, F, G were generated and analyzed by me.

Figure 3: Data for panels A, B were generated and analyzed by Cláudia Saraiva. Data for panels C, D, E, F were generated and analyzed by me.

Figure 4: Data for panels A, B were generated by Cláudia Saraiva. Panel A was analyzed by Kyriaki Barmpa and Alise Zagare. Panel B was analyzed by Cláudia Saraiva. Data for panels C, D were generated and analyzed by me.

Figure 5: All data were generated and analyzed by Cláudia Saraiva.

Figure 6: The upper part of Panel A was created by me, indicating sequences and genetic modification, while Panel A data (PCR gel and sequencing) were generated by Anne-Marie Marzesco and technicians. Timeline for Panel B was generated by me. Data for panels C and D were generated and analyzed by me. Data for panels E, F were generated by me, western blot performed by Alexandre Baron, and analyzed by me. Data for panel G were generated by Pierre Garcia. Data for panels H, I were generated and analyzed by Jaqueline Jung.

Supplementary figures 1, 2, 4, 6: Data were generated by Cláudia Saraiva and analyzed by Kyriaki Barmpa and Alise Zagare.

Supplementary figure 3: Data for were generated by me and analyzed by Jochen Ohnmacht.

Supplementary figure 5: Data for panel A were generated by Cláudia Saraiva and analyzed by Kyriaki Barmpa and Alise Zagare. Data for panel B were generated by me and analyzed by Jochen Ohnmacht.

Supplementary figure 7: Data for panels A, I, J, K were generated and analyzed by Jaqueline Jung. Data for panel B, C, D, E, F, G were generated and analyzed by me. Data for Panel H were generated by Pierre Garcia.

This manuscript refers to the characterization of the effect of the Miro1 p.R272Q in 3 different models, 2D iPSC-derived neurons, midbrain organoids, and mice.

First, we focused on *in vitro* models derived from a PD patient carrying the heterozygous p.R272Q mutation in Miro1. iPSC-derived neurons from this patient displayed disrupted calcium homeostasis. This was accompanied in 2D iPSC-derived neurons and midbrain organoids by impaired mitochondrial bioenergetics, reduced ATP production and elevated ROS.
Metabolomics analysis revealed that Miro1 mutant neurons have lower NAD cofactors levels, and also take more pyruvate, glutamate, and glycine up, which might be used to compensate for their bioenergetics deficits by increasing the uptake of specific metabolites to either fuel the TCA cycle, or fuel glutathione in order to decrease ROS levels.
Strikingly, we also found increased intracellular α-synuclein levels in mutant p.R272Q 2D neurons compared to their isogenic counterpart. Moreover, dopaminergic neurons (DAN) death was observed in p.R272Q MO increasing with aging, as shown by TUNEL analysis in 20 and 30 days old MO. By using both an isogenic control and cells derived from a healthy patient, this allowed us to 1) decipher the role of the Miro1 p.R272Q point mutation regardless of genetic background giving another argument in favor of its importance when studying PD and 2) show that Miro1 variants can also be used to model typical PD, as many of the phenotypes are present when comparing mutant cells to the WT control and are also found in other genetic forms of PD.

We also made use of a newly generated, KI mouse model carrying the p.R285Q Miro1 mutation (p.R272Q ortholog), which dysplayed three PD signs usually found in patients. Indeed, we observed an age-dependent loss of DANs in the SNpc of mice expressing the ortholog Miro1 mutation, increased levels of PS129 α-synuclein, accompanied by a significant impairment in anterograde procedural memory, three phenotypes that are rarely recapitulated by other *in vivo* genetic models of PD.

Our findings demonstrate that the p.R272Q Miro1 variant is sufficient to comprehensively model PD-relevant cellular phenotypes *in vitro* and *in vivo*, reinforcing a role of PD-specific Miro1 variants in dopaminergic neurodegeneration in PD.

Parkinson's disease-related Miro1 mutation induces mitochondrial dysfunction and loss of dopaminergic neurons *in vitro* and *in vivo*

Authors

Axel Chemla[1], Giuseppe Arena[1], Ginevra Sacripanti[1], Kyriaki Barmpa[1], Alise Zagare[1], Pierre Garcia[1,3], Paul Antony[1], Jochen Ohnmacht[2], Alexandre Baron[1], Jaqueline Jung[4], Anne-Marie Marzesco[1,§], Manuel Buttini[1,3], Thorsten Schmidt[4], Anne Grünewald[1,5], Jens C. Schwamborn[1,*], Rejko Krüger[1,2,6,*], Claudia Saraiva[1,*]

Affiliations

[1]Luxembourg Centre for Systems Biomedicine (LCSB), University of Luxembourg, Luxembourg

[2]Transversal Translational Medicine, Luxembourg Institute of Health (LIH), Luxembourg

[3]Luxembourg Center of Neuropathology (LCNP), LNS, Dudelange, Luxembourg

[4] Institute of Medical Genetics and Applied Genomics, University of Tübingen, Tübingen, Germany

[5]Institute of Neurogenetics, University of Lübeck, Lübeck, Germany

[6]Centre Hospitalier de Luxembourg, Luxembourg

§ Current address: Institute of Experimental Hematology, School of Medicine, Technical University of Munich, 81675 Munich, Germany

* Senior authors

Correspondence: jens.schwamborn@uni.lu (JCS), rejko.krueger@lih.lu (RK) and claudia.saraiva@uni.lu (CS)

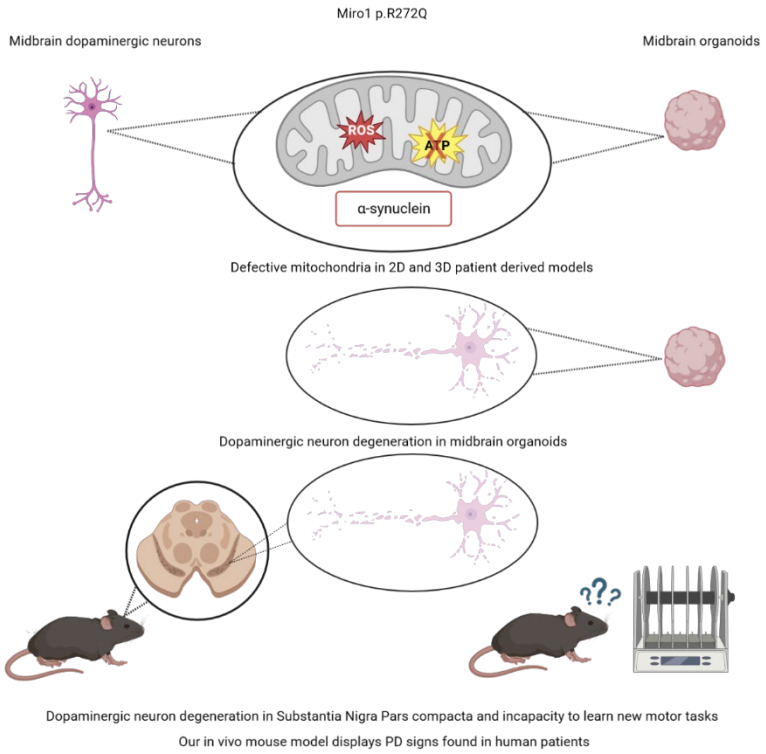

Created with BioRender

Summary

The complex and heterogeneous nature of Parkinson's disease (PD) is still not fully understood. Mitochondrial impairment is a major driver of neurodegeneration in PD. Recently, the regulator of mitochondrial homeostasis Miro1 has been linked genetically and pathophysiologically to PD. Using 2D and 3D patient-based induced pluripotent stem cells models, including isogenic control, showed that the Miro1 p.R272Q mutation leads to mitochondrial impairments including increased oxidative stress, disrupted mitochondrial bioenergetics and altered metabolism. This was accompanied by increased α-synuclein levels in 2D dopaminergic neurons and by a significant reduction of dopaminergic neurons within midbrain organoids. Knock-in mice expressing mutant p.R285Q Miro1 (orthologue of the human p.R272Q mutation) confirmed the PD-specific dopaminergic neuronal loss in the substantia nigra, accumulation of striatal phosphorylated α-synuclein accompanied by behavioral alterations. These findings demonstrate that mutant Miro1 is sufficient to comprehensively model PD-relevant phenotypes *in vitro* and *in vivo*, reinforcing its pivotal role in PD pathogenesis.

Keywords
Miro1, Parkinson's disease, mitochondrial dysfunction, bioenergetic defects, α-synuclein, neurodegeneration, isogenic control, induced pluripotent stem cells, midbrain organoids, knock-in mice.

Introduction

Parkinson's disease (PD) is the fastest growing neurodegenerative disorder worldwide (Ou et al., 2021). The majority of cases are sporadic, while around 5-15% are familial, caused by rare, high penetrance mutations in single genes showing autosomal dominant (e.g. *SNCA*, *LRRK2*) or recessive (e.g. *PINK1*, *PRKN*, *DJ-1*) inheritance (Kim and Alcalay, 2017). Studies on these rare monogenic PD forms provided important insight into cellular and molecular mechanisms underlying neurodegeneration, such as mitochondrial dysfunction, oxidative stress, calcium dyshomeostasis, impaired autophagy and mitophagy, protein misfolding and apoptosis, among others (Paul M A Antony et al., 2013). These could cause the massive loss of dopaminergic neurons observed in the substantia nigra pars compacta (SNpc) of the PD brain, which prompts the well-described motor and some of the non-motor symptoms typical of PD. Surviving neurons in affected brain regions usually display characteristic proteinaceous aggregates (Lewy bodies) containing α-synuclein as a major component (Paul M A Antony et al., 2013).

In sporadic PD patients, besides the impact of common genetic variants explored in large genome-wide association studies, the identification of disease-associated rare genetic variants is increasing, suggesting the contribution of low-frequency variants to disease susceptibility (Germer et al., 2019). We previously identified four PD patients carrying distinct heterozygous mutations in the *RHOT1* gene encoding Miro1 (Berenguer-Escuder et al., 2019b; Grossmann et al., 2019b). Miro1 (mitochondrial Rho GTPase protein) is a conserved element of the mitochondria motor/adaptor complex. It is composed of a C-terminal transmembrane domain, which binds to the outer mitochondrial membrane, and two EF-hand Ca^{2+}-binding domains flanked by two GTPase domains (Klosowiak et al., 2016b). Miro1 plays a fundamental role in regulating not only mitochondrial dynamics (including morphology and transport), but also calcium homeostasis and mitophagy (Grossmann et al., 2020b). Miro1 was also found to physically or functionally interact with well-established PD-related proteins, such as PINK1, Parkin, LRRK2 and α-synuclein, suggesting a possible converging role of Miro1 in controlling different cellular activities and pathways relevant for neurodegeneration in PD (Hsieh et al.,

2019b, 2016b; Shaltouki et al., 2018b; Tsai et al., 2014b; Wang et al., 2011).
Moreover, a pathological stabilization of Miro1, in which its degradation induced by mitochondrial depolarization is impaired, was observed in fibroblasts (Hsieh et al., 2019b) and induced pluripotent stem cells (iPSC) (Nguyen et al., 2021b) from both, sporadic and monogenic, PD patients. In accordance, the pharmacological reduction of Miro1 rescued mitochondrial dysfunction and neurodegeneration in different PD models *in vitro* and *in vivo*, including human iPSC-derived neurons from affected *LRRK2*-G2019S, *SNCA*-A53T carriers and sporadic PD patients as well as Drosophila (Hsieh et al., 2019b, 2016b; Shaltouki et al., 2018b). Moreover, human PD-related mutations in *RHOT1* showed deregulation of mitochondria in fibroblasts and iPSC-derived neurons (Berenguer-Escuder et al., 2020b; Grossmann et al., 2019b; Schwarz et al., 2022b; Schwarz and Fitzgerald, 2022).

In the current study, we dissected the importance of Miro1 in PD pathogenesis by using iPSC-derived dopaminergic neuronal cultures and 3D midbrain organoids (MO), including an isogenic control derived from a PD patient carrying the p.R272Q mutation in Miro1 together with sex and age-matched healthy individuals as controls. We demonstrate that p.R272Q Miro1 leads to an increase in reactive oxygen species (ROS) and altered mitochondrial bioenergetics. This was accompanied by higher α-synuclein levels and loss of dopaminergic neurons *in vitro*. Importantly, degeneration of dopaminergic neurons and accumulation of phospho-α-synuclein was observed in the SNpc of aged knock-in mice expressing the orthologue p.R285Q mutant Miro1, accompanied by deficits in the first trial of the Rotarod behavior test. Altogether, our findings indicate that PD-associated mutant Miro1 is sufficient to model PD *in vitro* and *in vivo*, supporting a role of Miro1 in the pathogenesis of PD.

Results

Miro1 p.R272Q mutation in midbrain organoids and dopaminergic neurons revealed transcriptomic deregulation of major PD-related pathways

To dissect the relevance of Miro1 in PD we used two different iPSC-derived *in vitro* models. We generated midbrain organoids, 3D complex structures with diverse cell types, including functional dopaminergic neurons, and defined spatial orientations mimicking the human midbrain (Monzel et al., 2017b; Zagare et al., 2022). Additionally, we used 2D dopaminergic neurons to dissect in more detail the effects on the main affected cellular population in PD.

These models were generated from iPSC obtained from a PD patient carrying the *RHOT1* c.815G>A (NM_001033568; Miro1 p.R272Q, first EF-hand domain) mutation (PD-R272Q), its correspondent line with point mutation correction (isogenic control, iCtrl) (Chemla et al., 2023) as well as control lines from age- and sex-matched healthy individuals (Ctrl) (Figure 1A; Table1).

Midbrain organoids derived from 1 healthy individual (Ctrl2), PD-R272Q and iCtrl were analyzed using single cell RNA sequencing (scRNAseq). The Seurat integration workflow identified 7 different cellular clusters (Figure 1B) based on the combination of the La Manno et al. gene list (La Manno et al., 2016) and the expression of cell and maturity specific markers (Supplementary Figure 1A-B). UMAP representation showed the presence of midbrain relevant cell types in the organoid model, including the presence of a neural progenitor cluster as well as two dopaminergic neuron clusters: dopaminergic neurons 1 and dopaminergic neurons 2, the later expressing higher levels of tyrosine hydroxylase (TH; Figure 1B, Supplementary Figure 1B). Hierarchical clustering of the top 500 variable genes showed that PD-R272Q organoids were separated from both healthy and isogenic controls, suggesting a significant influence of Miro1 p.R272Q mutation on the transcriptome (Figure 1C). Then, the computed differentially expressed genes (DEG) were used to perform pathway enrichment analysis between PD-R272Q and either Ctrl or iCtrl midbrain organoids. The most relevant shared dysregulated processes and pathways (Figure 1D) from the top 25 (Supplementary Figure 2A) showed a significant deregulation of processes related to neurogenesis, synapses contacts and exocytosis, endoplasmic reticulum (ER) and mitochondrial apoptosis. Pathway maps also showed deregulation of ROS, transcription of HIF-1 targets (important for iron homeostasis and oxidative stress defense (Zhang et al., 2021)), LRRK2 in PD neurons, and dynein-dynactin motor complex in axonal transport in neurons. Remarkably, the main transcriptomic alterations induced by mutant Miro1 seemed to be driven by the dopaminergic neuron clusters (Supplementary Figure 2B).

The transcriptomic profile of iPSC-derived dopaminergic neurons was also assessed using bulk RNAseq. Principal component analysis (PCA) showed a clear separation between PD-R272Q and controls (Figure 1E; Supplementary Figure 3). Gene ontology (GO) and enrich terms analyzed in PD-R272Q vs Ctrl and PD-R272Q vs iCtrl conditions showed deregulation in neuronal projections, axons, secretory vesicles, ER and lysosomal compartments (Figure 1F). These results further support specific Miro1 p.R272Q-dependent transcriptome alterations within dopaminergic neurons.

Miro1 p.R272Q mutant midbrain organoids and dopaminergic neurons showed signs of mitochondrial stress

Pathway enrichment analysis on midbrain organoids scRNAseq data revealed several deregulated genes associated with ROS production (Figure 2A, Supplementary Figure 4), including: i) *ADM*, which is also involved in neurotransmitter release and cell adhesion (Ferrero et al., 2018); ii) *FTL*, essential for iron metabolism and iron-induced stress (Zhang et al., 2021); iii) *PRKCB*, encoding protein kinase C beta type, which negatively correlates with mitochondrial energetic state and autophagy (Castellazzi et al., 2019); iv) *MAPK8* and *MAPK10*, mitogen-activated protein kinases, involved in misfolded protein-induced stress, autophagy, protein transport and apoptosis (Bohush et al., 2018); and v) *UBL5*, important for coping with mitochondrial stress (Benedetti et al., 2006). Deregulation of these ROS-related genes pointed to a possible impairment of mitochondrial homeostasis in PD-R272Q organoids. Western blotting against the mitochondrial outer membrane protein VDAC revealed that mitochondrial mass in organoids was similar between PD-R272Q and controls (Figure 2B). MitoSOX Red was used to measure mitochondrial superoxide levels via flow cytometry. Mutant Miro1 p.R272Q organoids showed a significant increase in the number of MitoSOX-positive events compared with healthy and isogenic controls (Figure 2C). Mitochondria membrane potential (MMP) was assessed by the percentage and the mean fluorescent intensity (MFI) of the TMRM-positive signal within the total mitochondria (MitoTracker Green signal). Midbrain organoids expressing mutant p.R272Q Miro1 showed a significant reduction of the percentage of mitochondria with intact MMP as well as an overall lower MMP in comparison to controls (Figure 2D). Midbrain organoids from the iCtrl showed a significantly higher MMP compared to healthy controls.

In order to understand which of these phenotypes were specific for dopaminergic neurons, we characterized Miro1 p.R272Q mitochondria using dopaminergic neuronal cultures. Imaging-based analyses were performed to assess intracellular ROS, MMP and calcium response. Intracellular ROS were quantified by the MFI of the CellROX Deep Red-positive cells from total cells (Cell Tracker Green-positive signal). In concordance with midbrain organoid data, PD-R272Q neurons showed a significant increase of ROS compared to controls (Figure 2E). For MMP measures, MFI of TMRE (marker of intact MMP) within the total mitochondrial signal was quantified both in basal conditions (DMSO) and under mitochondrial depolarization (FCCP). In DMSO-treated cells, MMP was significantly lower in PD-R272Q neurons compared to the Ctrl, but not to the iCtrl.

However, in response to mitochondrial depolarization, the Miro1 p.R272Q mutant neurons showed a reduced ability to cope with stress, and displayed a significantly reduced MMP compared with both controls (Figure 2F). Finally, due to the nature of the Miro1 p.R272Q mutation that affects Miro1 EF-calcium binding domain (Berenguer-Escuder et al., 2020b; Grossmann et al., 2019b; Schwarz et al., 2022b), and the existing link between impaired cytosolic calcium handling and mitochondrial stress (Baev et al., 2022), calcium response was evaluated. Fluo-4 Direct MFI was measured over time in presence of ionomycin, which promotes a rapid influx of Ca^{2+} into cells. PD-R272Q dopaminergic neurons showed the highest increase in the F1/F0 ratio upon ionomycin administration (Figure 2G). Herein, iCtrl dopaminergic neurons showed an intermediate response to the increased intracellular calcium levels, displaying significant differences compared to both Ctrl and PD-R272Q neurons (Figure 2G). Altogether, our results showed that despite some influence of the patient's genetic background, the Miro1 p.R272Q mutation seems to increase the susceptibility to mitochondrial damage, which might impact mitochondrial energy production.

Miro1 p.R272Q-induced mitochondria stress prompted bioenergetic deficits *in vitro*

To understand the influence of the Miro1 p.R272Q mutation on the energy status of the cells, we analyzed mitochondrial respiration in midbrain organoids using the Seahorse technology. As shown in Figure 3A (left panel), the pattern of oxygen consumption rate (OCR) curves was significantly different between PD-R272Q organoids and both, healthy and isogenic controls. In particular, PD-R272Q organoids showed a significantly lower basal respiration, proton leak and ATP-linked production. Moreover, PD-R272Q organoids displayed a significantly lower non-mitochondrial respiration compared to Ctrl but not to the iCtrl, suggesting a partial contribution of the patient's genetic background. However, when treated with the mitochondrial uncoupler FCCP, PD-R272Q midbrain organoids were still able to respond in a similar way as control organoids, shown by the similar levels of maximal respiration and higher spare respiratory capacity observed (Figure 3A, right panel). Midbrain organoids metabolomic analysis did not show a significant difference in ATP levels (Figure 3B i), indicating potentially compensatory mechanisms from non-mitochondrial metabolic pathways. Nevertheless, PD-R272Q organoids showed significant lower relative abundance of the co-factors NAD and FAD (Figure 3B ii, iii) as well as pyruvate, a key metabolite in the glucose metabolism that feeds the tricarboxylic acid (TCA) cycle (Figure 3B iv).

We further assessed the specific role of the p.R272Q mutation in 2D human dopaminergic neurons, which showed a significant decrease of all OCR-related parameters compared to healthy and isogenic controls (Figure 3C). Interestingly, different from Miro1 p.R272Q organoids, dopaminergic neurons also displayed a significant reduction of maximal respiration and spare respiratory capacity (Figure 3C, right panel), indicative of their inability to produce energy via oxidative phosphorylation under high energy demand. The mitochondrial phenotype observed in PD-R272Q dopaminergic neurons was also supported by the robust decrease of intracellular ATP levels in comparison with both controls (Figure 3D). Levels of NAD(H) (Figure 3E i) and NADP(H) co-factors (Figure 3E ii) were also affected in PD-R272Q neurons when compared to isogenic and/or healthy controls, although no significant alterations were observed in their ratio. Interestingly, these energy alterations seemed to be more pronounced between PD-R272Q vs iCtrl than PD-R272Q vs Ctrl, indicating a Miro1 p.R272Q mutation-dependent effect. Metabolomic analysis of dopaminergic neurons media revealed that PD-R272Q neurons released more lactate (Figure 3F i) while taking more pyruvate (Figure 3F ii), glutamate (Figure 3F iii) and glycine (Figure 3F iv) up than iCtrl. Surprisingly, no significant differences were observed in the relative abundance of these metabolites between Ctrl and PD-R272Q neurons. Overall, these results support mitochondria-related bioenergetic defects caused by the p.R272Q Miro1 mutation.

Miro1 p.R272Q mutant dopaminergic neurons showed increased levels of total α-synuclein

Recent evidence points to a direct role of α-synuclein in mitochondrial dynamics and quality control mechanisms (Thorne and Tumbarello, 2022) as well as a possible positive correlation between α-synuclein and Miro1 levels (Shaltouki et al., 2018b). In midbrain organoids, *RHOT1* gene expression levels were not different (Supplementary Figure 5A). Though, DEG analysis showed a significant increase in *SNCA* gene expression in PD-R272Q organoids compared with healthy and isogenic controls (Figure 4A). Nevertheless, no difference in α-synuclein protein levels were observed (Figure 4B). In 2D dopaminergic neurons, *RHOT1* was upregulated in PD-R272Q compared to Ctrl and iCtrl within the bulk RNAseq data (log2 fold change = 0.52 and 1.92, respectively; Supplementary Figure 5B). Likewise, *SNCA* transcript was upregulated in PD-R272Q compared to Ctrl and iCtrl (log2 fold change = 0.79 and 2.31, respectively) – (Figure 4C). In accordance, α-synuclein levels were significantly higher in PD-R272Q dopaminergic neurons compared to iCtrl but not to Ctrl (Figure 4D). These findings suggest that Miro1 p.R272Q might interfere with α-synuclein expression levels.

Increased dopaminergic neuronal cell death in Miro1 p.R272Q midbrain organoids

The loss of dopaminergic neurons is a key hallmark of PD. Immunoblotting analyses showed a significant reduction of the dopaminergic marker TH in PD-R272Q organoids compared with both healthy and isogenic controls (Figure 5A). Similar results were obtained by confocal microscopy, upon quantification of the TH-positive (TH+) signal within the total neuronal population (TUJ1+) (Figure 5B). High content image morphometric analysis (Bolognin et al., 2019; Monzel et al., 2020) revealed that, in mutant organoids, TH+ neurons have a reduced average length (skeleton) compared to Ctrl, but not to iCtrl (Figure 5C i), meaning that TH+ PD-R272Q neurons have in average a smaller cytoskeleton. Moreover, the neurite fragmentation index of TH+ neurons, which is an early indicator of neurodegeneration (Raff et al., 2002), was significantly increased in PD-R272Q organoids in comparison with both Ctrl and iCtrl (Figure 5C ii). In line, scRNAseq analysis showed a clear deregulation of genes related with apoptosis within the dopaminergic neuron clusters (Supplementary Figure 6). Lactate dehydrogenase (LDH) presence in organoids media and the TUNEL apoptotic assay were used to assess cell death. PD-R272Q organoids showed a significant increase in LDH abundance (Figure 5D) and higher levels of DNA fragmentation (as measured by the TUNEL staining; Figure 5E) within the dopaminergic neuron population, compared to Ctrl and iCtrl. Altogether, these findings suggest a selective loss of TH+ neurons in Miro1 mutant organoids, which is mediated, at least in part by apoptosis.

Aged Miro1 p.R285Q knock-in mice showed dopaminergic neuron degeneration and behavioral alterations

The Miro1 protein is evolutionary conserved among species (Grossmann et al., 2020b). The R285 amino acid in mice is the equivalent of the human R272 residue found mutated (i.e., p.R272Q) in the PD patient. Thus, to study the potential contribution of mutant Miro1 to PD pathogenesis *in vivo*, we created a knock-in mouse model by introducing the corresponding Miro1 p.R285Q mutation using CRISPR/Cas9 technology (Figure 6A). Successful generation of knock-in mice was validated by PCR and DNA sequencing analysis in wild-type animals (wt/wt) as well as in heterozygous (wt/R285Q) and homozygous (R285Q/ R285Q) mutant mice (Figure 6A). Miro1 mutation did not interfere with mice weight (Supplementary Figure 7A). Immunohistochemical analysis showed similar levels of TH-positive terminals and dopamine transporter (DAT) in the striatum (Supplementary Figure 7 B,C) and similar TH levels in the SNpc (Supplementary Figure 7D) of young mice (3-6 month-old, Figure 6B).

In 15-month-old mice, striatal TH (Figure 6 C), DAT levels (Supplementary figure 7E) and striatal dopamine (Supplementary Figure 7F) were also unaffected. However, 15-month-old mutant mice showed a significant decrease in the SNpc TH area, reflecting dopaminergic neuron loss in both heterozygous and homozygous mice, an effect that was more pronounced in females (Figure 6D and Supplementary figure 7G). Considering this and the lower number of male mice within the study we proceed the analysis focusing on female mice. Total levels of α-synuclein in the striatum of old mice did not differ (Figure 6E). Nevertheless, old homozygous mutant mice showed significantly more phosphorylated S129 α-synuclein in the striatum (Figure 6F). The presence of phosphorylated S129 α-synuclein inclusions were also qualitatively observed via immunofluorescence in the mice SNpc (Figure 6G and Supplementary figure 7H). 20 month-old mice were monitored for water and food consumption as well as global activity using Phenomaster® cages. No significant differences were observed between the mice (Supplementary Figure 7I, J, K). Then, Rotarod test was used to evaluate spontaneous motor activity (Jakkamsetti et al., 2021) and/or anterograde procedural memory (Richard J Siegert et al., 2006) in 20 (trial 1) and 21 (trial 2) month-old female mice. Heterozygous and homozygous Miro1 p.R285Q mice displayed a significantly reduced latency to fall compared to wild-type mice on their first trial (Figure 6H), but not in the second trial (Figure 6I), which is indicative of compromised motor or motor-learning processes. Taken together, characterization of Miro1 mutant mice suggests a pathological role of p.R285Q (human p.R272Q) point mutation in PD etiopathogenesis.

Discussion

PD is not only a clinically but also genetically heterogenous disease. Besides rare Mendelian mutations in monogenic forms and common variants in genes associated with the common sporadic form of PD, there is growing evidence pointing to an important role of low-frequency variants with substantial effect in PD pathogenesis (Wüllner et al., 2023). Recently, a large study investigating the burden of rare genetic variants in PD based on their predicted functional impact, identified *RHOT1* as one of four genes with the highest burden (4th out 2500 genes) (Makarious et al., 2023). This strongly supports a role for rare variants in the *RHOT1* gene, encoding Miro1, including those previously identified by us (Berenguer-Escuder et al., 2019b; Grossmann et al., 2019b).

Furthermore, a common molecular signature where Miro1 mitochondrial clearance is delayed (Miro1 retention phenotype) has been identified in both familial (*PINK1*, *PRKN*, *SNCA*, *LRRK2*) and sporadic PD cases (Hsieh et al., 2019b, 2016b; Shaltouki et al., 2018b), highlighting Miro1 as a potential convergent player, as well as a potential molecular biomarker in PD (Bharat and Wang, 2020). Due to limited pedigree size the genetic impact of *RHOT1* variants was not accessible to validation via classical Mendelian co-segregation patterns, urging the need for functional characterization. Herein, a novel mouse model in combination with patient-based iPSC-derived 2D and 3D cellular models, including a gene-corrected control, allowed for dissecting neuronal phenotypes related to the Miro1 p.R272Q mutation and their impact on PD pathogenesis. We demonstrated that Miro1 p.R272Q mutation causes mitochondrial dysfunction leading to dopaminergic neuron loss, both *in vitro* and *in vivo*. Importantly, we unveiled Miro1-dependent cellular processes and molecular signatures, providing convincing evidence to supporting its role in neurodegeneration in PD.

In vitro, transcriptomic analysis between Miro1 p.R272Q mutant and healthy or isogenic controls showed a mutation-specific deregulation on PD pathways, which are also known to be altered in sporadic and familial PD, such as LRRK2 and Tau deregulation, oxidative stress, iron homeostasis and apoptosis (Cherubini and Wade-Martins, 2018; Glaab and Schneider, 2015; Nicoletti et al., 2021). For example, the *ADM* gene encoding adrenomedullin – known to protect rat neurons against oxidative stress and apoptosis (Mahmoodazdeh et al., 2020) – was downregulated in PD-R272Q organoids. Of note, the shorter pro-adrenomedullin fragment is implicated in increasing kinesin-mediated mitochondrial velocity (Larráyoz and Martínez, 2012), in line with our previous findings showing reduced mitochondrial speed in Miro1 p.R272Q dopaminergic neurons (Berenguer-Escuder et al., 2020b).
Other ROS-related deregulated genes, such as *UBL5* (ubiquitin-related) and *FTL* (iron-related) have been previously linked to Miro1-mediated mitophagy regulation (Grossmann et al., 2020b) and to a putative iron-calcium-Miro axis (Bharat et al., 2022a), respectively. The iron-calcium-Miro1 axis hypothesis states that elevated iron levels in PD lead to mitochondrial calcium overflow, which might be preceded by reduced calcium sensing Miro1 capability (Bharat et al., 2022a). Indeed, in PD-R272Q condition, we observed high levels of ROS and a reduced number of functional mitochondria. Miro1 is able to sense both cytosolic calcium (Han et al., 2018b) and oxidative stress (L. Li et al., 2021b; Wasilewski and Chacinska, 2021b), with impairments in Miro1 leading to mitophagy alterations and bioenergetics deficits (Bharat et al., 2022a; L. Li et al., 2021b; Wasilewski and Chacinska, 2021b).

A recent study in iPSC-derived dopaminergic neurons, from a healthy individual in which the heterozygous Miro1 p.R272Q mutation had been artificially introduced, showed Ca^{2+} deregulation as well as altered mitochondrial morphology and basal respiration (Schwarz et al., 2022b). In our patient-specific PD-R272Q dopaminergic neurons, we also showed calcium handling dysregulation (Berenguer-Escuder et al., 2020b), which might contribute to the mitochondrial defects observed. Miro1 p.R272Q isogenic control showed an intermediate calcium response, further strengthening the concept that additional factors defining the individual 'genetic background' may influence the occurrence of particular phenotypes (Fahed et al., 2020).

Mitochondrial respiration and energy production were severely impaired in both Miro1 mutant midbrain organoids and dopaminergic neurons (i.e., OCR, NAD and FAD abundance as well as metabolic alterations). These phenotypes were seen more clearly in the 2D dopaminergic neurons, which can be explained by the presence of other cellular populations within midbrain organoids. In fact, Miro1 p.R272Q mutant organoids showed a specific loss of TH-positive dopaminergic neurons in comparison with healthy and isogenic controls. The dopaminergic neuron population found within the midbrain organoids produces dopamine and has pacemaker activity (Monzel et al., 2017b). These features can justify the higher vulnerability of the dopaminergic neuron population to stress and energy loss driven by the Miro1 p.R272Q mutation within the midbrain organoids, modeling the main hallmark of PD (Paul M A Antony et al., 2013). Furthermore, NAD(H) and NADP(H) co-factors were significantly reduced in PD-R272Q dopaminergic neurons, suggesting that energy deficits might come from low availability of these species – essential for cellular function – rather than their imbalance (Lautrup et al., 2019; Xiao et al., 2018). Supporting this, supplementation with NAD+ precursors niacin and nicotinamide riboside showed neuroprotective properties in PD patients (Brakedal et al., 2022; Pérez et al., 2021).

Alpha-synuclein has recently been implicated in mechanisms controlling mitochondrial quality control and dynamics, such as autophagosome-lysosome formation and function, mitophagy, MDV formation, among others (Thorne and Tumbarello, 2022). PD-R272Q dopaminergic neurons showed α-synuclein upregulation in a genetic background-dependent manner, suggesting a dopaminergic-specific α-synuclein accumulation. Previously, a positive correlation between Miro1 and α-synuclein levels was shown in the SNpc of sporadic PD patients (Shaltouki et al., 2018b), further supporting a possible functional link between both proteins.

This link, might be related to altered mitochondrial quality control mechanisms (Thorne and Tumbarello, 2022) or Miro1-dependent calcium deregulation, since disruption in intracellular calcium buffering promotes α-synuclein aggregation (Leandrou et al., 2019b), which can be caused by a direct interaction with the α-synuclein NAC domain (Han et al., 2018). Interestingly, transcriptomics in PD-R272Q organoids and dopaminergic neurons showed extracellular matrix-related genes dysregulation, which is involved in the pathological spreading of proteins (e.g. Tau, α-synuclein, beta-amyloid) typically observed in neurodegenerative disorders (Moretto et al., 2022). Altogether, our results further support a potential direct and/or indirect relation between Miro1 and α-synuclein dynamics, however further studies are needed to better understand the nature of their relationship.

In vivo, we generated the first knock-in mouse model of Miro1 p.R285Q mutant (ortholog of the human p.R272Q mutation) where physiological levels of Miro1 p.R285Q kept mimicking the human condition. Miro1 p.R285Q mutant mice presented significant dopaminergic neuronal loss in the SNpc of aged animals, corroborating the midbrain organoid experiments. Of note, these mice presented elevated levels of phosphorylated S129 α-synuclein, a post-translational modification that has been associated with α-synuclein toxicity and aggregation(Fujiwara et al., 2002b). Indeed, reduction of S129 phosphorylated α-synuclein levels decreased motor deficits in PD mice overexpressing human α-synuclein (Lee et al., 2011b). Furthermore, p.R285Q mice spent significantly less time in the rod at the first trial of the Rotarod task, which might be due to difficulties in performing precise movement (Jakkamsetti et al., 2021) or impaired anterograde procedural memory (Richard J Siegert et al., 2006). Dodson and colleagues showed that SNpc dopaminergic neurons stop firing at movement onset leading to slightly impairments in motor precision in humanized *SNCA* overexpression and *SNCA* knock-out mice models (Dodson et al., 2016). Procedural memory can be divided in the ability to learn new skills (anterograde), and the ability to remember and execute previously learned skills (retrograde). PD patients show decreased implicit learning abilities concerning new motor tasks (anterograde procedural memory), while their motor performance improves over time on pursuit rotor-motor task test (Frith et al., 1986b; Richard J Siegert et al., 2006). Interestingly, rotarod differences in Miro1 p.R285Q mice were dissipated on trial two, suggesting either compensatory mechanisms or lack of pure motor deficits. Similarly, impairments on the first but not consecutive trials of the rotarod test were observed in a transgenic ataxia mouse model(Boy et al., 2009b).

PD is commonly modeled by toxin-based acute challenges that, despite recapitulating SNpc neuronal loss, do not replicate the human PD pathological features (Blesa et al., 2016a). In other PD mouse models, including single knock-out (e.g. *DJ-1, PINK1*, *PRKN*), triple *PINK1*/*PRKN*/*DJ-1* knock-out or *LRKK2*-R1441G transgenic mice, no dopaminergic neurodegeneration was observed albeit their motor coordination is altered (Blesa et al., 2016a; Matthew S Goldberg et al., 2003; Kitada et al., 2009; Sanchez et al., 2014). Herein, we showed that physiological levels of Miro1 with p.R285Q mutation led to behavior impairments and SNpc TH loss in an age-dependent way. LRRK2 knock-in mice have also been used to model PD, showing subtle differences in striatal dopamine content and/or behavior defects (Chang et al., 2022). However, dopaminergic degeneration was only observed in *LRKK2*-G2019S knock-in mice when combined with *SNCA*-A53T overexpression (Novello et al., 2018). In sum, these results point to the unequivocal key role of Miro1 in PD pathogenesis. Interestingly, our knock-in model had a more pronounced effect in females, which could be a sample size limitation and/ or sex specific genetic or hormonal differences. Notably, the PD patient carrying the Miro1 p.R272Q is also female.

An important question still not addressed is how PD patient heterozygous Miro1 p.R272Q mutation affects Miro1 overall activity. The mutation is located in the calcium sensing domain, with a predicted toxic gain-of-function (Grossmann et al., 2019b), supported by our current data. However, considering the current experimental setup and the Miro1 different domains further experiments are needed to clearly understand if p.R272Q is a gain- or loss- of function mutation. Miro1 knock-out is lethal, while conditional neuronal Miro1 knock-out or long deletion led to mitochondrial dysfunction and neurodegeneration (Lpez-Doménech et al., 2016b; Lpez-Doménech et al., 2021). However, Miro1 overexpression in animal fibroblasts also resulted in mitochondrial morphology and transport issues (Fransson et al., 2003). Similarly, we and others showed mitochondrial dysfunction in Miro1 mutant cells (Berenguer-Escuder et al., 2020b; Grossmann et al., 2019b; Schwarz et al., 2022b; Schwarz and Fitzgerald, 2022). Remarkably, all Miro1 alterations culminate in similar mitochondrial dysfunction phenotypes, suggesting that a tight regulation of Miro1 levels and/or activity is needed for maintaining mitochondrial homeostasis, with slight changes being pathogenic for cells, especially for more sensitive cell types such as dopaminergic neurons. In fact, stabilization of wildtype Miro1 levels via downregulation (Hsieh et al., 2019b, 2016b; L. Li et al., 2021c; Shaltouki et al., 2018b) or overexpression (Moller et al., 2017) showed amelioration in mitochondrial-related phenotypes, relevant in PD.

In conclusion, the here presented *in vitro* and *in vivo* models demonstrated that Miro1 p.R272Q mutation is sufficient to cause dopaminergic neuron loss, which might occur via alteration of mitochondrial status. We also showed a possible functional link between p.R272Q mutant Miro1 and α-synuclein. Moreover, we highlighted the importance of rare pathogenic variants, such as those found in *RHOT1*, as key in PD pathogenesis, further demonstrating the importance of genetic variance in PD susceptibility. Altogether, we corroborate the potential of Miro1 as convergent biomolecule and drug target in both familial and sporadic cases of PD as well as its relevance as a model of PD to develop new disease-modifying therapies.

Acknowledgements:

We thank the LCSB sequencing platform (RRID: SCR_021931) and metabolomic platform for the bulk RNAseq and LC-MS and GC-MS experiments, respectively. We also thank Aurélien Ginolhac for developing the snakemake pipeline and François Massart for technical help in performing mouse genotyping. We acknowledge Wolfgang Wurst and Florian Giesert for hosting Anne-Marie Marzesco within the *Helmholtz Zentrum München* as part of the knowledge transfer program, from which the Miro1 p.R285Q mutant mice were generated. We thank Dr. Wagner Zago, Prothena Bioscience, for gifting the 11A5 antibody.

This work was mainly supported by the Luxembourg National Research Fund (FNR) under the CORE Junior Program (C19/BM/13535609; C.S. & J.C.S.) and the CORE grant MiRisk-PD (C17/BM/11676395; R.K., A.G. and G.A). R.K. also obtained funding from the FNR PEARL Excellence Program (FNR/P13/6682797), the Michael J. Fox Foundation, and the European Union's Horizon2020 research and innovation program (WIDESPREAD; CENTRE-PD; grant agreement no. 692320). A.C. is supported by the FNR within the framework of the PARK-QC DTU (PRIDE17/12244779/PARK-QC). G.A. is also supported by the FNR CORE Junior grant PINK1-DiaPDs (C21/BM/15850547). A.G. was supported by the FNR within the ATTRACT program (Model-IPD, FNR9631103). The authors also thank Prof. Michel Mittelbronn funded by FNR PEARL (P16/BM/11192868).

Author contribution:

A.C.: Design of experiment, performed, analyzed and interpret 2D and mice immunohistochemistry experiments, manuscript writing and illustration. G.A.: Study design, conceptualization and management of mice work, data collection and interpretation, supervision of work, manuscript revision. G.S.: collection of 3D data. K.B. & A.Z.: analysis and plotting of organoid scRNAseq. P.A.: MATLAB script development for image analysis. J.O.: analysis and plotting of dopaminergic neurons RNAseq. P.G. and M.B.: conceptualization, carry-through and troubleshooting of mice-related experiments. J.J.: mice behavioral experiments. A.M.M.: generation of mice models. T.S.: conceptualization of mice behavior experiments. A.G.: Study design. J.C.S. & R.K.: Conception and study design, supervision of work, administrative and financial support, data interpretation, manuscript revision. C.S.: Conception and study design, supervision of work, performed and analyzed 3D experiments, data interpretation, writing of manuscript, administrative and financial support. All authors approved the final manuscript.

Declaration of interests:

J.C.S. is co-inventor on a patent (WO2017060884A1) describing the midbrain organoid technology used and co-founder of OrganoTherapeutics (organoid-based biotech company). Other authors declare no competing interests.

Figure legends

Figure 1. Miro1 p.R272Q mutation deregulated Parkinson's disease (PD)-related pathways in midbrain organoids (MO) and dopaminergic (DA) neurons.

A) Schematic representation of the *in vitro* models and culture conditions used. **B)** UMAP visualization of healthy control (Ctrl 2), Miro1 p.R272Q mutant (PD-R272Q) and isogenic control (iCtrl) organoids single cell RNA sequencing (scRNAseq) data showed 7 unique cell clusters. Dots are color code by cell cluster and represent individual cells. **C)** Heatmap displaying the top 500 differential expressed genes (DEG) showed a separation between PD-R272Q MO and controls. **D)** Graphics depict the most PD-relevant deregulated network processes (left) and pathways (right) between MO PD-R272Q and Ctrl or iCtrl from the top 25 most deregulated ones (See also Supplementary Figure 2). **E)** Principal component analysis (PCA) plot showed separation at PC1 in PD-R272Q dopaminergic neurons compared with Ctrl and iCtrl, based on the top 500 DEG identified from bulk RNA sequencing analysis. **F)** Graphic displaying the deregulated gene ontology (GO) terms of PD-R272Q dopaminergic neurons *versus* healthy or isogenic controls. For all, significance was considered when p.adjusted value < 0.05.

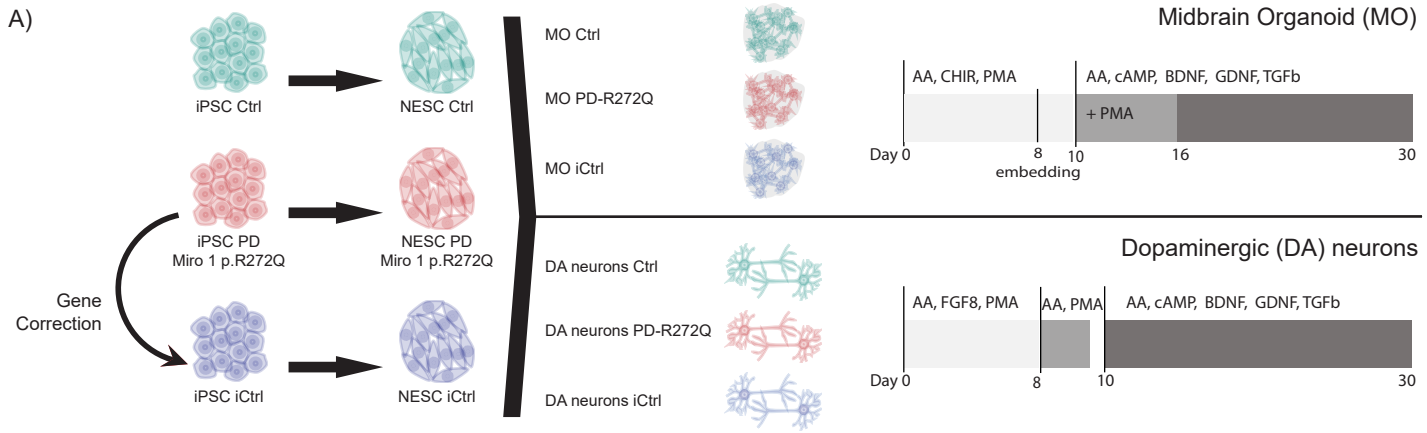

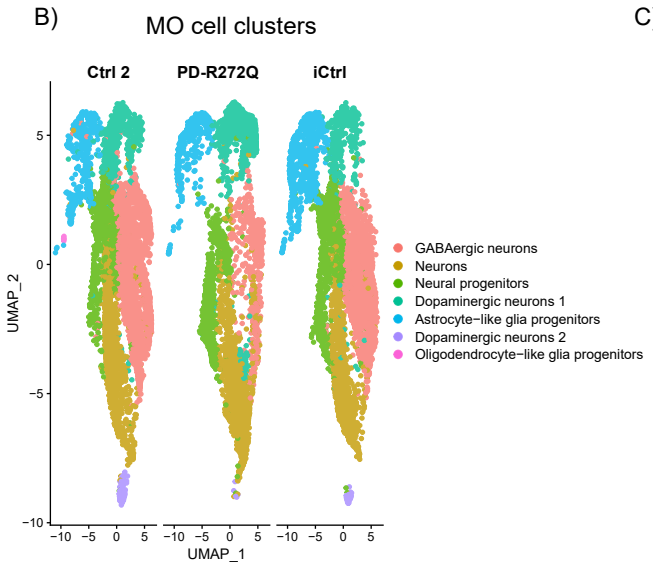

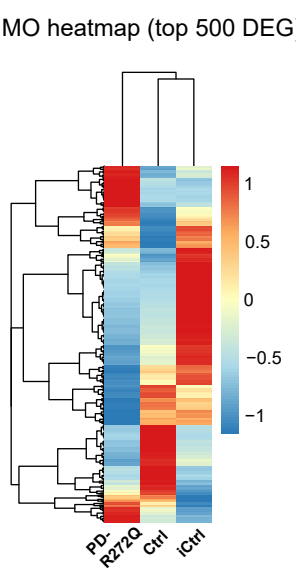

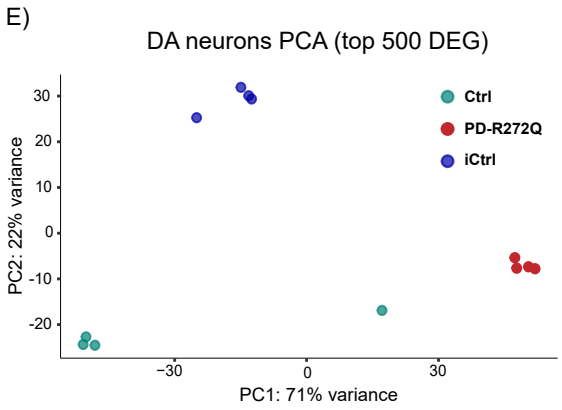

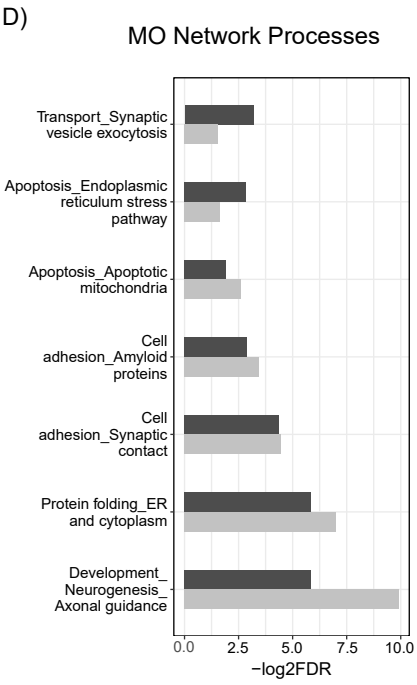

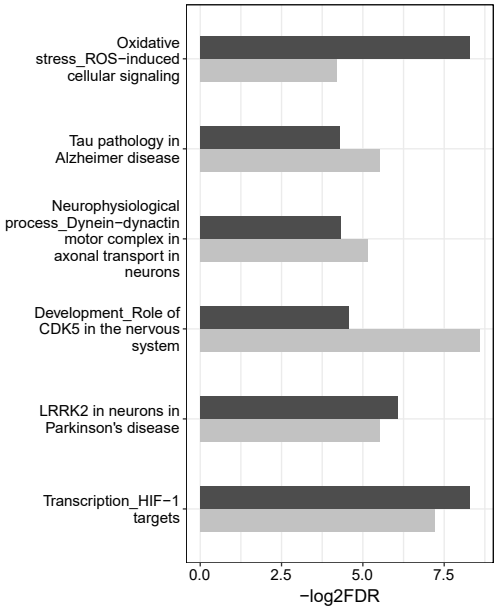

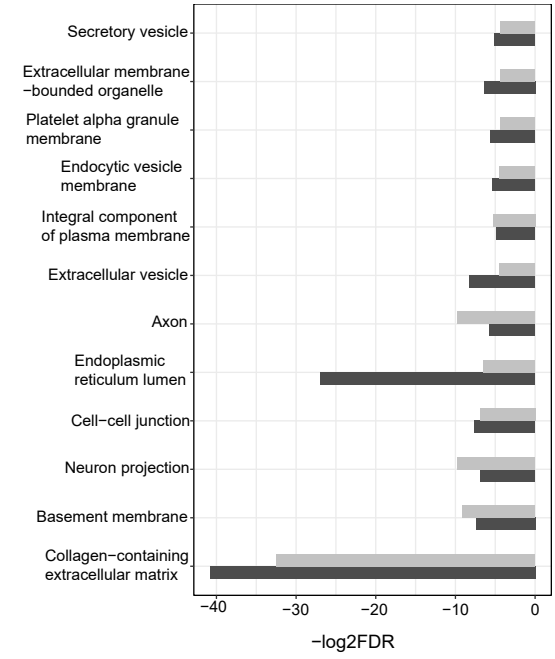

PD-R272Q vs Ctrl PD-R272Q vs iCtrl

Figure 2. Miro1 p.R272Q mutation increased ROS, impaired mitochondrial membrane potential (MMP) and calcium handling *in vitro*. A) Fold change of selected significantly differentially expressed genes between Miro1 p.R272Q midbrain organoids (PD-R272Q MO) and healthy (Ctrl) or isogenic (iCtrl) controls, obtained from the enriched deregulated pathway *'oxidative stress ROS-induced cellular signaling'* (see also Supplementary Figure 4). **B)** Box plot (bottom) showing MO Western blotting against the outer mitochondrial membrane protein VDAC (32 kDa) normalized to the housekeeping protein β-actin (42 kDa). n = 6-18 from 6 independent derivations. Representative images displayed on top. **C)** Flow cytometry representation (left) and quantification (right) of the percentage of MitoSox Red-positive events. n = 8-24 from 6 independent derivations. **D)** Evaluation of MMP using the specific marker TMRM by flow cytometry in organoids. **(i)** Percentage of double positive events for TMRM and Mito tracker Green. **(ii)** Mean fluorescent intensity (MFI) ratio between TMRM and Mito tracker Green within the double positive events. n = 5-21 from 5 independent derivations. **E)** Evaluation of cellular ROS in dopaminergic neurons using live imaging. Left: representative images of dopaminergic neurons containing CellRox deep red (ROS marker; red), Cell tracker green (cellular marker; green) and Hoechst (blue, nuclei) in Ctrl, PD-R272Q and iCtrl. Scalebar: 20 μm. Right: graphs depicting the intracellular CellRox MFI values normalized to iCtrl. n = 33-68, from 5 independent differentiations. **F)** MMP evaluation in dopaminergic neurons, in absence (DMSO) or presence of FCCP by live imaging quantification of mitochondrial TMRE MFI signal (boxplot). n = 63-84 from 4 independent differentiations. **G)** Left: representative images of dopaminergic neurons containing Fluo-4 direct (green), and Hoechst (blue, nuclei) before (zero seconds) and after (120 seconds) ionomycin injection. Scalebar: 50 μm. Middle: Bar plot shows F1/F0 area under the curve (AUC; right). Right: Graphical representation of Fluo-4 direct signal (F1) divided by its basal signal (F0) throughout time assessed by live imaging. n = 84 Ctrl1, n = 344 PD-R272Q, n = 82 iCtrl from 4 independent differentiations (left). All data is presented as median with max/min or mean ± SEM, *$P < 0.05$, **$P < 0.01$, ***$P < 0.001$ using non-parametric multiple comparison Kruskal-Wallis test.

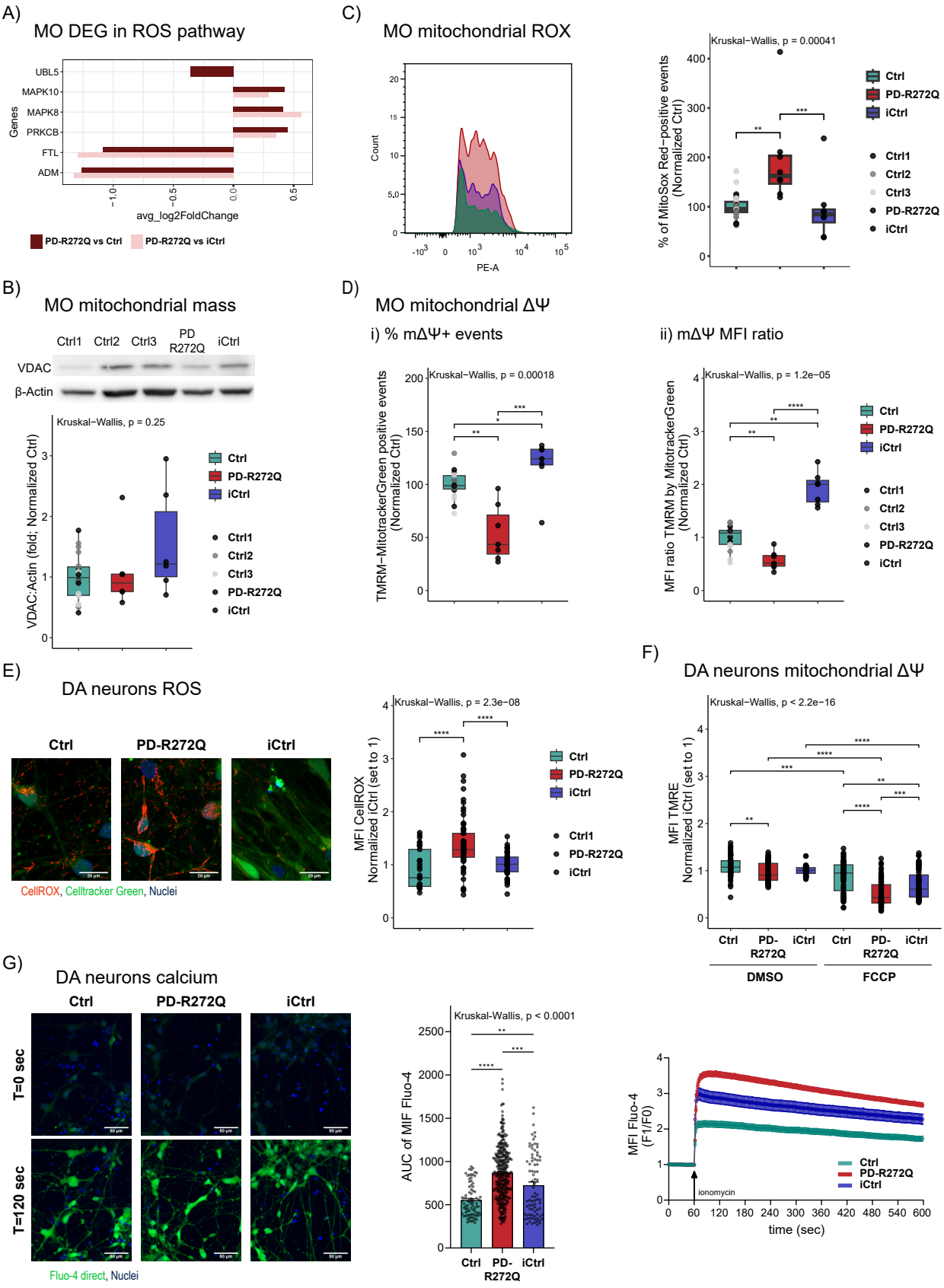
A)
MO DEG in ROS pathway
UBL5
MAPK10
MAPK8
PRKCB
FTL
ADM
Genes
avg_log2FoldChange
PD-R272Q vs Ctrl
PD-R272Q vs iCtrl
C)
MO mitochondrial ROX
Count
PE-A
Kruskal–Wallis, p = 0.00041
% of MitoSox Red–positive events (Normalized Ctrl)
Ctrl
PD-R272Q
iCtrl
Ctrl1
Ctrl2
Ctrl3
B)
MO mitochondrial mass
Ctrl1 Ctrl2 Ctrl3 PD R272Q iCtrl
VDAC
β-Actin
Kruskal–Wallis, p = 0.25
VDAC:Actin (fold; Normalized Ctrl)
D)
MO mitochondrial ΔΨ
i) % mΔΨ+ events
Kruskal–Wallis, p = 0.00018
TMRM–MitotrackerGreen positive events (Normalized Ctrl)
ii) mΔΨ MFI ratio
Kruskal–Wallis, p = 1.2e–05
MFI ratio TMRM by MitotrackerGreen (Normalized Ctrl)
E)
DA neurons ROS
Ctrl
PD-R272Q
iCtrl
CellROX, Celltracker Green, Nuclei
Kruskal–Wallis, p = 2.3e–08
MFI CellROX Normalized iCtrl (set to 1)
F)
DA neurons mitochondrial ΔΨ
Kruskal–Wallis, p < 2.2e–16
MFI TMRE Normalized iCtrl (set to 1)
DMSO
FCCP
G)
DA neurons calcium
T=0 sec
T=120 sec
Fluo-4 direct, Nuclei
Kruskal-Wallis, p < 0.0001
AUC of MIF Fluo-4
MFI Fluo-4 (F1/F0)
ionomycin
time (sec)

Figure 3. Miro1 p.R272Q mutation caused mitochondrial-based bioenergetic deficits *in vitro*. A) Assessment of Miro1 p.R272Q mutant (PD-R272Q), healthy (Ctrl) and isogenic (iCtrl) midbrain organoids (MO) mitochondrial function using Seahorse mito stress test from Agilent. Representative graphic depicts oxygen consumption rate (OCR) over time (minutes, min) under a specific set of drugs: oligomycin, FCCP and antimycin and rotenone. On the right, bar graph shows quantification of the different parameters calculated from the assay. Ctrl n = 197, PD n = 53, iCtrl n = 35 organoids from 5 (iCtrl) or 9 (Ctrl, PD-R272Q) independent derivations. **B)** Relative abundance of (i) ATP, (ii) NAD, (iii) FAD and (iv) pyruvate intracellular metabolites in MO upon targeted liquid chromatography – mass spectrometry (LC-MS)**.** n = 5-15 from 2 independent derivations. **C)** Graphics display OCR by time (left) and feature quantification (right) from Seahorse Mito stress test in dopaminergic neuronal cultures; n = 29-34 from 3 independent differentiations. **D)** Intracellular ATP levels in dopaminergic neurons. n = 14 from 5 independent differentiations. **E)** Intracellular NAD(H) and ratio **(i)** as well as NADP(H) and their ratio **(ii)** relative quantification in dopaminergic neurons. n = 12 from 4 independent differentiations. **F)** Relative quantification of polar metabolites in dopaminergic neuron extracellular media using gas chromatography (GC)-MS. Graphs showed release of **(i)** lactate and uptake of **(ii)** pyruvate, **(iii)** glutamate, **(iv)** glycine metabolites. All data is represented as mean ± SEM or median with max/min . *P < 0.05, **P < 0.01, ***P < 0.001, ****P < 0.0001 using non-parametric multiple comparison Kruskal-Wallis test.

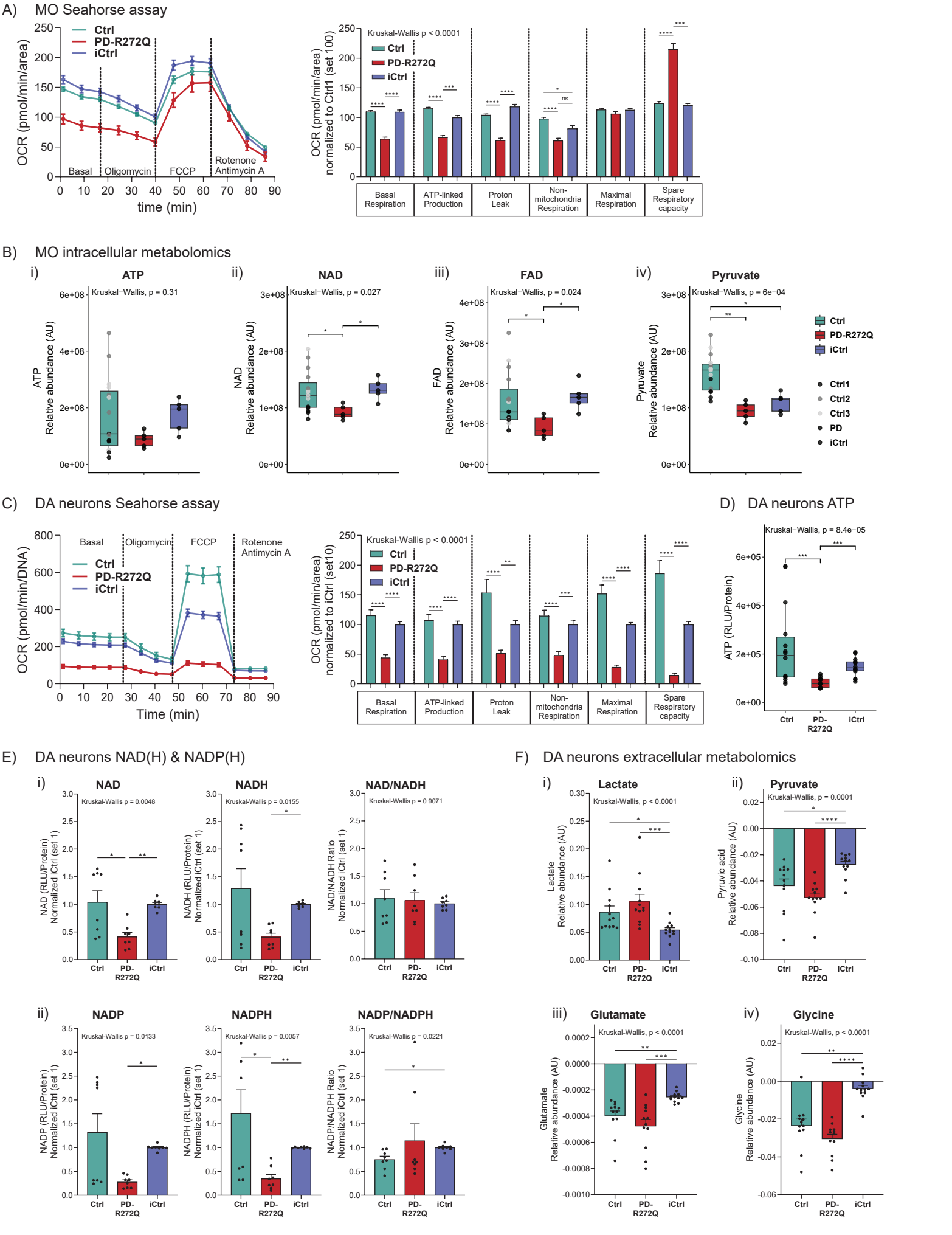
A) MO Seahorse assay
Ctrl
PD-R272Q
iCtrl
OCR (pmol/min/area)
time (min)
Basal
Oligomycin
FCCP
Rotenone
Antimycin A
Kruskal-Wallis p < 0.0001
OCR (pmol/min/area) normalized to Ctrl1 (set 100)
Basal Respiration
ATP-linked Production
Proton Leak
Non-mitochondria Respiration
Maximal Respiration
Spare Respiratory capacity
B) MO intracellular metabolomics
i) ATP
Kruskal–Wallis, p = 0.31
ATP Relative abundance (AU)
ii) NAD
Kruskal–Wallis, p = 0.027
NAD Relative abundance (AU)
iii) FAD
Kruskal–Wallis, p = 0.024
FAD Relative abundance (AU)
iv) Pyruvate
Kruskal–Wallis, p = 6e−04
Pyruvate Relative abundance (AU)
Ctrl1
Ctrl2
Ctrl3
PD
iCtrl
C) DA neurons Seahorse assay
OCR (pmol/min/DNA)
Time (min)
OCR (pmol/min/area) normalized to iCtrl (set10)
D) DA neurons ATP
Kruskal–Wallis, p = 8.4e−05
ATP (RLU/Protein)
E) DA neurons NAD(H) & NADP(H)
i) NAD
Kruskal-Wallis p = 0.0048
NAD (RLU/Protein) Normalized iCtrl (set 1)
NADH
Kruskal-Wallis p = 0.0155
NADH (RLU/Protein) Normalized iCtrl (set 1)
NAD/NADH
Kruskal-Wallis p = 0.9071
NAD/NADH Ratio Normalized iCtrl (set 1)
ii) NADP
Kruskal-Wallis p = 0.0133
NADP (RLU/Protein) Normalized iCtrl (set 1)
NADPH
Kruskal-Wallis p = 0.0057
NADPH (RLU/Protein) Normalized iCtrl (set 1)
NADP/NADPH
Kruskal-Wallis p = 0.0221
NADP/NADPH Ratio Normalized iCtrl (set 1)
F) DA neurons extracellular metabolomics
i) Lactate
Kruskal-Wallis, p < 0.0001
Lactate Relative abundance (AU)
ii) Pyruvate
Kruskal-Wallis, p = 0.0001
Pyruvic acid Relative abundance (AU)
iii) Glutamate
Kruskal-Wallis, p < 0.0001
Glutamate Relative abundance (AU)
iv) Glycine
Kruskal-Wallis, p < 0.0001
Glycine Relative abundance (AU)
Ctrl
PD-R272Q
iCtrl

Figure 4. Dopaminergic neurons with Miro1 p.R272Q mutation showed higher α-synuclein levels. A) SNCA expression levels in midbrain organoids (MO) obtained from transcriptomic data. **B)** MO showed similar levels of α-synuclein in immunofluorescent staining. n =9-27 from 5 independent derivations. **C)** SNCA expression levels in dopaminergic neurons infer from bulk RNA sequencing analysis. **D)** Top: Representative image of α-synuclein (15 kDa) and housekeeping gene β-actin (42 kDa) Western blotting in dopaminergic neurons. Bottom: α-synuclein levels quantification. n = 4. Data presented as median with max/min. *P < 0.05, **P < 0.01, using non-parametric multiple comparison Kruskal-Wallis test **(B)** or ANOVA with post-hoc Tukey HSD test **(D)**.

A) MO SNCA expression

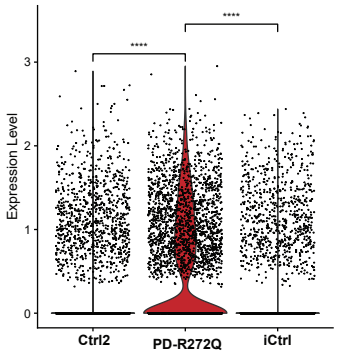

B) MO α-synuclein levels

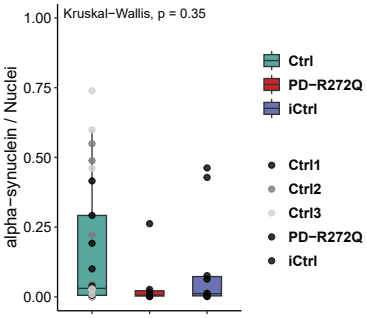

C) DA neurons SNCA expression

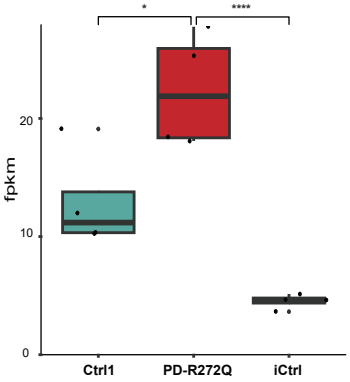

D) DA neurons α-synuclein levels

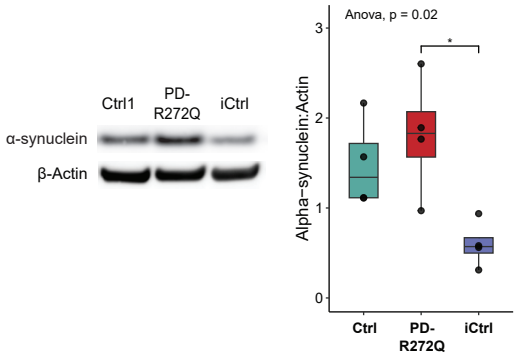

Figure 5. Miro1 p.R272Q mutant midbrain organoids (MO) showed signs of dopaminergic neuron loss. A) Tyrosine hydroxylase (TH) quantification (right) and representative image (left) evaluated in organoids by Western blotting (TH – 60 kDa; β-actin – 42 kDa). Ctrl n = 30, PD-R272Q n = 10, iCtrl n = 6 from 6 (iCtrl) or 10 (Ctrl, PD) independent derivations. **B)** Immunofluorescent analysis of TH-positive (TH+) signal, total neural marker TUJ1 and nuclei (Hoechst) in MO. TH area Scale bar: 200 μm. Graphic displays quantification of the total volume occupied by the TH and TUJ1 double positive signal within the total TUJ1. **C)** Immunofluorescent TH-based morphometric features **(i)** 3D Skeleton and **(ii)** fragmentation index. **B, C)** n = 12-36 from 5 independent derivations. **D)** Quantification of the relative abundance of lactate dehydrogenase (LDH) released into MO media. n = 8-28 from 3 independent derivations. **F)** Immunofluorescent identified TH+ neurons undergoing apoptosis (TUNEL assay). Nuclei are shown in blue. Scale bar: 200 μm. Box plot depicts volume of TH neurons undergoing apoptosis (TH+TUNEL+) normalized by the total TH. n = 7-16 organoids from 3 independent derivation. All data is presented as median with max/min. or mean ± SEM. *P < 0.05, **P < 0.01, ***P < 0.001, ****P < 0.0001 using non-parametric multiple comparison Kruskal-Wallis test **(A, Cii, D, E)** or ANOVA with post-hoc Tukey HSD test **(B, Ci)**.

A) Tyrosine hydroxylase (TH) levels

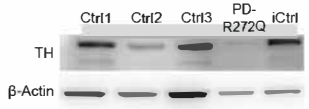

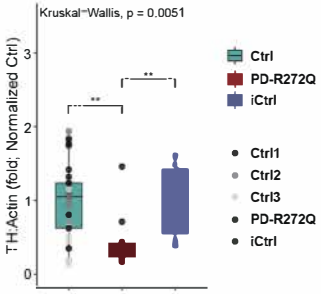

B) TH-positive neurons

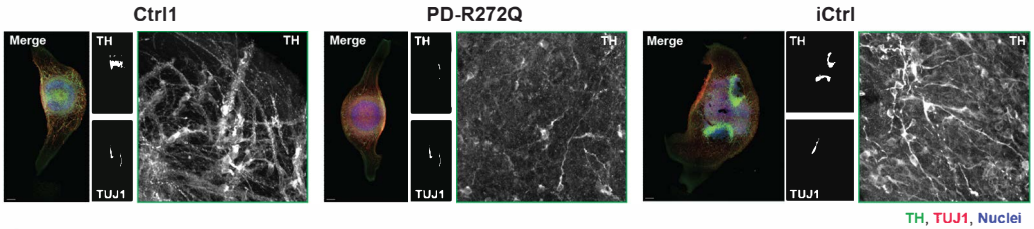

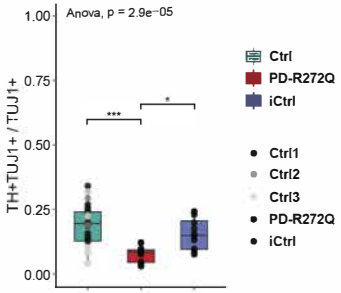

C) i) TH Skeleton

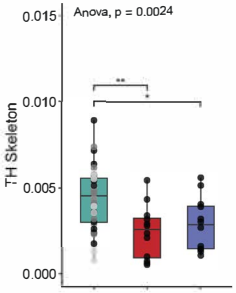

ii) TH Fragmentation

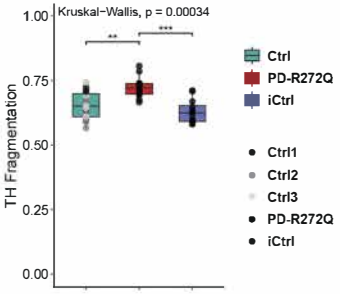

D) LDH release

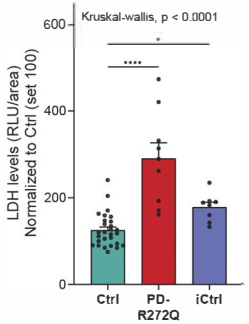

E) TH apoptotic cells

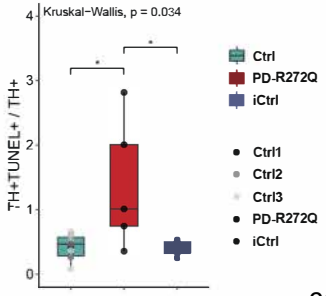

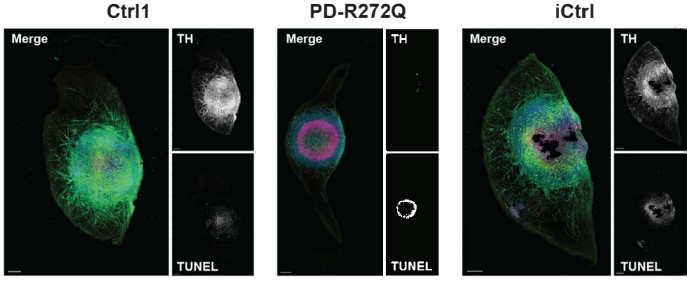

Figure 6. Miro 1 p.R285Q mutant aged mice presented dopaminergic neuron loss and behavior alterations. A) Protein amino acid sequencing and CRISPR/Cas9 guided RNA sequences used in the knock-in Miro1 p.R285Q mouse generation. Agarose gel (left) and DNA sequencing (right) confirming the successful integration of the Miro1 point mutation. **B)** Scheme illustrating the timeline of the experiments and mice used within the study: wildtype mice (wt/wt), heterozygous (wt/R285Q) and homozygous (R285Q/R285Q). **C)** Graphic depicts percentage of striatal tyrosine hydroxylase-positive (TH+) area. **D)** Representative image of SNpc TH immunoreactivity. Scale bar: 50µm. Quantification of the area occupied by TH in substantia nigra par compacta (SNpc) in 15 month-old mice (left) or in female only (right). **C, D)** wt/wt: n = 2M + 5F; wt/R285Q: n = 3M + 5F; R285/R285Q: n = 4M + 6F. **E, F)** Western blotting quantification (bottom) and representative image (top) of total α-synuclein **(E)** and phosphorylated (p)S129 α-synuclein **(F)** in the striatum of 15 old-month female mice. wt/wt n = 9, R285Q/R285Q n = 10. **G)** Representative confocal images of pS129 α-synuclein (red) and TH-positive (green) signal in the SNpc of 15 month-old female wildtype (top) and homozygous (bottom) mice. Arrows depicts pS129 α-synuclein intracellular inclusions. Scalebar 20µm. **H, I)** Bar graph display 21 month-old female mice latency to fall in seconds upon a first **(H)** and second **(I)** trials of Rotarod behavior test. wt/wt: n = 4; wt/R285Q: n = 5; R285/R285Q: n = 6. Graphs are represented as mean ± SEM, each point represents one mouse. *$P < 0.05$, **$P < 0.01$ using non-parametric multiple comparison Kruskal-Wallis test **(C, G, H)** or unpaired T test **(D, E)**. Abbreviation: F, female; M, male.

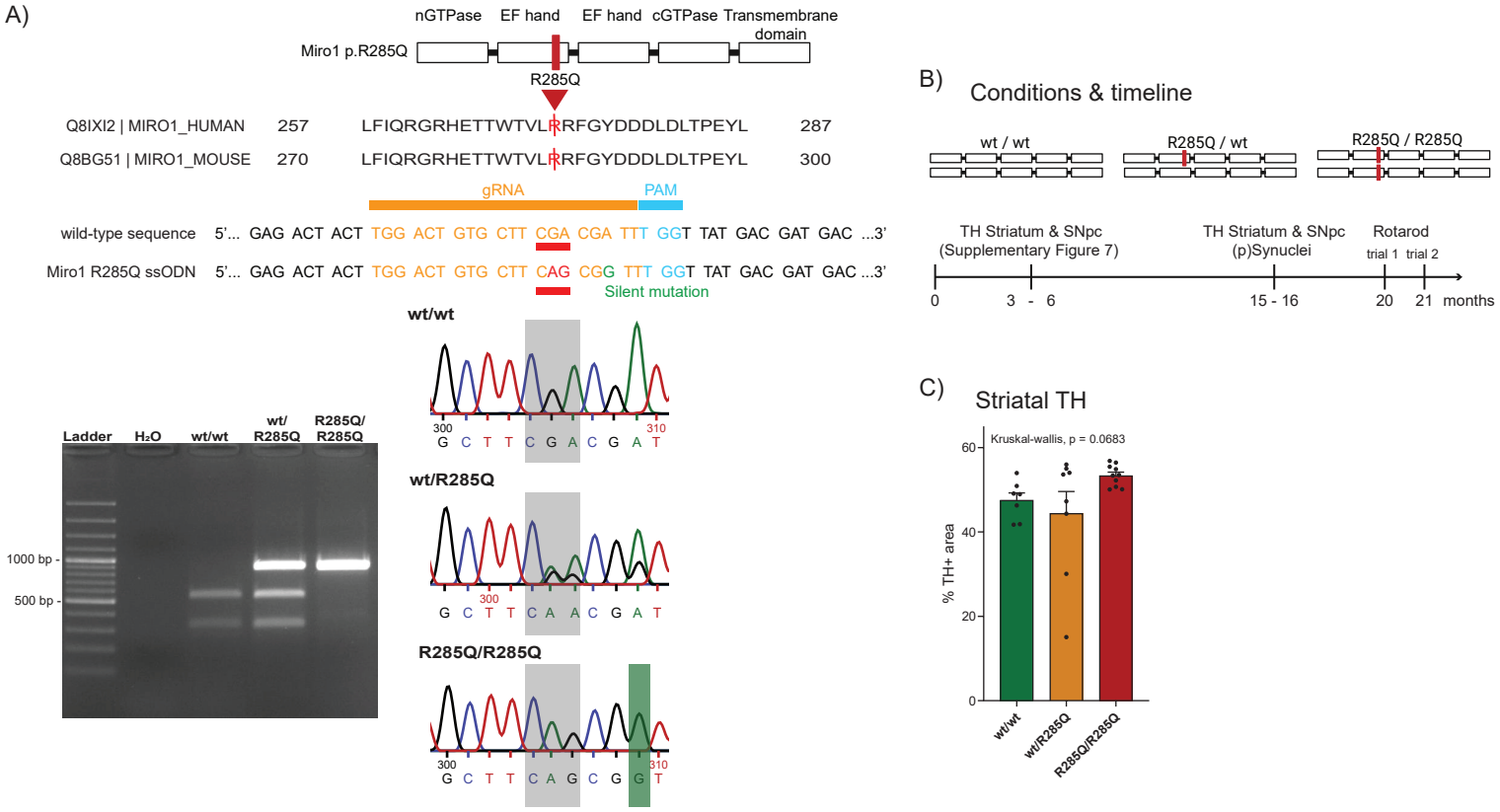
A)
nGTPase
EF hand
EF hand
cGTPase
Transmembrane domain
Miro1 p.R285Q
R285Q
Q8IXI2 | MIRO1_HUMAN 257 LFIQRGRHETTWTVLRRFGYDDDLDLTPEYL 287
Q8BG51 | MIRO1_MOUSE 270 LFIQRGRHETTWTVLRRFGYDDDLDLTPEYL 300
gRNA
PAM
wild-type sequence 5'... GAG ACT ACT TGG ACT GTG CTT CGA CGA TTT GGT TAT GAC GAT GAC ...3'
Miro1 R285Q ssODN 5'... GAG ACT ACT TGG ACT GTG CTT CAG CGG TTT GGT TAT GAC GAT GAC ...3'
Silent mutation
Ladder
H2O
wt/wt
wt/ R285Q
R285Q/ R285Q
1000 bp
500 bp
wt/wt
wt/R285Q
R285Q/R285Q
B)
Conditions & timeline
wt / wt
R285Q / wt
R285Q / R285Q
TH Striatum & SNpc (Supplementary Figure 7)
TH Striatum & SNpc (p)Synuclei
Rotarod
trial 1 trial 2
0
3 - 6
15 - 16
20
21 months
C)
Striatal TH
Kruskal-wallis, p = 0.0683
% TH+ area
wt/wt
wt/R285Q
R285Q/R285Q

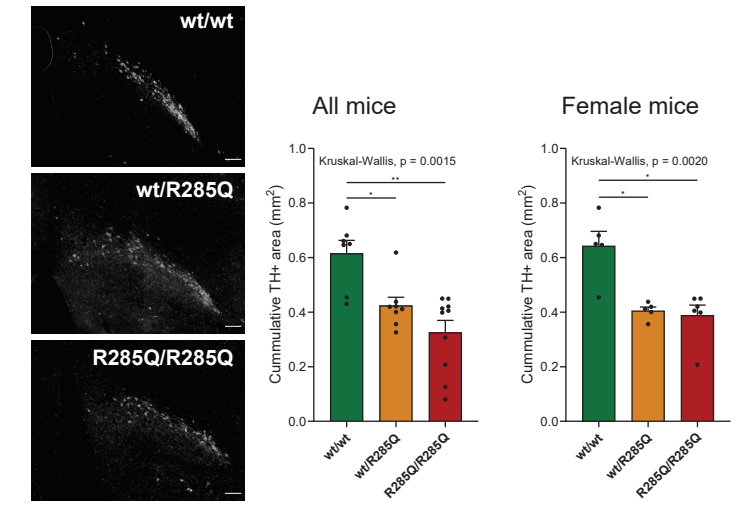
D)
SNpc TH
wt/wt
wt/R285Q
R285Q/R285Q
All mice
Female mice
Kruskal-Wallis, p = 0.0015
Kruskal-Wallis, p = 0.0020
Cummulative TH+ area (mm2)
wt/wt
wt/R285Q
R285Q/R285Q

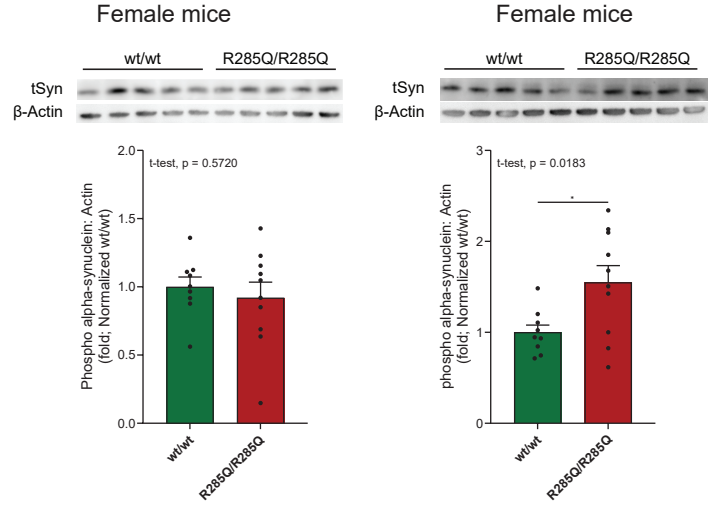
E)
Striatal total α-synuclein
Female mice
wt/wt
R285Q/R285Q
tSyn
β-Actin
t-test, p = 0.5720
Phospho alpha-synuclein: Actin (fold; Normalized wt/wt)
F)
Striatal phospho α-synuclein
Female mice
t-test, p = 0.0183
phospho alpha-synuclein: Actin (fold; Normalized wt/wt)

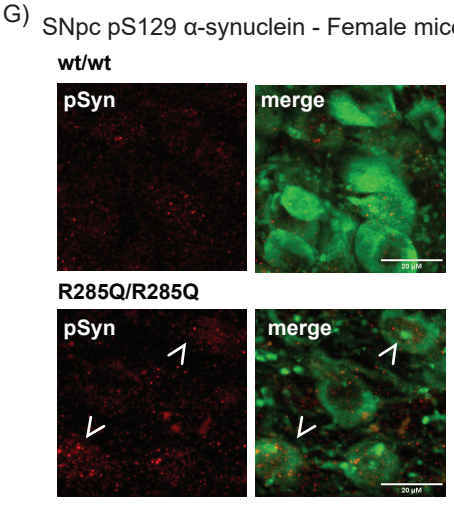
G)
SNpc pS129 α-synuclein - Female mice
wt/wt
pSyn
merge
R285Q/R285Q
phospho-Synuclein, TH

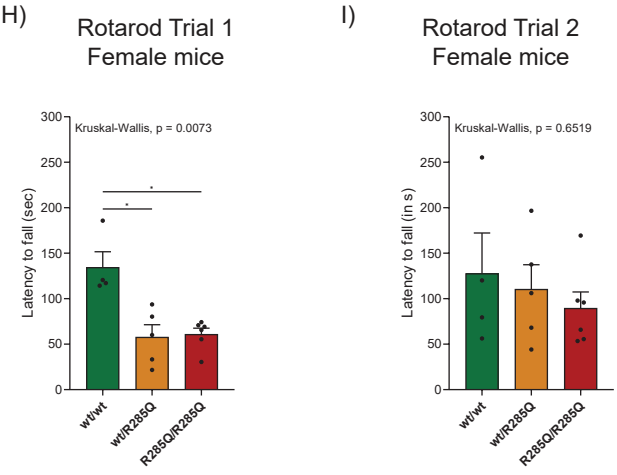
H)
Rotarod Trial 1
Female mice
Kruskal-Wallis, p = 0.0073
Latency to fall (sec)
I)
Rotarod Trial 2
Female mice
Kruskal-Wallis, p = 0.6519
Latency to fall (in s)
wt/wt
wt/R285Q
R285Q/R285Q

Table 1. Description of cell lines used in *in vitro* experiments, both for midbrain organoids and dopaminergic neuronal cultures.

ID	Diagnosis	Genotype	Sex	Age of sampling	Age onset	Reference/Source
Ctrl1	Healthy (Control)	wt/wt	Female	72	-	(Berenguer-Escuder et al., 2020b)
Ctrl2		wt/wt	Female	68		(Zagare et al., n.d.)
Ctrl3		wt/wt	Female	63	-	(Zagare et al., n.d.)
PD-R272Q	PD	Miro1 p.R272Q/wt	Female	78	70	(Chemla et al., 2023)
iCtrl	PD background / Healthy genotype (Isogenic control)	wt/wt	Female	78	70	(Chemla et al., 2023)

Table 2. Antibodies list used for Western blotting and immunostaining experiment in midbrain organoids (MO), dopaminergic neurons (DAN) and mice. aa: amino acid

Antibody	Species	Company	Cat. no	RRID	WB Dilution	IF Dilution	Model
β-Actin	Mouse	Cell Signaling	3700S	AB_2242334	1:50 000 1:20 000	-	MO DAN
DAT	Rat	Millipore	Ab369	AB_2190413	-	1:1000	Mice
MAP2	Chicken	Abcam	ab92434	AB_2138147	-	1:1500	MO
TH	Rabbit	Santa Cruz	sc-14007	AB_671397	1:1000	-	MO
TH	Rabbit	Abcam	ab112	AB_297840	-	1:1000	MO
TH	Rabbit	Millipore	Ab152	AB_390204	-	1:1000	Mice
TH	Chicken	Abcam	Ab76442	AB_1524535	-	1:1000	Mice
TUJ1	Mouse	BioLegend	801201	AB_2313773	1: 50 000	1:1000	MO
VDAC	Rabbit	Cell Signaling	4661	AB_10557420	1:1000	-	MO
α-Synuclein (2A7; aa 61-95)	Rabbit	Novus Biologicals	NBP1-05194	AB_1555287	-	1:1000	MO
α-Synuclein (C42; aa 15-123)	Mouse	BD Transduction	610787	AB_398107	1:1000	-	DAN Mice
α-Synuclein P-S129	Mouse	Prothena	1347	Non commercial	1:1000		Mice

(11A5)							
α-Synuclein P-S129	Rabbit	Abcam	ab51253	AB_869973	-	1:1000	Mice
anti-Rabbit IgG (H+L) Alexa Fluor™ 488	Goat	Thermo Fisher Scientific	**A-11034**	AB_2576217	-	1:1000	MO Mice
Anti-Chicken IgG (H+L) Alexa Fluor™ 488	Goat	Molecular probes	**A-11039**	AB_142924	-	1:1000	Mice
Anti-Chicken IgY (H+L) Alexa Fluor™ 647	Goat	Thermo Fisher Scientific	A-21449	AB_10374876	-	1:1000	MO
Anti-rat IgG (H+L) Alexa Fluor™ 647	Goat	Molecular Probes	A21247	AB_141778	-	1:1000	Mice
anti-Mouse IgM Alexa Fluor™ 568	Goat	Thermo Fisher Scientific	**A-21043**	AB_2535712	-	1:1000	MO
Anti-rabbit HRP	Donkey	Cytiva	NA934	AB_772206	1:1000	-	MO
Anti-mouse HRP	Sheep	Cytiva	NA931	AB_772210	1:1000	-	MO
Anti-mouse HRP	Goat	Novex	A24524	AB_ 2535993	1:10000	-	DAN

STAR Methods

Maintenance of NESC and midbrain organoids generation

Neuroepithelial stem cells (NESC), derived from human iPSC as described previously(Reinhardt et al., 2013), were used to generate midbrain organoids. 5 lines have been used in the current study: 3 lines from healthy individuals (Ctrl), 1 line from a PD patient carrying a heterozygous point mutation at the *RHOT1* gene (PD-R272Q), and the corresponding isogenic line in which the *RHOT1* mutation has been corrected by CRISPR/Cas9-mediated gene editing (iCtrl) (Table 1). Midbrain organoids were generated following our previously described procedure(Monzel et

al., 2017b; Zagare et al., 2021b). Briefly, N2B27 medium, composed of 50:50 DMEM-F12 (Thermo Fisher Scientific, cat. no 21331046) and Neurobasal (Thermo Fisher Scientific, cat. no 10888022), 1% penicillin/streptomycin (Thermo Fisher Scientific, cat. no 15140122), 1% GlutaMAX (Thermo Fisher Scientific, cat. no 35050061), 1:100 B27 supplement without vitamin A (Life technologies, cat. no 12587001) and 1:200 N2 supplement (Thermo Fisher Scientific, cat. no 17502001), was used as the base culture media. NESC were cultured in Geltrex-coated (1:90 dilution in media, Thermo Fisher Scientific, cat. no A1413302) 6-well plates in maintenance media (base culture media further supplemented with 150 µM ascorbic acid (AA, Sigma, cat. no A4544), 3 µM CHIR-99021 (Axon Medchem, cat. no CT99021) and 0.75 µM purmorphamine (PMA, Enzo Life Science, cat. no ALX-420-045) until reaching 80% confluency. NESC cell suspension was then obtained using accutase (Sigma, cat. no A6964) and cell density and viability assessed using Trypan Blue (Invitrogen, cat. no T10282) in an automated cell counter (Countess II, Invitrogen). A total of 9000 cells per well, diluted in 150 µl of maintenance media, were plated in 96-well ultra-low attachment plates (faCellitate, cat. no F202003). Plates were then centrifuged at 100g for 3 minutes at room temperature to promote cell contact and facilitate organoid formation. Organoids were cultured in maintenance media for 10 days with media changes every 2 days. At day 8, organoids were embedded in Geltrex droplets and kept in 24-well plates in dynamic conditions (80 rpm). From day 10 to 16, organoids were cultured in maturation media (base media further supplemented with 200 µM ascorbic acid, 500 µM dbcAMP (STEMCELL Technologies, cat. no 100-0244), 10 ng/ml hBDNF (Peprotech, cat. no 450-02), 10 ng/ml hGDNF (Peprotech, cat. no 450-10), 1 ng/ml TGF-β3 (Peprotech cat. no 100-36E) in the presence of 1 µM purmorphamine, with media changes performed every 2 days. From day 16 onward, organoids were cultured in maturation media with media changes occurring every 3 to 4 days. For assays, such as Seahorse and FACS, due to size limitations, non-embedded organoids were used. Here, organoids were kept in maintenance media for 2 days, then cultured for 6 days in maturation media containing 1 µM purmorphamine (media change every 2 days) and finally kept in maturation media until the assay day, with media changes every 3 to 4 days. To ensure cell quality, all cultures were monthly tested for mycoplasma contamination using the LookOut Mycoplasma PCR Detection Kit (Sigma, cat. no MP0035-1KT).

Generation of 2D midbrain dopaminergic neurons

iPSC-derived NESC (Ctrl1, PD-R272Q and iCtrl; Table 1) were seeded into Geltrex-coated 6-well plates at the density of $3x10^6$ cells/well, unless stated otherwise. Cells were kept in base

culture media supplemented with 1μM purmorphamine (Sigma-Aldrich, cat. no SML0868-25mg), 200μM ascorbic acid, and 100 ng/ml FGF8b (Peprotech, cat. no 10-25) from day 0 (seeding) up to day 8. Between day 8 and day 10, FGF8b was removed and differentiation media contained purmorphamine (0.5μM) and ascorbic acid (200μM) only. Finally, from day 10 onwards, differentiating neurons were kept in maturation media, containing 200 μM ascorbic acid, 500 μM dbcAMP (Santa Cruz, cat. no sc-201567C), 10 ng/ml hBDNF, 10 ng/ml hGDNF, and 1 ng/ml TGF-β3.

Single cell RNA sequencing (scRNAseq) in midbrain organoids

Midbrain organoids dissociation and single-cell isolation

30-days old midbrain organoids from one healthy control (Ctrl2), the PD patient carrying the Miro1 p.R272Q mutation (PD-R272Q) and the respective gene-corrected line (iCtrl) were used for scRNAseq analysis (GEO: GSE237133). A total of 30 embedded organoids per condition were pulled for the analysis. Midbrain organoids were collected from their culture medium and washed with 1x PBS (phosphate-buffered saline, Gibco, cat. no 10010-23). Organoids were digested in 1 ml sCelLive™ Tissue Dissociation Solution (Singleron Biotechnologies, cat. no 1190062) in a 15 ml conical tube (Sarstedt, cat. no 62.5544.003) and placed in a thermal shaker at 50 rpm at 37°C for 30 minutes. The state of dissociation was checked at regular intervals under a light microscope. Following digestion, the suspension was filtered using a 40 μm sterile strainer (Greiner, cat. no 542040). Cells were then centrifuged at 350g for 5 minutes at 4 °C, and the pellets resuspended in 500 μl PBS. Cells were stained with Acridine Orange/Propidium Iodide Stain (Logos Biosystems, cat. no F23001), and the cell number and viability were calculated using LUNA-FX7™ Automated Cell Counter (Logos Biosystems).

scRNAseq library Preparation

The scRNAseq libraries were constructed using GEXSCOPE™ Single Cell RNAseq Library Kit (Singleron Biotechnologies, cat. no 4161031) according to the manufacturer´s instructions.

Briefly, for each library, the concentration of the single-cell suspension was adjusted to $3x10^5$ cells/ml with PBS, and the suspension was loaded onto an SD microfluidic chip to capture 6000 cells. Paramagnetic beads conjugated to oligodT probes carrying a unique molecular identifier (UMI) and a barcode unique to each bead (from the same kit) were loaded, followed by cells lysis. The beads bound to polyadenylated mRNA were extracted from the chip and reverse transcribed into cDNA at 42 °C for 1.5 hours, followed by cDNA amplification by PCR. The cDNA was then fragmented and ligated to indexed Illumina adapters. The fragment size distribution of

the final amplified library was obtained using the Agilent Fragment Analyzer.

Library sequencing

The library concentration was calculated using the Qubit 4.0 fluorometer and the libraries were pooled in an equimolar fashion. The single cell libraries were sequenced on the Illumina NovaSeq 6000 using a 2x150-bp (base pair) approach to a final depth of 90 GB per library. The reads were demultiplexed according to the multiplexing index sequencing on Illumina's BaseCloud platform.

Transcriptome data pre-processing

Pre-processing of Fastq data were conducted using CeleScope® (v.1.3.0; www.github.com/singleron-RD/CeleScope; Singleron Biotechnologies GmbH, RRID SCR_023553) to generate raw data, using default parameters. Low-quality reads were removed. Sequences were mapped using STAR (https://github.com/alexdobin/STAR), and the human reference GRCh38 and genes were annotated using Ensembl 92. The reads were assigned to genes using featureCount (https://subread.sourceforge.net/; RRID SCR_009803) and the cell calling was performed by fitting a negative bimodal distribution and by determining the threshold between empty wells and cell-associated wells, to generate a count matrix file containing the number of Unique Molecular Identifier (UMI) for each gene within each cell.

Transcriptome data processing and plotting

scRNAseq data was analyzed using Seurat R toolkit for single cell genomics version 4.2.0[88] on R version 4.2.2. Cells with unique feature counts lower than 300 and higher than 7000 were removed as low-quality, empty droplets or probable doublets, respectively. Cells with mitochondrial genes higher than 10 or 15% were also filtered out as additional measure for low quality cells. Datasets were merged, log-normalized and integrated based on the 20 PCA components using Seurat integration workflow for better identification of shared cellular populations across the datasets(Stuart et al., 2019). After integration, merged data were scaled to reduce the variance in gene expression across cells. Seven distinct cell populations were identified applying Louvain algorithm modularity optimization with a resolution of 0.15, based on the top 20 principal components. Visualization was done based on their transcriptomic similarities according to the uniform manifold approximation and projection (UMAP) technique(Becht et al., 2019). Cell identities were determined using the online tool GeneAnalytics(Ben-Ari Fuchs et al., 2016), where marker genes of each cell cluster (identified

using the *FindAllMarkers* function of Seurat) were given in the tool for cell type identification choosing *in vitro* parameter for brain cells. The identity of each cluster was further validated by the expression pattern of known cell type specific markers. DEG were detected using the *FindMarkers* function of Seurat, comparing the PD-R272Q midbrain (ident.1) against the Control (Ctrl) midbrain (ident.2) or PD-R272Q midbrain (ident.1) against the isogenic control (iCtrl) midbrain (ident.2) in the whole dataset and for each cellular population separately. Significantly differentially expressed genes (p.adjust < 0.05 and logfc threshold = 0.25) were selected for further enrichment analysis using MetaCore (version 2022 Clarivate; RRID SCR_008125), and Rstudio (R version 4.2.2) used to visualize genes fold change from the most relevant enriched pathways.

Midbrain organoids Western blotting

A total of 3 embedded organoids per cell line per organoid generation (batch) were pulled and snap frozen, followed by protein extraction using RIPA buffer (Abcam, cat. no ab156034) supplemented with 1x Complete™ Protease Inhibitor Cocktail (Roche, cat. no 11697498001) and 1x Phosphatase Inhibitor Cocktail Set V (Merck, cat. no 524629). First, organoids were mechanically dissociated by pipetting in 100 µl of supplemented RIPA buffer followed by a 20 minutes incubation on ice. Lysates were then sonicated at 4 °C for 10 cycles of 30 seconds (sec) on, 30 sec off intervals using the Bioruptor Pico (Diagenode). Lysates were centrifuged at 14,000g for 30 minutes at 4°C, and supernatant was collected. Proteins were then quantified using Pierce™ BCA Protein Assay Kit (Thermo Fisher Scientific, cat. no 23225), according to the manufacturer's instructions. 15 µg of proteins were diluted in 20 µl of 1x loading buffer (62.5 mM Tris (AppliChem GmbH, cat. no 141940), 1.5% Sodium dodecyl sulfate (SDS; GE Healthcare, cat. no 17-1313-01), 8% glycerol (Alfa Aesar, cat. no A16205), 0.03% bromophenolblue (Carl Roth, cat. no T116.1), 0.5 M DL-Dithiothreitol (DTT; Sigma, cat. no 43816-50ml) and then boiled for 5 min at 95 °C. SDS-PAGE using Bolt™ 4-12% Bis-Tris Plus gels, 1.0 mm (Thermo Fisher Scientific, cat. no NW04127BOX or NW04122BOX or NW04120BOX) in either MOPS (Invitrogen™, cat. no B0001-02, MW > 30) or MES (Invitrogen™, cat. no B000202, MW < 30) buffer was used to separate the proteins by mass. Proteins were then transferred into a PVDF membrane, using the iBlot™ 2 Transfer Stacks (Thermo Fisher Scientific, cat. no IB24001 or IB24002) in the iBlot™ 2 Gel Transfer Device (Thermo Fisher Scientific) for 7 minutes. Membranes were fixed with 0.4% paraformaldehyde (Sigma, cat. no 1.00496.5000) at room temperature for 30 minutes, followed by two 10 minutes washes with PBS and 1 hour incubation with 5% skimmed milk (Carl Roth, cat. no T145.4). Membranes were incubated overnight at 4°C

with primary antibodies (table 2) in 5% BSA (Carl Roth, cat. no 8076.3) in PBS with 0.2% tween (Applichem GmbH, cat. no A4974,0500). The following day, membranes were washed 3x for 15 minutes with PBS-T (PBS with 0.02% Tween) and incubated for 2 hours with either anti-rabbit HRP-linked (VWR, cat. no NA934) or anti-mouse HRP-linked (VWR, cat. no NA931) antibodies at 1:1000 dilution (table 2). Finally, membranes were again rinsed 3x for 15 min with PBS-T and revealed using STELLA 8300 imaging system (Raytest) after incubation with chemiluminescent substrate (Life Technologies, cat. no 34580). Proteins of interest were quantified using Image J software (Wayne Rasband; RRID SCR_003070) and normalized for the housekeeping gene beta-actin.

Midbrain organoid immunofluorescence staining

Organoids were fixed overnight in 4% paraformaldehyde at 4 °C under shaking conditions. The following day, midbrain organoids were washed 3x for 15 minutes and embedded in 3% low melting agarose (Biozym Scientific GmbH, cat. no 840100). Seventy micrometer sections were then cut using the Leica VT1000s vibratome and kept at 4 °C in PBS with 0.1% sodium azide until further use. For staining, sections were first blocked and permeabilized in a 5% normal goat serum (Thermo Fisher Scientific, cat. no 10000C) and 0.5% Triton X-100 (Carl Roth, cat. no 3051.3) in PBS with 0.1% sodium azide for 2 hours at room temperature under a shaker. Primary antibodies (table 2), diluted in antibody solution (0.1% sodium azide in PBS, 0.01% triton X-100 and 5% goat serum), were incubated at 4 °C for 48 hours on an orbital shaker. Afterwards, sections were rinsed 3x for 10 minutes with PBS containing 0.01% triton X-100 followed by a 2 hours incubation at room temperature under shaking conditions with the respective secondary antibodies (table 2) and the nuclear marker Hoechst-33342 (Invitrogen, cat. no 62249) diluted 1: 10,000 in antibody solution. Finally, organoids sections were further rinsed 3x for 10 minutes with 0.01% triton X-100 PBS and once with miliQ water and, mounted with Fluoromount-G® mounting media (Southern Biotech, cat.no 0100-01) on DBM Teflon® Slides (De Beer Medicals, cat.no BM-9244).

To assess apoptosis, TUNEL assay was performed using the *In Situ* Cell Death Detection Kit, TMR red (Merck, cat. no 12156792910) in combination TH staining. For this, the abovementioned protocol was followed except the secondary antibody incubation. Secondary antibodies (table 2) and Hoechst-33342 were diluted in the TUNEL kit components (label solution with enzyme solution, 1:9) and incubated for 1 hour at room temperature under an orbital shaker.

Midbrain organoid image acquisition and analysis

Organoids were imaged and analyzed following a pipeline previously described by us(Bolognin et al., 2019; Monzel et al., 2020). Briefly, Yokogawa CV8000 standalone high content screening confocal microscope was used. Cell Voyager and Wako software allowed the automated imaging of organoids section in the x, y and z fields with a 20x objective. Images were then analyzed using adapted in-housed developed MATLAB scripts (v.2021a; RRID SCR_001622). For all experiments, at least one section from 2 organoids per cell line from 3 independent organoid derivations (batches) were quantify unless stated otherwise.

Midbrain organoids Mito stress test (Seahorse XF)

Seahorse XF Cell Mito Stress Test (Agilent) allowed the evaluation of organoids metabolic state using the Seahorse XFe96 Spheroid FluxPak (Agilent, cat. no 102905-100) in 35 day-old non-embedded organoids. The assay measures OCR over a period of time under a specific order of mitochondrial respiration modulators: oligomycin (complex V inhibitor, which inhibits the electron transport reducing OCR), FCCP (uncoupling agent that disrupts proton gradient, when administrated after oligomycin leads to maximal OCR consumption), and finally, rotenone and antimycin (complex I and III inhibitors, respectively, that block any mitochondrial respiration). First, the cartridge containing the O_2 and pH sensors was hydrated with 200 µl of calibrant solution and incubated overnight at 37 °C in a non-CO_2 incubator. On the assay day, spheroids microplates were coated with Corning® Cell-Tak™ Cell and Tissue Adhesive (1:60 dilution in 0.1 M sodium bicarbonate; Corning, cat. no 354240) for 1 hour at 37 °C, followed by 2 washes with warm miliQ water. Organoids were then seeded on the spheroid microplates and incubated for at least 1 hour in a non-CO_2 incubator in Seahorse XF DMEM medium, pH 7.4 (Agilent, cat. no 103575-100) further supplemented with 1 mM L-glutamine (Gibco, cat. no 25030-024), 1 mM pyruvate (Thermo Fisher Scientific, cat. no 11360070), and 21.25 mM glucose (Sigma, cat. no G7021-100g). Cartridge was loaded with assay drugs: 5 µM oligomycin (Sigma, cat. no 75351-5mg), 1 µM FCCP (Abcam, cat. no ab120081), 1 µM antimycin A (Abcam, cat. no ab141904) and 1 µM Rotenone (Sigma, cat. no R8875-1G); and the assay run in Seahorse XFe96 analyzer. Data analysis was done using Seahorse Wave Desktop software (Agilent, RRID SCR_014526). OCR results were normalized by the respective area of each organoids, obtained using Cytation5M reader (BioTek). Datapoints which did not respond to drugs or presented abnormal OCR values were excluded from the analysis. A total of at least 3 organoids per cell line from at least 3 independent organoid generations were used.

Midbrain organoid flow cytometry:

Mitochondrial ROS (MitoSox Red)

5 to 10 non-embedded 30 day-old organoids, per cell line, were pulled into 1 well of a 24-well plate and dissociated into single cells with accutase. Replicates were obtained from pulling different independently culture organoids. For organoid dissociation, pulled organoids were incubated with 300 µl of accutase for 1 hour at 37 °C under dynamic conditions, followed by mechanical dissociation with 1000 µl pipette and 200 µl pipette. Incubation with accutase was repeated for 15 to 25 minutes followed by further trituration with a 200 µl pipette. Cell suspension was then collected, centrifuged at 400g for 5 minutes and wash once with assay media. Samples were then stained with 1 nM MitoSOX™ Mitochondrial Superoxide Indicators (Invitrogen™, cat. no M36008) in phenol-red free DMEM-F12 in combination with live-dead stain Zombie NIR (1: 10,000 dilution; Biolegend, cat. no 423106) and incubated for 25 minutes at 37 °C and 5% CO_2 conditions. Flow cytometer BD LSRFortessa (BD Biosciences) using the BD FACSDiva™ Software (BD Biosciences, RRID SCR_001456) was used to record 10,000 single-cell events per sample. Events counts and intensity were analyzed with FlowJo software (v.10.8.1; RRID SCR_008520). Organoids from at least 3 independent derivations were analyzed.

Mitochondrial membrane potential (TMRM & Mitotracker Green)

Organoid single cell suspension was obtained as described above. Once cells were washed in assay media followed by incubation for 30 minutes at 37 °C and 5% CO_2 with base media containing 1 nM tetramethylrhodamine, TMRM (Invitrogen, cat. no I34361), 100 nM MitoTracker Green (Invitrogen, cat. no M7514) and 1: 10,000 Zombie NIR. Cells were then 2x rinsed in PBS by 400g centrifugation for 5 minutes. Cells were resuspended in PBS and 10,000 single-cell events per sample were recorded at BD LSRFortessa using the BD FACSDiva™ Software. The number and intensity of the events that are double positive for TMRM and Mitotracker Green within the live cell population were analyzed by using FlowJo software (v.10.8.1). Values were obtained from at least 3 independent organoid derivations in 30 days old midbrain organoids.

Midbrain organoids metabolomics

Polar intracellular metabolites were analyzed in 30 day-old organoids. 5 embedded organoids per line were pulled into Precellys tubes, washed 3 times in miliQ sterile water, snap frozen and kept at -80 °C until processed. A total of 5 independent samples coming from 5 pulled organoids from 2 independent organoid derivations (2 batches) were analyzed. Metabolite extraction and relative quantification were done in a blind way.

Metabolite extractions

Metabolite extraction of batch 1 and batch 2 were done separately. Snap frozen organoids were transferred to 2 ml Precellys tubes and 1600 µl (batch 1) or 1500 µl (batch 2) of cold extraction fluid was used. Precellys tubes were prefilled with 600 mg of ceramic beads (1.4 mm, Qiagen, cat. no 1103955) to facilitate metabolite extraction. Pre-cooled (4°C) extraction fluid was composed of 4:1 ratio of methanol (Carl Roth, cat. no AE71.1; Rotisolv, purity ≥ 99.95%) and Mill-Q water (in-house, Milli-Q Advantage A10, 18.2 MΩ•cm, <3 ppb TOC) with 0.8 µg/ml internal standards: internal standards, [$_{13}C^{10}$,$_{15}N^{5}$] AMP sodium (Sigma-Aldrich, cat. no 650676), 6-chloropurine riboside (Sigma-Aldrich, cat. no 852481), 2-Chloroquinoline-3-carboxylic acid (Sigma-Aldrich, cat. no 688517), 4-Chloro-DL-phenylalanine salt (Sigma-Aldrich, cat. no C6506), Nε-Trifluoroacetyl-L-lysine (Sigma-Aldrich, cat. no 53604), sucralose (Sigma-Aldrich, cat. no 69293) and $^{13}C_3$-caffeine-trimethyl (Eurisotop, cat. no CLM-514-1).

Precellys tubes were homogenized with a 30 sec cycle at 6000 rpm (0 to 5 °C). For batch 1, the total volume was divided into 2 Precellys tubes follow by addition of 800 µl of extraction fluid in each followed by a second round of homogenization. A total of 1800 µl of solution from both tubes (batch 1) were transferred to a 2 ml Eppendorf and vortexed (Eppendorf Thermomixer C) for 15 minutes at 2000 rpm (4 °C). For batch 2, after homogenization, 1400 µl of solution was transfer to a 1.5 ml Eppendorf. In both cases, Eppendorf tubes were centrifuged at 21,000g for 10 minutes at 4 °C. After, either two times 500 µl (batch 1) or 800 µl (batch 2) supernatant were transfer to new 1.5 mL Eppendorf tubes, which were evaporated overnight at -4 °C on a refrigerated centrifugal vacuum concentrator (CentriVap 7310000, Labconco). The dried metabolite pellets were stored at -80 °C until LC-MS analysis.

Hydrophilic Interaction Liquid Chromatography- Mass Spectrometry (HILIC-MS) measurements

Targeted HILIC-MS measurement was done using a Themo UHPLC Vanquish UHPLC equipped with a binary pump and coupled to a Thermo Exploris 240 mass-spectrometer. Dried metabolite pellets were reconstituted in 50% ACN and filtered using PHENEX-RC 4 mm syringe filter (Phenomenex, cat. no AF0-3203-52). Metabolites were separated using a Hydrophilic Interaction Liquid Chromatography (HILIC) column (SeQuant ZIC pHILIC, 5 µm particles, 2.1 x 150 mm) protected with a guard column (SeQuant ZIC-pHILIC Guard 20 x 2.1 mm). Detailed LC-MS setting are provided in Supplementary Methodology 1. Peak areas were integrated and exported to Microsoft Excel via the Thermo TraceFinder software (version 5.1; RRID SCR_023045).

Metabolite identification confidence was level 1[92] with all metabolites being verified by an in-house library of standards. Raw values were exported using the sum of all peak areas within a sample. Normalized data was further analyzed using RStudio software (Version 4.3.0; RRID SCR_000432) and further normalized between the different cell lines, to account for cell number differences between conditions, using the Perform Probabilistic Quotient Normalization (PQN).

Midbrain organoids LDH assay

Cell death was evaluated in 30 day-old non-embedded organoids using LDH-Glo™ Cytotoxicity Assay (Promega, cat. no J2380) accordingly to the manufacturer' instructions. Briefly, organoid media was changed to freshly prepared media 24 h before the assay. For the assay, 25 µl of media from at least 2 organoids per cell line from 3 independent organoid derivation were used. 25 µl of LDH detection reagent (25 µl LDH Detection Enzyme Mix with 0.125 µl Reductase Substrate) were added to the 25 µl of organoid media and incubated in lumitrac-600 96-well plate (Greiner, cat. no 655074), at room temperature, for 1 hour under shaking at 400 rpm using a ThermoMixer C (Eppendorf). Luminescent was read at the Cytation5M reader (BioTek). Relative levels of LDH were calculated by LDH luminescence normalized by organoid area set to 100.

Bulk RNA sequencing in dopaminergic neurons

RNA extraction was performed using the RNeasy Kit (Qiagen, cat. no 74104) according to manufacturer's instructions in dopaminergic neurons after 30 days of differentiation using 600 µl RLT lysis buffer containing 1:1,000 2-mercaptoethanol (Sigma Aldrich, cat. no M3148). After RNA extraction, eluted RNA concentration was assessed using a NanoDrop™ spectrophotometer. RNA quality was further assessed using the Agilent 2100 Bioanalyzer showing RNA integrity (RIN) values > 8.

RNA library preparation was performed using TruSeq Stranded mRNA library prep kit (Illumina, cat. no 20020594) according to the manufacturer's protocol, and then sequenced using NextSeq2000 (Illumina) at the LCSB Genomics platform (RRID SCR_021931). For all samples paired end reads of 51 bp length were generated.

Data (GEO: GSE238129) was processed using an in-house snakemake workflow (https://git-r3lab.uni.lu/aurelien.ginolhac/snakemake-rna-seq; release v0.2.3 and singularity image v0.4). Snakemake pipeline is under license https://git-r3lab.uni.lu/aurelien.ginolhac/snakemake-rna-seq/-/blob/main/LICENSE. Raw read quality was assessed by FastQC (v0.11.9; RRID SCR_014583)(Andrews, 2010). Adapters were removed using AdapterRemoval (v2.3.2;

RRID:SCR_011834)(Schubert et al., 2016), with a minimum length of the remaining reads set to 35 bp. Reads were mapped to hg38 (GRCh38.p13) using STAR (v.2.7.9a)(Dobin et al., 2013), and reads were counted using featureCounts from the R package Rsubread (v2.8.1; RRID SCR_016945)(Liao et al., 2019). All transcripts with counts > 10 were used for differential gene expression analysis using the R package DESeq2 (v1.34.0; RRID SCR_015687)(Love et al., 2014). apeglm was used for normalization in DEseq2 (v.1.16.0)(Zhu et al., 2019). FPKM (fragments per kilobase of exon per million mapped fragments) were calculated using DESeq2 package. Pathway analysis on DEG with minimum FPKM of > 1, false discovery rate < 0.05, and a minimum log2-fold change cut-off of +/- 1.5 was performed using Ingenuity Pathway Analysis tool (Qiagen, version: 60467501) and the EnrichR online tool (https://maayanlab.cloud/Enrichr; RRID SCR_001575).

Dopaminergic neurons imaging

iPSC-derived dopaminergic neurons were re-plated on day 15 of differentiation at a density of 100,000 cells per well into PerkinElmer Phenoplate 96-well plates (PerkinElmer, cat. no 6055300) and kept in maturation media until imaged (day of differentiation 30, approximately). Yokogawa CV8000 standalone high content screening microscope using a 60x (intracellular ROS and calcium imaging) or 20x (mitochondrial membrane potential) objective was used for dopaminergic neurons live-cell imaging experiments. To maintain cell integrity during image acquisition, neurons were kept under controlled conditions: 5 % CO_2, 37 °C temperature and 80% humidity. A total of 17 fields for intracellular ROS, 1 field for calcium imaging, and 21 fields in the x, y, z axis were acquired per well. MATLAB scripts (v.2021a) developed in-house were further used for image analysis.

Intracellular ROS (CellROX Deep Red & CellTracker Green)

The cell-permeant CellROX Deep Red dye (Thermo Fisher Scientific, cat. no C10422), which allows for live assessment of intracellular ROS, was used in combination with the general cellular marker CellTracker Green (Thermo Fisher Scientific, cat. no C7025), and nuclei dye Hoechst-33342 (Invitrogen, cat. no 21492) to evaluate intracellular ROS using live imaging. Two days before the assay cells were changed to maturation media without antioxidants (without B27 and ascorbic acid). At the day of the assay, dopaminergic neurons were incubated for 30 minutes with 10 µM CellROX Deep Red, 0.5 µM CellTracker Green and 1 µg/ml Hoechst-33342 at 37 °C with 5% CO_2, washed once with PBS and kept in maturation media during imaging acquisition.

Mitochondrial membrane potential (TMRE & Mitotracker Green)

Dopaminergic neurons were stained with the specific mitochondria membrane potential maker TMRE (Invitrogen™, cat. no T669) at concentration of 20 µM, combined with 0.1 nM MitoTracker Green (Invitrogen™, cat. no M7514) and 1 µg/ml Hoechst-33342 in base culture media for 30 minutes in a cell culture incubator (37 °C with 5% CO_2). Cells were washed once in PBS and further re-incubated in base culture media with 20 µM TMRE followed by live imaging.

Calcium imaging

For calcium imaging, dopaminergic neurons were incubated for 1 hour with 50% maturation media 50% of 2X calcium indicator Fluo4-Direct (Thermo Fisher Scientific, cat. no F10471) following the manufacturer's instructions, and Hoechst-33342 (1 µg/ml). Imaging was done for a total of 10 minutes at 0.5 Hz. For the first minute, imaging was done at basal conditions to establish baseline calcium levels (F0). At minute 1, dopaminergic neurons were exposed to the calcium ionophore ionomycin (10 µM; Sigma-Aldrich, cat. no I0634-1MG), dispensed in an automated way by Yokogawa CV8000, allowing to understand dopaminergic neurons response to calcium influx increase (F1).

Dopaminergic neurons Seahorse mitochondrial stress test

OCR and pH was measured in whole cells using the Seahorse Xfe96 Cell Metabolism Analyzer (Agilent) and Seahorse FluxPak (Agilent, cat. no 103775-100) following Agilent Seahorse mito stress test. Dopaminergic neurons were re-plated at a density of 100,000 cells per well, in maturation media, into Geltex-coated Seahorse Xfe96 well plate 24 hour prior to the assay. After seeding, the plate was left at room temperature for 1 hour to prevent edge-effects. Outer wells were filled with media only and not used for cells seeding to avoid cell stress occurring due to evaporation. Dopaminergic neurons were then kept in a cell culture incubator overnight. Also, at day before the assay, XFe96 sensor cartridge was hydrated using 200 µl of XF-calibrant solution. Seahorse base medium (Agilent, cat. no 102353) was further supplemented with 382 µg/ml D-glucose (Sigma, cat. no D8375), 2 mM (1%) L-glutamine (Gibco, cat. no 35050061) and 40 µg/ml sodium pyruvate (Sigma, cat. no P5280; pH = 7.4 ± 0.05 at 37 °C). Both, cartridge and media were incubated overnight at 37 °C in a non-CO_2 incubator.

At the assay day (day of differentiation 30), the media of dopaminergic neurons was replaced by Seahorse assay media by removing 80 µl of maturation media (leaving 20 µl) from each well, rinsed 2x with 200 µl of Seahorse assay media and finally adding 155 µl of Seahorse assay

media per well to a total final volume of 175 µl/well. The plate was then incubated in a non-CO_2 incubator for at least 1 hour to allow cells to equilibrate. Mitochondria targeted drugs dissolved in Seahorse assay media (25 µl) were loaded into the cartridge: 1 µM oligomycin, 1 µM FCCP (Sigma, cat. no C2920), 0.5 µM antimycin A (Sigma, cat. no A8674) and 0.5 µM Rotenone. After, Mito stress test assay was run in the Seahorse Xfe96 Cell Metabolism Analyzer and OCR and pH measure through time.

Assay normalization was done by DNA quantification using the CyQUANT® assay (Invitrogen, cat. no C7026). For that, the Seahorse assay media was removed and dopaminergic neurons were frozen and stored at -80 °C in the Seahorse cell culture plate until DNA quantification. CyQUANT® components as well as dopaminergic neurons were brought to room temperature. The CyQUANT® GR stock solution was diluted 400-fold into the 1X cell-lysis buffer, 200 µl of solution were added to each well and incubated for 2–5 minutes at room temperature, protected from light. Samples were then transferred into a new 96-well plate and fluorescence measure by Cytation5M reader at 480 nm excitation and ~520 nm emission.

Dopaminergic neurons NAD(P)/NAD(P)H and ATP measurement

At day of differentiation 30, dopaminergic neurons were harvest with accutase for ATP measurement (40,000 cells per replicate), NAD(P)/NAD(P)H (25,000 cells per replicate). Measurements were done using commercially available kits from Promega, following the manufacturer's protocol: CellTiter-Glo (Promega, cat. no G7570), NAD/NADH-Glo (Promega, cat. no G9071) and NADP/NADPH-Glo (Promega, cat. no G9081). Luminescence was read using the Cytation5M reader. All values were normalized to protein amount quantified with the Pierce™ BCA Protein Assay Kit according to manufacturer instructions. For all assays, a total of 4 independent batches (derivations) with 2 technical replicates per batch were performed.

Extracellular metabolomics on dopaminergic neurons

Sample collection and metabolite extraction

At day 30 of differentiation, maturation media that has been in contact with dopaminergic neurons for the previous 48 hours was collected, filtered using Phenex Regenerated Cellulose (RC) syringe filters to remove any cells or debris, and frozen at -80 °C until extraction and gas chromatography (GC)-MS measurement. Metabolite derivatization was performed by using a multi-purpose sample preparation robot (Gerstel). Dried medium extracts were dissolved in 30 µl pyridine, containing 20 mg/ml methoxyamine hydrochloride (Sigma-Aldrich, cat. no 89803), for 120 min at 45 °C under shaking. After adding 30 µl of N-methyl-N-trimethylsilyl-

trifluoroacetamide (Macherey-Nagel, cat. no 701270.510) samples were further incubated for 30 minutes at 45 °C under continuous shaking followed by GC-MS analysis.

Gas chromatography – Mass spectrometry

GC-MS analysis was performed on an Agilent 8890 GC coupled to an Agilent 5977B MS (Agilent Technologies). A sample volume of 1 µl was injected into a Split/Splitless inlet, operating in split mode (20:1) at 270 °C. The gas chromatograph was equipped with a 30 m (I.D. 0.25 mm, film 0.25 µm) ZB-5MSplus capillary column (Phenomenex, cat. no 7HG-G030-11-GGA) with 5 m guard column in front of the analytical column. Helium was used as carrier gas with a constant flow rate of 1.4 ml/minute. The GC oven temperature was held at 90 °C for 1 minute and increased to 220 °C at 10 °C/minute. Then, the temperature was increased to 300 °C at 20 °C/minute followed by 4 min post run time at 325 °C. The total run time was 22 minutes. The transfer line temperature was set to 280 °C. The MSD was operating under electron ionization at 70 eV. The MS source was held at 230 °C and the quadrupole at 150 °C. Mass spectra were acquired in selected ion monitoring (SIM) mode for precise quantification of medium components. Supplementary Material 2 shows the masses used for quantification and qualification of the derivatized target analytes (dwell times between 20 and 70 ms).

Data processing and normalization

All GC-MS chromatograms were processed using MetaboliteDetector (v3.2.20190704)(Hiller et al., 2009). Compounds were annotated by retention time and mass spectrum using an in-house mass spectral (SIM) library (overall similarity > 0.80). The following deconvolution settings were applied: peak threshold: 2; minimum peak height: 2; bins per scan: 10; deconvolution width: 8 scans; no baseline adjustment; minimum 1 peak per spectrum; no minimum required base peak intensity. The internal standards (U-13C5-ribitol and pentanedioic-d6 acid) were added at the same concentration to every sample to correct for uncontrolled sample losses, and analyte degradation during metabolite extraction and sensitivity drifts during measurements. The dataset was normalized by using the response ratio of the integrated peak area of the analyte and the integrated peak area of the internal standard. Further normalization based on the total cell number that the media was in contact with was performed and the relative abundance of metabolites was plotted in GraphPad Prism v10 (RRID SCR_002798) using negative values for metabolites consumed and positive values for metabolites released by the dopaminergic neurons.

Dopaminergic neurons Western blotting

Neurons were lysed with 200 µl SDS lysis buffer (1% SDS with protease inhibitor cocktail tablet; Roche, cat. no 04693159001) per well in 6-well plates and scraping. Lysates were transferred into 1.5 ml tubes and boiled for 5 minutes at 95 °C. Protein quantification was performed using the Pierce BCA assay kit according to manufacturer's instructions. NuPAGE™ 4 to 12%, Bis-Tris, 1.0 mm, Mini Protein Gels with 12-wells were used for all blots (Invitrogen™, cat. no NP0329PK2). Prior to loading, samples were diluted with 6x Lämmli loading buffer and boiled for 5 minutes at 95 °C. As ladder, PageRuler Plus Prestained Protein Ladder was used (Thermo Fisher Scientific, cat. no 26619). Electrophoresis were runed in NuPAGE™ MES SDS running buffer. After the run, wet transfer ran for 75 minutes at 100 V in transfer buffer: 1:5 99% ethanol and 1x Tris glycine in MilliQ water. After protein transfer, Ponceau red was used to assess total protein levels. The membrane was then rinsed with TBS-T (Tris-buffered saline with 0.1% Tween 20 detergent) and blocked with 5% BSA in TBS-T for 1 hour prior to incubation of the primary antibody overnight at 4 °C with rotation: α-synuclein (C42) and β-actin (8H10D10) – Table 2. The next day, membrane was washed 3x for 10 minutes in TBS-T with shaking and incubated with the respective secondary antibody (Table 2) for 1 hour at room temperature with shaking. Then, membrane was further washed 3x for 10 minutes in TBS-T with shaking. Protein bands were detected with ECL Prime Western blotting Amersham (Sigma Aldrich, cat. no GERPN2232) detection reagent and images acquired with STELLA imaging system. Western Blot membranes were analyzed with Image J software.

In vivo

All mouse experiments were performed according the European FELASA guidelines for animal experimentation (see ethical approval section).

Housing

Mice were housed and bred in dedicated facilities under specific pathogen free (SPF) conditions, then transferred to a conventional mouse facility at least one week before any manipulation or measurement. Both facilities had 12 hours alternating dark/light cycles. Mice always had *ad libitum* access to standard mouse food (Sniff, cat. no V 1534-300) and water. Health monitoring was performed quarterly and yearly, according to the FELASA 2014 pathogen list.

Generation of Miro1 p.R285Q knock-in mice

Miro1 p.R285Q knock-in mice (which represent the human Miro1 p.R272Q ortholog mutation) were generated by CRISPR/Cas9-mediated gene editing in mouse zygotes. Briefly, pronuclear stage zygotes were harvested from C57BL/6N mice super ovulated C57BL/6N females mated with C57BL/6N males. The pronucleus of embryos were microinjected with a mix containing 25 ng/µl Cas9 mRNA, 60 ng/µl Recombinant S. pyogenes Cas9 nuclease, 0.6 pmol/µl Alt-R® CRISPR-Cas9 crRNA (protospacer TGGACTGTGCTTCGACGATT; IDT, Inc.): 0.6 pmol/µl Alt-R® CRISPR-Cas9 tracrRNA duplex (IDT, Inc.) and 50 ng/µl of specific mutagenic ssODN Miro1 R285Q (5' - GGTTTTCTCTTTTTACATACACTTTTTATCCAGAGGGGGAGGCATGAGACTACTTGGACTGT GCTTCAGCGGTTTGGTTATGACGATGACCTGGACCTGACGCCTGAGTATTTATTCCCCCTG TATGTACCTCAGCGCTC - 3', synthetized by Metabion international AG), comprising the R285Q substitution and an additional silent mutation for genotyping purposes. After microinjections, zygotes were transferred into pseudopregnant CD-1 foster mice.

To identify Miro1 p.R285Q knock-in founder mice (F0 generation) derived from microinjected zygotes, genomic (g)DNA was isolated from tissue biopsies from mice at the age of 3 - 4 weeks and used to assess Miro1 p.R285Q substitution by PCR (see *Mice genotyping* section below).

The knock-in founder mice (F0) were generated at the Institute of Developmental Genetics (Helmholtz Zentrum München, Germany), according to protocols approved by the government of Upper Bavaria and in accordance with the guidelines of the European Community Council Directives.

The animals of Miro1 p.R285Q knock-in mouse line (B6.Miro1^{tmR285QHmgu}) were raised and handled at the University of Luxembourg following the European Union directive 2010/63/EU (see ethical approval section). Wild-type (wt/wt) were used to generate heterozygous (wt/R285Q) and homozygous (R285Q /R285Q) Miro1 p.R285Q mutant mice (B6.Miro1^{tmR285QHmgu}), which represent the human Miro1 p.R272Q ortholog mutation, using an heterozygous x heterozygous and homozygous x homozygous breading strategy.

Mice genotyping

Genomic DNA from biopsies was extracted using the Nucleospin DNA RapidLyse kit (Macherey Nagel, cat. no 740100.250) and quantified using a NanoDrop™ spectrophotometer. DNA was then used to assess Miro1 p.R285Q point mutation integration by PCR. 300 ng of gDNA and 0.2 µM Miro1 forward and reversed primers (Table 3) were used in a total of 50 µl reaction. PCR reaction was done in Biometra Thermocycler T Professional Basic 96 (Montreal Biotech, cat. no 846-070-701) for 5 minutes at 94 °C, followed by 35 cycles of 1 minute at 94 °C denaturation

step, 1 minute at 60 °C annealing and 3 minutes 72 °C elongation step, and a final extension step of 7 minutes at 72 °C. PCR products were further digested by TAQI (GoTaq® G2 Flexi DNA Polymerase; Promega, cat. no M7805) to assess if the point mutation is or not present, since its restriction site will be only present in wt Miro1 protein. For that, 12 µl of ddH2O, 10 µl PCR product (no purification is necessary), 0.5 µl NEB Taq1 enzyme and 2.5 µl 10x smart cut NEB Buffer (Bioke cat. no R0149S) were amplified by PCR using the thermocycling program: 40 minutes at 65 °C digestion, 20 minutes 80 °C inactivation step, and a final hold at 7 °C. PCR products and the GeneRuler™ 100 bp Plus DNA ladder were then ran in 1.5% agarose gel at 130 V for 45 minutes and revealed in a Biodoc Analyse GBOX machine (Syngene) under UV light using Midori Green advance (Biozyl, cat. no 617004). Considering the primers used, wt Miro1 will present 2 bands at 334 bp and 569 bp, while homozygous Miro1 p.R285Q mutant will only present one band with 903 bp.

Table 3. PCR primers used for PCR of mice.

Name:	Nucleotide Sequence (5' - 3')
Miro1R285Q forward	AAGCCAGGAGACTTGTCCAC
Miro1R285Q reverse	TGACCTGCTCCGTACAGTAAG

Mice Behavior

Mice weight was assessed throughout the study at month 12, 15, 18 and 21.

Home cage activity

The LabMaster system (TSE Systems) was used to record and analyze the spontaneous home cage activity of the mice. The mouse cage was surrounded by sensor frames with which the number of beam brakes was quantified and analyzed in 15 minutes intervals. The recorded data provided information on total activity, movement and rearing. Additionally, the volume of consumed food and water was quantified. The data was recorded over a period of 22 hours, which started with about 30 minutes of light phase before a 12 hour phase of darkness. The measurement happened in the same day and night cycle that mice were used to. All mice were analyzed in individual cages and afterwards reunited with their cage mates. Measurements were done in 20 month-old mice.

RotaRod

An accelerating rotarod (TSE Systems) was used to measure the motor coordination abilities, balance and spontaneous motor activity/movement anterograde procedural memory of the mice. The analysis was performed in a room with only red light illumination during the night time of the animals. Mice were placed on the rod which accelerated from 4 to 40 rpm over a duration of 300 sec. The latency to fall off the rotating rod was recorded in each trial. If a mouse fell within the first 10 sec of a trial the measurement was repeated. Per test day three trials were carried out with a minimum 15 minutes rest between trials. The mean latency to fall per mouse was calculated as the mean value of the three trials. Rotarod was performed twice with the same female mice at age 20 and 21 months. There was no training prior to the first trial. One female was excluded based on their significant higher weight.

Mice brain dissection

Mice were deeply anesthetized with ketamine-medetomidine anesthesia (150 mg/kg ketamine lot nr. 136472 and 1 mg/kg medetomidine lot nr. 2033.85) and transcardiacally perfused with PBS. After perfusion, brains were placed on ice, and split along the longitudinal fissure into the two hemispheres. For molecular biology analyses, one part was dissected into different regions of interest (striatum and midbrain), put on dry ice and stored at -80 °C. The other hemisphere were fixed for immunohistochemistry in 4% PFA for 48 hours at 4 °C and then stored in PBS with 0.2% sodium-azide until further processing.

Immunohistochemistry (mice)

Female and male young (3 to 6 month-old) and aged (15 month-old) mice were used for analyzing striatal DAT and TH as well as SNpc TH levels. Serialized parasagittal free floating, 50 µm-thick sections were obtained using a Leica VT-1000S vibratome and collected in cryoprotective medium composed of a 1:1 ethylene glycol (Sigma Aldrich, cat. no 61941) and PBS solution, supplemented with 1% w/v polyvinyl pyrrolidone (Sigma Aldrich, cat. no PVP40). Sections were stored at -20 °C, in tubes, each containing series of every 4th section.

For staining, sections were washed 2x 5 minutes in washing buffer (PBS with 0.1% Triton X-100) with agitation, permeabilized for 30 minutes in PBS containing 1.5% Triton X-100 and 3% hydrogen peroxide, to deactivate endogenous peroxidases. Sections were further washed 2x 5 minutes in washing buffer and blocked in PBS with 5% BSA and 0.1% Triton X-100 for 30 minutes. After, sections were rinsed 2x 5 minutes in washing buffer followed by incubation with primary antibodies: rabbit anti-TH, rat anti-DAT Nter for the striatum; chicken anti-TH for SNpc (Table 2) in antibody buffer (PBS with 0.3% Triton X-100 and 2% BSA) overnight under strong

shaking at room temperature. After three more washing steps (10 minutes each), sections were incubated with appropriate secondary antibodies (Table 2) in antibody buffer, in the dark, on shaking conditions for 2 hours at room temperature. Next, the sections were washed again (3x 10 minutes) in washing buffer, and once in TBS (Trizma base 6.06 g/l (Sigma Aldrich, cat. no T1503), 8.77 g/l NaCl (Sigma Aldrich, cat. no S9888), adjusted with HCl to pH 7.4). Finally, sections were mounted on glass slides, cover slipped using Dako fluorescent mounting medium (DAKO, cat. no S302380).

Imaging acquisition and quantification (mice)

Imaging was done using a Zeiss *AxioImager Z1* upright microscope, coupled to a "*Colibri*" LED system to generate fluorescence light of defined wavelengths, an *Mrm3* digital camera for image capture, and equipped with a PRIOR motorized slide stage. The complete Zeiss imaging system was controlled by Zeiss Blue Vision software. To measure TH and DAT, 2-3 striatal sections per mouse containing 3 fields in the dorsal striatum were taken in a 40X objective using the Apotome. Apotome captured image were then modified with the parameters "display optical sectioning" to correct phase errors. Obtained images were converted to TIFF. Then, after thresholding, the percent area occupied by TH and DAT staining were determined using the publicly available imaging software FIJI (RRID SCR_002285), using the "restrict to threshold" parameter. Qualitative assessment of phosphor S129 α-synuclein was performed on 15 µM deep stacks at a 40 % magnification, followed by maximum intensity projection.

For TH quantification, we first carry a careful anatomical observation to distinguish SNpc specific TH-positive neurons from the ones present in other anatomical regions. We recognized the SNpc at four anatomically distinguishable levels using 6-10 sections of 50 µm (spaced 200 µm) per mouse, covering the entire space occupied by the SNpc in each mouse brain. Then, for each section, tiled pictures (2x2) were taken at 10x magnification using the above-mentioned Zeiss imaging system. Next, the region-of-interest (ROI) tool in the FIJI software was used to segment the area occupied only by SNpc TH-positive neurons within each section. After thresholding, the area occupied (in pixels) by TH-positive neurons was measured. The four distinguishable anatomical levels of the SNpc were measured using 2-3 sections/level in each mouse. Values for each level were averaged separately. Thus, 4 final area values, representative of the areas occupied by TH-positive neurons in each anatomical level of the SN, were obtained for each mouse. To obtain one representative value for each brain hemisphere, these 4 values were summed up ("cumulated SN surface"), and converted to mm^2 for graphical

representation(Ashrafi et al., 2017). Detailed information on the method and its correlation with stereological cell counts can be found in Ashrafi et al.(Ashrafi et al., 2017).

Striatal dopamine measurement

Striatum, dissected as abovementioned, was used to quantify the abundance of the neurotransmitter dopamine in 15 month-old mice. Tissue was used to extract and measure dopamine by GS-MS based on previously published method(Jaeger et al., 2015; Jäger et al., 2016). Briefly, 500 µl of methanolic extraction fluid (4:1, methanol/water mixture, v/v) were added to 50 mg mouse brain (striatum). The extraction fluid contained an internal standard mix, consisting of U-13C5 ribitol (c = 2 µg/ml; Omicron Biochemicals, cat. no ALD-062) and pentanedioic-d6 acid (c = 2 µg/ml; C/D/N Isotopes Inc., cat. no D-5227). Samples were subsequently homogenized using a Precellys24 homogenizer (Bertin Technologies) using 600 mg ceramic beads (1.4 mm) and one 30 sec cycle at 6,000 rpm at 0 to 5 °C. Then, 250 µl of a 0.1 mol/l hydrochloric acid solution, including dopamine-D4 (c = 15 µmol/l) was added to the homogenate. Polar metabolites were extracted by adding 400 µl of chloroform. After incubation under shaking for 15 minutes at 2,000 rpm at 4 °C (Eppendorf ThermoMix Comfort), samples were centrifuged for 5 minutes at 21,000g at 4 °C. 80 µl of the upper phase containing the polar metabolites were transferred into a GC glass vial with micro insert and evaporated at -4 °C for 4 hours, followed by an adaptation phase to room temperature for 25 minutes (Labconco CentriVap). Samples were submitted to subsequent GC-MS analysis.

Data analysis and statistics

GraphPad Prism (version 10) was used to plot and statistically analyzed midbrain organoids LDH assay, organoids and dopaminergic neurons Seahorse data, dopaminergic neurons metabolomics, calcium imaging and ATP, NAD(H) and NADP(H) assays, while RStudio software (version R 4.3.0) was used to plot and statistically analyzed dopaminergic neurons and/or midbrain organoids Western blotting, image analysis and metabolomic data. Data are expressed as mean ± standard error of mean (SEM). For midbrain organoids LDH and dopaminergic neurons single cell calcium imaging assays outlier removal was performed with ROUT test (Q=5%) using GraphPad Prism. For TUNEL assay, Rosner Test (from EnvStats package) was used to detect outliers using RStudio. Statistical significance was determined with GraphPad Prism 10 software or with RStudio. First, data was analyzed for normality using Shapiro test. For normal distributed data (Shapiro test not significant) ANOVA with post-hoc Tukey HSD test was used, while in non-normal data (Shapiro test significant) the statistical significance was

calculated using the non-parametric Kruskall-walis test. $P < 0.05$ was considered to represent statistical significance, with * $P < 0.05$, ** $P < 0.01$ and *** $P < 0.001$.

Ethical approval

All necessary ethical approvals have been obtained in accordance with the Règlement grand-ducal du 11 janvier 2013 relatif à la protection des animaux utilisés à des fins scientifiques" adapted from and in line with the European Directive 2010/63/EU.w (on the use of clinical samples and on the Care and Use of laboratory animals, where applicable). The Luxembourgish National Research Ethics Committee (CNER) provided ethical approval for the following projects: "Disease modelling of Parkinson's disease using patient-derived fibroblasts and induced pluripotent stem cells" (DiMo-PD, CNER #201411/05) and, *'In vitro* modeling of Parkinson's disease (ivPD)' (ERP 18-082 ivPD).

Data availability

All the data used in the current study, both raw and processed, as well as all the scripts developed are publicly available at https://doi.org/10.17881/vm4y-sv50. The scripts generated from the current are also available on gitlab: https://gitlab.lcsb.uni.lu/dvb/saraiva_2023. Midbrain organoid scRNAseq and dopaminergic neurons bulk RNAseq data are also available on Gene Expression Omnibus (GEO) repository under the accession code GSE237133 and GSE238129, respectively.

Supplementary Figures

Supplementary figure 1. Midbrain organoid (MO) single cell RNA sequencing quality control and cell cluster markers. A) Plots representing the gene number (nFeature_RNA), total molecules number (nCount_RNA), mitochondrial gene percentage as well as the correlation between the number of genes and total molecules before (unfiltered; left) and after (filtered; right) applying the quality control thresholding in **(i)** healthy MO (Ctrl2), **(ii)** Miro1 p.R272Q mutant organoids (PD-R272Q), and **(iii)** isogenic control (iCtrl). **B)** Expression levels of cell specific markers for oligodendrocyte progenitors, glia progenitors, neural progenitors, dopaminergic neurons, other neuronal subtypes and mature neurons, respectively, in the different MO clusters identified.

A)

i)

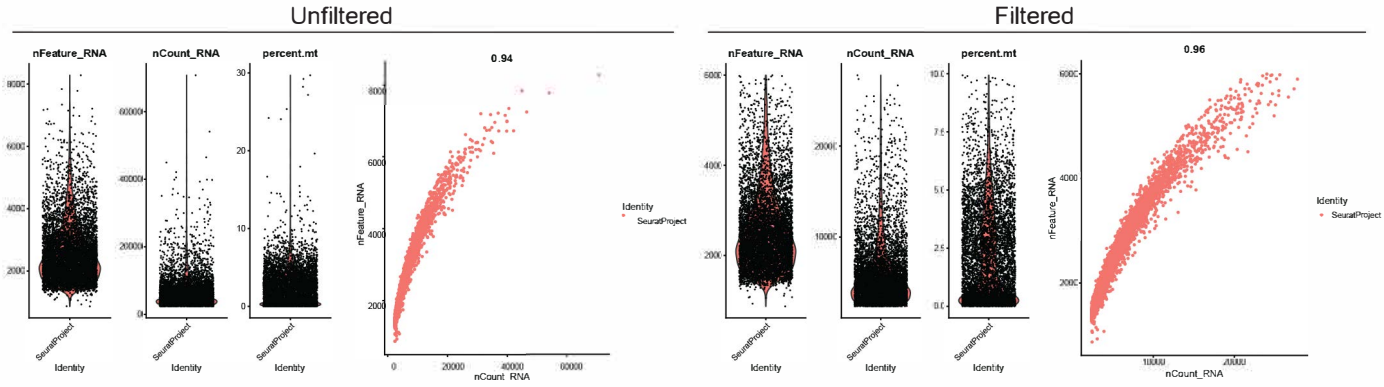
Unfiltered
Filtered
nFeature_RNA
nCount_RNA
percent.mt
0.94
0.96
Identity
SeuratProject

ii)

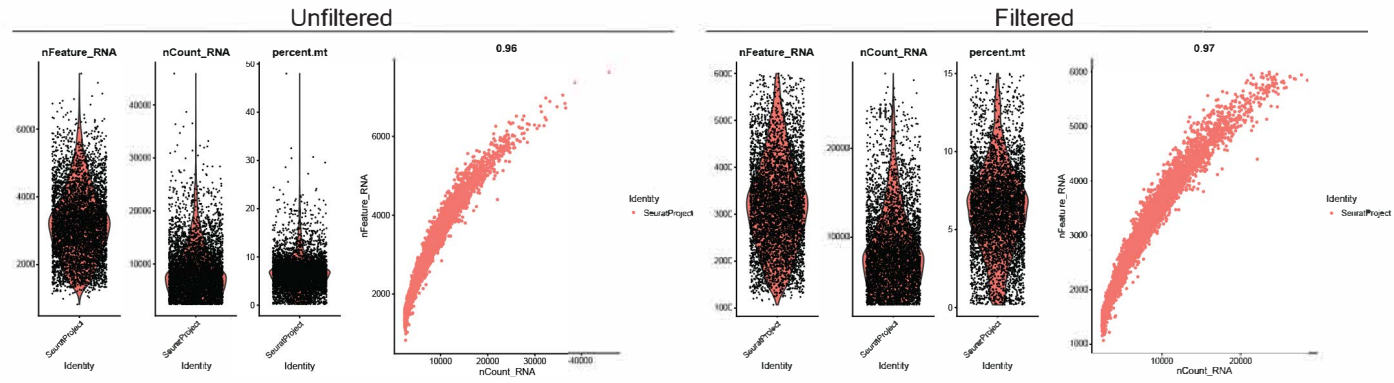
Unfiltered
Filtered
nFeature_RNA
nCount_RNA
percent.mt
0.96
0.97
Identity
SeuratProject

iii)

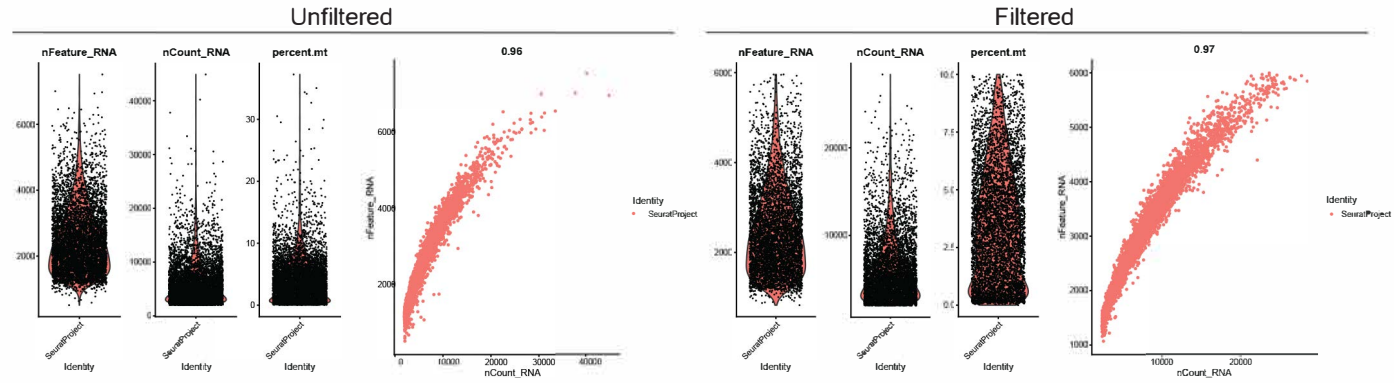
Unfiltered
Filtered
nFeature_RNA
nCount_RNA
percent.mt
0.96
0.97
Identity
SeuratProject

B)

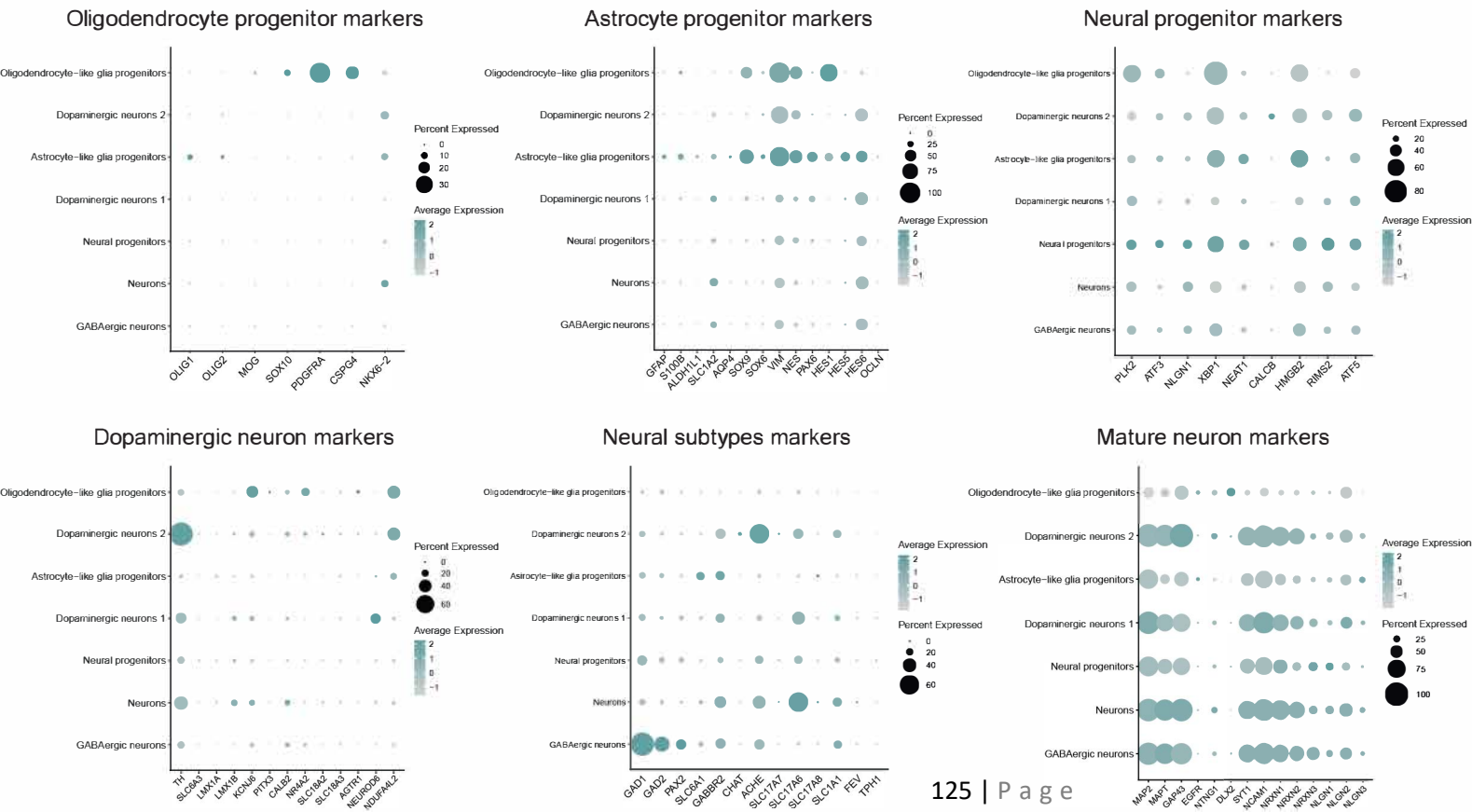
Oligodendrocyte progenitor markers
Astrocyte progenitor markers
Neural progenitor markers
Dopaminergic neuron markers
Neural subtypes markers
Mature neuron markers
Oligodendrocyte−like glia progenitors
Dopaminergic neurons 2
Astrocyte−like glia progenitors
Dopaminergic neurons 1
Neural progenitors
Neurons
GABAergic neurons
Percent Expressed
Average Expression
OLIG1
OLIG2
MOG
SOX10
PDGFRA
CSPG4
NKX6−2
GFAP
S100B
ALDH1L1
SLC1A2
AQP4
SOX9
SOX6
VIM
NES
PAX6
HES1
HES5
HES6
OCLN
PLK2
ATF3
NLGN1
XBP1
NEAT1
CALC8
HMGB2
RIMS2
ATF5
TH
SLC6A3
LMX1A
LMX1B
KCNJ6
PITX3
CALB2
NR4A2
SLC18A2
SLC18A3
AGTR1
NEUROD6
NDUFA4L2
Asirocyte−like glia progenitors
GAD1
GAD2
PAX2
SLC6A1
GABBR2
CHAT
ACHE
SLC17A7
SLC17A6
SLC17A8
SLC1A1
FEV
TPH1
MAP2
MAPT
GAP43
EGFR
NTNG1
DLX2
STT1
NCAM1
NRXN1
NRXN2
NRXN3
NLGN1
NLGN2
NLGN3

Supplementary figure 2. Deregulated process and pathways in midbrain organoids (MO). **A)** Top 25 most deregulated process (left) and pathways (right) in Miro1 p.R272Q mutant MO (PD-R272Q) when compared with healthy control (Ctrl) or isogenic control (iCtrl) (PD-R272Q vs Ctrl; PD-R272Q vs iCtrl) based on differential express gene analysis of the single cell RNA sequencing data. **B)** Top 25 most deregulated process (left) and pathways (right) in PD-R272Q vs Ctrl and PD-R272Q vs iCtrl in the dopaminergic neuron clusters (dopaminergic neurons 1 and dopaminergic neurons 2).

A)

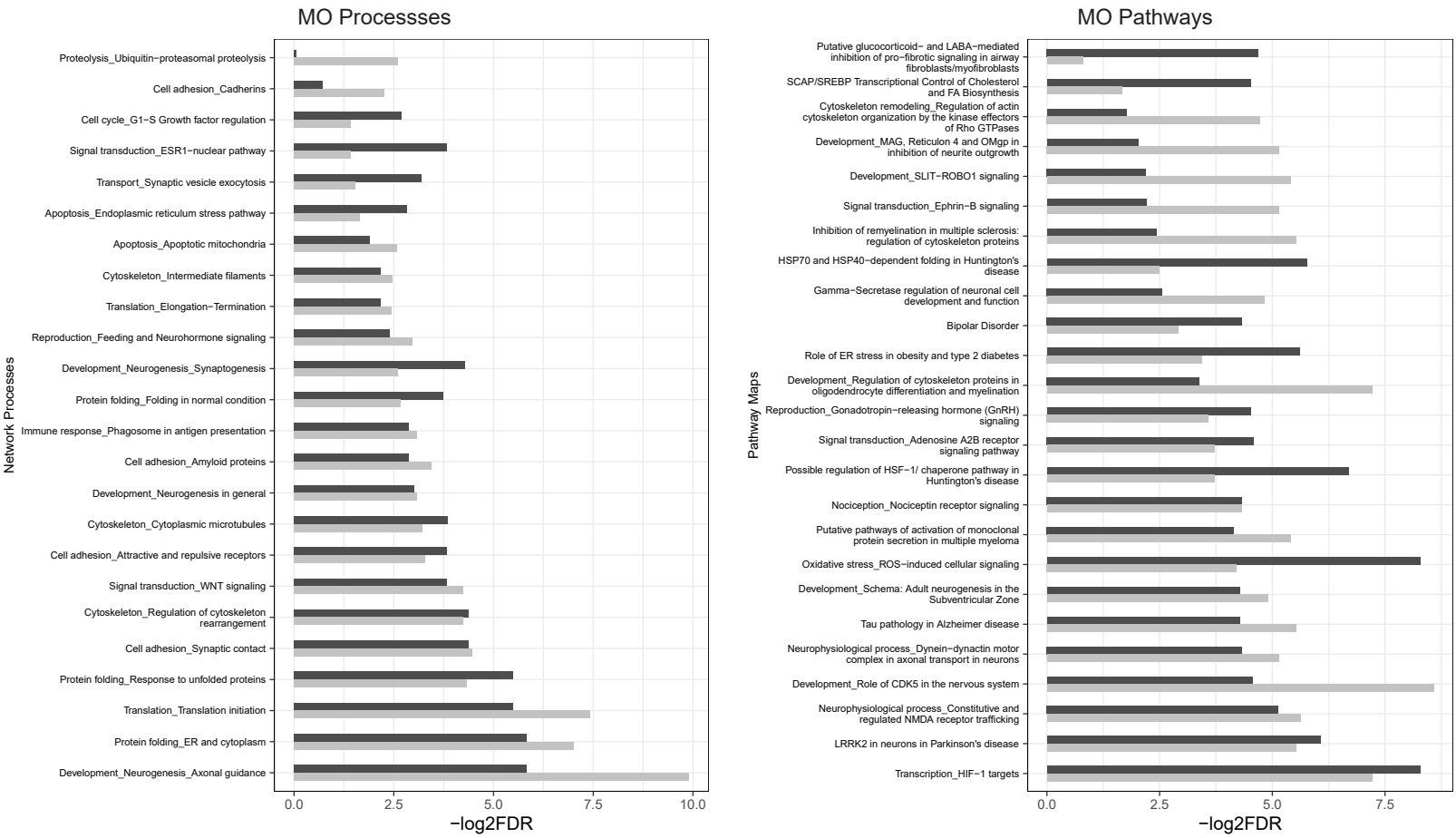

B)

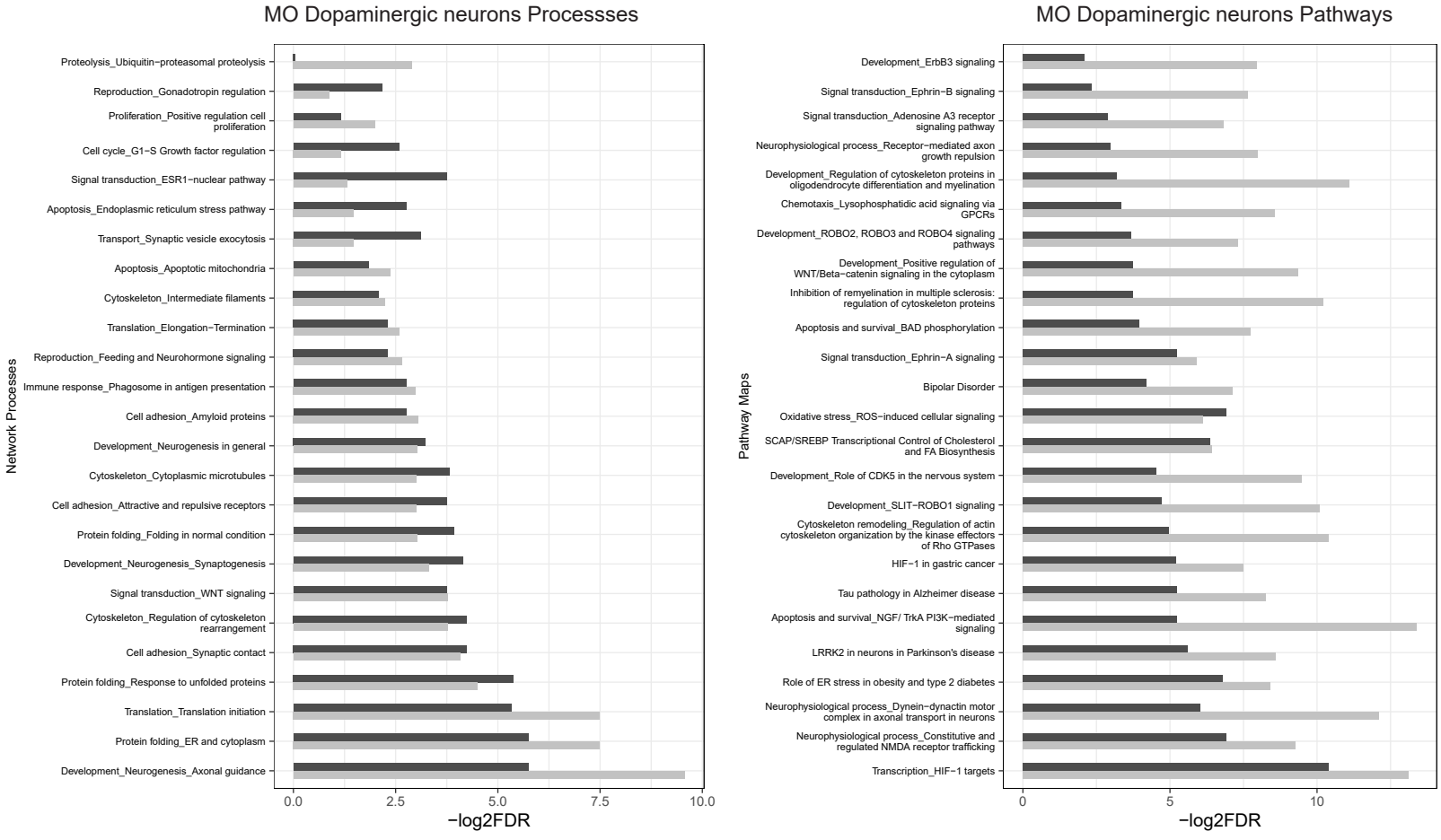

PD-R272Q vs Ctrl **PD-R272Q vs iCtrl**

Supplementary figure 3. Expression levels in fpkm (fragments per kilobase per million mapped fragments) of dopaminergic neuronal markers (top) and glial markers (bottom) expressed by dopaminergic neurons in the bulk RNA sequencing dataset.

Dopaminergic neuron markers

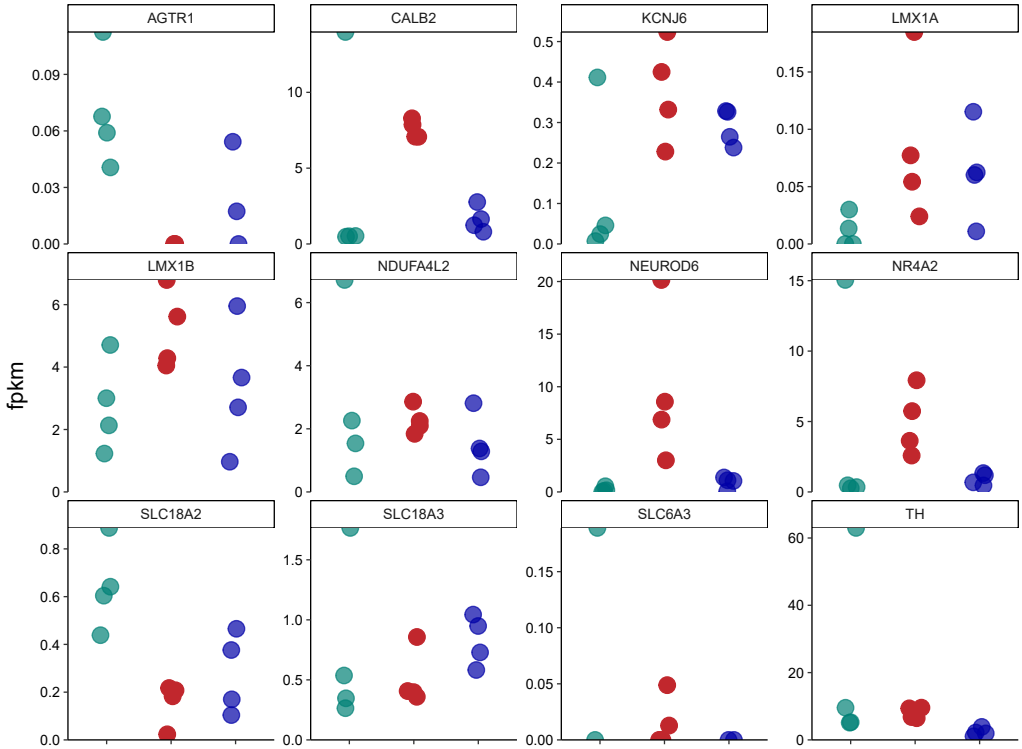

Glia markers

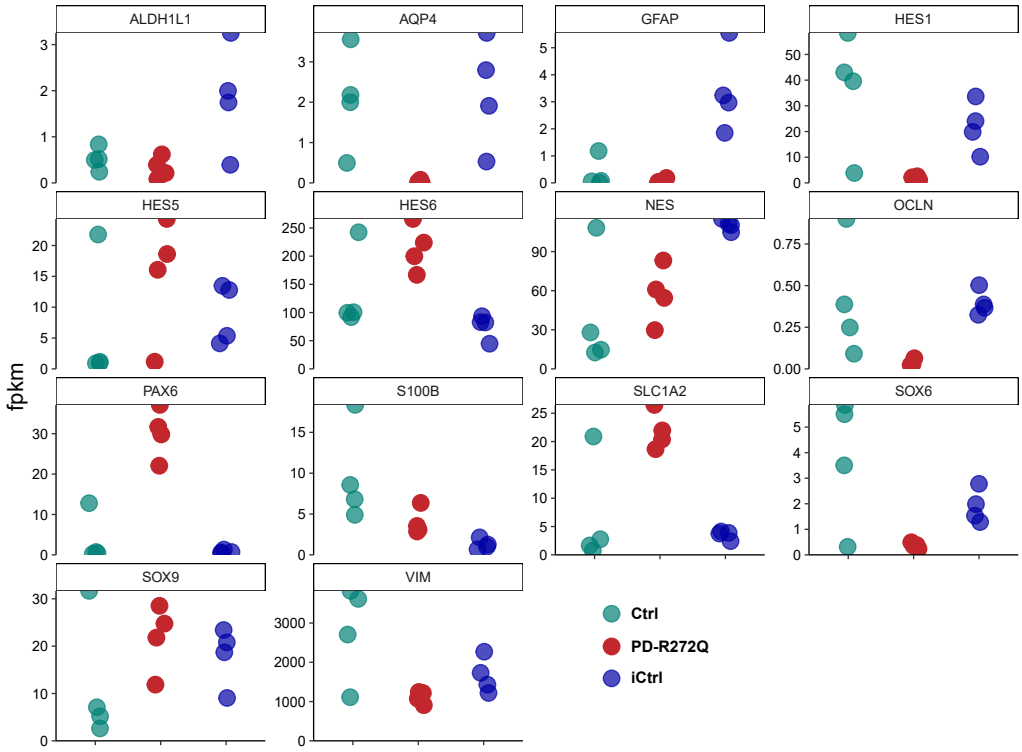

Supplementary figure 4. Fold change of the significant differentially expressed genes contributing to the deregulation of the *'oxidative stress ROS-induced cellular signaling'* pathway in midbrain organoids comparing Miro1 p.R272Q midbrain organoids (PD-R272Q MO) and healthy (Ctrl) or isogenic (iCtrl) controls (i.e. PD-R272Q vs Ctrl and PD-R272Q vs iCtrl).

MO deregulated genes in the *Oxidative Stress_ROS-induced cellular signaling* pathway

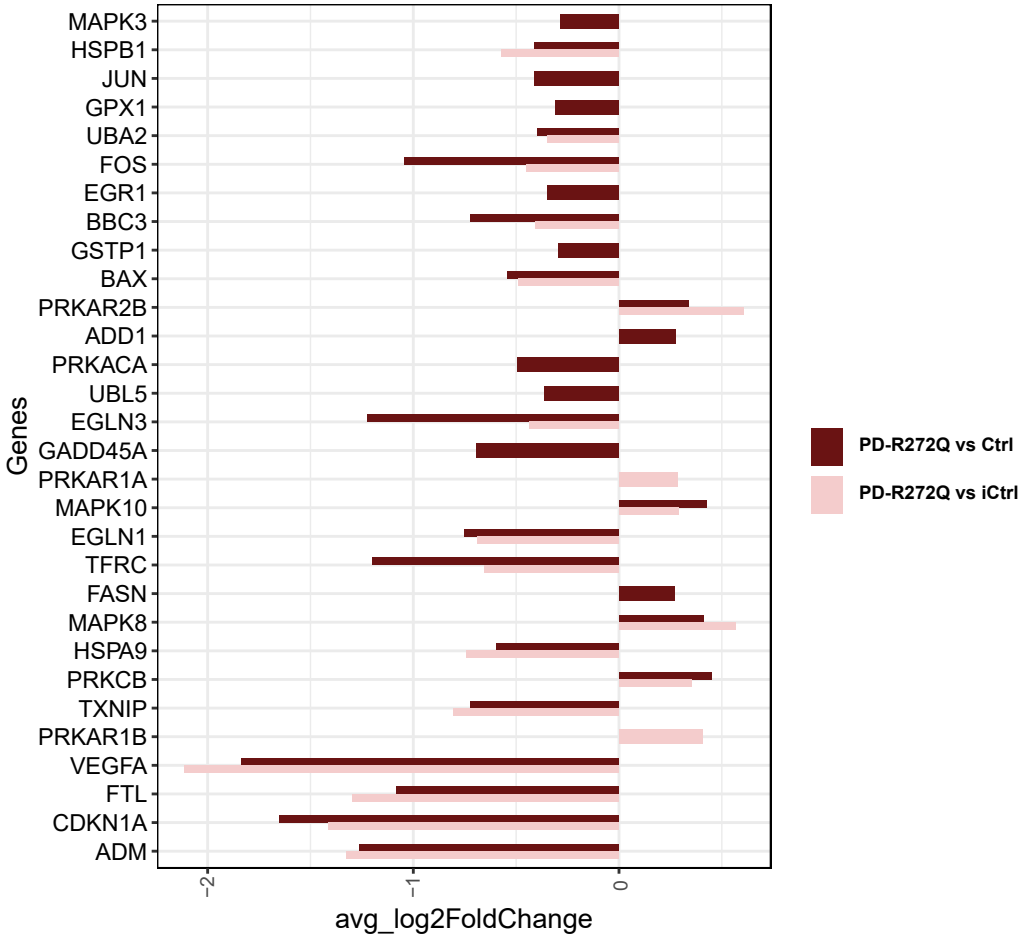

Supplementary figure 5. *RHOT1* expression levels *in vitro*. A) Ridge plot of midbrain organoids *RHOT1* gene expression in Miro1 p.R272Q mutant (PD-R272Q), healthy (Ctrl) and isogenic (iCtrl) controls conditions based on the single cell RNA sequencing data. **B)** Ctrl, PD-R272Q and iCtrl expression levels of *RHOT1* in dopaminergic neuronal cultures in the bulk RNA sequencing dataset.

A)

Midbrain organoids *RHOT1* expression levels

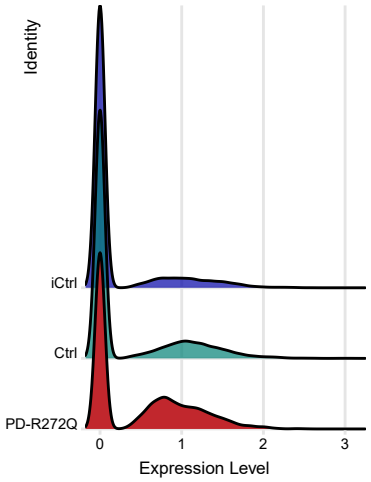

B)

Dopaminergic neurons *RHOT1* expression levels

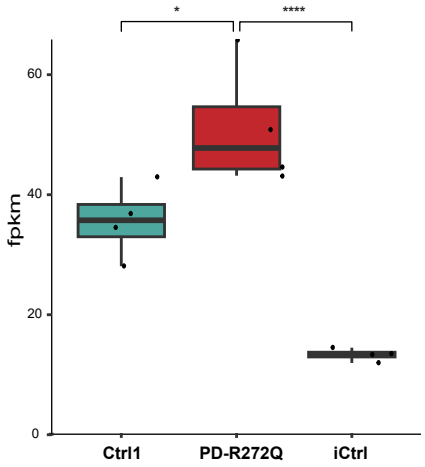

Supplementary figure 6. Significant differentially expressed genes contributing to the deregulation of the process "*Apoptosis_Apoptotic mitochondria*" (left) and the pathway "*Apoptosis and survival_NGF/TrkA PI3K−mediated signaling*" found within the dopaminergic neuron clusters (dopaminergic neurons 1 and dopaminergic neurons 2 clusters) of the midbrain organoids. Graph displays gene fold-changes comparing Miro1 p.R272Q midbrain organoids (PD-R272Q MO) and healthy (Ctrl) or isogenic (iCtrl) controls (i.e. PD-R272Q vs Ctrl and PD-R272Q vs iCtrl).

Genes in "*Apoptosis_Apoptotic mitochondria*" MO dopaminergic neuron clusters deregulated process

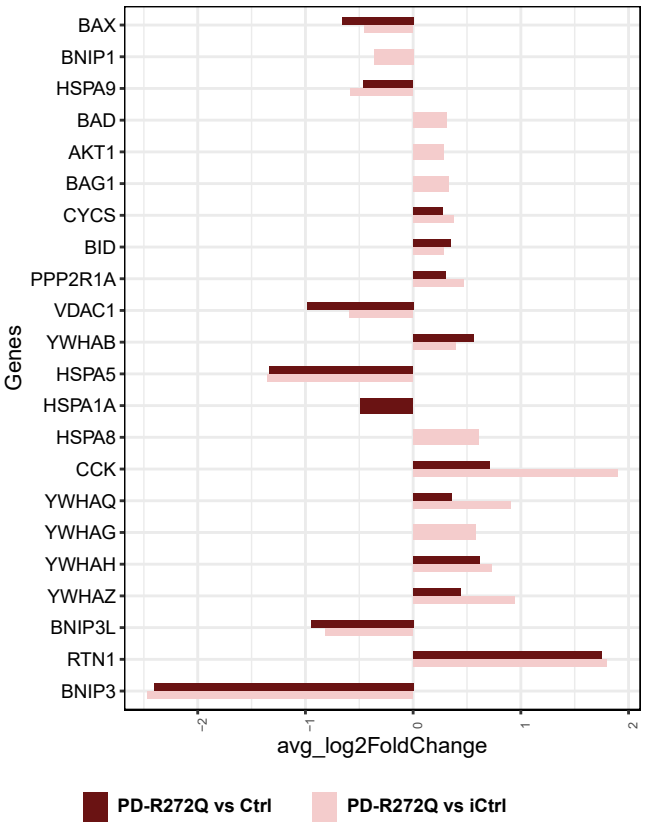

Genes in "*Apoptosis and survival_NGF/TrkA PI3K−mediated signaling*" MO dopaminergic neuron clusters deregulated pathway

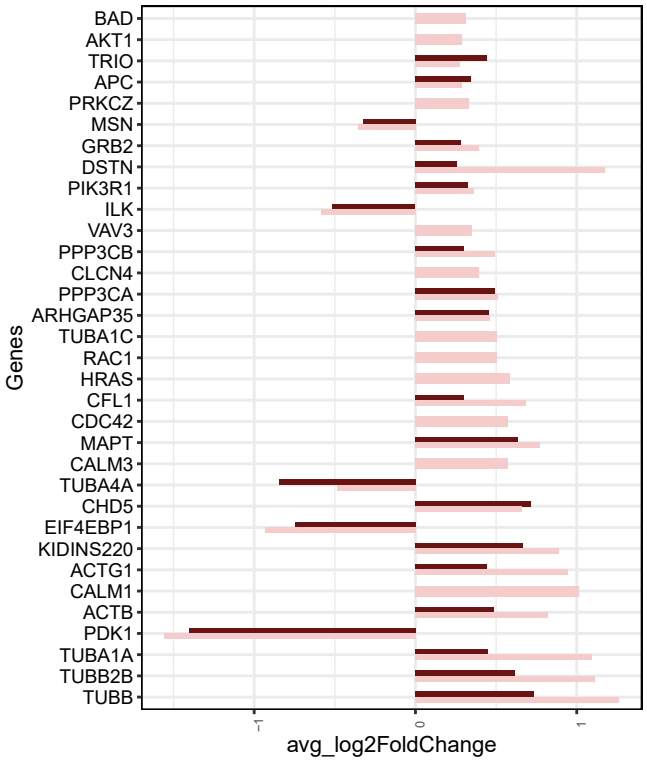

Supplementary figure 7: Miro1 p.R285Q mutant C57BL/6 mice features. A) Body weight of Wilde-type (wt/wt, green) and Miro1 p.R285Q mutant heterozygous (wt/R285Q, orange) and homozygous (R285Q/R285Q, red) mice at month 12, 15, 18 and 21 of age. **B-C)** Quantification of tyrosine hydroxylase (TH; **B)** and dopamine transporter (DAT; **C**) terminals in the striatum of 3 to 6 month-old mice. **D)** TH cumulative area in the substantia nigra (SNpc) of 3 to 6 month-old mice. **B-D)** wt/wt: n = 6F; wt/R285Q: n = 6F; R285/R285Q: n = 10F. **E)** DAT quantification in the striatum of 15 month-old mice. **F)** Graphic depicts striatal dopamine quantification (pmol/mg) in wt/wt and R285Q/R285Q 15 month-old mice using gas-chromatography-mass spectrometry (GC-MS). **15 month-old mice:** wt/wt: n = 2M + 5F; wt/R285Q: n = 3M + 5F; R285/R285Q: n = 4M + 6F. **G)** Quantification of SNpc TH positive area in 15 month-old male mice. **H)** Representative image of pS129 α-synuclein and TH immunoreactivity in the SNpc of old male wildtype and Miro1 p.R285Q homozygous mice. Scalebar 20µm. **J, K)** Consumption of water **(J)** and food **(K)** for 22 hours in 20 month-old mice measured with the Phenomaster® Cage. **L)** Total activity, expressed as number of beam brakes every 15 minutes, for 22 hours, in 20 month-old mice measured with the Phenomaster® Cage.

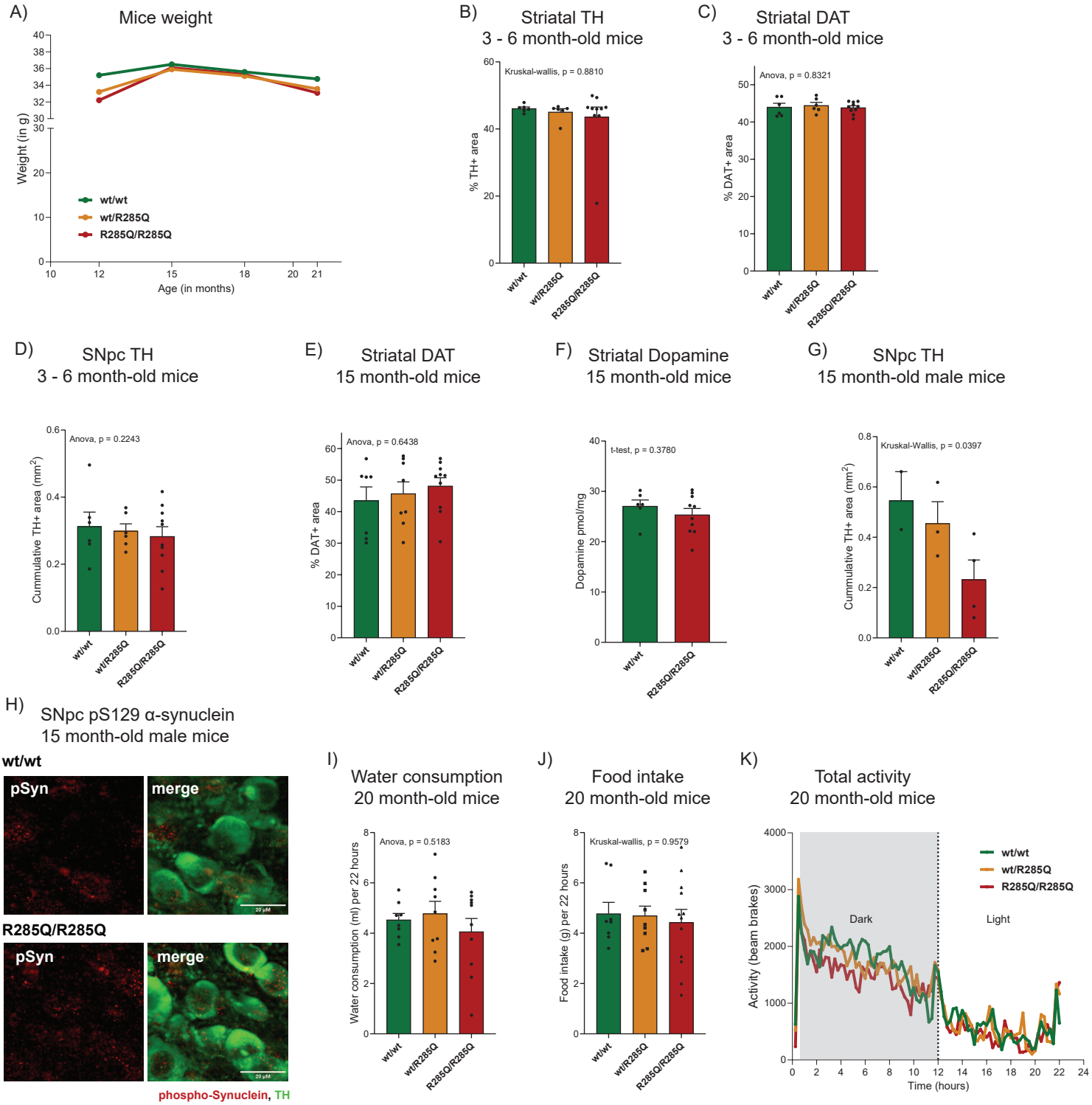
A)
Mice weight
Weight (in g)
Age (in months)
wt/wt
wt/R285Q
R285Q/R285Q
B)
Striatal TH
3 - 6 month-old mice
Kruskal-wallis, p = 0.8810
% TH+ area
C)
Striatal DAT
3 - 6 month-old mice
Anova, p = 0.8321
% DAT+ area
D)
SNpc TH
3 - 6 month-old mice
Anova, p = 0.2243
Cummulative TH+ area (mm2)
E)
Striatal DAT
15 month-old mice
Anova, p = 0.6438
% DAT+ area
F)
Striatal Dopamine
15 month-old mice
t-test, p = 0.3780
Dopamine pmol/mg
G)
SNpc TH
15 month-old male mice
Kruskal-Wallis, p = 0.0397
Cummulative TH+ area (mm2)
H)
SNpc pS129 α-synuclein
15 month-old male mice
wt/wt
pSyn
merge
R285Q/R285Q
phospho-Synuclein, TH
I)
Water consumption
20 month-old mice
Anova, p = 0.5183
Water consumption (ml) per 22 hours
J)
Food intake
20 month-old mice
Kruskal-wallis, p = 0.9579
Food intake (g) per 22 hours
K)
Total activity
20 month-old mice
Activity (beam brakes)
Dark
Light
Time (hours)

Supplementary Material 1:
Midbrain organoids metabolomics:

. Detailed LC-MS setting for assessing polar intracellular midbrain organoids metabolites:
Analytical column: SeQuant® ZIC-pHILIC 5µm polymer 150 x 2.1 mm
Guard column: SeQuant® ZIC-pHILIC Guard 20 x 2.1 mm

Mobile phase A: 20 mmol/L ammonium acetate in H2O (pH 9.2, + 5 µM MA)
Mobile phase B: ACN (pH unadjusted, 5 µM MA)

Gradient:	Time (min)	%B	Flow rate (µL/min)
	0.00	80	200
	3.00	80	200
	18.00	20	200
	19.00	80	200
	24.5	80	200
	25.5	80	400
	29.5	80	400
	30.00	80	200

Flow rate: 0.20-0.40 mL/min
Column temp.: 45 °C
Injection volume: 5 µL
Autosampler temp.: 4 °C

MS parameters
Instrument: Exploris 240
Ion mode: Polarity Switching (positive/negative ESI in Full scan)

ESI Source
Sheath gas flow rate: 35
Aux gas flow rate: 7
Sweep gas flow rate: 0
Spray voltage kV: 3.5
Capillary temp. (°C): 400
S-lens RF level: 70.0
Aux gas heater temp. (°C): 275

Scan parameters Full MS
MS1 Scan range: 75 – 1000 m/z
Polarity: POS/NEG
Spray voltage of 3 kV in both positive and negative mode
MS1 Resolution: 60,000
MS1 AGC target: ¨standard”
MS1 Maximum injection time: 100 ms

MS1 Scan range: 75 – 1000 m/z
Polarity: POS/NEG
Spray voltage of 3 kV in both positive and negative mode
MS2 Resolution: 30,000

MS2 AGC target: ¨standard”
MS2 Maximum injection time: “auto”
MS2 isolation window: 0.4 m/z
Collision energy: 30 V
Loop count: 3
Dynamic exclusion time: 3 s with exclusion after 1 acquisition.

Supplementary Material 2:
Extracellular metabolomics on dopaminergic neurons:
Masses used for quantification and qualification of the derivatized target analytes (dwell times between 20 and 70 ms).

Analyte Name	Quantification Ions (m/z)	Qualification Ion I (m/z)	Qualification Ion II (m/z)
Pyruvic acid 1MEOX 1TMS	174-179	158.1	189.1
Lactic acid 2TMS	219.1-224.1	190.1	117.1
Alanine 2TMS	218.1-223.1	190.1	116.1
Valine 2TMS	144.1	218.1	246.2
Urea 2TMS	189.1	103.1	171.1
Leucine 2TMS	158.1	218.1	232.2
Isoleucine 2TMS	158.1	218.1	232.2
Glycine 3TMS	276.1-280.1	248.1	174
Serine 3TMS	306.1-311.1	218.1	204.1
Threonine 3TMS	218.1	291.2	320.2
IS Pentanedioic acid-D6 2TMS	267.1	163.1	239.1
Methionine 2TMS	176.1	250.1	293.1
Glutamic acid 3TMS	363.2-371.2	246.1	348.2
Phenylalanine 2TMS	192.1	218.1	266.1
Asparagine 3TMS	231.1-236.1	132.1	348.1
IS [UL-13C5]-Ribitol 5TMS	220.1	310.2	323.2
Glutamine 3TMS	347.2-354.2	245.1	156.1
Fructose 1MeOX 5TMS	307.2, 310.2	217.1, 220.1	
Glucose 1MEOX 5TMS	319.2, 323.2	217.1, 220.1	
Lysine 4TMS	174.1	317.2	434.3
Tyrosine 3TMS	218.1	179.1	280.2
Inositol 6TMS	305.1	318.1	507.3
Tryptophan 2TMS	218.1-223.1	130	348.2
Alanyl-glutamine 3TMS	418.2	347.2	216.1
Cystine 4TMS	218.1-223.1	297.1	411.2

References

Acurex Biosciences to Present Early Clinical Results Supporting its Novel Parkinson's Disease Biomarkers at a Michael J. Fox Foundation Biomarkers Workshop [WWW Document], 2023. URL https://www.businesswire.com/news/home/20230515005012/en/Acurex-Biosciences-to-Present-Early-Clinical-Results-Supporting-its-Novel-Parkinson%E2%80%99s-Disease-Biomarkers-at-a-Michael-J.-Fox-Foundation-Biomarkers-Workshop (accessed 5.21.23).

Ahmad, T., Mukherjee, S., Pattnaik, B., Kumar, M., Singh, S., Kumar, M., Rehman, R., Tiwari, B.K., Jha, K.A., Barhanpurkar, A.P., Wani, M.R., Roy, S.S., Mabalirajan, U., Ghosh, B., Agrawal, A., 2014. Miro1 regulates intercellular mitochondrial transport & enhances mesenchymal stem cell rescue efficacy. EMBO J n/a-n/a. https://doi.org/10.1002/embj.201386030

Akita, H., Ogata, M., Jitsuki, S., Ogura, T., Oh-Nishi, A., Hoka, S., Saji, M., 2006. Nigral injection of antisense oligonucleotides to synaptotagmin I using HVJ–liposome vectors causes disruption of dopamine release in the striatum and impaired skill learning. Brain Research 1095, 178–189. https://doi.org/10.1016/j.brainres.2006.04.039

Anderson, J.P., Walker, D.E., Goldstein, J.M., Laat, R. de, Banducci, K., Caccavello, R.J., Barbour, R., Huang, J., Kling, K., Lee, M., Diep, L., Keim, P.S., Shen, X., Chataway, T., Schlossmacher, M.G., Seubert, P., Schenk, D., Sinha, S., Gai, W.P., Chilcote, T.J., 2006. Phosphorylation of Ser-129 Is the Dominant Pathological Modification of α-Synuclein in Familial and Sporadic Lewy Body Disease *. Journal of Biological Chemistry 281, 29739–29752. https://doi.org/10.1074/jbc.M600933200

Andrews, S., 2010. FASTQC. A quality control tool for high throughput sequence data.

Antony, Paul M. A., Diederich, N.J., Krüger, R., Balling, R., 2013. The hallmarks of Parkinson's disease. The FEBS Journal 280, 5981–5993. https://doi.org/10.1111/febs.12335

Antony, Paul M A, Diederich, N.J., Krüger, R., Balling, R., 2013. The hallmarks of Parkinson's disease. The FEBS journal 280, 5981–93. https://doi.org/10.1111/febs.12335

Arena, G., Landoulsi, Z., Grossmann, D., Vitali, A., Delcambre, S., Baron, A., Antony, P., Boussaad, I., Bobbili, D.R., Sreelatha, A.A.K., Pavelka, L., Klein, C., Seibler, P., Glaab, E., Sharma, M., Krüger, R., May, P., Grünewald, A., 2023. Polygenic risk scores validated in patient-derived cells stratify for mitochondrial subtypes of Parkinson's disease. https://doi.org/10.1101/2023.05.12.23289877

Arias-Fuenzalida, J., Jarazo, J., Walter, J., Gomez-Giro, G., Forster, J.I., Krueger, R., Antony, P.M.A., Schwamborn, J.C., 2019. Automated high-throughput high-content autophagy and mitophagy analysis platform. Sci Rep 9, 9455. https://doi.org/10.1038/s41598-019-45917-2

Ashrafi, A., Garcia, P., Kollmus, H., Schughart, K., Del Sol, A., Buttini, M., Glaab, E., 2017. Absence of regulator of G-protein signaling 4 does not protect against dopamine neuron dysfunction and injury in the mouse 6-hydroxydopamine lesion model of Parkinson's disease. Neurobiology of Aging 58, 30–33. https://doi.org/10.1016/j.neurobiolaging.2017.06.008

Ashrafi, G., Juan-Sanz, J. de, Farrell, R.J., Ryan, T.A., 2020. Molecular Tuning of the Axonal Mitochondrial Ca2+ Uniporter Ensures Metabolic Flexibility of Neurotransmission. Neuron 105, 678-687.e5. https://doi.org/10.1016/j.neuron.2019.11.020

Babenko, V., Silachev, D., Popkov, V., Zorova, L., Pevzner, I., Plotnikov, E., Sukhikh, G., Zorov, D., 2018. Miro1 Enhances Mitochondria Transfer from Multipotent Mesenchymal Stem Cells (MMSC) to Neural Cells and Improves the Efficacy of Cell Recovery. Molecules 23, 687. https://doi.org/10.3390/molecules23030687

Babic, M., Russo, G.J., Wellington, A.J., Sangston, R.M., Gonzalez, M., Zinsmaier, K.E., 2015. Miro's N-Terminal GTPase Domain Is Required for Transport of Mitochondria into Axons and Dendrites. Journal of Neuroscience 35, 5754–5771. https://doi.org/10.1523/JNEUROSCI.1035-14.2015

Baev, A.Y., Vinokurov, A.Y., Novikova, I.N., Dremin, V. V, Potapova, E. V, Abramov, A.Y., 2022. Interaction of Mitochondrial Calcium and ROS in Neurodegeneration. Cells 11, 706.

https://doi.org/10.3390/cells11040706
Balderas, E., Eberhardt, D.R., Lee, S., Pleinis, J.M., Sommakia, S., Balynas, A.M., Yin, X., Parker, M.C., Maguire, C.T., Cho, S., Szulik, M.W., Bakhtina, A., Bia, R.D., Friederich, M.W., Locke, T.M., Van Hove, J.L.K., Drakos, S.G., Sancak, Y., Tristani-Firouzi, M., Franklin, S., Rodan, A.R., Chaudhuri, D., 2022. Mitochondrial calcium uniporter stabilization preserves energetic homeostasis during Complex I impairment. Nat Commun 13, 2769. https://doi.org/10.1038/s41467-022-30236-4
Barasa, A., Wang, J., Dewey, R.B., 2021. Probable REM Sleep Behavior Disorder Is a Risk Factor for Symptom Progression in Parkinson Disease. Frontiers in Neurology 12.
Barbuti, P.A., Santos, B.FR., Antony, P.M., Massart, F., Cruciani, G., Dording, C.M., Pavelka, L., Kwon, Y.-J., Krüger, R., 2020. Gene-corrected Parkinson's disease neurons show the A30P alpha-synuclein point mutation leads to reduced neuronal branching and function (preprint). Neuroscience. https://doi.org/10.1101/2020.11.05.369389
Bayne, A.N., Trempe, J.-F., 2019. Mechanisms of PINK1, ubiquitin and Parkin interactions in mitochondrial quality control and beyond. Cell. Mol. Life Sci. 76, 4589–4611. https://doi.org/10.1007/s00018-019-03203-4
Becht, E., McInnes, L., Healy, J., Dutertre, C.-A., Kwok, I.W.H., Ng, L.G., Ginhoux, F., Newell, E.W., 2019. Dimensionality reduction for visualizing single-cell data using UMAP. Nature Biotechnology 37, 38–44. https://doi.org/10.1038/nbt.4314
Beckervordersandforth, R., Ebert, B., Schäffner, I., Moss, J., Fiebig, C., Shin, J., Moore, D.L., Ghosh, L., Trinchero, M.F., Stockburger, C., Friedland, K., Steib, K., von Wittgenstein, J., Keiner, S., Redecker, C., Hölter, S.M., Xiang, W., Wurst, W., Jagasia, R., Schinder, A.F., Ming, G.-L., Toni, N., Jessberger, S., Song, H., Lie, D.C., 2017. Role of Mitochondrial Metabolism in the Control of Early Lineage Progression and Aging Phenotypes in Adult Hippocampal Neurogenesis. Neuron 93, 560-573.e6. https://doi.org/10.1016/j.neuron.2016.12.017
Ben-Ari Fuchs, S., Lieder, I., Stelzer, G., Mazor, Y., Buzhor, E., Kaplan, S., Bogoch, Y., Plaschkes, I., Shitrit, A., Rappaport, N., Kohn, A., Edgar, R., Shenhav, L., Safran, M., Lancet, D., Guan-Golan, Y., Warshawsky, D., Shtrichman, R., 2016. GeneAnalytics: An Integrative Gene Set Analysis Tool for Next Generation Sequencing, RNAseq and Microarray Data. OMICS: A Journal of Integrative Biology 20, 139–151. https://doi.org/10.1089/omi.2015.0168
Benedetti, C., Haynes, C.M., Yang, Y., Harding, H.P., Ron, D., 2006. Ubiquitin-Like Protein 5 Positively Regulates Chaperone Gene Expression in the Mitochondrial Unfolded Protein Response. Genetics 174, 229–239. https://doi.org/10.1534/genetics.106.061580
Bentea, E., Verbruggen, L., Massie, A., 2017. The Proteasome Inhibition Model of Parkinson's Disease. J Parkinsons Dis 7, 31–63. https://doi.org/10.3233/JPD-160921
Berenguer-Escuder, C., Grossmann, D., Antony, P., Arena, G., Wasner, K., Massart, F., Jarazo, J., Walter, J., Schwamborn, J.C., Grünewald, A., Krüger, R., 2020a. Impaired mitochondrial–endoplasmic reticulum interaction and mitophagy in Miro1-mutant neurons in Parkinson's disease. Human Molecular Genetics ddaa066. https://doi.org/10.1093/hmg/ddaa066
Berenguer-Escuder, C., Grossmann, D., Antony, P., Arena, G., Wasner, K., Massart, F., Jarazo, J., Walter, J., Schwamborn, J.C., Grünewald, A., Krüger, R., 2020b. Impaired mitochondrial-endoplasmic reticulum interaction and mitophagy in Miro1-mutant neurons in Parkinson's disease. Human molecular genetics 29, 1353–1364. https://doi.org/10.1093/hmg/ddaa066
Berenguer-Escuder, C., Grossmann, D., Massart, F., Antony, P., Burbulla, L.F., Glaab, E., Imhoff, S., Trinh, J., Seibler, P., Grünewald, A., Krüger, R., 2019a. Variants in Miro1 Cause Alterations of ER-Mitochondria Contact Sites in Fibroblasts from Parkinson's Disease Patients. JCM 8, 2226. https://doi.org/10.3390/jcm8122226
Berenguer-Escuder, C., Grossmann, D., Massart, F., Antony, P., Burbulla, L.F., Glaab, E., Imhoff, S., Trinh, J., Seibler, P., Grünewald, A., Krüger, R., 2019b. Variants in Miro1 Cause Alterations of ER-

Mitochondria Contact Sites in Fibroblasts from Parkinson's Disease Patients. Journal of Clinical Medicine 8, 2226. https://doi.org/10.3390/jcm8122226
Bharat, V., Hsieh, C.-H., Wang, X., 2021. Mitochondrial Defects in Fibroblasts of Pathogenic MAPT Patients. Front. Cell Dev. Biol. 9, 765408. https://doi.org/10.3389/fcell.2021.765408
Bharat, V., Vanhauwaert, R., Li, L., Muir, C.M., Durairaj, A.S., Chandra, S., Guen, Y. Le, Nandakishore, P., Hsieh, C.-H., Rensi, S.E., Altman, R.B., Greicius, M.D., Feng, L., Wang, X., 2022a. An Iron-Calcium-Miro Axis Influences Parkinson's Risk and Neurodegeneration. bioRxiv 2022.10.30.513580. https://doi.org/10.1101/2022.10.30.513580
Bharat, V., Vanhauwaert, R., Li, L., Muir, C.M., Durairaj, A.S., Chandra, S., Guen, Y.L., Nandakishore, P., Hsieh, C.-H., Rensi, S.E., Altman, R.B., Greicius, M.D., Feng, L., Wang, X., 2022b. An Iron-Calcium-Miro Axis Influences Parkinson's Risk and Neurodegeneration (preprint). Cell Biology. https://doi.org/10.1101/2022.10.30.513580
Bharat, V., Wang, X., 2020. Precision Neurology for Parkinson's Disease: Coupling Miro1-Based Diagnosis With Drug Discovery. Movement disorders : official journal of the Movement Disorder Society 35, 1502–1508. https://doi.org/10.1002/mds.28194
Blesa, J., Trigo-Damas, I., Quiroga-Varela, A., del Rey, N.L.-G., 2016a. Animal Models of Parkinson's Disease, in: Challenges in Parkinson's Disease. InTech. https://doi.org/10.5772/63328
Blesa, J., Trigo-Damas, I., Quiroga-Varela, A., Rey, N.L.-G. del, Blesa, J., Trigo-Damas, I., Quiroga-Varela, A., Rey, N.L.-G. del, 2016b. Animal Models of Parkinson's Disease, in: Challenges in Parkinson's Disease. IntechOpen. https://doi.org/10.5772/63328
Bohush, A., Niewiadomska, G., Filipek, A., 2018. Role of Mitogen Activated Protein Kinase Signaling in Parkinson's Disease. International Journal of Molecular Sciences 19, 2973. https://doi.org/10.3390/ijms19102973
Bolognin, S., Fossépré, M., Qing, X., Jarazo, J., Ščančar, J., Moreno, E.L., Nickels, S.L., Wasner, K., Ouzren, N., Walter, J., Grünewald, A., Glaab, E., Salamanca, L., Fleming, R.M.T., Antony, P.M.A., Schwamborn, J.C., 2019. 3D Cultures of Parkinson's Disease-Specific Dopaminergic Neurons for High Content Phenotyping and Drug Testing. Advanced Science 6, 1800927. https://doi.org/10.1002/advs.201800927
Boy, J., Schmidt, T., Wolburg, H., Mack, A., Nuber, S., Böttcher, M., Schmitt, I., Holzmann, C., Zimmermann, F., Servadio, A., Riess, O., 2009a. Reversibility of symptoms in a conditional mouse model of spinocerebellar ataxia type 3. Hum Mol Genet 18, 4282–4295. https://doi.org/10.1093/hmg/ddp381
Boy, J., Schmidt, T., Wolburg, H., Mack, A., Nuber, S., Böttcher, M., Schmitt, I., Holzmann, C., Zimmermann, F., Servadio, A., Riess, O., 2009b. Reversibility of symptoms in a conditional mouse model of spinocerebellar ataxia type 3. Human Molecular Genetics 18, 4282–4295. https://doi.org/10.1093/hmg/ddp381
Brakedal, B., Dölle, C., Riemer, F., Ma, Y., Nido, G.S., Skeie, G.O., Craven, A.R., Schwarzlmüller, T., Brekke, N., Diab, J., Sverkeli, L., Skjeie, V., Varhaug, K., Tysnes, O.-B., Peng, S., Haugarvoll, K., Ziegler, M., Grüner, R., Eidelberg, D., Tzoulis, C., 2022. The NADPARK study: A randomized phase I trial of nicotinamide riboside supplementation in Parkinson's disease. Cell Metabolism 34, 396-407.e6. https://doi.org/10.1016/j.cmet.2022.02.001
Brand, M.D., 2010. The sites and topology of mitochondrial superoxide production. Exp Gerontol 45, 466–472. https://doi.org/10.1016/j.exger.2010.01.003
Brembati, V., Faustini, G., Longhena, F., Bellucci, A., 2023. Alpha synuclein post translational modifications: potential targets for Parkinson's disease therapy? Front Mol Neurosci 16, 1197853. https://doi.org/10.3389/fnmol.2023.1197853
Burbulla, L.F., Song, P., Mazzulli, J.R., Zampese, E., Wong, Y.C., Jeon, S., Santos, D.P., Blanz, J., Obermaier, C.D., Strojny, C., Savas, J.N., Kiskinis, E., Zhuang, X., Krüger, R., Surmeier, D.J., Krainc, D., 2017.

Dopamine oxidation mediates mitochondrial and lysosomal dysfunction in Parkinson's disease. Science 357, 1255–1261. https://doi.org/10.1126/science.aam9080

Bus, C., Zizmare, L., Feldkaemper, M., Geisler, S., Zarani, M., Schaedler, A., Klose, F., Admard, J., Mageean, C.J., Arena, G., Fallier-Becker, P., Ugun-Klusek, A., Maruszczak, K.K., Kapolou, K., Schmid, B., Rapaport, D., Ueffing, M., Casadei, N., Krüger, R., Gasser, T., Vogt Weisenhorn, D.M., Kahle, P.J., Trautwein, C., Gloeckner, C.J., Fitzgerald, J.C., 2020. Human Dopaminergic Neurons Lacking PINK1 Exhibit Disrupted Dopamine Metabolism Related to Vitamin B6 Co-Factors. iScience 23, 101797. https://doi.org/10.1016/j.isci.2020.101797

Byers, B., Cord, B., Nguyen, H.N., Schüle, B., Fenno, L., Lee, P.C., Deisseroth, K., Langston, J.W., Pera, R.R., Palmer, T.D., 2011. SNCA triplication Parkinson's patient's iPSC-derived DA neurons accumulate α-synuclein and are susceptible to oxidative stress. PLoS One 6, e26159. https://doi.org/10.1371/journal.pone.0026159

Cai, H., Liu, G., Sun, L., Ding, J., 2014. Aldehyde Dehydrogenase 1 making molecular inroads into the differential vulnerability of nigrostriatal dopaminergic neuron subtypes in Parkinson's disease. Transl Neurodegener 3, 27. https://doi.org/10.1186/2047-9158-3-27

Castellazzi, M., Patergnani, S., Donadio, M., Giorgi, C., Bonora, M., Fainardi, E., Casetta, I., Granieri, E., Pugliatti, M., Pinton, P., 2019. Correlation between auto/mitophagic processes and magnetic resonance imaging activity in multiple sclerosis patients. Journal of neuroinflammation 16, 131. https://doi.org/10.1186/s12974-019-1526-0

Castro, I.G., Richards, D.M., Metz, J., Costello, J.L., Passmore, J.B., Schrader, T.A., Gouveia, A., Ribeiro, D., Schrader, M., 2018. A role for Mitochondrial Rho GTPase 1 (MIRO1) in motility and membrane dynamics of peroxisomes. Traffic 19, 229–242. https://doi.org/10.1111/tra.12549

Castro, I.G., Schrader, M., 2018. Miro1 - the missing link to peroxisome motility. Commun Integr Biol 11, e1526573. https://doi.org/10.1080/19420889.2018.1526573

Chang, E.E.S., Ho, P.W.-L., Liu, H.-F., Pang, S.Y.-Y., Leung, C.-T., Malki, Y., Choi, Z.Y.-K., Ramsden, D.B., Ho, S.-L., 2022. LRRK2 mutant knock-in mouse models: therapeutic relevance in Parkinson's disease. Translational Neurodegeneration 11, 10. https://doi.org/10.1186/s40035-022-00285-2

Chang, K.T., Niescier, R.F., Min, K.-T., 2011. Mitochondrial matrix Ca2+ as an intrinsic signal regulating mitochondrial motility in axons. Proceedings of the National Academy of Sciences 108, 15456–15461. https://doi.org/10.1073/pnas.1106862108

Chaudhuri, K.R., Schapira, A.H.V., 2009. Non-motor symptoms of Parkinson's disease: dopaminergic pathophysiology and treatment. Lancet Neurol 8, 464–474. https://doi.org/10.1016/S1474-4422(09)70068-7

Chemla, A., Arena, G., Onal, G., Walter, J., Berenguer-Escuder, C., Grossmann, D., Grünewald, A., Schwamborn, J.C., Krüger, R., 2023. Generation of two induced pluripotent stem cell lines and the corresponding isogenic controls from Parkinson's disease patients carrying the heterozygous mutations c.815G{\textgreater}A (p.R272Q) or c.1348C{\textgreater}T (p.R450C) in the RHOT1 gene encod. Stem Cell Research 103145. https://doi.org/10.1016/j.scr.2023.103145

Chen, L., Liu, C., Gao, J., Xie, Z., Chan, L.W.C., Keating, D.J., Yang, Y., Sun, J., Zhou, F., Wei, Y., Men, X., Yang, S., 2017. Inhibition of Miro1 disturbs mitophagy and pancreatic β-cell function interfering insulin release via IRS-Akt-Foxo1 in diabetes. Oncotarget 8, 90693–90705. https://doi.org/10.18632/oncotarget.20963

Cherubini, M., Wade-Martins, R., 2018. Convergent pathways in Parkinson's disease. Cell and Tissue Research 373, 79–90. https://doi.org/10.1007/s00441-017-2700-2

Chesselet, M.-F., Fleming, S., Mortazavi, F., Meurers, B., 2008. Strengths and Limitations of Genetic Mouse Models of Parkinson's Disease. Parkinsonism Relat Disord 14, S84–S87. https://doi.org/10.1016/j.parkreldis.2008.04.004

Choi, M.L., Chappard, A., Singh, B.P., Maclachlan, C., Rodrigues, M., Fedotova, E.I., Berezhnov, A.V., De,

S., Peddie, C.J., Athauda, D., Virdi, G.S., Zhang, W., Evans, J.R., Wernick, A.I., Zanjani, Z.S., Angelova, P.R., Esteras, N., Vinokurov, A.Y., Morris, K., Jeacock, K., Tosatto, L., Little, D., Gissen, P., Clarke, D.J., Kunath, T., Collinson, L., Klenerman, D., Abramov, A.Y., Horrocks, M.H., Gandhi, S., 2022. Pathological structural conversion of α-synuclein at the mitochondria induces neuronal toxicity. Nat Neurosci 25, 1134–1148. https://doi.org/10.1038/s41593-022-01140-3

Chung, K.K.K., Dawson, V.L., Dawson, T.M., 2003. New insights into Parkinson's disease. J Neurol 250 Suppl 3, III15-24. https://doi.org/10.1007/s00415-003-1304-9

Chung, S.Y., Kishinevsky, S., Mazzulli, J.R., Graziotto, J., Mrejeru, A., Mosharov, E.V., Puspita, L., Valiulahi, P., Sulzer, D., Milner, T.A., Taldone, T., Krainc, D., Studer, L., Shim, J., 2016. Parkin and PINK1 Patient iPSC-Derived Midbrain Dopamine Neurons Exhibit Mitochondrial Dysfunction and α-Synuclein Accumulation. Stem Cell Reports 7, 664–677. https://doi.org/10.1016/j.stemcr.2016.08.012

Cieri, D., Vicario, M., Giacomello, M., Vallese, F., Filadi, R., Wagner, T., Pozzan, T., Pizzo, P., Scorrano, L., Brini, M., Calì, T., 2018. SPLICS: a split green fluorescent protein-based contact site sensor for narrow and wide heterotypic organelle juxtaposition. Cell Death Differ 25, 1131–1145. https://doi.org/10.1038/s41418-017-0033-z

Cmarko, L., Weiss, N., 2020. Selective inhibition of neuronal Cav3.3 T-type calcium channels by TAT-based channel peptide. Mol Brain 13, 95. https://doi.org/10.1186/s13041-020-00636-y

Colicelli, J., 2004. Human RAS Superfamily Proteins and Related GTPases. Science Signaling 2004, re13–re13. https://doi.org/10.1126/stke.2502004re13

Collatz, M.B., Rüdel, R., Brinkmeier, H., 1997. Intracellular calcium chelator BAPTA protects cells against toxic calcium overload but also alters physiological calcium responses. Cell Calcium 21, 453–459. https://doi.org/10.1016/S0143-4160(97)90056-7

Congdon, E.E., 2018. Sex Differences in Autophagy Contribute to Female Vulnerability in Alzheimer's Disease. Frontiers in Neuroscience 12.

Conner, M.R., Jang, D., Anderson, B.J., Kritzer, M.F., 2020. Biological Sex and Sex Hormone Impacts on Deficits in Episodic-Like Memory in a Rat Model of Early, Pre-motor Stages of Parkinson's Disease. Frontiers in Neurology 11.

Corsini, N.S., Knoblich, J.A., 2022. Human organoids: New strategies and methods for analyzing human development and disease. Cell 185, 2756–2769. https://doi.org/10.1016/j.cell.2022.06.051

Costello, J.L., Castro, I.G., Camões, F., Schrader, T.A., McNeall, D., Yang, J., Giannopoulou, E.-A., Gomes, S., Pogenberg, V., Bonekamp, N.A., Ribeiro, D., Wilmanns, M., Jedd, G., Islinger, M., Schrader, M., 2017. Predicting the targeting of tail-anchored proteins to subcellular compartments in mammalian cells. J Cell Sci 130, 1675–1687. https://doi.org/10.1242/jcs.200204

Course, M.M., Wang, X., 2016. Transporting mitochondria in neurons. F1000Res 5, 1735. https://doi.org/10.12688/f1000research.7864.1

Covill-Cooke, C., Toncheva, V.S., Drew, J., Birsa, N., López-Doménech, G., Kittler, J.T., 2020. Peroxisomal fission is modulated by the mitochondrial Rho-GTPases, Miro1 and Miro2. EMBO Rep 21. https://doi.org/10.15252/embr.201949865

Day, J.O., Mullin, S., 2021. The Genetics of Parkinson's Disease and Implications for Clinical Practice. Genes 12, 1006. https://doi.org/10.3390/genes12071006

de Lau, L.M.L., Breteler, M.M.B., 2006. Epidemiology of Parkinson's disease. Lancet Neurol 5, 525–535. https://doi.org/10.1016/S1474-4422(06)70471-9

Dias, V., Junn, E., Mouradian, M.M., 2013. The role of oxidative stress in Parkinson's disease. J Parkinsons Dis 3, 461–491. https://doi.org/10.3233/JPD-130230

Diepenbroek, M., Casadei, N., Esmer, H., Saido, T.C., Takano, J., Kahle, P.J., Nixon, R.A., Rao, M.V., Melki, R., Pieri, L., Helling, S., Marcus, K., Krueger, R., Masliah, E., Riess, O., Nuber, S., 2014. Overexpression of the calpain-specific inhibitor calpastatin reduces human alpha-Synuclein

processing, aggregation and synaptic impairment in [A30P]αSyn transgenic mice. Hum Mol Genet 23, 3975–3989. https://doi.org/10.1093/hmg/ddu112

Dixit, E., Boulant, S., Zhang, Y., Lee, A.S.Y., Odendall, C., Shum, B., Hacohen, N., Chen, Z.J., Whelan, S.P., Fransen, M., Nibert, M.L., Superti-Furga, G., Kagan, J.C., 2010. Peroxisomes are signaling platforms for antiviral innate immunity. Cell 141, 668–681. https://doi.org/10.1016/j.cell.2010.04.018

Dobin, A., Davis, C.A., Schlesinger, F., Drenkow, J., Zaleski, C., Jha, S., Batut, P., Chaisson, M., Gingeras, T.R., 2013. STAR: ultrafast universal RNA-seq aligner. Bioinformatics 29, 15–21. https://doi.org/10.1093/bioinformatics/bts635

Dodson, P.D., Dreyer, J.K., Jennings, K.A., Syed, E.C.J., Wade-Martins, R., Cragg, S.J., Bolam, J.P., Magill, P.J., 2016. Representation of spontaneous movement by dopaminergic neurons is cell-type selective and disrupted in parkinsonism. Proceedings of the National Academy of Sciences of the United States of America 113, E2180-8. https://doi.org/10.1073/pnas.1515941113

Dorsey, E.R., Elbaz, A., Nichols, E., Abd-Allah, F., Abdelalim, A., Adsuar, J.C., Ansha, M.G., Brayne, C., Choi, J.-Y.J., Collado-Mateo, D., Dahodwala, N., Do, H.P., Edessa, D., Endres, M., Fereshtehnejad, S.-M., Foreman, K.J., Gankpe, F.G., Gupta, R., Hankey, G.J., Hay, S.I., Hegazy, M.I., Hibstu, D.T., Kasaeian, A., Khader, Y., Khalil, I., Khang, Y.-H., Kim, Y.J., Kokubo, Y., Logroscino, G., Massano, J., Ibrahim, N.M., Mohammed, M.A., Mohammadi, A., Moradi-Lakeh, M., Naghavi, M., Nguyen, B.T., Nirayo, Y.L., Ogbo, F.A., Owolabi, M.O., Pereira, D.M., Postma, M.J., Qorbani, M., Rahman, M.A., Roba, K.T., Safari, H., Safiri, S., Satpathy, M., Sawhney, M., Shafieesabet, A., Shiferaw, M.S., Smith, M., Szoeke, C.E.I., Tabarés-Seisdedos, R., Truong, N.T., Ukwaja, K.N., Venketasubramanian, N., Villafaina, S., Weldegwergs, K. gidey, Westerman, R., Wijeratne, T., Winkler, A.S., Xuan, B.T., Yonemoto, N., Feigin, V.L., Vos, T., Murray, C.J.L., 2018a. Global, regional, and national burden of Parkinson's disease, 1990–2016: a systematic analysis for the Global Burden of Disease Study 2016. The Lancet Neurology 17, 939–953. https://doi.org/10.1016/S1474-4422(18)30295-3

Dorsey, E.R., Sherer, T., Okun, M.S., Bloem, B.R., 2018b. The Emerging Evidence of the Parkinson Pandemic. JPD 8, S3–S8. https://doi.org/10.3233/JPD-181474

Dufty, B.M., Warner, L.R., Hou, S.T., Jiang, S.X., Gomez-Isla, T., Leenhouts, K.M., Oxford, J.T., Feany, M.B., Masliah, E., Rohn, T.T., 2007. Calpain-cleavage of alpha-synuclein: connecting proteolytic processing to disease-linked aggregation. Am J Pathol 170, 1725–1738. https://doi.org/10.2353/ajpath.2007.061232

Ebrahimi-Fakhari, D., Wahlster, L., McLean, P.J., 2012. PROTEIN DEGRADATION PATHWAYS IN PARKINSON'S DISEASE – CURSE OR BLESSING. Acta Neuropathol 124, 153–172. https://doi.org/10.1007/s00401-012-1004-6

Emmanouilidou, E., Melachroinou, K., Roumeliotis, T., Garbis, S.D., Ntzouni, M., Margaritis, L.H., Stefanis, L., Vekrellis, K., 2010. Cell-Produced α-Synuclein Is Secreted in a Calcium-Dependent Manner by Exosomes and Impacts Neuronal Survival. J Neurosci 30, 6838–6851. https://doi.org/10.1523/JNEUROSCI.5699-09.2010

English, K., Shepherd, A., Uzor, N.-E., Trinh, R., Kavelaars, A., Heijnen, C.J., 2020. Astrocytes rescue neuronal health after cisplatin treatment through mitochondrial transfer. acta neuropathol commun 8, 36. https://doi.org/10.1186/s40478-020-00897-7

Fahed, A.C., Wang, M., Homburger, J.R., Patel, A.P., Bick, A.G., Neben, C.L., Lai, C., Brockman, D., Philippakis, A., Ellinor, P.T., Cassa, C.A., Lebo, M., Ng, K., Lander, E.S., Zhou, A.Y., Kathiresan, S., Khera, A. V, 2020. Polygenic background modifies penetrance of monogenic variants for tier 1 genomic conditions. Nature communications 11, 3635. https://doi.org/10.1038/s41467-020-17374-3

Fang, C., Hernandez, P., Liow, K., Damiano, E., Zetterberg, H., Blennow, K., Feng, D., Chen, M., Maccecchini, M., 2023. Buntanetap, a Novel Translational Inhibitor of Multiple Neurotoxic

Proteins, Proves to Be Safe and Promising in Both Alzheimer's and Parkinson's Patients. J Prev Alzheimers Dis 10, 25–33. https://doi.org/10.14283/jpad.2022.84

Feigin, V.L., Abajobir, A.A., Abate, K.H., Abd-Allah, F., Abdulle, A.M., Abera, S.F., Abyu, G.Y., Ahmed, M.B., Aichour, A.N., Aichour, I., Aichour, M.T.E., Akinyemi, R.O., Alabed, S., Al-Raddadi, R., Alvis-Guzman, N., Amare, A.T., Ansari, H., Anwari, P., Ärnlöv, J., Asayesh, H., Asgedom, S.W., Atey, T.M., Avila-Burgos, L., Frinel, E., Avokpaho, G.A., Azarpazhooh, M.R., Barac, A., Barboza, M., Barker-Collo, S.L., Bärnighausen, T., Bedi, N., Beghi, E., Bennett, D.A., Bensenor, I.M., Berhane, A., Betsu, B.D., Bhaumik, S., Birlik, S.M., Biryukov, S., Boneya, D.J., Bulto, L.N.B., Carabin, H., Casey, D., Castañeda-Orjuela, C.A., Catalá-López, F., Chen, H., Chitheer, A.A., Chowdhury, R., Christensen, H., Dandona, L., Dandona, R., de Veber, G.A., Dharmaratne, S.D., Do, H.P., Dokova, K., Dorsey, E.R., Ellenbogen, R.G., Eskandarieh, S., Farvid, M.S., Fereshtehnejad, S.-M., Fischer, F., Foreman, K.J., Geleijnse, J.M., Gillum, R.F., Giussani, G., Goldberg, E.M., Gona, P.N., Goulart, A.C., Gugnani, H.C., Gupta, Rahul, Hachinski, V., Gupta, Rajeev, Hamadeh, R.R., Hambisa, M., Hankey, G.J., Hareri, H.A., Havmoeller, R., Hay, S.I., Heydarpour, P., Hotez, P.J., Jakovljevic, M. (Michael) B., Javanbakht, M., Jeemon, P., Jonas, J.B., Kalkonde, Y., Kandel, A., Karch, A., Kasaeian, A., Kastor, A., Keiyoro, P.N., Khader, Y.S., Khalil, I.A., Khan, E.A., Khang, Y.-H., Tawfih, A., Khoja, A., Khubchandani, J., Kulkarni, C., Kim, D., Kim, Y.J., Kivimaki, M., Kokubo, Y., Kosen, S., Kravchenko, M., Krishnamurthi, R.V., Defo, B.K., Kumar, G.A., Kumar, R., Kyu, H.H., Larsson, A., Lavados, P.M., Li, Y., Liang, X., Liben, M.L., Lo, W.D., Logroscino, G., Lotufo, P.A., Loy, C.T., Mackay, M.T., El Razek, H.M.A., El Razek, M.M.A., Majeed, A., Malekzadeh, R., Manhertz, T., Mantovani, L.G., Massano, J., Mazidi, M., McAlinden, C., Mehata, S., Mehndiratta, M.M., Memish, Z.A., Mendoza, W., Mengistie, M.A., Mensah, G.A., Meretoja, A., Mezgebe, H.B., Miller, T.R., Mishra, S.R., Ibrahim, N.M., Mohammadi, A., Mohammed, K.E., Mohammed, S., Mokdad, A.H., Moradi-Lakeh, M., Velasquez, I.M., Musa, K.I., Naghavi, M., Ngunjiri, J.W., Nguyen, C.T., Nguyen, G., Le Nguyen, Q., Nguyen, T.H., Nichols, E., Ningrum, D.N.A., Nong, V.M., Norrving, B., Noubiap, J.J.N., Ogbo, F.A., Owolabi, M.O., Pandian, J.D., Parmar, P.G., Pereira, D.M., Petzold, M., Phillips, M.R., Piradov, M.A., Poulton, R.G., Pourmalek, F., Qorbani, M., Rafay, A., Rahman, M., Rahman, M.H., Rai, R.K., Rajsic, S., Ranta, A., Rawaf, S., Renzaho, A.M.N., Rezai, M.S., Roth, G.A., Roshandel, G., Rubagotti, E., Sachdev, P., Safiri, S., Sahathevan, R., Sahraian, M.A., Samy, A.M., Santalucia, P., Santos, I.S., Sartorius, B., Satpathy, M., Sawhney, M., Saylan, M.I., Sepanlou, S.G., Shaikh, M.A., Shakir, R., Shamsizadeh, M., Sheth, K.N., Shigematsu, M., Shoman, H., Silva, D.A.S., Smith, M., Sobngwi, E., Sposato, L.A., Stanaway, J.D., Stein, D.J., Steiner, T.J., Stovner, L.J., Abdulkader, R.S., El Szoeke, C., Tabarés-Seisdedos, R., Tanne, D., Theadom, A.M., Thrift, A.G., Tirschwell, D.L., Topor-Madry, R., Tran, B.X., Truelsen, T., Tuem, K.B., Ukwaja, K.N., Uthman, O.A., Varakin, Y.Y., Vasankari, T., Venketasubramanian, N., Vlassov, V.V., Wadilo, F., Wakayo, T., Wallin, M.T., Weiderpass, E., Westerman, R., Wijeratne, T., Wiysonge, C.S., Woldu, M.A., Wolfe, C.D.A., Xavier, D., Xu, G., Yano, Y., Yimam, H.H., Yonemoto, N., Yu, C., Zaidi, Z., El Sayed Zaki, M., Zunt, J.R., Murray, C.J.L., Vos, T., 2017. Global, regional, and national burden of neurological disorders during 1990–2015: a systematic analysis for the Global Burden of Disease Study 2015. The Lancet Neurology 16, 877–897. https://doi.org/10.1016/S1474-4422(17)30299-5

Fernie, A.R., Carrari, F., Sweetlove, L.J., 2004. Respiratory metabolism: glycolysis, the TCA cycle and mitochondrial electron transport. Curr Opin Plant Biol 7, 254–261. https://doi.org/10.1016/j.pbi.2004.03.007

Ferrero, H., Larrayoz, I.M., Martisova, E., Solas, M., Howlett, D.R., Francis, P.T., Gil-Bea, F.J., Martínez, A., Ramírez, M.J., 2018. Increased Levels of Brain Adrenomedullin in the Neuropathology of Alzheimer's Disease. Molecular Neurobiology 55, 5177–5183. https://doi.org/10.1007/s12035-017-0700-6

Franco-Iborra, S., Vila, M., Perier, C., 2016. The Parkinson Disease Mitochondrial Hypothesis: Where Are

We at? Neuroscientist 22, 266–277. https://doi.org/10.1177/1073858415574600
Fransson, Å., Ruusala, A., Aspenström, P., 2003. Atypical Rho GTPases Have Roles in Mitochondrial Homeostasis and Apoptosis. Journal of Biological Chemistry 278, 6495–6502. https://doi.org/10.1074/jbc.M208609200
Friedman, J.R., Nunnari, J., 2014. Mitochondrial form and function. Nature 505, 335–343. https://doi.org/10.1038/nature12985
Frith, C.D., Bloxham, C.A., Carpenter, K.N., 1986a. Impairments in the learning and performance of a new manual skill in patients with Parkinson's disease. Journal of Neurology, Neurosurgery & Psychiatry 49, 661–668. https://doi.org/10.1136/jnnp.49.6.661
Frith, C.D., Bloxham, C.A., Carpenter, K.N., 1986b. Impairments in the learning and performance of a new manual skill in patients with Parkinson's disease. Journal of neurology, neurosurgery, and psychiatry 49, 661–8. https://doi.org/10.1136/jnnp.49.6.661
Fu, H., Zhou, H., Yu, X., Xu, J., Zhou, J., Meng, X., Zhao, J., Zhou, Y., Chisholm, A.D., Xu, S., 2020. Wounding triggers MIRO-1 dependent mitochondrial fragmentation that accelerates epidermal wound closure through oxidative signaling. Nat Commun 11, 1050. https://doi.org/10.1038/s41467-020-14885-x
Fujiwara, H., Hasegawa, M., Dohmae, N., Kawashima, A., Masliah, E., Goldberg, M.S., Shen, J., Takio, K., Iwatsubo, T., 2002a. alpha-Synuclein is phosphorylated in synucleinopathy lesions. Nat Cell Biol 4, 160–164. https://doi.org/10.1038/ncb748
Fujiwara, H., Hasegawa, M., Dohmae, N., Kawashima, A., Masliah, E., Goldberg, M.S., Shen, J., Takio, K., Iwatsubo, T., 2002b. alpha-Synuclein is phosphorylated in synucleinopathy lesions. Nature cell biology 4, 160–4. https://doi.org/10.1038/ncb748
Furnish, M., Boulton, D.P., Genther, V., Grofova, D., Ellinwood, M.L., Romero, L., Lucia, M.S., Cramer, S.D., Caino, M.C., 2022. MIRO2 Regulates Prostate Cancer Cell Growth via GCN1-Dependent Stress Signaling. Mol Cancer Res 20, 607–621. https://doi.org/10.1158/1541-7786.MCR-21-0374
Gaig, C., Martí, M.J., Ezquerra, M., Cardozo, A., Rey, M.J., Tolosa, E., 2009. G2019S LRRK2 mutation causing Parkinson's disease without Lewy bodies. BMJ Case Rep 2009, bcr08.2008.0632. https://doi.org/10.1136/bcr.08.2008.0632
Gao, J., Sang, M., Zhang, X., Zheng, T., Pan, J., Dai, M., Zhou, L., Yang, S., 2015. Miro1-mediated mitochondrial dysfunction under high nutrient stress is linked to NOD-like receptor 3 (NLRP3)-dependent inflammatory responses in rat pancreatic beta cells. Free Radical Biology and Medicine 89, 322–332. https://doi.org/10.1016/j.freeradbiomed.2015.09.002
GBD 2015 Disease and Injury Incidence and Prevalence Collaborators, 2016. Global, regional, and national incidence, prevalence, and years lived with disability for 310 diseases and injuries, 1990-2015: a systematic analysis for the Global Burden of Disease Study 2015. Lancet 388, 1545–1602. https://doi.org/10.1016/S0140-6736(16)31678-6
Germer, E.L., Imhoff, S., Vilariño-Güell, C., Kasten, M., Seibler, P., Brüggemann, N., Klein, C., Trinh, J., 2019. The Role of Rare Coding Variants in Parkinson's Disease GWAS Loci. Frontiers in Neurology 10, 1284. https://doi.org/10.3389/fneur.2019.01284
Gialluisi, A., Reccia, M.G., Modugno, N., Nutile, T., Lombardi, A., Di Giovannantonio, L.G., Pietracupa, S., Ruggiero, D., Scala, S., Gambardella, S., Iacoviello, L., Gianfrancesco, F., Acampora, D., D'Esposito, M., Simeone, A., Ciullo, M., Esposito, T., 2021. Identification of sixteen novel candidate genes for late onset Parkinson's disease. Mol Neurodegener 16, 35. https://doi.org/10.1186/s13024-021-00455-2
Gispert, S., Ricciardi, F., Kurz, A., Azizov, M., Hoepken, H.-H., Becker, D., Voos, W., Leuner, K., Müller, W.E., Kudin, A.P., Kunz, W.S., Zimmermann, A., Roeper, J., Wenzel, D., Jendrach, M., García-Arencíbia, M., Fernández-Ruiz, J., Huber, L., Rohrer, H., Barrera, M., Reichert, A.S., Rüb, U., Chen, A., Nussbaum, R.L., Auburger, G., 2009. Parkinson phenotype in aged PINK1-deficient mice is

accompanied by progressive mitochondrial dysfunction in absence of neurodegeneration. PLoS One 4, e5777. https://doi.org/10.1371/journal.pone.0005777
Glaab, E., Schneider, R., 2015. Comparative pathway and network analysis of brain transcriptome changes during adult aging and in Parkinson's disease. Neurobiology of Disease 74, 1–13. https://doi.org/10.1016/j.nbd.2014.11.002
Goldberg, Matthew S., Fleming, S.M., Palacino, J.J., Cepeda, C., Lam, H.A., Bhatnagar, A., Meloni, E.G., Wu, N., Ackerson, L.C., Klapstein, G.J., Gajendiran, M., Roth, B.L., Chesselet, M.-F., Maidment, N.T., Levine, M.S., Shen, J., 2003. Parkin-deficient Mice Exhibit Nigrostriatal Deficits but Not Loss of Dopaminergic Neurons *. Journal of Biological Chemistry 278, 43628–43635. https://doi.org/10.1074/jbc.M308947200
Goldberg, Matthew S, Fleming, S.M., Palacino, J.J., Cepeda, C., Lam, H.A., Bhatnagar, A., Meloni, E.G., Wu, N., Ackerson, L.C., Klapstein, G.J., Gajendiran, M., Roth, B.L., Chesselet, M.-F., Maidment, N.T., Levine, M.S., Shen, J., 2003. Parkin-deficient Mice Exhibit Nigrostriatal Deficits but Not Loss of Dopaminergic Neurons. Journal of Biological Chemistry 278, 43628–43635. https://doi.org/10.1074/jbc.M308947200
Goldman, S.M., Marek, K., Ottman, R., Meng, C., Comyns, K., Chan, P., Ma, J., Marras, C., Langston, J.W., Ross, G.W., Tanner, C.M., 2019. Concordance for Parkinson's disease in twins: A 20-year update. Ann Neurol 85, 600–605. https://doi.org/10.1002/ana.25441
Grossmann, D., Berenguer-Escuder, C., Bellet, M.E., Scheibner, D., Bohler, J., Massart, F., Rapaport, D., Skupin, A., Fouquier d'Hérouël, A., Sharma, M., Ghelfi, J., Raković, A., Lichtner, P., Antony, P., Glaab, E., May, P., Dimmer, K.S., Fitzgerald, J.C., Grünewald, A., Krüger, R., 2019a. Mutations in *RHOT1* Disrupt Endoplasmic Reticulum–Mitochondria Contact Sites Interfering with Calcium Homeostasis and Mitochondrial Dynamics in Parkinson's Disease. Antioxidants & Redox Signaling 31, 1213–1234. https://doi.org/10.1089/ars.2018.7718
Grossmann, D., Berenguer-Escuder, C., Bellet, M.E., Scheibner, D., Bohler, J., Massart, F., Rapaport, D., Skupin, A., Fouquier d'Hérouël, A., Sharma, M., Ghelfi, J., Raković, A., Lichtner, P., Antony, P., Glaab, E., May, P., Dimmer, K.S., Fitzgerald, J.C., Grünewald, A., Krüger, R., 2019b. Mutations in RHOT1 Disrupt Endoplasmic Reticulum–Mitochondria Contact Sites Interfering with Calcium Homeostasis and Mitochondrial Dynamics in Parkinson's Disease. Antioxidants & Redox Signaling 31, 1213–1234. https://doi.org/10.1089/ars.2018.7718
Grossmann, D., Berenguer-Escuder, C., Chemla, A., Arena, G., Krüger, R., 2020a. The Emerging Role of RHOT1/Miro1 in the Pathogenesis of Parkinson's Disease. Front. Neurol. 11, 587. https://doi.org/10.3389/fneur.2020.00587
Grossmann, D., Berenguer-Escuder, C., Chemla, A., Arena, G., Krüger, R., 2020b. The Emerging Role of RHOT1/Miro1 in the Pathogenesis of Parkinson's Disease. Frontiers in neurology 11, 587. https://doi.org/10.3389/fneur.2020.00587
Grossmann, D., Krüger, R., 2020. The Emerging Role of RHOT1/Miro1 in the Pathogenesis of Parkinson's Disease. Frontiers in Neurology 11, 20.
Groten, C.J., MacVicar, B.A., 2022. Mitochondrial Ca2+ uptake by the MCU facilitates pyramidal neuron excitability and metabolism during action potential firing. Commun Biol 5, 1–15. https://doi.org/10.1038/s42003-022-03848-1
Grünewald, A., Kumar, K.R., Sue, C.M., 2019. New insights into the complex role of mitochondria in Parkinson's disease. Prog Neurobiol 177, 73–93. https://doi.org/10.1016/j.pneurobio.2018.09.003
Grünewald, A., Rygiel, K.A., Hepplewhite, P.D., Morris, C.M., Picard, M., Turnbull, D.M., 2016. Mitochondrial DNA Depletion in Respiratory Chain-Deficient Parkinson Disease Neurons. Ann Neurol 79, 366–378. https://doi.org/10.1002/ana.24571
Guardia-Laguarta, C., Area-Gomez, E., Rüb, C., Liu, Y., Magrané, J., Becker, D., Voos, W., Schon, E.A.,

Przedborski, S., 2014. α-Synuclein Is Localized to Mitochondria-Associated ER Membranes. J. Neurosci. 34, 249–259. https://doi.org/10.1523/JNEUROSCI.2507-13.2014
Guo, X., Macleod, G.T., Wellington, A., Hu, F., Panchumarthi, S., Schoenfield, M., Marin, L., Charlton, M.P., Atwood, H.L., Zinsmaier, K.E., 2005. The GTPase dMiro Is Required for Axonal Transport of Mitochondria to Drosophila Synapses. Neuron 47, 379–393. https://doi.org/10.1016/j.neuron.2005.06.027
Haddad, D., Nakamura, K., 2016. Understanding the susceptibility of dopamine neurons to mitochondrial stressors in Parkinson's disease 28.
Haenseler, W., Sansom, S.N., Buchrieser, J., Newey, S.E., Moore, C.S., Nicholls, F.J., Chintawar, S., Schnell, C., Antel, J.P., Allen, N.D., Cader, M.Z., Wade-Martins, R., James, W.S., Cowley, S.A., 2017. A Highly Efficient Human Pluripotent Stem Cell Microglia Model Displays a Neuronal-Co-culture-Specific Expression Profile and Inflammatory Response. Stem Cell Reports 8, 1727–1742. https://doi.org/10.1016/j.stemcr.2017.05.017
Han, J.Y., Choi, T.S., Kim, H.I., 2018a. Molecular Role of Ca2+ and Hard Divalent Metal Cations on Accelerated Fibrillation and Interfibrillar Aggregation of α-Synuclein. Sci Rep 8, 1895. https://doi.org/10.1038/s41598-018-20320-5
Han, J.Y., Choi, T.S., Kim, H.I., 2018b. Molecular Role of Ca2+ and Hard Divalent Metal Cations on Accelerated Fibrillation and Interfibrillar Aggregation of α-Synuclein. Scientific Reports 8, 1895. https://doi.org/10.1038/s41598-018-20320-5
Hawkes, C.H., 2008. The prodromal phase of sporadic Parkinson's disease: does it exist and if so how long is it? Mov Disord 23, 1799–1807. https://doi.org/10.1002/mds.22242
Hely, M.A., Morris, J.G.L., Reid, W.G.J., Trafficante, R., 2005. Sydney Multicenter Study of Parkinson's disease: non-L-dopa-responsive problems dominate at 15 years. Mov Disord 20, 190–199. https://doi.org/10.1002/mds.20324
Hiller, K., Hangebrauk, J., Jäger, C., Spura, J., Schreiber, K., Schomburg, D., 2009. MetaboliteDetector: comprehensive analysis tool for targeted and nontargeted GC/MS based metabolome analysis. Analytical chemistry 81, 3429–39. https://doi.org/10.1021/ac802689c
Hinkle, K.M., Yue, M., Behrouz, B., Dächsel, J.C., Lincoln, S.J., Bowles, E.E., Beevers, J.E., Dugger, B., Winner, B., Prots, I., Kent, C.B., Nishioka, K., Lin, W.-L., Dickson, D.W., Janus, C.J., Farrer, M.J., Melrose, H.L., 2012. LRRK2 knockout mice have an intact dopaminergic system but display alterations in exploratory and motor co-ordination behaviors. Mol Neurodegener 7, 25. https://doi.org/10.1186/1750-1326-7-25
Hirokawa, N., Noda, Y., Okada, Y., 1998. Kinesin and dynein superfamily proteins in organelle transport and cell division. Current Opinion in Cell Biology 10, 60–73. https://doi.org/10.1016/S0955-0674(98)80087-2
Howlett, E.H., Jensen, N., Belmonte, F., Zafar, F., Hu, X., Kluss, J., Schüle, B., Kaufman, B.A., Greenamyre, J.T., Sanders, L.H., 2017. LRRK2 G2019S-induced mitochondrial DNA damage is LRRK2 kinase dependent and inhibition restores mtDNA integrity in Parkinson's disease. Hum Mol Genet 26, 4340–4351. https://doi.org/10.1093/hmg/ddx320
Hsieh, C.-H., Li, L., Vanhauwaert, R., Nguyen, K.T., Davis, M.D., Bu, G., Wszolek, Z.K., Wang, X., 2019a. Miro1 Marks Parkinson's Disease Subset and Miro1 Reducer Rescues Neuron Loss in Parkinson's Models. Cell Metabolism 30, 1131-1140.e7. https://doi.org/10.1016/j.cmet.2019.08.023
Hsieh, C.-H., Li, L., Vanhauwaert, R., Nguyen, K.T., Davis, M.D., Bu, G., Wszolek, Z.K., Wang, X., 2019b. Miro1 Marks Parkinson's Disease Subset and Miro1 Reducer Rescues Neuron Loss in Parkinson's Models. Cell metabolism 30, 1131-1140.e7. https://doi.org/10.1016/j.cmet.2019.08.023
Hsieh, C.-H., Shaltouki, A., Gonzalez, A.E., Bettencourt da Cruz, A., Burbulla, L.F., St. Lawrence, E., Schüle, B., Krainc, D., Palmer, T.D., Wang, X., 2016a. Functional Impairment in Miro Degradation and Mitophagy Is a Shared Feature in Familial and Sporadic Parkinson's Disease. Cell Stem Cell 19,

709–724. https://doi.org/10.1016/j.stem.2016.08.002
Hsieh, C.-H., Shaltouki, A., Gonzalez, A.E., Bettencourt da Cruz, A., Burbulla, L.F., St. Lawrence, E., Schüle, B., Krainc, D., Palmer, T.D., Wang, X., 2016b. Functional Impairment in Miro Degradation and Mitophagy Is a Shared Feature in Familial and Sporadic Parkinson's Disease. Cell Stem Cell 19, 709–724. https://doi.org/10.1016/j.stem.2016.08.002
Jackson, J.G., Robinson, M.B., 2015. Reciprocal Regulation of Mitochondrial Dynamics and Calcium Signaling in Astrocyte Processes. Journal of Neuroscience 35, 15199–15213. https://doi.org/10.1523/JNEUROSCI.2049-15.2015
Jaeger, C., Glaab, E., Michelucci, A., Binz, T.M., Koeglsberger, S., Garcia, P., Trezzi, J.-P., Ghelfi, J., Balling, R., Buttini, M., 2015. The mouse brain metabolome: region-specific signatures and response to excitotoxic neuronal injury. The American journal of pathology 185, 1699–712. https://doi.org/10.1016/j.ajpath.2015.02.016
Jäger, C., Hiller, K., Buttini, M., 2016. Metabolic Profiling and Quantification of Neurotransmitters in Mouse Brain by Gas Chromatography-Mass Spectrometry. Current protocols in mouse biology 6, 333–342. https://doi.org/10.1002/cpmo.15
Jakkamsetti, V., Scudder, W., Kathote, G., Ma, Q., Angulo, G., Dobariya, A., Rosenberg, R.N., Beutler, B., Pascual, J.M., 2021. Quantification of early learning and movement sub-structure predictive of motor performance. Scientific Reports 11, 14405. https://doi.org/10.1038/s41598-021-93944-9
Jankovic, J., 2008. Parkinson's disease: clinical features and diagnosis. J Neurol Neurosurg Psychiatry 79, 368–376. https://doi.org/10.1136/jnnp.2007.131045
Jo, D.S., Park, N.Y., Cho, D.-H., 2020. Peroxisome quality control and dysregulated lipid metabolism in neurodegenerative diseases. Exp Mol Med 52, 1486–1495. https://doi.org/10.1038/s12276-020-00503-9
Johansen, K.K., Torp, S.H., Farrer, M.J., Gustavsson, E.K., Aasly, J.O., 2018. A Case of Parkinson's Disease with No Lewy Body Pathology due to a Homozygous Exon Deletion in Parkin. Case Rep Neurol Med 2018, 6838965. https://doi.org/10.1155/2018/6838965
Johnson, B., 2022. Parkinson's disease drug hunters think outside the α-synuclein box. Nature Biotechnology 40, 1705–1707. https://doi.org/10.1038/s41587-022-01610-w
Joksimovic, S.Lj., Joksimovic, S.M., Tesic, V., García-Caballero, A., Feseha, S., Zamponi, G.W., Jevtovic-Todorovic, V., Todorovic, S.M., 2018. Selective inhibition of Cav3.2 channels reverses hyperexcitability of peripheral nociceptors and alleviates post-surgical pain. Sci Signal 11, eaao4425. https://doi.org/10.1126/scisignal.aao4425
Jouaville, L.S., Pinton, P., Bastianutto, C., Rutter, G.A., Rizzuto, R., 1999. Regulation of mitochondrial ATP synthesis by calcium: Evidence for a long-term metabolic priming. Proc. Natl. Acad. Sci. U.S.A. 96, 13807–13812. https://doi.org/10.1073/pnas.96.24.13807
Kalia, L.V., Lang, A.E., 2015. Parkinson's disease. Lancet 386, 896–912. https://doi.org/10.1016/S0140-6736(14)61393-3
Kalinski, A.L., Kar, A.N., Craver, J., Tosolini, A.P., Sleigh, J.N., Lee, S.J., Hawthorne, A., Brito-Vargas, P., Miller-Randolph, S., Passino, R., Shi, L., Wong, V.S.C., Picci, C., Smith, D.S., Willis, D.E., Havton, L.A., Schiavo, G., Giger, R.J., Langley, B., Twiss, J.L., 2019. Deacetylation of Miro1 by HDAC6 blocks mitochondrial transport and mediates axon growth inhibition. J. Cell Biol. 218, 1871–1890. https://doi.org/10.1083/jcb.201702187
Kang, K., Kim, J., Ryu, B., Lee, S.-G., Oh, M.-S., Baek, J., Ren, X., Canavero, S., Kim, C.-Y., Chung, H.M., 2021. BAPTA, a calcium chelator, neuroprotects injured neurons in vitro and promotes motor recovery after spinal cord transection in vivo. CNS Neuroscience & Therapeutics 27, 919–929. https://doi.org/10.1111/cns.13651
Karampetsou, M., Ardah, M.T., Semitekolou, M., Polissidis, A., Samiotaki, M., Kalomoiri, M., Majbour, N., Xanthou, G., El-Agnaf, O.M.A., Vekrellis, K., 2017. Phosphorylated exogenous alpha-synuclein

fibrils exacerbate pathology and induce neuronal dysfunction in mice. Sci Rep 7, 16533. https://doi.org/10.1038/s41598-017-15813-8

Karbowski, M., Youle, R.J., 2003. Dynamics of mitochondrial morphology in healthy cells and during apoptosis. Cell Death Differ 10, 870–880. https://doi.org/10.1038/sj.cdd.4401260

Kay, L., Pienaar, I.S., Cooray, R., Black, G., Soundararajan, M., 2018. Understanding Miro GTPases: Implications in the Treatment of Neurodegenerative Disorders. Mol Neurobiol 55, 7352–7365. https://doi.org/10.1007/s12035-018-0927-x

Keller, M.F., Saad, M., Bras, J., Bettella, F., Nicolaou, N., Simón-Sánchez, J., Mittag, F., Büchel, F., Sharma, M., Gibbs, J.R., Schulte, C., Moskvina, V., Durr, A., Holmans, P., Kilarski, L.L., Guerreiro, R., Hernandez, D.G., Brice, A., Ylikotila, P., Stefánsson, H., Majamaa, K., Morris, H.R., Williams, N., Gasser, T., Heutink, P., Wood, N.W., Hardy, J., Martinez, M., Singleton, A.B., Nalls, M.A., International Parkinson's Disease Genomics Consortium (IPDGC), Wellcome Trust Case Control Consortium 2 (WTCCC2), 2012. Using genome-wide complex trait analysis to quantify "missing heritability" in Parkinson's disease. Hum Mol Genet 21, 4996–5009. https://doi.org/10.1093/hmg/dds335

Kia, D.A., Zhang, D., Guelfi, S., Manzoni, C., Hubbard, L., Reynolds, R.H., Botía, J., Ryten, M., Ferrari, R., Lewis, P.A., Williams, N., Trabzuni, D., Hardy, J., Wood, N.W., United Kingdom Brain Expression Consortium (UKBEC) and the International Parkinson's Disease Genomics Consortium (IPDGC), Noyce, A.J., Kaiyrzhanov, R., Middlehurst, B., Kia, D.A., Tan, M., Houlden, H., Morris, H.R., Plun-Favreau, H., Holmans, P., Hardy, J., Trabzuni, D., Bras, J., PhD, J.Q., Mok, K.Y., Kinghorn, K.J., Billingsley, K., Wood, N.W., Lewis, P., Schreglmann, S., Guerreiro, R., Lovering, R., R'Bibo, L., Manzoni, C., Rizig, M., Ryten, M., Guelfi, S., Escott-Price, V., Chelban, V., Foltynie, T., Williams, N., Brice, A., Danjou, F., Lesage, S., Corvol, J.-C., Martinez, M., Schulte, C., Brockmann, K., Simón-Sánchez, J., Heutink, P., Rizzu, P., Sharma, M., Gasser, T., Nicolas, A., Cookson, M.R., Bandres-Ciga, S., Blauwendraat, C., Craig, D.W., Faghri, F., Gibbs, J.R., Hernandez, D.G., Van Keuren-Jensen, K., Shulman, J.M., Leonard, H.L., Nalls, M.A., Robak, L., Lubbe, S., Finkbeiner, S., Mencacci, N.E., Lungu, C., Singleton, A.B., Scholz, S.W., Reed, X., Alcalay, R.N., Gan-Or, Z., Rouleau, G.A., Krohn, L., van Hilten, J.J., Marinus, J., Adarmes-Gómez, A.D., Aguilar, M., Alvarez, I., Alvarez, V., Javier Barrero, F., Bergareche Yarza, J.A., Bernal-Bernal, I., Blazquez, M., Bonilla-Toribio, M., Botía, J.A., Boungiorno, M.T., Buiza-Rueda, D., Càmara, A., Carrillo, F., Carrión-Claro, M., Cerdan, D., Clarimón, J., Compta, Y., Diez-Fairen, M., Dols-Icardo, O., Duarte, J., Duran, R., Escamilla-Sevilla, F., Ezquerra, M., Feliz, C., Fernàndez, M., Fernàndez-Santiago, R., Garcia, C., García-Ruiz, P., Gómez-Garre, P., Gomez Heredia, M.J., Gonzalez-Aramburu, I., Pagola, A.G., Hoenicka, J., Infante, J., Jimenez-Escrig, A., Kulisevsky, J., Labrador-Espinosa, M.A., Lopez-Sendon, J.L., Arregui, A.L. de M., Macias, D., Torres, I.M., Marín, J., Marti, M.J., Martínez-Castrillo, J.C., Mèndez-del-Barrio, C., González, M.M., Adolfo Mínguez, M.M., Mir, P., Rezola, E.M., Muñoz, E., Pagonabarraga, J., Pastor, P., Errazquin, F.P., Perinán-Tocino, T., Ruiz-Martínez, J., Ruz, C., Rodriguez, A.S., Sierra, M., Suarez-Sanmartin, E., Tabernero, C., Tartari, J.P., Tejera-Parrado, C., Tolosa, E., Valldeoriola, F., Vargas-González, L., Vela, L., Vives, F., Zimprich, A., Pihlstrom, L., Toft, M., Koks, S., Taba, P., Hassin-Baer, S., Weale, M., Ramasamy, A., Smith, C., Guelfi, M.S., D'sa, K., Forabosco, P., Botiá, J.A., 2021. Identification of Candidate Parkinson Disease Genes by Integrating Genome-Wide Association Study, Expression, and Epigenetic Data Sets. JAMA Neurol. https://doi.org/10.1001/jamaneurol.2020.5257

Kim, C., Alcalay, R., 2017. Genetic Forms of Parkinson's Disease. Seminars in Neurology 37, 135–146. https://doi.org/10.1055/s-0037-1601567

Kitada, T., Tong, Y., Gautier, C.A., Shen, J., 2009. Absence of nigral degeneration in aged parkin/DJ-1/PINK1 triple knockout mice. Journal of Neurochemistry 111, 696–702. https://doi.org/10.1111/j.1471-4159.2009.06350.x

Klosowiak, J.L., Focia, P.J., Chakravarthy, S., Landahl, E.C., Freymann, D.M., Rice, S.E., 2013. Structural coupling of the EF hand and C-terminal GTPase domains in the mitochondrial protein Miro. EMBO Rep 14, 968–974. https://doi.org/10.1038/embor.2013.151

Klosowiak, J.L., Park, S., Smith, K.P., French, M.E., Focia, P.J., Freymann, D.M., Rice, S.E., 2016a. Structural insights into Parkin substrate lysine targeting from minimal Miro substrates. Sci Rep 6, 33019. https://doi.org/10.1038/srep33019

Klosowiak, J.L., Park, S., Smith, K.P., French, M.E., Focia, P.J., Freymann, D.M., Rice, S.E., 2016b. Structural insights into Parkin substrate lysine targeting from minimal Miro substrates. Scientific reports 6, 33019. https://doi.org/10.1038/srep33019

König, T., Nolte, H., Aaltonen, M.J., Tatsuta, T., Krols, M., Stroh, T., Langer, T., McBride, H.M., 2021. MIROs and DRP1 drive mitochondrial-derived vesicle biogenesis and promote quality control. Nat Cell Biol 23, 1271–1286. https://doi.org/10.1038/s41556-021-00798-4

Koshiba, T., Holman, H.A., Kubara, K., Yasukawa, K., Kawabata, S., Okamoto, K., Macfarlane, J., Shaw, J.M., 2011. Structure-Function Analysis of the Yeast Mitochondrial Rho GTPase, Gem1p: IMPLICATIONS FOR MITOCHONDRIAL INHERITANCE. J. Biol. Chem. 286, 354–362. https://doi.org/10.1074/jbc.M110.180034

Krüger, R., Kuhn, W., Müller, T., Woitalla, D., Graeber, M., Kösel, S., Przuntek, H., Epplen, J.T., Schöls, L., Riess, O., 1998. Ala30Pro mutation in the gene encoding alpha-synuclein in Parkinson's disease. Nat Genet 18, 106–108. https://doi.org/10.1038/ng0298-106

Kruman, I.I., Mattson, M.P., 1999. Pivotal role of mitochondrial calcium uptake in neural cell apoptosis and necrosis. J Neurochem 72, 529–540. https://doi.org/10.1046/j.1471-4159.1999.0720529.x

Kumar, A., Kopra, J., Varendi, K., Porokuokka, L.L., Panhelainen, A., Kuure, S., Marshall, P., Karalija, N., Härma, M.-A., Vilenius, C., Lilleväli, K., Tekko, T., Mijatovic, J., Pulkkinen, N., Jakobson, Madis, Jakobson, Maili, Ola, R., Palm, E., Lindahl, M., Strömberg, I., Võikar, V., Piepponen, T.P., Saarma, M., Andressoo, J.-O., 2015. GDNF Overexpression from the Native Locus Reveals its Role in the Nigrostriatal Dopaminergic System Function. PLOS Genetics 11, e1005710. https://doi.org/10.1371/journal.pgen.1005710

La Manno, G., Gyllborg, D., Codeluppi, S., Nishimura, K., Salto, C., Zeisel, A., Borm, L.E., Stott, S.R.W., Toledo, E.M., Villaescusa, J.C., Lönnerberg, P., Ryge, J., Barker, R.A., Arenas, E., Linnarsson, S., 2016. Molecular Diversity of Midbrain Development in Mouse, Human, and Stem Cells. Cell 167, 566-580.e19. https://doi.org/10.1016/j.cell.2016.09.027

LaMonte, B.H., Wallace, K.E., Holloway, B.A., Shelly, S.S., Ascaño, J., Tokito, M., Van Winkle, T., Howland, D.S., Holzbaur, E.L.F., 2002. Disruption of Dynein/Dynactin Inhibits Axonal Transport in Motor Neurons Causing Late-Onset Progressive Degeneration. Neuron 34, 715–727. https://doi.org/10.1016/S0896-6273(02)00696-7

Langston, J.W., 2006. The Parkinson's complex: parkinsonism is just the tip of the iceberg. Ann Neurol 59, 591–596. https://doi.org/10.1002/ana.20834

Langston, J.W., Ballard, P., Tetrud, J.W., Irwin, I., 1983. Chronic Parkinsonism in humans due to a product of meperidine-analog synthesis. Science 219, 979–980. https://doi.org/10.1126/science.6823561

Langston, J.W., Forno, L.S., Rebert, C.S., Irwin, I., 1984. Selective nigral toxicity after systemic administration of 1-methyl-4-phenyl-1,2,5,6-tetrahydropyrine (MPTP) in the squirrel monkey. Brain Res 292, 390–394. https://doi.org/10.1016/0006-8993(84)90777-7

Larráyoz, I.M., Martínez, A., 2012. Proadrenomedullin N-terminal 20 peptide increases kinesin's velocity both in vitro and in vivo. Endocrinology 153, 1734–42. https://doi.org/10.1210/en.2011-1685

Larsen, S.B., Hanss, Z., Krüger, R., 2018. The genetic architecture of mitochondrial dysfunction in Parkinson's disease. Cell Tissue Res 373, 21–37. https://doi.org/10.1007/s00441-017-2768-8

Lautenschläger, J., Stephens, A.D., Fusco, G., Ströhl, F., Curry, N., Zacharopoulou, M., Michel, C.H., Laine, R., Nespovitaya, N., Fantham, M., Pinotsi, D., Zago, W., Fraser, P., Tandon, A., St George-Hyslop,

P., Rees, E., Phillips, J.J., De Simone, A., Kaminski, C.F., Schierle, G.S.K., 2018. C-terminal calcium binding of α-synuclein modulates synaptic vesicle interaction. Nat Commun 9, 712. https://doi.org/10.1038/s41467-018-03111-4

Lautrup, S., Sinclair, D.A., Mattson, M.P., Fang, E.F., 2019. NAD+ in Brain Aging and Neurodegenerative Disorders. Cell Metabolism 30, 630–655. https://doi.org/10.1016/j.cmet.2019.09.001

Leandrou, E., Emmanouilidou, E., Vekrellis, K., 2019a. Voltage-Gated Calcium Channels and α-Synuclein: Implications in Parkinson's Disease. Front. Mol. Neurosci. 12, 237. https://doi.org/10.3389/fnmol.2019.00237

Leandrou, E., Emmanouilidou, E., Vekrellis, K., 2019b. Voltage-Gated Calcium Channels and α-Synuclein: Implications in Parkinson's Disease. Frontiers in Molecular Neuroscience 12, 237. https://doi.org/10.3389/fnmol.2019.00237

Lee, K.-S., Huh, S., Lee, S., Wu, Z., Kim, A.-K., Kang, H.-Y., Lu, B., 2018. Altered ER–mitochondria contact impacts mitochondria calcium homeostasis and contributes to neurodegeneration in vivo in disease models. Proc Natl Acad Sci U S A 115, E8844–E8853. https://doi.org/10.1073/pnas.1721136115

Lee, K.-W., Chen, W., Junn, E., Im, J.-Y., Grosso, H., Sonsalla, P.K., Feng, X., Ray, N., Fernandez, J.R., Chao, Y., Masliah, E., Voronkov, M., Braithwaite, S.P., Stock, J.B., Mouradian, M.M., 2011a. Enhanced Phosphatase Activity Attenuates α-Synucleinopathy in a Mouse Model. J. Neurosci. 31, 6963–6971. https://doi.org/10.1523/JNEUROSCI.6513-10.2011

Lee, K.-W., Chen, W., Junn, E., Im, J.-Y., Grosso, H., Sonsalla, P.K., Feng, X., Ray, N., Fernandez, J.R., Chao, Y., Masliah, E., Voronkov, M., Braithwaite, S.P., Stock, J.B., Mouradian, M.M., 2011b. Enhanced phosphatase activity attenuates α-synucleinopathy in a mouse model. The Journal of neuroscience : the official journal of the Society for Neuroscience 31, 6963–71. https://doi.org/10.1523/JNEUROSCI.6513-10.2011

Lee, S., Lee, K.-S., Huh, S., Liu, S., Lee, D.-Y., Hong, S.H., Yu, K., Lu, B., 2016. Polo Kinase Phosphorylates Miro to Control ER-Mitochondria Contact Sites and Mitochondrial Ca2+ Homeostasis in Neural Stem Cell Development. Developmental Cell 37, 174–189. https://doi.org/10.1016/j.devcel.2016.03.023

Li, B., Guo, Y.-S., Sun, M.-M., Dong, H., Wu, S.-Y., Wu, D.-X., Li, C.-Y., 2008. The NADPH oxidase is involved in lipopolysaccharide-mediated motor neuron injury. Brain Research 1226, 199–208. https://doi.org/10.1016/j.brainres.2008.06.024

Li, B., Zhang, Y., Li, H., Shen, H., Wang, Y., Li, X., Cui, G., Chen, G., 2021. Miro1 Regulates Neuronal Mitochondrial Transport and Distribution to Alleviate Neuronal Damage in Secondary Brain Injury After Intracerebral Hemorrhage in Rats. Cell Mol Neurobiol 41, 795–812. https://doi.org/10.1007/s10571-020-00887-2

Li, J.-M., Li, X., Chan, L.W.C., Hu, R., Zheng, T., Li, H., Yang, S., 2023. Lipotoxicity-polarised macrophage-derived exosomes regulate mitochondrial fitness through Miro1-mediated mitophagy inhibition and contribute to type 2 diabetes development in mice. Diabetologia 66, 2368–2386. https://doi.org/10.1007/s00125-023-05992-7

Li, L., Conradson, D.M., Bharat, V., Kim, M.J., Hsieh, C.-H., Minhas, P.S., Papakyrikos, A.M., Durairaj, A.S., Ludlam, A., Andreasson, K.I., Partridge, L., Cianfrocco, M.A., Wang, X., 2021a. A mitochondrial membrane-bridging machinery mediates signal transduction of intramitochondrial oxidation. Nat Metab 3, 1242–1258. https://doi.org/10.1038/s42255-021-00443-2

Li, L., Conradson, D.M., Bharat, V., Kim, M.J., Hsieh, C.-H., Minhas, P.S., Papakyrikos, A.M., Durairaj, A.S., Ludlam, A., Andreasson, K.I., Partridge, L., Cianfrocco, M.A., Wang, X., 2021b. A mitochondrial membrane-bridging machinery mediates signal transduction of intramitochondrial oxidation. Nature Metabolism 3, 1242–1258. https://doi.org/10.1038/s42255-021-00443-2

Li, L., Conradson, D.M., Bharat, V., Kim, M.J., Hsieh, C.-H., Minhas, P.S., Papakyrikos, A.M., Durairaj, A.S.,

Ludlam, A., Andreasson, K.I., Partridge, L., Cianfrocco, M.A., Wang, X., 2021c. A mitochondrial membrane-bridging machinery mediates signal transduction of intramitochondrial oxidation. Nature metabolism 3, 1242–1258. https://doi.org/10.1038/s42255-021-00443-2

Li, X., Tao, Yezheng, Bradley, R., Du, Z., Tao, Yunlong, Kong, L., Dong, Y., Jones, J., Yan, Y., Harder, C.R.K., Friedman, L.M., Bilal, M., Hoffmann, B., Zhang, S.-C., 2018. Fast Generation of Functional Subtype Astrocytes from Human Pluripotent Stem Cells. Stem Cell Reports 11, 998–1008. https://doi.org/10.1016/j.stemcr.2018.08.019

Li, Xujun, Chan, L.W.C., Li, Xianyu, Liu, C., Yang, G., Gao, J., Dai, M., Wang, Y., Xie, Z., Liu, J., Zhou, F., Zheng, T., Feng, D., Guo, S., Li, H., Sun, K., Yang, S., 2020. Obesity-Induced Regulator of Calcineurin 1 Overexpression Leads to β-Cell Failure Through Mitophagy Pathway Inhibition. Antioxidants & Redox Signaling 32, 413–428. https://doi.org/10.1089/ars.2019.7806

Liao, Y., Smyth, G.K., Shi, W., 2019. The R package Rsubread is easier, faster, cheaper and better for alignment and quantification of RNA sequencing reads. Nucleic Acids Research 47, e47–e47. https://doi.org/10.1093/nar/gkz114

Liu, G., Yu, J., Ding, J., Xie, C., Sun, L., Rudenko, I., Zheng, W., Sastry, N., Luo, J., Rudow, G., Troncoso, J.C., Cai, H., 2014. Aldehyde dehydrogenase 1 defines and protects a nigrostriatal dopaminergic neuron subpopulation. J Clin Invest 124, 3032–3046. https://doi.org/10.1172/JCI72176

Liu, S., Sawada, T., Lee, S., Yu, W., Silverio, G., Alapatt, P., Millan, I., Shen, A., Saxton, W., Kanao, T., Takahashi, R., Hattori, N., Imai, Y., Lu, B., 2012. Parkinson's Disease–Associated Kinase PINK1 Regulates Miro Protein Level and Axonal Transport of Mitochondria. PLoS Genet 8, e1002537. https://doi.org/10.1371/journal.pgen.1002537

López-Doménech, G., Higgs, N.F., Vaccaro, V., Roš, H., Arancibia-Cárcamo, I.L., MacAskill, A.F., Kittler, J.T., 2016a. Loss of Dendritic Complexity Precedes Neurodegeneration in a Mouse Model with Disrupted Mitochondrial Distribution in Mature Dendrites. Cell Reports 17, 317–327. https://doi.org/10.1016/j.celrep.2016.09.004

López-Doménech, G., Higgs, N.F., Vaccaro, V., Roš, H., Arancibia-Cárcamo, I.L., MacAskill, A.F., Kittler, J.T., 2016b. Loss of Dendritic Complexity Precedes Neurodegeneration in a Mouse Model with Disrupted Mitochondrial Distribution in Mature Dendrites. Cell reports 17, 317–327. https://doi.org/10.1016/j.celrep.2016.09.004

López-Doménech, G., Howden, J.H., Covill-Cooke, C., Morfill, C., Patel, J.V., Bürli, R., Crowther, D., Birsa, N., Brandon, N.J., Kittler, J.T., 2021. Loss of neuronal Miro1 disrupts mitophagy and induces hyperactivation of the integrated stress response. The EMBO Journal 40, e100715. https://doi.org/10.15252/embj.2018100715

López-Doménech, G., Howden, J.H., Covill-Cooke, C., Morfill, C., Patel, J. V, Bürli, R., Crowther, D., Birsa, N., Brandon, N.J., Kittler, J.T., 2021. Loss of neuronal Miro1 disrupts mitophagy and induces hyperactivation of the integrated stress response. The EMBO Journal 40, e100715. https://doi.org/10.15252/embj.2018100715

Love, M.I., Huber, W., Anders, S., 2014. Moderated estimation of fold change and dispersion for RNA-seq data with DESeq2. Genome Biology 15, 550. https://doi.org/10.1186/s13059-014-0550-8

Luo, Y., Hoffer, A., Hoffer, B., Qi, X., 2015. Mitochondria: A Therapeutic Target for Parkinson's Disease? Int J Mol Sci 16, 20704–20730. https://doi.org/10.3390/ijms160920704

MacAskill, A.F., Brickley, K., Stephenson, F.A., Kittler, J.T., 2009a. GTPase dependent recruitment of Grif-1 by Miro1 regulates mitochondrial trafficking in hippocampal neurons. Molecular and Cellular Neuroscience 40, 301–312. https://doi.org/10.1016/j.mcn.2008.10.016

MacAskill, A.F., Rinholm, J.E., Twelvetrees, A.E., Arancibia-Carcamo, I.L., Muir, J., Fransson, A., Aspenstrom, P., Attwell, D., Kittler, J.T., 2009b. Miro1 Is a Calcium Sensor for Glutamate Receptor-Dependent Localization of Mitochondria at Synapses. Neuron 61, 541–555. https://doi.org/10.1016/j.neuron.2009.01.030

Mahmoodazdeh, A., Shafiee, S.M., Sisakht, M., Khoshdel, Z., Takhshid, M.A., 2020. Adrenomedullin protects rat dorsal root ganglion neurons against doxorubicin-induced toxicity by ameliorating oxidative stress. Iranian journal of basic medical sciences 23, 1197–1206. https://doi.org/10.22038/ijbms.2020.45134.10514

Makarious, M.B., Lake, J., Pitz, V., Fu, A.Y., Guidubaldi, J.L., Solsberg, C.W., Bandres-Ciga, S., Leonard, H.L., Kim, J.J., Billingsley, K.J., Grenn, F.P., Jerez, P.A., Alvarado, C.X., Iwaki, H., Ta, M., Vitale, D., Hernandez, D., Torkamani, A., Ryten, M., Hardy, J., Scholz, S.W., Traynor, B.J., Dalgard, C.L., Ehrlich, D.J., Tanaka, T., Ferrucci, L., Beach, T.G., Serrano, G.E., Real, R., Morris, H.R., Ding, J., Gibbs, J.R., Singleton, A.B., Nalls, M.A., Bhangale, T., Blauwendraat, C., 2023. Large-scale rare variant burden testing in Parkinson's disease. Brain awad214. https://doi.org/10.1093/brain/awad214

Marchitti, S.A., Deitrich, R.A., Vasiliou, V., 2007. Neurotoxicity and metabolism of the catecholamine-derived 3,4-dihydroxyphenylacetaldehyde and 3,4-dihydroxyphenylglycolaldehyde: the role of aldehyde dehydrogenase. Pharmacol Rev 59, 125–150. https://doi.org/10.1124/pr.59.2.1

Marras, C., Lang, A., van de Warrenburg, B.P., Sue, C.M., Tabrizi, S.J., Bertram, L., Mercimek-Mahmutoglu, S., Ebrahimi-Fakhari, D., Warner, T.T., Durr, A., Assmann, B., Lohmann, K., Kostic, V., Klein, C., 2016. Nomenclature of genetic movement disorders: Recommendations of the international Parkinson and movement disorder society task force. Mov Disord 31, 436–457. https://doi.org/10.1002/mds.26527

Mätlik, K., Võikar, V., Vilenius, C., Kulesskaya, N., Andressoo, J.-O., 2018. Two-fold elevation of endogenous GDNF levels in mice improves motor coordination without causing side-effects. Sci Rep 8, 11861. https://doi.org/10.1038/s41598-018-29988-1

Matsuda, W., Furuta, T., Nakamura, K.C., Hioki, H., Fujiyama, F., Arai, R., Kaneko, T., 2009. Single Nigrostriatal Dopaminergic Neurons Form Widely Spread and Highly Dense Axonal Arborizations in the Neostriatum. J Neurosci 29, 444–453. https://doi.org/10.1523/JNEUROSCI.4029-08.2009

McBride, H.M., Neuspiel, M., Wasiak, S., 2006. Mitochondria: more than just a powerhouse. Curr Biol 16, R551-560. https://doi.org/10.1016/j.cub.2006.06.054

McCormack, J.G., Halestrap, A.P., Denton, R.M., 1990. Role of calcium ions in regulation of mammalian intramitochondrial metabolism. Physiological Reviews 70, 391–425. https://doi.org/10.1152/physrev.1990.70.2.391

McLelland, G.-L., Goiran, T., Yi, W., Dorval, G., Chen, C.X., Lauinger, N.D., Krahn, A.I., Valimehr, S., Rakovic, A., Rouiller, I., Durcan, T.M., Trempe, J.-F., Fon, E.A., 2018. Mfn2 ubiquitination by PINK1/parkin gates the p97-dependent release of ER from mitochondria to drive mitophagy. eLife 7, e32866. https://doi.org/10.7554/eLife.32866

McLelland, G.-L., Soubannier, V., Chen, C.X., McBride, H.M., Fon, E.A., 2014. Parkin and PINK1 function in a vesicular trafficking pathway regulating mitochondrial quality control. The EMBO Journal 33, 282–295. https://doi.org/10.1002/embj.201385902

Mhyre, T.R., Boyd, J.T., Hamill, R.W., Maguire-Zeiss, K.A., 2012. Parkinson's disease. Subcell Biochem 65, 389–455. https://doi.org/10.1007/978-94-007-5416-4_16

Moller, A., Bauer, C.S., Cohen, R.N., Webster, C.P., De Vos, K.J., 2017. Amyotrophic lateral sclerosis-associated mutant SOD1 inhibits anterograde axonal transport of mitochondria by reducing Miro1 levels. Human Molecular Genetics 26, 4668–4679. https://doi.org/10.1093/hmg/ddx348

Monzel, A.S., Hemmer, K., Kaoma, T., Smits, L.M., Bolognin, S., Lucarelli, P., Rosety, I., Zagare, A., Antony, P., Nickels, S.L., Krueger, R., Azuaje, F., Schwamborn, J.C., 2020. Machine learning-assisted neurotoxicity prediction in human midbrain organoids. Parkinsonism & Related Disorders 75, 105–109. https://doi.org/10.1016/j.parkreldis.2020.05.011

Monzel, A.S., Smits, L.M., Hemmer, K., Hachi, S., Moreno, E.L., van Wuellen, T., Jarazo, J., Walter, J., Brüggemann, I., Boussaad, I., Berger, E., Fleming, R.M.T., Bolognin, S., Schwamborn, J.C., 2017a.

Derivation of Human Midbrain-Specific Organoids from Neuroepithelial Stem Cells. Stem Cell Reports 8, 1144–1154. https://doi.org/10.1016/j.stemcr.2017.03.010
Monzel, A.S., Smits, L.M., Hemmer, K., Hachi, S., Moreno, E.L., van Wuellen, T., Jarazo, J., Walter, J., Brüggemann, I., Boussaad, I., Berger, E., Fleming, R.M.T., Bolognin, S., Schwamborn, J.C., 2017b. Derivation of Human Midbrain-Specific Organoids from Neuroepithelial Stem Cells. Stem Cell Reports 8, 1144–1154. https://doi.org/10.1016/j.stemcr.2017.03.010
Moretto, E., Stuart, S., Surana, S., Vargas, J.N.S., Schiavo, G., 2022. The Role of Extracellular Matrix Components in the Spreading of Pathological Protein Aggregates. Frontiers in cellular neuroscience 16, 844211. https://doi.org/10.3389/fncel.2022.844211
Morlino, G., Barreiro, O., Baixauli, F., Robles-Valero, J., Gonzalez-Granado, J.M., Villa-Bellosta, R., Cuenca, J., Sanchez-Sorzano, C.O., Veiga, E., Martin-Cofreces, N.B., Sanchez-Madrid, F., 2014. Miro-1 Links Mitochondria and Microtubule Dynein Motors To Control Lymphocyte Migration and Polarity. Molecular and Cellular Biology 34, 1412–1426. https://doi.org/10.1128/MCB.01177-13
Nalls, M.A., Blauwendraat, C., Vallerga, C.L., Heilbron, K., Bandres-Ciga, S., Chang, D., Tan, M., Kia, D.A., Noyce, A.J., Xue, A., Bras, J., Young, E., von Coelln, R., Simón-Sánchez, J., Schulte, C., Sharma, M., Krohn, L., Pihlstrøm, L., Siitonen, A., Iwaki, H., Leonard, H., Faghri, F., Gibbs, J.R., Hernandez, D.G., Scholz, S.W., Botia, J.A., Martinez, M., Corvol, J.-C., Lesage, S., Jankovic, J., Shulman, L.M., Sutherland, M., Tienari, P., Majamaa, K., Toft, M., Andreassen, O.A., Bangale, T., Brice, A., Yang, J., Gan-Or, Z., Gasser, T., Heutink, P., Shulman, J.M., Wood, N.W., Hinds, D.A., Hardy, J.A., Morris, H.R., Gratten, J., Visscher, P.M., Graham, R.R., Singleton, A.B., 23andMe Research Team, System Genomics of Parkinson's Disease Consortium, International Parkinson's Disease Genomics Consortium, 2019. Identification of novel risk loci, causal insights, and heritable risk for Parkinson's disease: a meta-analysis of genome-wide association studies. Lancet Neurol 18, 1091–1102. https://doi.org/10.1016/S1474-4422(19)30320-5
Nath, S., Goodwin, J., Engelborghs, Y., Pountney, D.L., 2011. Raised calcium promotes α-synuclein aggregate formation. Molecular and Cellular Neuroscience 46, 516–526. https://doi.org/10.1016/j.mcn.2010.12.004
Nemani, N., Carvalho, E., Tomar, D., Dong, Z., Ketschek, A., Breves, S.L., Jaña, F., Worth, A.M., Heffler, J., Palaniappan, P., Tripathi, A., Subbiah, R., Riitano, M.F., Seelam, A., Manfred, T., Itoh, K., Meng, S., Sesaki, H., Craigen, W.J., Rajan, S., Shanmughapriya, S., Caplan, J., Prosser, B.L., Gill, D.L., Stathopulos, P.B., Gallo, G., Chan, D.C., Mishra, P., Madesh, M., 2018. MIRO-1 Determines Mitochondrial Shape Transition upon GPCR Activation and Ca2+ Stress. Cell Reports 23, 1005–1019. https://doi.org/10.1016/j.celrep.2018.03.098
Nguyen, D., Bharat, V., Conradson, D.M., Nandakishore, P., Wang, X., 2021a. Miro1 Impairment in a Parkinson's At-Risk Cohort. Frontiers in Molecular Neuroscience 14.
Nguyen, D., Bharat, V., Conradson, D.M., Nandakishore, P., Wang, X., 2021b. Miro1 Impairment in a Parkinson's At-Risk Cohort. Frontiers in Molecular Neuroscience 14, 734273. https://doi.org/10.3389/fnmol.2021.734273
Nguyen, T.T., Oh, S.S., Weaver, D., Lewandowska, A., Maxfield, D., Schuler, M.-H., Smith, N.K., Macfarlane, J., Saunders, G., Palmer, C.A., Debattisti, V., Koshiba, T., Pulst, S., Feldman, E.L., Hajnoczky, G., Shaw, J.M., 2014. Loss of Miro1-directed mitochondrial movement results in a novel murine model for neuron disease. Proceedings of the National Academy of Sciences 111, E3631–E3640. https://doi.org/10.1073/pnas.1402449111
Nickels, S.L., Modamio, J., Mendes-Pinheiro, B., Monzel, A.S., Betsou, F., Schwamborn, J.C., 2020. Reproducible generation of human midbrain organoids for in vitro modeling of Parkinson's disease. Stem Cell Res 46, 101870. https://doi.org/10.1016/j.scr.2020.101870
Nicoletti, V., Palermo, G., Del Prete, E., Mancuso, M., Ceravolo, R., 2021. Understanding the Multiple Role of Mitochondria in Parkinson's Disease and Related Disorders: Lesson From Genetics and

Protein–Interaction Network. Frontiers in Cell and Developmental Biology 9, 636506. https://doi.org/10.3389/fcell.2021.636506
Niescier, R.F., Chang, K.T., Min, K.-T., 2013. Miro, MCU, and calcium: bridging our understanding of mitochondrial movement in axons. Front. Cell. Neurosci. 7. https://doi.org/10.3389/fncel.2013.00148
Niescier, R.F., Hong, K., Park, D., Min, K.-T., 2018. MCU Interacts with Miro1 to Modulate Mitochondrial Functions in Neurons. J. Neurosci. 38, 4666–4677. https://doi.org/10.1523/JNEUROSCI.0504-18.2018
Nolfi-Donegan, D., Braganza, A., Shiva, S., 2020. Mitochondrial electron transport chain: Oxidative phosphorylation, oxidant production, and methods of measurement. Redox Biology 37, 101674. https://doi.org/10.1016/j.redox.2020.101674
Novello, S., Arcuri, L., Dovero, S., Dutheil, N., Shimshek, D.R., Bezard, E., Morari, M., 2018. G2019S LRRK2 mutation facilitates α-synuclein neuropathology in aged mice. Neurobiology of Disease 120, 21–33. https://doi.org/10.1016/j.nbd.2018.08.018
Nuber, S., Selkoe, D.J., 2023. The Parkinson-Associated Toxin Paraquat Shifts Physiological α-Synuclein Tetramers toward Monomers That Can Be Calpain-Truncated and Form Oligomers. Am J Pathol 193, 520–531. https://doi.org/10.1016/j.ajpath.2023.01.010
Okuzumi, A., Hatano, T., Matsumoto, G., Nojiri, S., Ueno, S.-I., Imamichi-Tatano, Y., Kimura, H., Kakuta, S., Kondo, A., Fukuhara, T., Li, Y., Funayama, M., Saiki, S., Taniguchi, D., Tsunemi, T., McIntyre, D., Gérardy, J.-J., Mittelbronn, M., Kruger, R., Uchiyama, Y., Nukina, N., Hattori, N., 2023. Propagative α-synuclein seeds as serum biomarkers for synucleinopathies. Nat Med. https://doi.org/10.1038/s41591-023-02358-9
Ortner, N.J., 2021. Voltage-Gated Ca2+ Channels in Dopaminergic Substantia Nigra Neurons: Therapeutic Targets for Neuroprotection in Parkinson's Disease? Frontiers in Synaptic Neuroscience 13.
Ou, Z., Pan, J., Tang, S., Duan, D., Yu, D., Nong, H., Wang, Z., 2021. Global Trends in the Incidence, Prevalence, and Years Lived With Disability of Parkinson's Disease in 204 Countries/Territories From 1990 to 2019. Frontiers in Public Health 9, 776847. https://doi.org/10.3389/fpubh.2021.776847
Pagano, G., Taylor, K.I., Anzures-Cabrera, J., Marchesi, M., Simuni, T., Marek, K., Postuma, R.B., Pavese, N., Stocchi, F., Azulay, J.-P., Mollenhauer, B., López-Manzanares, L., Russell, D.S., Boyd, J.T., Nicholas, A.P., Luquin, M.R., Hauser, R.A., Gasser, T., Poewe, W., Ricci, B., Boulay, A., Vogt, A., Boess, F.G., Dukart, J., D'Urso, G., Finch, R., Zanigni, S., Monnet, A., Pross, N., Hahn, A., Svoboda, H., Britschgi, M., Lipsmeier, F., Volkova-Volkmar, E., Lindemann, M., Dziadek, S., Holiga, Š., Rukina, D., Kustermann, T., Kerchner, G.A., Fontoura, P., Umbricht, D., Doody, R., Nikolcheva, T., Bonni, A., 2022. Trial of Prasinezumab in Early-Stage Parkinson's Disease. New England Journal of Medicine 387, 421–432. https://doi.org/10.1056/NEJMoa2202867
Panchal, K., Tiwari, A.K., 2021. Miro (Mitochondrial Rho GTPase), a key player of mitochondrial axonal transport and mitochondrial dynamics in neurodegenerative diseases. Mitochondrion 56, 118–135. https://doi.org/10.1016/j.mito.2020.10.005
Pekkurnaz, G., Wang, X., 2022. Mitochondrial heterogeneity and homeostasis through the lens of a neuron. Nat Metab 4, 802–812. https://doi.org/10.1038/s42255-022-00594-w
Pérez, M.J., Baden, P., Deleidi, M., 2021. Progresses in both basic research and clinical trials of NAD+ in Parkinson's disease. Mechanisms of Ageing and Development 197, 111499. https://doi.org/10.1016/j.mad.2021.111499
Periñán, M.T., Gómez-Garre, P., Blauwendraat, C., Mir, P., Bandres-Ciga, S., 2020. The role of RHOT1 and RHOT2 genetic variation on Parkinson disease risk and onset. Neurobiology of Aging S0197458020302190. https://doi.org/10.1016/j.neurobiolaging.2020.07.003
Polymeropoulos, M.H., Lavedan, C., Leroy, E., Ide, S.E., Dehejia, A., Dutra, A., Pike, B., Root, H.,

Rubenstein, J., Boyer, R., Stenroos, E.S., Chandrasekharappa, S., Athanassiadou, A., Papapetropoulos, T., Johnson, W.G., Lazzarini, A.M., Duvoisin, R.C., Di Iorio, G., Golbe, L.I., Nussbaum, R.L., 1997. Mutation in the alpha-synuclein gene identified in families with Parkinson's disease. Science 276, 2045–2047. https://doi.org/10.1126/science.276.5321.2045

Poppe, M., Reimertz, C., Düssmann, H., Krohn, A.J., Luetjens, C.M., Böckelmann, D., Nieminen, A.L., Kögel, D., Prehn, J.H., 2001. Dissipation of potassium and proton gradients inhibits mitochondrial hyperpolarization and cytochrome c release during neural apoptosis. J Neurosci 21, 4551–4563. https://doi.org/10.1523/JNEUROSCI.21-13-04551.2001

Pulido, C., Ryan, T.A., 2021. Synaptic vesicle pools are a major hidden resting metabolic burden of nerve terminals. Sci Adv 7, eabi9027. https://doi.org/10.1126/sciadv.abi9027

Raff, M.C., Whitmore, A. V, Finn, J.T., 2002. Axonal Self-Destruction and Neurodegeneration. Science 296, 868–871. https://doi.org/10.1126/science.1068613

Ramsay, R.R., Kowal, A.T., Johnson, M.K., Salach, J.I., Singer, T.P., 1987. The inhibition site of MPP+, the neurotoxic bioactivation product of 1-methyl-4-phenyl-1,2,3,6-tetrahydropyridine is near the Q-binding site of NADH dehydrogenase. Arch Biochem Biophys 259, 645–649. https://doi.org/10.1016/0003-9861(87)90531-5

Ramsay, R.R., Salach, J.I., Singer, T.P., 1986. Uptake of the neurotoxin 1-methyl-4-phenylpyridine (MPP+) by mitochondria and its relation to the inhibition of the mitochondrial oxidation of NAD+-linked substrates by MPP+. Biochem Biophys Res Commun 134, 743–748. https://doi.org/10.1016/s0006-291x(86)80483-1

Reeve, A., Simcox, E., Turnbull, D., 2014. Ageing and Parkinson's disease: why is advancing age the biggest risk factor? Ageing Res Rev 14, 19–30. https://doi.org/10.1016/j.arr.2014.01.004

Reinhardt, P., Glatza, M., Hemmer, K., Tsytsyura, Y., Thiel, C.S., Höing, S., Moritz, S., Parga, J.A., Wagner, L., Bruder, J.M., Wu, G., Schmid, B., Röpke, A., Klingauf, J., Schwamborn, J.C., Gasser, T., Schöler, H.R., Sterneckert, J., 2013. Derivation and Expansion Using Only Small Molecules of Human Neural Progenitors for Neurodegenerative Disease Modeling. PLoS ONE 8, e59252. https://doi.org/10.1371/journal.pone.0059252

Richard, M., Kaufmann, P., Kornberger, R., Dingemanse, J., 2019. First-in-man study of ACT-709478, a novel selective triple T-type calcium channel blocker. Epilepsia 60, 968–978. https://doi.org/10.1111/epi.14732

Richard, M., Kaufmann, P., Ort, M., Kornberger, R., Dingemanse, J., 2020. Multiple-Ascending Dose Study in Healthy Subjects to Assess the Pharmacokinetics, Tolerability, and CYP3A4 Interaction Potential of the T-Type Calcium Channel Blocker ACT-709478, A Potential New Antiepileptic Drug. CNS Drugs 34, 311–323. https://doi.org/10.1007/s40263-019-00697-1

Riederer, P., Berg, D., Casadei, N., Cheng, F., Classen, J., Dresel, C., Jost, W., Krüger, R., Müller, T., Reichmann, H., Rieß, O., Storch, A., Strobel, S., van Eimeren, T., Völker, H.-U., Winkler, J., Winklhofer, K.F., Wüllner, U., Zunke, F., Monoranu, C.-M., 2019. α-Synuclein in Parkinson's disease: causal or bystander? J Neural Transm 126, 815–840. https://doi.org/10.1007/s00702-019-02025-9

Rizzuto, R., De Stefani, D., Raffaello, A., Mammucari, C., 2012. Mitochondria as sensors and regulators of calcium signalling. Nat Rev Mol Cell Biol 13, 566–578. https://doi.org/10.1038/nrm3412

Rousseaux, M.W.C., Marcogliese, P.C., Qu, D., Hewitt, S.J., Seang, S., Kim, R.H., Slack, R.S., Schlossmacher, M.G., Lagace, D.C., Mak, T.W., Park, D.S., 2012. Progressive dopaminergic cell loss with unilateral-to-bilateral progression in a genetic model of Parkinson disease. Proceedings of the National Academy of Sciences 109, 15918–15923. https://doi.org/10.1073/pnas.1205102109

Russo, G.J., Louie, K., Wellington, A., Macleod, G.T., Hu, F., Panchumarthi, S., Zinsmaier, K.E., 2009. Drosophila Miro Is Required for Both Anterograde and Retrograde Axonal Mitochondrial Transport. Journal of Neuroscience 29, 5443–5455. https://doi.org/10.1523/JNEUROSCI.5417-

08.2009
Ryan, S.D., Dolatabadi, N., Chan, S.F., Zhang, X., Akhtar, M.W., Parker, J., Soldner, F., Sunico, C.R., Nagar, S., Talantova, M., Lee, B., Lopez, K., Nutter, A., Shan, B., Molokanova, E., Zhang, Y., Han, X., Nakamura, T., Masliah, E., Yates, J.R., Nakanishi, N., Andreyev, A.Y., Okamoto, S., Jaenisch, R., Ambasudhan, R., Lipton, S.A., 2013. Isogenic human iPSC Parkinson's model shows nitrosative stress-induced dysfunction in MEF2-PGC1α transcription. Cell 155, 1351–1364. https://doi.org/10.1016/j.cell.2013.11.009
Ryan, T., Bamm, V.V., Stykel, M.G., Coackley, C.L., Humphries, K.M., Jamieson-Williams, R., Ambasudhan, R., Mosser, D.D., Lipton, S.A., Harauz, G., Ryan, S.D., 2018. Cardiolipin exposure on the outer mitochondrial membrane modulates α-synuclein. Nat Commun 9, 817. https://doi.org/10.1038/s41467-018-03241-9
Sabari, S.S., Balasubramani, K., Iyer, M., Sureshbabu, H.W., Venkatesan, D., Gopalakrishnan, A.V., Narayanaswamy, A., Senthil Kumar, N., Vellingiri, B., 2023. Type 2 Diabetes (T2DM) and Parkinson's Disease (PD): a Mechanistic Approach. Mol Neurobiol 1–27. https://doi.org/10.1007/s12035-023-03359-y
Saeed, M., 2018. Genomic convergence of locus-based GWAS meta-analysis identifies AXIN1 as a novel Parkinson's gene. Immunogenetics 70, 563–570. https://doi.org/10.1007/s00251-018-1068-0
Sanchez, G., Varaschin, R.K., Büeler, H., Marcogliese, P.C., Park, D.S., Trudeau, L.-E., 2014. Unaltered Striatal Dopamine Release Levels in Young Parkin Knockout, Pink1 Knockout, DJ-1 Knockout and LRRK2 R1441G Transgenic Mice. PLoS ONE 9, e94826. https://doi.org/10.1371/journal.pone.0094826
Sanders, L.H., Laganière, J., Cooper, O., Mak, S.K., Vu, B.J., Huang, Y.A., Paschon, D.E., Vangipuram, M., Sundararajan, R., Urnov, F.D., Langston, J.W., Gregory, P.D., Zhang, H.S., Greenamyre, J.T., Isacson, O., Schüle, B., 2014. LRRK2 mutations cause mitochondrial DNA damage in iPSC-derived neural cells from Parkinson's disease patients: reversal by gene correction. Neurobiol Dis 62, 381–386. https://doi.org/10.1016/j.nbd.2013.10.013
Santiago, J.A., Potashkin, J.A., 2013. Shared dysregulated pathways lead to Parkinson's disease and diabetes. Trends in Molecular Medicine 19, 176–186. https://doi.org/10.1016/j.molmed.2013.01.002
Saotome, M., Safiulina, D., Szabadkai, G., Das, S., Fransson, A., Aspenstrom, P., Rizzuto, R., Hajnoczky, G., 2008. Bidirectional Ca2+-dependent control of mitochondrial dynamics by the Miro GTPase. Proceedings of the National Academy of Sciences 105, 20728–20733. https://doi.org/10.1073/pnas.0808953105
Saxton, W.M., Hollenbeck, P.J., 2012. The axonal transport of mitochondria. Journal of Cell Science 125, 2095–2104. https://doi.org/10.1242/jcs.053850
Scheiblich, H., Dansokho, C., Mercan, D., Schmidt, S.V., Bousset, L., Wischhof, L., Eikens, F., Odainic, A., Spitzer, J., Griep, A., Schwartz, S., Bano, D., Latz, E., Melki, R., Heneka, M.T., 2021. Microglia jointly degrade fibrillar alpha-synuclein cargo by distribution through tunneling nanotubes. Cell 184, 5089-5106.e21. https://doi.org/10.1016/j.cell.2021.09.007
Schneider, T., Dibué, M., Hescheler, J., 2013. How "Pharmacoresistant" is Cav2.3, the Major Component of Voltage-Gated R-type Ca2+ Channels? Pharmaceuticals (Basel) 6, 759–776. https://doi.org/10.3390/ph6060759
Schöndorf, D.C., Aureli, M., McAllister, F.E., Hindley, C.J., Mayer, F., Schmid, B., Sardi, S.P., Valsecchi, M., Hoffmann, S., Schwarz, L.K., Hedrich, U., Berg, D., Shihabuddin, L.S., Hu, J., Pruszak, J., Gygi, S.P., Sonnino, S., Gasser, T., Deleidi, M., 2014. iPSC-derived neurons from GBA1-associated Parkinson's disease patients show autophagic defects and impaired calcium homeostasis. Nat Commun 5, 4028. https://doi.org/10.1038/ncomms5028
Schubert, M., Lindgreen, S., Orlando, L., 2016. AdapterRemoval v2: rapid adapter trimming,

identification, and read merging. BMC Research Notes 9, 88. https://doi.org/10.1186/s13104-016-1900-2
Schwab, A.J., Sison, S.L., Meade, M.R., Broniowska, K.A., Corbett, J.A., Ebert, A.D., 2017. Decreased Sirtuin Deacetylase Activity in LRRK2 G2019S iPSC-Derived Dopaminergic Neurons. Stem Cell Reports 9, 1839–1852. https://doi.org/10.1016/j.stemcr.2017.10.010
Schwarz, L., Fitzgerald, J.C., 2022. Steady-State Levels of Miro1 Linked to Phosphorylation at Serine 156 and Mitochondrial Respiration in Dopaminergic Neurons. Cells 11, 1269. https://doi.org/10.3390/cells11081269
Schwarz, L., Sharma, K., Dodi, L.D., Rieder, L.-S., Fallier-Becker, P., Casadei, N., Fitzgerald, J.C., 2022a. Miro1 R272Q disrupts mitochondrial calcium handling and neurotransmitter uptake in dopaminergic neurons. Front. Mol. Neurosci. 15, 966209. https://doi.org/10.3389/fnmol.2022.966209
Schwarz, L., Sharma, K., Dodi, L.D., Rieder, L.-S., Fallier-Becker, P., Casadei, N., Fitzgerald, J.C., 2022b. Miro1 R272Q disrupts mitochondrial calcium handling and neurotransmitter uptake in dopaminergic neurons. Frontiers in Molecular Neuroscience 15, 966209. https://doi.org/10.3389/fnmol.2022.966209
Scialò, F., Fernández-Ayala, D.J., Sanz, A., 2017. Role of Mitochondrial Reverse Electron Transport in ROS Signaling: Potential Roles in Health and Disease. Frontiers in Physiology 8.
Segura-Aguilar, J., Paris, I., Muñoz, P., Ferrari, E., Zecca, L., Zucca, F.A., 2014. Protective and toxic roles of dopamine in Parkinson's disease. J Neurochem 129, 898–915. https://doi.org/10.1111/jnc.12686
Shahmoradian, S.H., Lewis, A.J., Genoud, C., Hench, J., Moors, T.E., Navarro, P.P., Castaño-Díez, D., Schweighauser, G., Graff-Meyer, A., Goldie, K.N., Sütterlin, R., Huisman, E., Ingrassia, A., Gier, Y. de, Rozemuller, A.J.M., Wang, J., Paepe, A.D., Erny, J., Staempfli, A., Hoernschemeyer, J., Großerüschkamp, F., Niedieker, D., El-Mashtoly, S.F., Quadri, M., Van IJcken, W.F.J., Bonifati, V., Gerwert, K., Bohrmann, B., Frank, S., Britschgi, M., Stahlberg, H., Van de Berg, W.D.J., Lauer, M.E., 2019. Lewy pathology in Parkinson's disease consists of crowded organelles and lipid membranes. Nat Neurosci 22, 1099–1109. https://doi.org/10.1038/s41593-019-0423-2
Shaltouki, A., Hsieh, C.-H., Kim, M.J., Wang, X., 2018a. Alpha-synuclein delays mitophagy and targeting Miro rescues neuron loss in Parkinson's models. Acta Neuropathol 136, 607–620. https://doi.org/10.1007/s00401-018-1873-4
Shaltouki, A., Hsieh, C.-H., Kim, M.J., Wang, X., 2018b. Alpha-synuclein delays mitophagy and targeting Miro rescues neuron loss in Parkinson's models. Acta neuropathologica 136, 607–620. https://doi.org/10.1007/s00401-018-1873-4
Shulman, J.M., De Jager, P.L., Feany, M.B., 2011. Parkinson's Disease: Genetics and Pathogenesis. Annu. Rev. Pathol. Mech. Dis. 6, 193–222. https://doi.org/10.1146/annurev-pathol-011110-130242
Siegert, Richard J., Taylor, K.D., Weatherall, M., Abernethy, D.A., 2006. Is implicit sequence learning impaired in Parkinson's disease? A meta-analysis. Neuropsychology 20, 490–495. https://doi.org/10.1037/0894-4105.20.4.490
Siegert, Richard J, Taylor, K.D., Weatherall, M., Abernethy, D.A., 2006. Is implicit sequence learning impaired in Parkinson's disease? A meta-analysis. Neuropsychology 20, 490–495. https://doi.org/10.1037/0894-4105.20.4.490
Smith, K.P., Focia, P.J., Chakravarthy, S., Landahl, E.C., Klosowiak, J.L., Rice, S.E., Freymann, D.M., 2019. Structural assembly of the human Miro1/2 GTPases based on the crystal structure of the N-terminal GTPase domain (preprint). Cell Biology. https://doi.org/10.1101/729251
Song, P., Trajkovic, K., Tsunemi, T., Krainc, D., 2016. Parkin Modulates Endosomal Organization and Function of the Endo-Lysosomal Pathway. J. Neurosci. 36, 2425–2437. https://doi.org/10.1523/JNEUROSCI.2569-15.2016
Sonustun, B., Altay, M.F., Strand, C., Ebanks, K., Hondhamuni, G., Warner, T.T., Lashuel, H.A.,

Bandopadhyay, R., 2022. Pathological Relevance of Post-Translationally Modified Alpha-Synuclein (pSer87, pSer129, nTyr39) in Idiopathic Parkinson's Disease and Multiple System Atrophy. Cells 11, 906. https://doi.org/10.3390/cells11050906

Sorrentino, Z.A., Giasson, B.I., 2020. The emerging role of α-synuclein truncation in aggregation and disease. Journal of Biological Chemistry 295, 10224–10244. https://doi.org/10.1074/jbc.REV120.011743

Spillantini, M.G., Schmidt, M.L., Lee, V.M., Trojanowski, J.Q., Jakes, R., Goedert, M., 1997. Alpha-synuclein in Lewy bodies. Nature 388, 839–840. https://doi.org/10.1038/42166

Stephen, T.-L., Higgs, N.F., Sheehan, D.F., Al Awabdh, S., Lopez-Domenech, G., Arancibia-Carcamo, I.L., Kittler, J.T., 2015. Miro1 Regulates Activity-Driven Positioning of Mitochondria within Astrocytic Processes Apposed to Synapses to Regulate Intracellular Calcium Signaling. Journal of Neuroscience 35, 15996–16011. https://doi.org/10.1523/JNEUROSCI.2068-15.2015

Stock, D., Leslie, A.G., Walker, J.E., 1999. Molecular architecture of the rotary motor in ATP synthase. Science 286, 1700–1705. https://doi.org/10.1126/science.286.5445.1700

Stuart, T., Butler, A., Hoffman, P., Hafemeister, C., Papalexi, E., Mauck, W.M., Hao, Y., Stoeckius, M., Smibert, P., Satija, R., 2019. Comprehensive Integration of Single-Cell Data. Cell 177, 1888-1902.e21. https://doi.org/10.1016/j.cell.2019.05.031

Sugiura, A., McLelland, G.-L., Fon, E.A., McBride, H.M., 2014. A new pathway for mitochondrial quality control: mitochondrial-derived vesicles. EMBO J 33, 2142–2156. https://doi.org/10.15252/embj.201488104

Surmeier, D.J., Schumacker, P.T., 2013. Calcium, bioenergetics, and neuronal vulnerability in Parkinson's disease. J Biol Chem 288, 10736–10741. https://doi.org/10.1074/jbc.R112.410530

Tabata, Y., Imaizumi, Y., Sugawara, M., Andoh-Noda, T., Banno, S., Chai, M., Sone, T., Yamazaki, K., Ito, M., Tsukahara, K., Saya, H., Hattori, N., Kohyama, J., Okano, H., 2018. T-type Calcium Channels Determine the Vulnerability of Dopaminergic Neurons to Mitochondrial Stress in Familial Parkinson Disease. Stem Cell Reports 11, 1171–1184. https://doi.org/10.1016/j.stemcr.2018.09.006

Takahashi, K., Tanabe, K., Ohnuki, M., Narita, M., Ichisaka, T., Tomoda, K., Yamanaka, S., 2007. Induction of pluripotent stem cells from adult human fibroblasts by defined factors. Cell 131, 861–872. https://doi.org/10.1016/j.cell.2007.11.019

Takahashi, K., Yamanaka, S., 2006. Induction of pluripotent stem cells from mouse embryonic and adult fibroblast cultures by defined factors. Cell 126, 663–676. https://doi.org/10.1016/j.cell.2006.07.024

Thorne, N.J., Tumbarello, D.A., 2022. The relationship of alpha-synuclein to mitochondrial dynamics and quality control. Frontiers in Molecular Neuroscience 15, 947191. https://doi.org/10.3389/fnmol.2022.947191

Tran, J., Anastacio, H., Bardy, C., 2020. Genetic predispositions of Parkinson's disease revealed in patient-derived brain cells. npj Parkinsons Dis. 6, 1–18. https://doi.org/10.1038/s41531-020-0110-8

Tsai, P.-I., Course, M.M., Lovas, J.R., Hsieh, C.-H., Babic, M., Zinsmaier, K.E., Wang, X., 2014a. PINK1-mediated Phosphorylation of Miro Inhibits Synaptic Growth and Protects Dopaminergic Neurons in Drosophila. Sci Rep 4, 6962. https://doi.org/10.1038/srep06962

Tsai, P.-I., Course, M.M., Lovas, J.R., Hsieh, C.-H., Babic, M., Zinsmaier, K.E., Wang, X., 2014b. PINK1-mediated Phosphorylation of Miro Inhibits Synaptic Growth and Protects Dopaminergic Neurons in Drosophila. Scientific Reports 4, 6962. https://doi.org/10.1038/srep06962

Tseng, N., Lambie, S.C., Huynh, C.Q., Sanford, B., Patel, M., Herson, P.S., Ormond, D.R., 2021. Mitochondrial transfer from mesenchymal stem cells improves neuronal metabolism after oxidant injury in vitro: The role of Miro1. J Cereb Blood Flow Metab 41, 761–770. https://doi.org/10.1177/0271678X20928147

Turconi, G., Kopra, J., Võikar, V., Kulesskaya, N., Vilenius, C., Piepponen, T.P., Andressoo, J.-O., 2020. Chronic 2-Fold Elevation of Endogenous GDNF Levels Is Safe and Enhances Motor and Dopaminergic Function in Aged Mice. Molecular Therapy - Methods & Clinical Development 17, 831–842. https://doi.org/10.1016/j.omtm.2020.04.003

Van Laar, V.S., Berman, S.B., 2009. Mitochondrial dynamics in Parkinson's disease. Exp Neurol 218, 247–256. https://doi.org/10.1016/j.expneurol.2009.03.019

Vander Heiden, M.G., Chandel, N.S., Williamson, E.K., Schumacker, P.T., Thompson, C.B., 1997. Bcl-xL regulates the membrane potential and volume homeostasis of mitochondria. Cell 91, 627–637. https://doi.org/10.1016/s0092-8674(00)80450-x

van Spronsen, M., Mikhaylova, M., Lipka, J., Schlager, M.A., van den Heuvel, D.J., Kuijpers, M., Wulf, P.S., Keijzer, N., Demmers, J., Kapitein, L.C., Jaarsma, D., Gerritsen, H.C., Akhmanova, A., Hoogenraad, C.C., 2013. TRAK/Milton Motor-Adaptor Proteins Steer Mitochondrial Trafficking to Axons and Dendrites. Neuron 77, 485–502. https://doi.org/10.1016/j.neuron.2012.11.027

Vlahou, G., Eliáš, M., von Kleist-Retzow, J.-C., Wiesner, R.J., Rivero, F., 2011. The Ras related GTPase Miro is not required for mitochondrial transport in Dictyostelium discoideum. European Journal of Cell Biology 90, 342–355. https://doi.org/10.1016/j.ejcb.2010.10.012

Wang, X., Schwarz, T.L., 2009. The Mechanism of Ca2+-Dependent Regulation of Kinesin-Mediated Mitochondrial Motility. Cell 136, 163–174. https://doi.org/10.1016/j.cell.2008.11.046

Wang, X., Winter, D., Ashrafi, G., Schlehe, J., Wong, Y.L., Selkoe, D., Rice, S., Steen, J., LaVoie, M.J., Schwarz, T.L., 2011. PINK1 and Parkin Target Miro for Phosphorylation and Degradation to Arrest Mitochondrial Motility. Cell 147, 893–906. https://doi.org/10.1016/j.cell.2011.10.018

Wasilewski, M., Chacinska, A., 2021a. MIC60 relays oxidation to block mitophagy. Nat Metab 3, 1146–1147. https://doi.org/10.1038/s42255-021-00460-1

Wasilewski, M., Chacinska, A., 2021b. MIC60 relays oxidation to block mitophagy. Nature Metabolism 3, 1146–1147. https://doi.org/10.1038/s42255-021-00460-1

Wong, H.-S., Dighe, P.A., Mezera, V., Monternier, P.-A., Brand, M.D., 2017. Production of superoxide and hydrogen peroxide from specific mitochondrial sites under different bioenergetic conditions. J Biol Chem 292, 16804–16809. https://doi.org/10.1074/jbc.R117.789271

Wu, J., Kung, J., Dong, J., Chang, L., Xie, C., Habib, A., Hawes, S., Yang, N., Chen, V., Liu, Z., Evans, R., Liang, B., Sun, L., Ding, J., Yu, J., Saez-Atienzar, S., Tang, B., Khaliq, Z., Lin, D.-T., Le, W., Cai, H., 2019. Distinct Connectivity and Functionality of Aldehyde Dehydrogenase 1a1-Positive Nigrostriatal Dopaminergic Neurons in Motor Learning. Cell Rep 28, 1167-1181.e7. https://doi.org/10.1016/j.celrep.2019.06.095

Wüllner, U., Borghammer, P., Choe, C., Csoti, I., Falkenburger, B., Gasser, T., Lingor, P., Riederer, P., 2023. The heterogeneity of Parkinson's disease. Journal of Neural Transmission 130, 827–838. https://doi.org/10.1007/s00702-023-02635-4

Xiao, W., Wang, R.-S., Handy, D.E., Loscalzo, J., 2018. NAD(H) and NADP(H) Redox Couples and Cellular Energy Metabolism. Antioxidants & Redox Signaling 28, 251–272. https://doi.org/10.1089/ars.2017.7216

Yellen, G., 2018. Fueling thought: Management of glycolysis and oxidative phosphorylation in neuronal metabolism. J Cell Biol 217, 2235–2246. https://doi.org/10.1083/jcb.201803152

Yoon, Y.-S., You, J.S., Kim, T.-K., Ahn, W.J., Kim, M.J., Son, K.H., Ricarte, D., Ortiz, D., Lee, S.-J., Lee, H.-J., 2022. Senescence and impaired DNA damage responses in alpha-synucleinopathy models. Exp Mol Med 54, 115–128. https://doi.org/10.1038/s12276-022-00727-x

Zagare, A., Barmpa, K., Smajic, S., Smits, L.M., Grzyb, K., Grünewald, A., Skupin, A., Nickels, S.L., Schwamborn, J.C., 2022. Midbrain organoids mimic early embryonic neurodevelopment and recapitulate LRRK2-p.Gly2019Ser-associated gene expression. American journal of human genetics 109, 311–327. https://doi.org/10.1016/j.ajhg.2021.12.009

Zagare, A., Gobin, M., Monzel, A.S., Schwamborn, J.C., 2021a. A robust protocol for the generation of human midbrain organoids. STAR Protoc 2, 100524. https://doi.org/10.1016/j.xpro.2021.100524
Zagare, A., Gobin, M., Monzel, A.S., Schwamborn, J.C., 2021b. A robust protocol for the generation of human midbrain organoids. STAR Protocols 2, 100524. https://doi.org/10.1016/j.xpro.2021.100524
Zagare, A., Preciat, G., Nickels, Sarah.L., Luo, X., Monzel, A.S., Gomez-Giro, G., Robertson, G., Jaeger, C., Sharif, J., Koseki, H., Diederich, N.J., Glaab, E., Fleming, R.M.T., Schwamborn, J.C., n.d. Omics data integration allows the dentification of an idiopathic Parkinson's disease signature. under revision Nature Communications. https://doi.org/10.17881/v8jg-pw83
Zhang, N., Yu, X., Xie, J., Xu, H., 2021. New Insights into the Role of Ferritin in Iron Homeostasis and Neurodegenerative Diseases. Molecular Neurobiology 58, 2812–2823. https://doi.org/10.1007/s12035-020-02277-7
Zhang, Y., Yu, Z., Jiang, D., Liang, X., Liao, S., Zhang, Z., Yue, W., Li, X., Chiu, S.-M., Chai, Y.-H., Liang, Y., Chow, Y., Han, S., Xu, A., Tse, H.-F., Lian, Q., 2016. iPSC-MSCs with High Intrinsic MIRO1 and Sensitivity to TNF-α Yield Efficacious Mitochondrial Transfer to Rescue Anthracycline-Induced Cardiomyopathy. Stem Cell Reports 7, 749–763. https://doi.org/10.1016/j.stemcr.2016.08.009
Zhao, R.-Z., Jiang, S., Zhang, L., Yu, Z.-B., 2019. Mitochondrial electron transport chain, ROS generation and uncoupling (Review). Int J Mol Med 44, 3–15. https://doi.org/10.3892/ijmm.2019.4188
Zhu, A., Ibrahim, J.G., Love, M.I., 2019. Heavy-tailed prior distributions for sequence count data: removing the noise and preserving large differences. Bioinformatics 35, 2084–2092. https://doi.org/10.1093/bioinformatics/bty895
Zhuang, Aojia, Zhuang, Aobo, Chen, Y., Qin, Z., Zhu, D., Ren, L., Wei, Y., Zhou, P., Yue, X., He, F., Xu, J., Ding, C., 2023. Proteomic characteristics reveal the signatures and the risks of T1 colorectal cancer metastasis to lymph nodes. eLife 12, e82959. https://doi.org/10.7554/eLife.82959
Zigmond, M.J., Hastings, T.G., Perez, R.G., 2002. Increased dopamine turnover after partial loss of dopaminergic neurons: compensation or toxicity?q 5.

V Conclusion and perspectives

This study provided evidence of the pathogenic relevance of Miro1, and Miro1 variants in neurodegeneration in PD, as well as its potential as a novel, robust, PD model.

Our data revealed that the Miro1 p.R272Q mutation impaired proper management of ionomycin induced calcium stress (Manuscript III, Figure 2, panel G) mitochondrial bioenergetics and ATP production (Manuscript III, Figure 3, all panels), as well as increased ROS levels in two different *in vitro* models of PD (Manuscript III, Figure 2, panels A, C and E). Moreover, we found elevated levels of α-synuclein (Manuscript III, Figure 4, panels A, C, and D), a major hallmark of the disease, as well as a phenotype that can be explained by the aforementioned issues caused by Miro1 p.R272Q, namely increased dopaminergic neuron death (Manuscript III, Figure 5, panel E). Furthermore, genetic correction of the R272Q mutation rescued PD related impairments.

The relevance of Miro1 in PD pathogenesis was also demonstrated *in vivo*, as we showed that Miro1 p.R285Q KI model displayed dopaminergic loss in the SNpc (Manuscript III, Figure 6, panel D), increased PS129 α-synuclein (Manuscript III, Figure 6, panel F), as well as impaired anterograde procedural memory (Manuscript III, Figure 6, panels H and I). On top of being three PD signs found in patients, this also places our Miro1 R285 mice as a strong PD model, as other well-known genetic models of PD do not always display the two aforementioned alterations.

One follow up study could be to measure whether the synaptic activity and endocytosis of synaptic vesicles are impaired, as it was shown that that mitochondrial Ca^{2+} uptake was required to sustain ATP levels during activity, and thereby maintained synaptic vesicle endocytosis (Ashrafi et al., 2020). This is even more important given that 50% of axonal mitochondria are found at the synapses, and that in resting state, maintaining the pool of synaptic vesicles consumes a major part of the energy produced (Pekkurnaz and Wang, 2022; Pulido and Ryan, 2021) The calcium related impairment was accompanied by deficits in mitochondrial bioenergetics, as expected due to the link between calcium entry into the mitochondria and ATP production. Knowing that Miro1 regulated the calcium entry via the MCU, it would be interesting to also measure the integrity and activity of complex I of the ETC, as Balderas and colleagues demonstrated that impaired complex I prevented degradation of the MCU, allowing the cell to increase calcium flux into the mitochondria to compensate for deficits in energy production (Balderas et al., 2022).

Moreover, given the bioenergetics impairments induced by the p.R272Q Miro1 mutation (Manuscript III, Figure 3, all panels), one could later investigate the activity of NAD producing and consuming enzymes, which could give us a potential NAD precursors-based therapeutics strategy.

One could also go deeper into our previously published analysis of MERCs in Miro1 mutant patient derived fibroblasts and p.R272Q mutant iPSC-derived neurons, since all four mutations affected these structures (Berenguer-Escuder et al., 2020a, 2019a; Grossmann et al., 2019a). In particular, multiplexing calcium imaging with the SPLICS (split Green Fluorescent Protein-based contact sites sensors, which allows us to see both wide, involved in autophagy and narrow MERCS, involved in calcium exchange, (Cieri et al., 2018) constructs or the Mitorosella sensor (Arias-Fuenzalida et al., 2019) could expand our knowledge on the calcium and/or mitophagy related molecular mechanisms associated with PD pathogenesis caused by Miro1 variants and Miro1 regulatory role in MERCs.
The involvement of exosomes in PD grew over recent years, and we see extracellular vesicles among the gene ontology (GO) terms from our RNA seq data (Manuscript III, Figure 1, panel F). Moreover, we know that α-synuclein is secreted in a calcium dependent manner by exosomes, and that calcium elevation positively contributes to α-synuclein aggregation (Emmanouilidou et al., 2010; Leandrou et al., 2019a). One would need to investigate whether these exosomes secreted by 2D neurons and MO contain α-synuclein and in which state, as well as whether the p.R272Q Miro1 mutation affects their release and composition.

We can also identify one main limitation to our study. First, while the increase of ROS in dopaminergic neurons was seen in older MO, as it was higher after 30 days of differentiation, but not in younger ones (20 days old, data not shown) we lack this information for the calcium imaging performed in 2D neurons. In order to confirm whether the variant located in Miro1 EF hand, affecting calcium sensing, is the first insult leading to PD in this model, one could also perform this experiment in younger neurons, as well as *in vivo*.

Regarding our in vivo Miro1 p.R285Q KI model, one could further investigate if calcium signaling is disrupted by the p.R285Q mutation, if Miro1 KI mice are affected by oxidative stress, as well as investigate the involvement of other PD hallmarks such as inflammation, microglia, and astrocytes activation.

The upregulation of SNCA in Miro1 mutant *in vitro* may provide another lead helping towards PD therapeutics. Unfortunately, the last therapies to date targeting α-synuclein failed. Clinical trials of Cinpanemab, a monoclonal antibody binding α-synuclein developed by Biogen stopped in phase 2 after finding that it was not more effective than placebo (Johnson, 2022). On the other hand, Prasinezumab, developed by Roche and Prothena Bioscences, which seemed not to have meaningful effects on global clinical or imaging measures of PD progression in the context of the PASADENA study, is still under investigation (Johnson, 2022; Pagano et al., 2022). Indeed, following positive evaluation of secondary outcome parameters of the PASADENA study, further investigation are ongoing within the PADOVA study. The final outcome of the PADOVA study is open and results (including 6 patients from Luxembourg that are currently treated with Prasinezumab) are expected in 2024 (ClinicalTrials.gov identifier: NCT04777331).
Strategies targeting not one protein only are promising. Buntanetap, a molecule developed by Annovis Bio, which suppresses messenger RNA (mRNA) translation of amyloid amyloid precursor protein (APP), Tau, α-synuclein, was recently tested in Alzheimer's and Parkinson's disease patients (Fang et al., 2023). The drug was safe, lowered α-synuclein aggregates, and improved cognition in patients (Fang et al., 2023). A phase 3 trial is expected to start in patients with early PD this year. As a long-established protein in PD pathogenesis, α-synuclein can now be used as a biomarker in a synuclein aggregation assay with the immunoprecipitation-based real-time quaking-induced conversion (IP/RT-QuIC) method(Okuzumi et al., 2023). Interestingly, Miro1, via its pathological stabilization preventing proper mitophagy in PD patients, is already used as a biomarker ("Acurex Biosciences to Present Early Clinical Results Supporting its Novel Parkinson's Disease Biomarkers at a Michael J. Fox Foundation Biomarkers Workshop," 2023; Hsieh et al., 2019a), and thanks to our study, is established as a gene whose at least one rare variant (p.R272Q) causes PD.

Dysregulated calcium homeostasis, as a hallmark of PD, is found in many PD cases. PARKIN mutant iPSC-derived midbrain dopaminergic neurons display dysregulated calcium homeostasis, increased susceptibility to rotenone-induced mitochondrial damages and cell death (Tabata et al., 2018). Since we hypothesize that most of the phenotypes are due to the incapacity of Miro1 to properly sense calcium, therapies based on calcium would be especially promising. Tabata and colleagues demonstrated that by using benidipine, a voltage gated calcium channel antagonist (affecting Long lasting "L" Cav1, Resting "N" Cav2.2, and Transient "T" Cav3, type calcium channels), PARKIN mutant neurons were protected against rotenone-induced apoptosis and calcium increase, and impaired neurites outgrowth was rescued (Tabata et al., 2018).

Rescue of neurite outgrowth with benidipine was also demonstrated in PINK1 mutant iPSC-derived neurons, further strengthening the potential of calcium modulation as a therapeutic target in PD (Tabata et al., 2018). L type calcium channel (LTCC) inhibitors have been used in mice, and shown to protect against dopaminergic neurons loss. Moreover, intake of LTCC reduces the risk to develop PD (Ortner, 2021). R type calcium channels (RTCC) calcium channels would be a more difficult target to modulate, as no specific inhibitor exists (Schneider et al., 2013). T type calcium channels (TTCC), however, would be a promising target, as their expression is elevated in a PD model, and inhibition of TTCC was beneficial in their PD iPSC-derived model (Tabata et al., 2018). Recently, Cav3.2 calcium channels were linked to nociception and inhibition of T-type calcium channels was found to alleviate pain (Joksimovic et al., 2018). An inhibitor of TTCC, zonisamide had a positive effect in PD patient, but could not be used further due to its broad side effects. To date, the TTCC specific blocker ACT-709478 was well tolerated and safe in phase 2 clinical trials (Richard et al., 2020, 2019). Another phase two trial uses the selective blocker CX 8998. Additional studies are needed to decipher to which extent subtypes of T-type calcium channels are functionally different, and if developing a drug that targets one subtype specifically could benefit PD patients (Cmarko and Weiss, 2020). Further work is needed to assess whether modulating calcium channels activity would be working in our Miro1 mutant PD model.

On the specific case of our Miro1 p.R272Q mutant, one could also further investigate mitochondrial calcium by preventing its uptake by the ER, using thapsigargin, forcing the cell to control calcium levels via the mitochondria, while also treating control neurons with MCU inhibitors such as Ru360, to see if the higher peak of calcium after ionomycin treatment we saw in the p.R272Q iPSC-derived neurons is truly due to a faulty interaction between Miro1 p.R272Q and the MCU.

Another approach could also be using calcium channel blockers, as it was shown that increased calcium levels led to augmentation of α-synuclein levels, and using isradipine lowered α-synuclein aggregation in primary rat ventral midbrain neurons (Lautenschläger et al., 2018; Leandrou et al., 2019a). Besides, another calcium targeted approach could be taken, not by blocking calcium channels, but by using a calcium chelator, (1,2-bis (o-aminophenoxy) ethane-N, N, N′, N'-tetraacetic acid) (BAPTA), as this compound was shown to be neuroprotective. In a spinal cord injury mouse model, this chelator protected neurons by inhibiting apoptosis and ROS generation, preserved their electrophysiological properties, and alleviated motor impairments in treated animals (Kang et al., 2021).

An earlier study also demonstrated its effect on lowering ionomycin induced calcium overload using neuroblastoma cell lines, which is of particular interest given our experimental setup used in this thesis for calcium imaging (Collatz et al., 1997). BAPTA was also used in the context of motor neuron diseases, and protected neurons against lipopolysaccharide-induced toxicity (Li et al., 2008).

Even though it is not directly linked to the results presented in this thesis, and ineffective in clinical trial to this date, but slightly working in pre-clinical models of PD (Turconi et al., 2020), ectopic delivery of glial cell line-derived neurotrophic factor-based (GDNF) could be tested in our Miro1 p.R285Q KI model. Indeed, elevating GDNF levels increased motor and dopaminergic function in young PD animals (Kumar et al., 2015; Mätlik et al., 2018). More recently, Turconi and colleagues demonstrated that a long-term, two-fold increase of GDNF levels improved motor learning, striatal dopamine concentration, as well as the number of SNpc TH positive cells (Turconi et al., 2020). Given the issues seen with motor learning, and loss of DA neurons in old, Miro1 R.285Q KI mice, GDNF based therapy remains a promising area to investigate.

As discussed earlier in this thesis (page 37, articles from Sijun Yang and colleagues), Miro1 seems to have a significant importance in T2D. Therefore, if an assessment of T2D related phenotypes in the Miro1 p.R285Q mice reveals significant alterations in this regard, our Miro1 model could also prove its usefulness to study the association between PD and T2D.

To conclude, taking the results presented in this thesis into account, we would like to exploit the Miro1 p.R272Q models for future pharmalogical screening.

Lastly, one could make use of the Luxembourg Parkinson Study (NCER-PD cohort) and its high level of phenotyping both at the genetic and clinical level, associated with sampling of blood and fibroblasts from participants, to further confirm the Miro1 retention phenotype in several patients. Regarding the use of the Miro1 retention phenotype as a prediction biomarker, the recent RBD study from Luxembourg could be of particular interest, as blood sampling from participants is performed, and their possible conversion towards PD is assessed.

VI Appendix

Appendix I: review
The emerging role of *RHOT1*/Miro1 in the pathogenesis of Parkinson's disease

Appendix II:
Oxygen consumption rate of. Native fibroblasts Miro1 p.R272Q with galactose

Appendix III:
Densitometric analysis of overexposed α-synuclein Western blot in iPSC-derived PD-R272Q Miro1 neurons (performed on the same membrane as in Manuscript III, figure 4 D)

Appendix IV and V:
Miro1 Fibroblasts (III) treated with cccp from Christiane Oleksy and Armelle Vitali, and Mirisk fibroblasts (IV)

Appendix VI:
Pictures Miro1 mice

frontiers in Neurology

REVIEW
published: 15 September 2020
doi: 10.3389/fneur.2020.00587

The Emerging Role of *RHOT1*/Miro1 in the Pathogenesis of Parkinson's Disease

Dajana Grossmann[1,2*], *Clara Berenguer-Escuder*[1], *Axel Chemla*[1], *Giuseppe Arena*[1] and *Rejko Krüger*[1,3,4*]

[1] Luxembourg Centre for Systems Biomedicine (LCSB), University of Luxembourg, Belvaux, Luxembourg, [2] Section for Translational Neurodegeneration "Albrecht Kossel", Department of Neurology, Universitätsmedizin Rostock, Rostock, Germany, [3] Parkinson Research Clinic, Centre Hospitalier de Luxembourg (CHL), Luxembourg, Luxembourg, [4] Transversal Translational Medicine, Luxembourg Institute of Health (LIH), Strassen, Luxembourg

The expected increase in prevalence of Parkinson's disease (PD) as the most common neurodegenerative movement disorder over the next years underscores the need for a better understanding of the underlying molecular pathogenesis. Here, first insights provided by genetics over the last two decades, such as dysfunction of molecular and organellar quality control, are described. The mechanisms involved relate to impaired intracellular calcium homeostasis and mitochondrial dynamics, which are tightly linked to the cross talk between the endoplasmic reticulum (ER) and mitochondria. A number of proteins related to monogenic forms of PD have been mapped to these pathways, i.e., PINK1, Parkin, LRRK2, and α-synuclein. Recently, Miro1 was identified as an important player, as several studies linked Miro1 to mitochondrial quality control by PINK1/Parkin-mediated mitophagy and mitochondrial transport. Moreover, Miro1 is an important regulator of mitochondria-ER contact sites (MERCs), where it acts as a sensor for cytosolic calcium levels. The involvement of Miro1 in the pathogenesis of PD was recently confirmed by genetic evidence based on the first PD patients with heterozygous mutations in *RHOT1*/Miro1. Patient-based cellular models from *RHOT1*/Miro1 mutation carriers showed impaired calcium homeostasis, structural alterations of MERCs, and increased mitochondrial clearance. To account for the emerging role of Miro1, we present a comprehensive overview focusing on the role of this protein in PD-related neurodegeneration and highlighting new developments in our understanding of Miro1, which provide new avenues for neuroprotective therapies for PD patients.

Keywords: Miro1, Parkinson's disease, mitochondrial dynamics, mitophagy, calcium signaling

OPEN ACCESS

Edited by:
Andrew Anthony Hicks, Eurac Research, Italy

Reviewed by:
Georgia Xiromerisiou, University of Thessaly, Greece
Irene Pichler, Eurac Research, Italy

***Correspondence:**
Dajana Grossmann
dajana.grossmann@med.uni-rostock.de
Rejko Krüger
rejko.krueger@uni.lu

Specialty section:
This article was submitted to Neurogenetics, a section of the journal Frontiers in Neurology

Received: *30 January 2020*
Accepted: *22 May 2020*
Published: *15 September 2020*

Citation:
Grossmann D, Berenguer-Escuder C, Chemla A, Arena G and Krüger R (2020) The Emerging Role of RHOT1/Miro1 in the Pathogenesis of Parkinson's Disease. Front. Neurol. 11:587. doi: 10.3389/fneur.2020.00587

INTRODUCTION

The mitochondrial Rho GTPase Miro1 was first described in yeast, and these studies already reported a link of Miro1 to calcium homeostasis. Yeast strains devoid of the Miro1-ortholog Gem1p displayed a calcium-dependent growth defect (1). Later, mammalian Miro1 was described as an adaptor for calcium-dependent mitochondrial transport (2–4).

The link between Miro1 dysfunction and Parkinson's disease (PD) arose from studies that identified Miro1 as a target of the PD-associated proteins PINK1 and Parkin. These proteins are mutated in autosomal recessively inherited early-onset PD, and functional studies revealed a key role of PINK1-mediated phosphorylation of Parkin for the regulation of mitophagy as a key mechanism in mitochondrial quality control (5, 6). Therefore, the functional interplay of Miro1 with these key proteins for the maintenance of mitochondrial homeostasis was the first link between mitochondrial dynamics and degradation (7, 8). Further studies *in vivo* revealed that the overexpression of Miro1 in flies led to loss of dopaminergic neurons (9), likely due to a delay of clearance of dysfunctional mitochondria via mitophagy triggered by an excess of Miro1. In contrast, knockout of Miro1 in primary mouse neurons caused a decrease in dendrite complexity as a result of impaired mitochondrial distribution (10). The link between Miro1 dysregulation and neurodegeneration was further substantiated by first studies in human patient-based models showing that impaired Miro1 degradation, and the resulting inhibition of mitophagy, was a shared phenotype in fibroblasts and neurons from different sporadic and monogenic PD patients (11, 12). Recently, our group described the first mitochondria-related cellular phenotypes in fibroblasts from PD patients carrying mutations in *RHOT1*, the gene encoding the Miro1 protein (13, 14), thereby further supporting the involvement of Miro1 in the pathogenesis of PD.

Investigations in yeast showed that Gem1p not only is involved in the regulation of mitochondrial function but also regulates the interplay between mitochondria and the endoplasmic reticulum (ER) (15, 16). This interplay came into the focus of PD research, since several PD-associated proteins were recently identified as regulators of mitochondria-ER contact sites (MERCs), i.e., PINK1, Parkin, LRRK2, or α-synuclein (17–20), all of which are also interacting with Miro1 (7, 11, 12, 21).

Moreover, Miro1 was associated with peroxisomal transport (22–24). Aberrant peroxisome-related metabolism was observed in PD patients (25), and mice with impaired peroxisome activity displayed increased aggregation of α-synuclein (26), providing another potential link between Miro1 and PD via altered peroxisome function. Together, these findings point to an emerging role of Miro1 in neurodegeneration in PD that underscores the need for summarizing the current knowledge about Miro1 and new developments that provide new perspectives for future causative therapies in PD.

STRUCTURE AND PHYSIOLOGICAL FUNCTION OF THE MIRO1 PROTEIN

In mammals, two Miro GTPases, named as Miro1 and Miro2, are encoded by the *RHOT1* and *RHOT2* genes located on chromosome 17. Miro1 and Miro2 are both ubiquitously expressed, consisting of 662 amino acid residues, and display a 60% peptide sequence homology (27–29). Miro GTPases are conserved in almost all eukaryotes containing mitochondria (30), and they were first considered as atypical members of the RAS superfamily of GTPases, particularly as two of the 23 members of the RHO (Ras homolog) protein subfamily (27).

However, in contrast to other RHO family members, Miro GTPases contain no C-terminal cysteine and they also lack the typical RHO insert, which led to their classification as a definite subfamily of small GTPases (29, 31–34).

Structurally distinct N-terminal and C-terminal GTP-binding motifs are present in both Miro proteins, with a linker region (called "MiroS") connecting two EF-hand domains to the C-terminal GTPase domain (35, 36).

In contrast to the yeast Miro1 homolog Gem1p, which needs both GTPase domains to maintain its function as an adaptor for transport (34, 37), the influence and requirement of these two GTPase domains on mitochondrial trafficking have been widely debated in metazoans, especially in neurons. Several studies suggested that the N-terminal and C-terminal GTPases of Miro1 might have different functions. For instance, it was shown in fly and rat neurons that the C-terminal GTPase domain of Miro is only involved in retrograde transport, while its N-terminal GTPase domain is essential for mitochondrial transport in both retrograde and anterograde directions (2, 38). However, another study provided evidence that alterations of mitochondrial transport in *Drosophila* neurons were exclusively caused by mutations in the N-terminal GTPase domain, but not in the C-terminal GTPase domain of dMiro (*Drosophila* homolog of mammalian Miro1) (37).

Further reinforcing this hypothesis, only mutations in the N-terminal GTPase domain led to the disruption of the mitochondrial network in mammalian cells (28). Moreover, recent work developed by Kalinski et al. describes that the deacetylation of the lysine 105 on the N-terminal GTPase domain of Miro1 could inhibit mitochondrial transport in primary mouse neurons, subsequently affecting axonal growth (39).

While earlier structural studies were performed on dMiro, recent work gave us new insights on human Miro1, demonstrating that both N-terminal and C-terminal GTPases were not only structurally but also functionally different. The N-terminal GTPase was shown to have exclusively GTPase activity, while the C-terminal GTPase also displayed NTPase activity (34, 36, 40), thus making Miro1 the only currently known human protein that contains two different GTPase domains (41). On the other hand, the C-terminal GTPase domain seems to be crucial for the calcium-related functions of Miro1, by interacting with and stabilizing the two EF-hand domains of the protein, which are involved in calcium binding (35, 42).

Miro1 also contains two ligand-mimicking α-helices (LM1 and LM2), which connect each canonical EF hand to a non-canonical "hidden" EF-hand domain (hEF) (35). The calcium-binding amino acids are exposed to the cytosol via an helix-loop-helix-motif in both EF hands, facilitating a conformational change of the protein upon binding to calcium (43, 44).

Moreover, Miro1 harbors a C-terminal transmembrane domain (TMD), which anchors the protein into the outer mitochondrial membrane (OMM), exposing the protein and the N-terminal GTPase to the cytoplasm (2, 35). Fransson et al. demonstrated that the deletion of the TMD in both

mammalian Miro proteins led to their mislocalization to the cytoplasm, proving that the TMD is required for mitochondrial targeting (28).

Our group recently described the first heterozygous mutations in the human *RHOT1* gene, found in four individuals diagnosed with PD (13, 14). The identified mutations R272Q, T351A, and R450C were located within highly conserved protein domains of Miro1: R272Q within the LM1 of the N-terminal EF-hand domain, T351A within the C-terminal EF-hand domain, and R450C within the C-terminal GTPase domain (13, 14). The T610A mutation is located within the C-terminus section of the protein, close to the TMD (14). The homology models of the 3D structure of the Miro1 protein showed that all four mutations were localized on the protein surface and exposed to the cytosol. Due to their position, these mutations could therefore impact on calcium binding and sensing, GTP hydrolysis, and mitochondrial localization features of Miro1 (13, 14).

MIRO1 AND PARKINSON'S DISEASE

Mitochondria are the main source of cellular energy, and on top of that, they have an essential role in intracellular calcium buffering and regulation of lipid homeostasis (45, 46). For these reasons, dopaminergic neurons critically depend on mitochondrial function, since they require a constant supply of energy and calcium to maintain the integrity of their long axons and to regulate their pacemaking activity for the release and recycling of neurotransmitters (47, 48).

Mitochondrial dyshomeostasis is a central factor in PD pathophysiology, and indeed several genes involved in the development of familial PD are associated with mitochondrial homeostasis (49–51). Increasing evidence indicates that proteins encoded by several PD-linked genes physically interact with Miro1, modifying its function and hence contributing to the dysregulation of neuronal integrity. For this reason, the link between Miro1 and neurodegeneration is a topic of growing interest in PD research.

Bioinformatic analyses indicated that PINK1 and Parkin are direct protein interactors of Miro1 (52). In line with this structural finding, several studies described functional links between these proteins using *in vitro* cellular models from different species. Functional connections between PINK1, Parkin, and Miro1 were first described in flies, where PD-associated deletions in *Drosophila* PINK1 were shown to cause disruption of mitochondrial transport in neuronal axons through interaction with dMiro in a Parkin-dependent manner (9, 53). On top of affecting mitochondrial movement, the loss of PINK1 and Parkin in flies promoted the disruption of other mitochondrial-related mechanisms, such as impairment of mitochondrial clearance, altered the abundance of mitochondria-ER appositions and mitochondrial calcium overload, finally leading to the death of dopaminergic neurons (9, 17). Notably, all these mentioned phenotypes were rescued by a reduction in the amount of dMiro protein in these cells (9, 17), emphasizing the importance of the multifunctional role of Miro1 for mitochondrial homeostasis in PD.

Despite the clear link between mitochondrial dyshomeostasis in PD and Miro proteins, single-nucleotide polymorphisms (SNPs) in *RHOT1/2* were not associated with PD using genome-wide association studies (GWAS) (54), and recent meta-analyses of GWAS data did not identified *RHOT1/2* as risk loci for PD (55, 56). However, GWAS are not designed to detect rare variants due to a minor allele frequency of the used SNPs of >5% in most studies, and therefore, sequencing methods to identify rare variants are needed. Of note, gene-based association clustering methods recently allowed the identification of *RHOT2*, the gene encoding for Miro2, as a PD-associated gene (57). Recently, our group identified the first heterozygous mutations in the *RHOT1* gene in four independent PD patients by exome sequencing (13, 14), further strengthening the impact of Miro1 in the development of PD and defining *RHOT1* as a potential novel risk gene for the pathogenesis of this disorder.

The knowledge about the role of human Miro1 in neurodegeneration, particularly in the pathogenesis of PD, is growing rapidly. In the next sections, we will discuss the molecular and cellular effects of mutant human Miro1 in PD.

MIRO1 AS A TARGET FOR PINK1/PARKIN-MEDIATED MITOPHAGY

An impressive number of studies over the last 30 years shed light on the so-called mitochondrial life cycle, during which these highly dynamic organelles continuously experience fission and fusion events to meet the functional needs of the cells. Maintaining this mitochondrial network requires the coordinated activity of mitochondrial biogenesis and clearance pathways, which ensure the replacement of damaged organelles with metabolically active mitochondria. Consequently, impairing this fine-tuned quality control mechanism leads to the accumulation of dysfunctional mitochondria, which in turn increases oxidative stress and deteriorates cellular activity (58, 59). Removal of damaged mitochondria is even more important in post-mitotic cells like neurons, which are not able to dilute harmful components through cell division.

In accordance, mitochondrial dysfunction plays an essential role in a large number of neurodegenerative diseases, including PD, and the accurate mitochondrial turnover is now considered a key neuroprotective mechanism against chronic disease conditions (60).

Mitochondrial degradation is a well-orchestrated process involving the two main intracellular clearance machineries, namely, the ubiquitin–proteasome system (UPS) and the autophagy pathway (61). The PD-linked PINK1 and Parkin proteins are the master and commander of this multistep mechanism: (i) the mitochondrial kinase PINK1 selectively recognizes depolarized mitochondria and rapidly accumulates on their surface, where it starts a massive phosphorylation of ubiquitinated proteins; (ii) the cytosolic ubiquitin-ligase Parkin recognizes PINK1-catalyzed phospho-ubiquitin and translocates to mitochondria, supplying further ubiquitin chains to PINK1

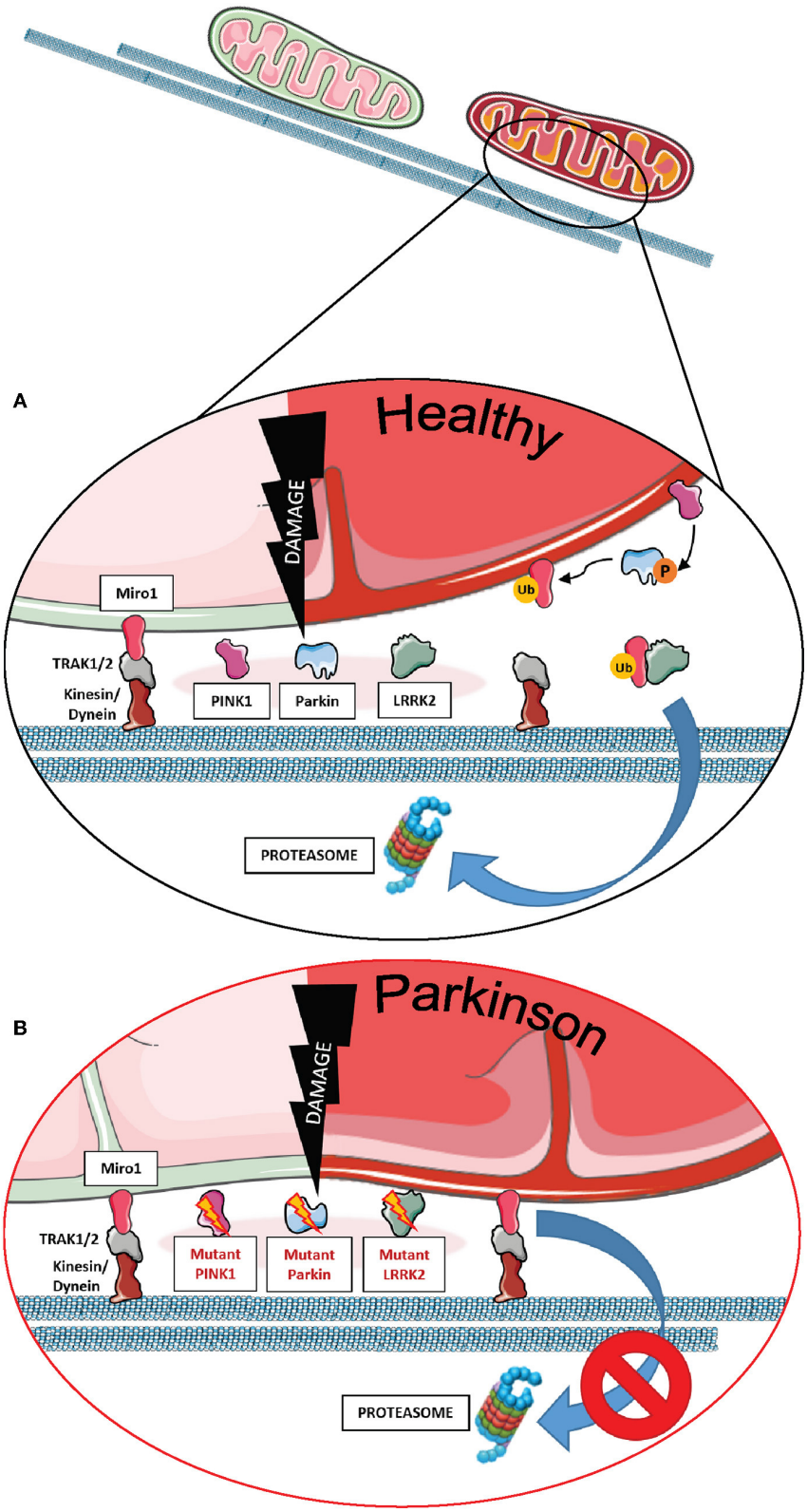

FIGURE 1 | The role of Miro1 in mitophagy. **(A)** Lysosomal degradation of dysfunctional mitochondria requires the stop of mitochondrial transport and detachment from the cytoskeleton. Mitochondrial damage leads to the accumulation of PINK1 at mitochondria and the recruitment of the E3 ubiquitin ligase Parkin. PINK1

(Continued)

FIGURE 1 | phosphorylates and activates Parkin, which in turn ubiquitinates proteins at the outer mitochondrial membrane, including Miro1. Additionally, PINK1 might also phosphorylate ubiquitin chains on mitochondrial proteins. Ubiquitinated proteins, including Miro1, are then targeted for proteasomal degradation, thereby disconnecting mitochondria from the cytoskeleton and stopping transport. Isolated mitochondria are then ready for uptake by autophagosomes. LRRK2 was shown to be involved in the removal of Miro1 from the surface of impaired mitochondria. **(B)** In cell models expressing PD-associated mutations in PINK1, Parkin, or LRRK2, the proteasomal degradation of Miro1 is impaired, consequently interfering with the arrest of mitochondrial transport and the initiation of mitophagy. This figure was created using elements from Servier Medical Art, licensed under a Creative Common Attribution 3.0 Generic License (www.smart.servier.com).

and amplifying the signal in a positive feedback loop; (iii) Parkin ubiquitinates a number of substrates on the OMM, leading to the inhibition of mitochondrial fusion and arrest of mitochondrial movement; (iv) the coating of dysfunctional mitochondria with phospho-ubiquitin chains recruits specific components of the autophagic receptor machinery to mitochondria, which are then engulfed by autophagosomes; and (v) finally degraded into lysosomes (62).

Miro1 plays an essential role in this process, being one of the first substrates of Parkin E3-ligase activity. As a key component of the mitochondrial transport machinery that anchors the organelle to the motor proteins of the cytoskeleton, Miro1 is ubiquitinated by Parkin and consequently degraded by the UPS (**Figure 1A**), which leads to mitochondrial arrest and facilitates mitophagy (7–9, 36, 42, 63, 64). Particularly in the context of PD, PD-associated mutations in Parkin were shown to disrupt the ubiquitination of Miro1 for proteasomal degradation in patient-derived fibroblasts, leading to the inhibition of Miro1 turnover and the subsequent failure of mitochondrial arrest for mitophagy (**Figure 1B**) (7). Further supporting the functional interaction of Miro1 with other PD gene products linked to mitochondrial quality control, previous findings also showed that Miro1 physically interacts with PINK1 and is phosphorylated by the kinase on the serine 156, which could represent a signal for the following ubiquitination by Parkin (7, 65).

In addition to the PINK1-Parkin axis, Miro1 removal from the OMM of depolarized organelles could also be mediated by its association with other PD-related proteins (**Figures 1A,B**). Two studies supported this hypothesis by the discovery that LRRK2 and α-synuclein cooperate with Miro1 to stop mitochondrial movement prior to mitophagy (11, 12). In fact, the pathogenic PD mutations LRRK2 G2019S and α-synuclein A53T disrupt this process, resulting in Miro1 accumulation, delayed mitochondria arrest, and impaired mitophagy activation in patient-derived fibroblasts and induced pluripotent stem cell (iPSC)-derived neurons (11, 12).

Based on these findings, clearing Miro1 from depolarized mitochondria is emerging as a potential neuroprotective mechanism against PD, as the failure of its removal from mitochondria was demonstrated in cells from PD patients. Interestingly, in some PD cases, Miro1 degradation is impaired even in the presence of functional Parkin and LRRK2, indicating the existence of additional mechanisms accounting for Miro1 removal from dysfunctional mitochondria (66). Hence, Hsieh et al. demonstrated that genetically or pharmacologically reducing Miro1 levels improved mitochondrial arrest, activated mitophagy, and prevented dopaminergic neurodegeneration in both iPSC-derived human neurons and fly models of PD, without significantly affecting the movement of healthy mitochondria (11, 12, 66).

Further confirming an important role for Miro1 in the pathogenesis of PD, we recently described mitophagy alterations in fibroblasts from PD patients harboring heterozygous mutations in the *RHOT1* gene encoding Miro1 (13, 14). Interestingly, all mutant fibroblast lines demonstrated alterations in mitophagy flux, but the resulting phenotype was different depending on the Miro1 mutation. In fact, the R272Q and R450C mutants demonstrated increased levels of mitophagy compared to controls, reflected by increased mitochondria co-localizing with LC3 puncta and decreased Parkin protein levels under baseline conditions. CCCP treatment was not sufficient to further increase mitophagy, suggesting that mitophagy was already running at maximal capacity (13). In contrast, the T351A and T610A mutants displayed no increase in mitophagy under baseline conditions. CCCP treatment leads to increased co-localization of LC3 puncta with mitochondria in control cells, but not in Miro1-T351A or -T610A fibroblasts, suggesting an impaired mitophagy mechanism in these mutants (14).

It is worth noting that, in contrast to the increased mitophagic turnover observed in R272Q mutant fibroblasts, iPSC-derived neurons harboring the same Miro1 mutation displayed an opposite phenotype compared to the fibroblasts (67). Mitophagy was not inducible in Miro1-R272Q neurons, either by oxidative stress or by CCCP treatment. Furthermore, bafilomycin A1 treatment did not lead to an accumulation of the autophagic cargo protein p62 in these cells, suggesting a reduced autophagic turnover (68). Based on these observations, mitophagy seems to be regulated differentially in fibroblasts and neurons.

Remarkably, the mitophagy phenotype in these cells seems to be tightly related to the degree of topographic association between mitochondria and ER, as represented by the distance between both organelles (68). In 2018, McLelland et al. described that the initiation step of mitophagy in human cancer cell lines and iPSC-derived neurons occurs at mitochondria and ER appositions where the cleft that separates both organelles is wider than ∼30 nm (**Figure 2A**) (69). These "wide" appositions serve as a platform for Parkin-mediated ubiquitination of OMM proteins at depolarized mitochondria, subsequently promoting the uncoupling of mitochondria from the ER and the mitophagy process (13, 14). This hypothesis was drawn from the observation that iPSC-derived neurons from a PD patient with a deletion in Parkin did not show a decrease of these "wide" MERCs after initiation of mitophagy with CCCP (**Figure 2B**) (69). Fitting, our results showed that Miro1-mutant lines with an unchanged number of "wide" MERCs compared to controls displayed the

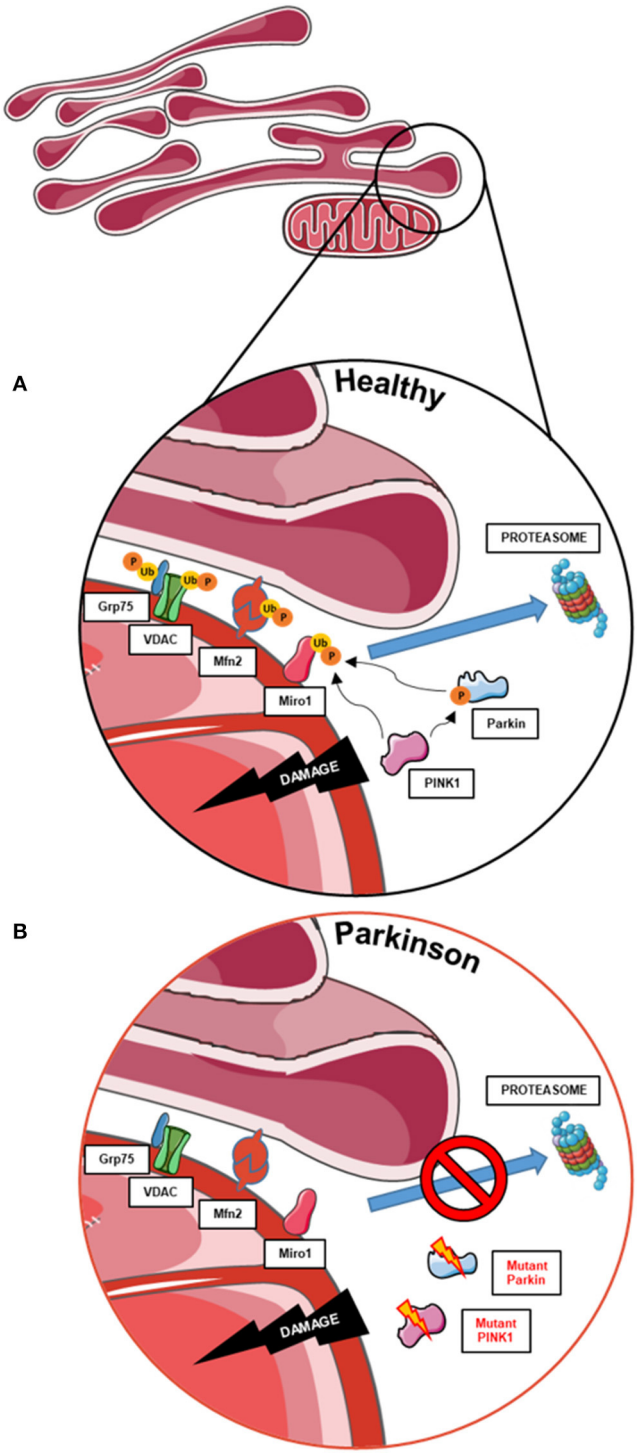

FIGURE 2 | The role of MERCs in mitophagy and the contribution of PD-associated proteins. **(A)** Mitophagy also requires the untethering of impaired mitochondria from the ER. Therefore, PINK1 and Parkin work together to ubiquitinate and phosphorylate proteins involved in subtypes of MERCs (i.e., Grp75, VDAC, Mfn2, and Miro1) for subsequent proteasomal degradation and disassembly of MERCs, allowing the degradation of impaired mitochondria. **(B)** In cells with impaired PINK1 or Parkin function, MERCs *(Continued)*

FIGURE 2 | are not disassembled upon mitochondrial dysfunction, hence hampering the initiation of mitophagy. This figure was created using elements from Servier Medical Art, licensed under a Creative Common Attribution 3.0 Generic License (www.smart.servier.com).

ability to induce mitophagy after CCCP treatment (13, 14), while mutants with reduced amount of "wide" MERCs revealed a deficit to initiate mitophagy after treatment with CCCP (14). These findings suggest that the regulation of mitochondrial quality control by Miro1 might crucially depend on the structure of MERCs.

MIRO1 AS A REGULATOR OF MITOCHONDRIAL-ER CONTACT SITES

MERCs are discrete areas of proximity between mitochondria and the ER that coordinate essential physiological processes, such as lipid biosynthesis, cellular calcium handling, and mitochondrial homeostasis (70–72). These mechanisms are reported to be affected in neurodegeneration (73, 74); hence, MERCs are one of the most studied organelle juxtapositions and a current spotlight in PD research (75).

Several mitochondria-related proteins involved in PD pathogenesis modulate the physiological function of the MERCs by acting as regulatory factors. Overexpression of Parkin in HeLa cells was shown to increase physical and functional coupling between mitochondria and ER, stimulating mitochondrial calcium uptake and ATP production, while Parkin knockdown had the opposite effect (18). Similarly, overexpression of α-synuclein and DJ-1 proteins increased the number of MERCs in HeLa cells, subsequently increasing mitochondrial calcium uptake (18, 76). LRRK2 was recently found to also modulate MERC amount and function, since LRRK2-null MEFs express reduced MERC abundance and dysregulated mitochondrial calcium uptake (77). Moreover, α-synuclein was found in MERCs from mouse and human brain tissue, where it seems to modulate mitochondrial morphology (78). Like α-synuclein, PINK1 was recently found to also localize to MERCs, and its continuous degradation in healthy mitochondria is regulated by the interplay of mitochondria and the ER (79). It is worth noting that the PD-related proteins PINK1, Parkin, LRRK2, and α-synuclein that are involved in MERCs have also been shown to directly or indirectly interact with Miro1 (7, 11, 12, 21). Hence, impaired mitophagy and dysregulation of MERCs seems a shared feature in different cases of PD.

The relationship between Miro proteins and MERCs started to be investigated when, in 2011, two research groups identified Gem1p, the yeast ortholog of mammalian Miro1, as a crucial regulator of the ER-mitochondrial encounter structure (ERMES), a protein complex that tethers mitochondria and ER in yeast (15, 80). Association of Gem1p to ERMES controls phospholipid exchange for lipid biosynthesis between mitochondria and ER (15) and regulates mitochondrial division and morphology (81–83). The localization of dMiro at MERCs was also demonstrated

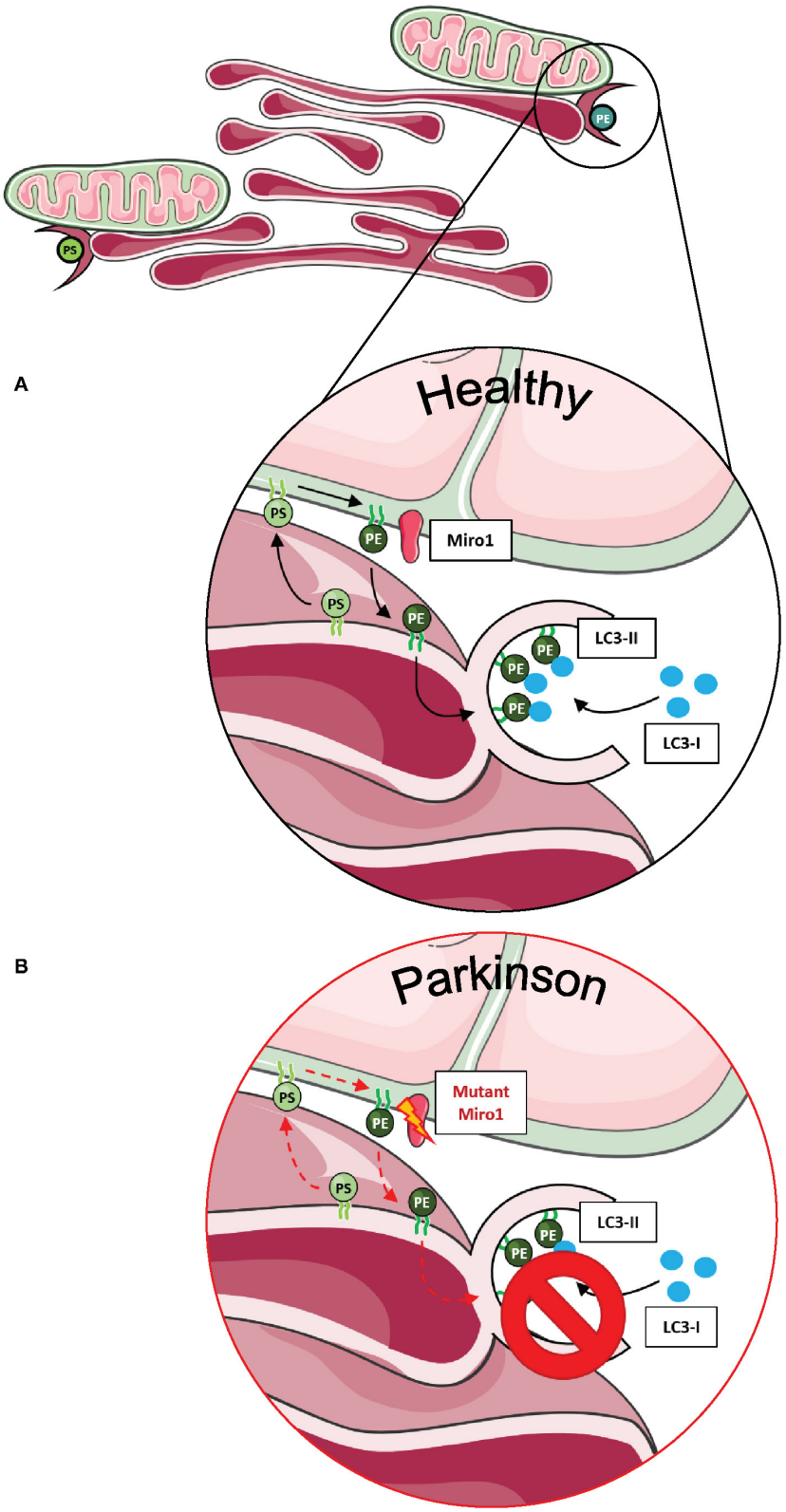

FIGURE 3 | Phospholipid synthesis and autophagosome formation at MERCs. **(A)** Phospholipids are synthesized in mitochondria and the ER, requiring the exchange of metabolites at MERCs. Phosphatidylserine (PS) is synthesized in the ER, shuttled to mitochondria via MERCs, where it is transferred into phosphatidylethanolamine

(Continued)

FIGURE 3 | (PE) and shuttled back into the ER. PE is necessary for the assembly of isolation membranes at the ER for the integration of cytosolic LC3-I into the autophagosome membrane, forming LC3-II. **(B)** A number of studies suggest that Miro1 is involved in phospholipid shuttling via MERCs. Disruption of Miro1 function might impair phospholipid synthesis, consequently interfering with the formation of autophagosomes. This figure was created using elements from Servier Medical Art, licensed under a Creative Common Attribution 3.0 Generic License (www.smart.servier.com).

in *Drosophila* neural stem cells and dopaminergic neurons (17, 84), as well as mammalian Miro1 in COS-7 cells, HeLa cells, MEFs, human fibroblasts, and human iPSC-derived neurons (14, 15, 67, 84, 85).

In human-derived cells, the contribution of Miro1 in lipid exchange and biosynthesis was confirmed by the discovery that patient-derived fibroblasts with PD-associated mutations in Miro1 displayed an altered formation of autophagosomes, which is dependent on the conversion of phosphatidylserine (PS) to phosphatidylethanolamine (PE) at MERCs (13, 14). In mammalian cells, PS is synthesized in the ER, transferred through the MERCs to the mitochondria, and transformed into PE (72). A fraction of the mitochondrial-generated PE is then shuttled back to the ER for the generation of isolation membranes, where PE is used for the lipidation of specific adaptor proteins that recruit autophagic cargoes (**Figure 3A**) (86, 87). In our studies, none of the Miro1-mutant fibroblast lines showed an increase in the amount of newly synthesized autophagosomes following starvation conditions (13, 14). In line with these results, all Miro1-mutant fibroblast lines showed an overall reduction in MERCs, suggesting that PD-associated Miro1 mutations disturb the formation of appositions between mitochondria and ER, affecting lipid exchange and, consequently, autophagy initiation (**Figure 3B**) (13, 14).

In contrast to our observations in patient-derived fibroblasts, Miro1-R272Q neurons showed an increased number of contacts between mitochondria and ER (67). Remarkably, only control neurons exhibited accumulation of the autophagic cargo protein p62 upon bafilomycin A1 treatment, but not Miro1-R272Q neurons (67). These results point toward a functional impairment of MERCs that may affect the initiation of autophagy in patient-derived neurons, possibly triggered by the pathogenic effect of mutant Miro1.

Importantly, two Miro1 interactor proteins, PINK1 and Parkin, were also shown to be involved in the organization and lipid-related function of MERCs (**Figure 4A**). Neurons derived from flies and patients carrying mutations in PINK1 and Parkin displayed increased amounts of MERCs and a disturbed exchange of the phospholipid PS, resulting in an impaired synthesis of dense core vesicles from the ER (**Figure 4B**) (88). Altogether, these findings argue in favor of an important role of Miro1 in lipid homeostasis at MERCs and an impairment of this function in conditions linked to neurodegeneration.

Other studies in metazoans also supported a key role of Miro in the regulation of MERCs. In *Drosophila* neural-derived cultures, Polo kinase-induced phosphorylation of dMiro enhances the localization of dMiro to MERCS and the interaction with calcium transporters to regulate calcium homeostasis and the integrity of the tethering complex (17, 84). Moreover, in our studies, we were able to observe a reduced co-localization of Miro1 with MERCs in Miro1-mutant fibroblasts from PD patients compared to control fibroblasts (14) and, conversely, an increased co-localization of Miro1 with MERCs in Miro1-R272Q iPSC-derived neurons (67), underscoring the importance of Miro1 localization to MERCs and a potential role in neurodegeneration.

As mentioned in the previous section, MERCs were recently shown to act as regulators of mitophagy initiation (**Figure 2A**). Coupled mitochondria and ER in human iPSC-derived dopaminergic neurons are untethered upon Parkin-mediated ubiquitination of MERC-residing proteins, such as Mfn2 and VDAC (63, 89, 90), as a starting point for mitochondrial clearance (69). Based on the evidence that targeting of Miro1 by the PINK1/Parkin pathway is required as an initial step for mitophagy (7, 9, 91), these studies provide strong evidence that PINK1/Parkin-mediated mitophagy is organized at MERCs and that Miro1 might be directly involved in that process. Indeed, fibroblasts obtained from PD patients harboring Miro1 mutations show significant alterations in mitophagy flux accompanied by dysregulation of the abundance of specific subtypes of MERCs, supporting the previous hypothesis (13, 14).

Moreover, based on the increased amount of overall MERCs and impaired CCCP-induced mitochondrial clearance observed in iPSC-derived Miro1-R272Q neurons, we speculate that damaged mitochondria may not uncouple from the ER, consequently hampering the initiation and flux of mitophagy (67).

In conclusion, the communication between mitochondria and ER is crucial to maintaining cellular homeostasis and is a potential investigation target of growing interest in neurodegenerative diseases, such as PD. Miro1 was demonstrated to be crucially involved in the regulation of the function of the MERCs; therefore, the study of this interaction between Miro1, mitochondria, and ER will help to better comprehend the complex pathogenicity of PD.

MIRO1 AS A REGULATOR OF CELLULAR CALCIUM HOMEOSTASIS

Calcium ions act as important second messengers that control several cellular mechanisms. Therefore, cytosolic calcium levels need to be tightly regulated, and cells manage to maintain calcium homeostasis mainly via buffering calcium by specific organelles, such as the ER and mitochondria (84, 92).

One of the main functions of Miro1 is to orchestrate calcium homeostasis in mitochondria and calcium-dependent mitochondrial positioning. To fulfill this function, calcium-binding is facilitated via both of its EF-hand domains (33, 93) and

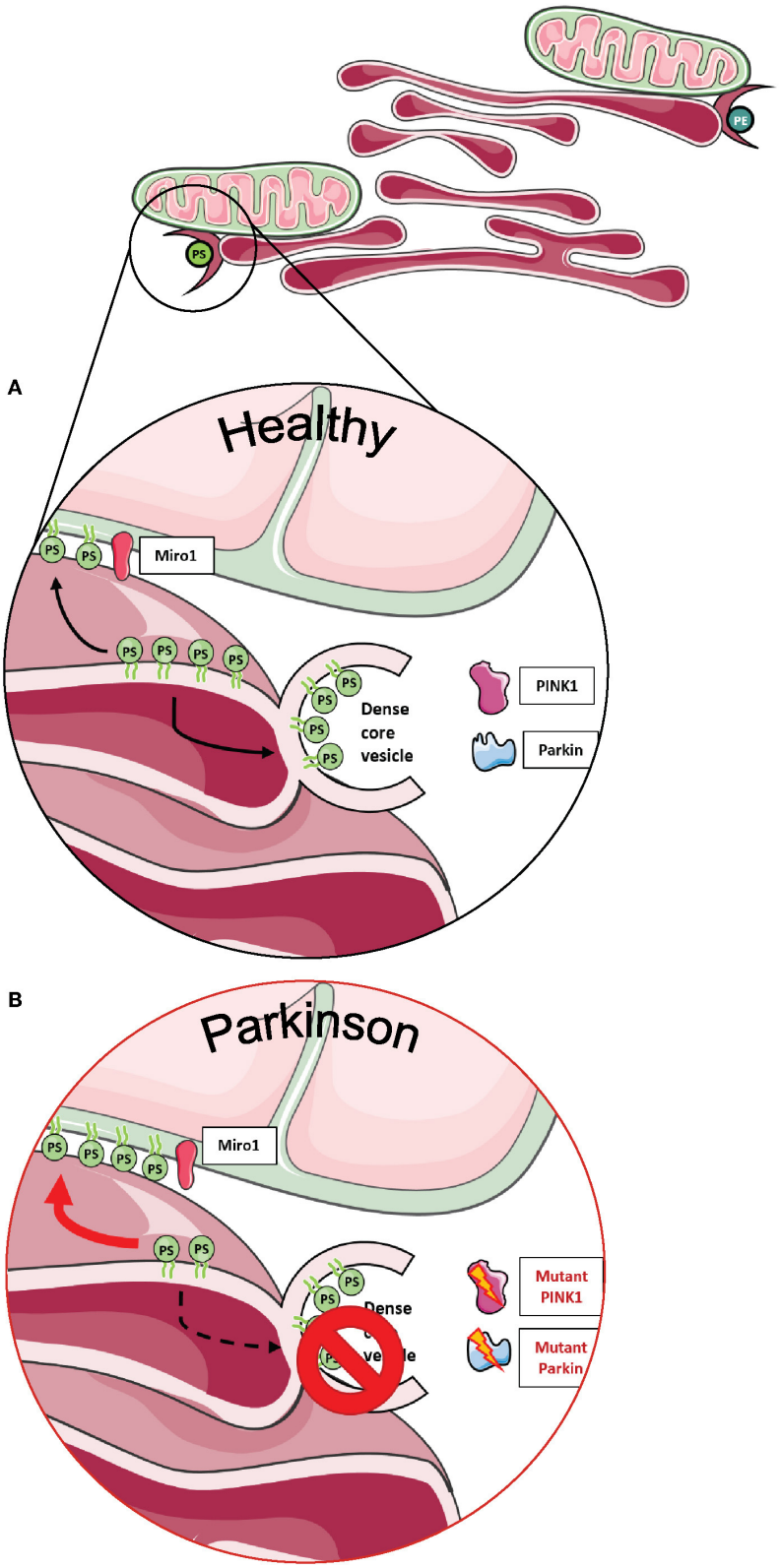

FIGURE 4 | Phospholipid synthesis and the formation of dense core vesicles at MERCs. **(A)** Phospholipids are required not only for the formation of autophagosomes, but PS is also required to provide membranes for dense core vesicles. **(B)** Fly neurons expressing mutant PINK1 or Parkin show impaired formation of dense core vesicles, resulting in alterations of neurotransmission. This figure was created using elements from Servier Medical Art, licensed under a Creative Common Attribution 3.0 Generic License (www.smart.servier.com).

the C-terminal GTPase domain (35, 42). Miro1 was suggested to have a high calcium-binding affinity (33) and consequently binds calcium only upon elevation of cytosolic calcium levels (3, 42, 94).

Interestingly, Chang et al. found in 2011 that intra-mitochondrial calcium levels correlated with mitochondrial transport speed, suggesting that mitochondrial transport was not only controlled by cytosolic calcium transients but also by mitochondrial matrix calcium levels (4). Furthermore, primary mouse neurons overexpressing Miro1 with calcium-insensitive EF-hand domains showed a decreased influx of calcium into the mitochondrial matrix, suggesting that Miro1 also regulates intra-mitochondrial calcium levels (4).

This finding was later supported by a study in primary fly neurons. Knockdown of dMiro caused a decreased histamine-induced calcium uptake in the mitochondrial matrix, while overexpression of dMiro led to increased calcium uptake (84). Lee et al. concluded that dMiro specifically promotes the flux of calcium from the ER to mitochondria and that this mechanism is independent of mitochondrial transport and intracellular distribution (**Figure 5A**) (84).

While the effect of intra-mitochondrial calcium levels on mitochondrial transport seems surprising at first glance, it is known that increased cytosolic calcium transients lead to an unavoidable influx of calcium into the mitochondrial matrix (4). The observed regulation of mitochondrial matrix calcium by Miro1 (4, 84) raised the question how a protein bound to the OMM and facing the cytosol can possibly regulate the influx of calcium into the matrix.

Uptake of calcium into mitochondria is facilitated by the mitochondrial calcium uniporter (MCU), a protein complex of several subunits residing in the inner mitochondrial membrane. Only in 2018, Niescier et al. revealed that the N-terminus of the MCU reaches through the mitochondrial intermembrane space and the outer membrane to directly interact with Miro1 (**Figures 5A,B**). This study finally solved the question how Miro1 residing in the outer membrane is able to regulate intra-mitochondrial calcium homeostasis (95).

Regulation of mitochondrial matrix calcium levels is important for mitochondrial energy production (96–98). Hence, loss-of-function mutations in Miro1 were suggested to affect mitochondrial energy production by disrupting the mitochondrial matrix calcium uptake (86). Indeed, the ATP production was decreased in brains of *Drosophila* larvae expressing the loss-of-function mutation dMiro B682 (84), in GemA (ortholog of Miro) knockout *Dictyostelium discoideum* (30), and in fibroblasts from patients carrying PD-associated Miro1 mutations (13). Together, these findings suggest that Miro1 plays a crucial role in the maintenance of mitochondrial function via regulation of mitochondrial calcium levels.

The importance of Miro1 for the maintenance of calcium homeostasis in the context of PD was highlighted in our recently published studies with PD patient-derived fibroblasts (13, 14). In these studies, we used thapsigargin, an inhibitor of the sarco-/ER calcium ATPase (99). When the ER calcium uptake was blocked by thapsigargin treatment: (i) calcium levels in the cytosol rose rapidly due to depletion of the ER calcium store (100), and (ii) calcium buffering relied on other mechanisms, i.e., mitochondrial calcium uptake. We found that buffering of cytosolic calcium after thapsigargin treatment was delayed in patient-derived fibroblasts harboring mutations in Miro1 (13, 14), suggesting that mitochondrial calcium buffering is impaired in Miro1-mutant fibroblasts. In addition, combined treatment of thapsigargin with the MCU inhibitor Ru360 (4, 101, 102) caused a reduction in cytosolic calcium buffering in the control fibroblast lines similarly to Miro1-mutant fibroblasts. These results confirmed that calcium buffering relies mostly on mitochondria when calcium uptake via the ER is blocked (13, 14).

Our studies also supported previous observations where mutations in the EF-hand domains of Miro1 caused an elevation of the frequency of calcium spikes and an increase in the time constant of calcium transients in primary rat astrocytes (103). A similar disruption of calcium homeostasis with increased frequency and amplitudes of calcium spikes was observed in rat hippocampal cultures with deletion of Miro1 EF-hand domains (Miro1-ΔEF) (104). In contrast, overexpression of wild-type Miro1 led to decreased thapsigargin-induced calcium spikes in primary fly neuron cultures (84).

Maintenance of calcium transients is important for the function of astrocytes and neurons. High levels of calcium enter the cell at active synapses and need to be buffered via mitochondria (103, 104). Impaired cellular calcium homeostasis is a shared phenotype observed in different models of PD (105–110). In line with this, iPSC-derived neurons with heterozygous Miro1-R272Q display a significantly higher peak of cytosolic calcium and delayed buffering capacity after ionomycin treatment compared to control neurons (67). Hence, one might speculate that mutations in Miro1 drive neurodegeneration by impairing calcium homeostasis, subsequently affecting mitochondrial function and energy production in the pathogenesis of PD. Indeed, *Drosophila* expressing loss-of-function mutations in the EF-hand domains of dMiro show a decreased neuronal survival because the impaired Miro-mediated calcium-dependent mitochondrial positioning affects calcium homeostasis and thereby increasing the susceptibility to glutamate excitotoxicity (3).

Another function of Miro1 is the regulation of mitochondrial dynamics in a calcium-dependent fashion. Glutamate application to primary rat neuronal cultures caused a reduction in mitochondrial length. However, these calcium-dependent changes in mitochondrial morphology were abolished in cells expressing Miro1-ΔEF (104). In 2018, Nemani et al. revealed that this Miro1-mediated calcium-dependent mitochondrial fragmentation was independent of the mitochondrial fission protein Drp1, the mitochondrial membrane potential, or the production of reactive oxygen species (ROS) and is an important prerequisite of mitophagy (94).

In our studies, PD patient-derived Miro1-mutant fibroblasts and iPSC-derived Miro1-R272Q neurons demonstrated an increased mitochondrial fragmentation after treatment compared to control cells. This finding was not surprising given the delayed buffering of calcium transients and resulting retained high levels of calcium in the cytosol (13, 14, 67).

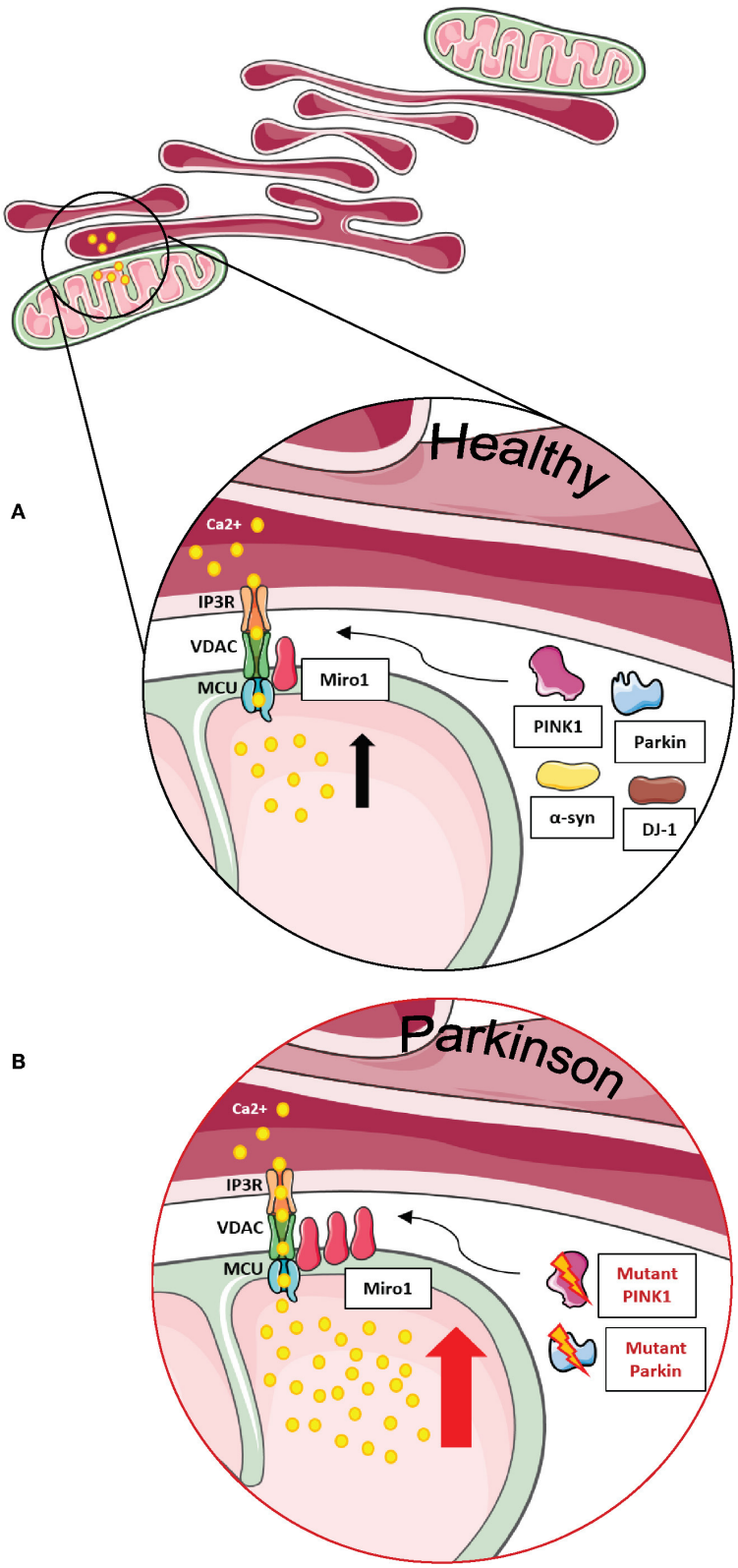

FIGURE 5 | Miro1 is involved in calcium regulation at MERCs. **(A)** Calcium homeostasis is tightly regulated. ER and mitochondria buffer cytosolic calcium transients and specialized subtypes of MERCs composed of IP3R, VDAC, MCU, and Miro1 are required for regulation of calcium uptake. Miro1 acts as sensor of cytosolic

(Continued)

FIGURE 5 | calcium levels, interacting directly with the MCU and orchestrating the mitochondrial calcium uptake at MERCs. PD-associated proteins PINK1, Parkin, α-synuclein, and DJ-1 participate in the regulation of calcium homeostasis at MERCs. **(B)** Impaired PINK1 or Parkin function leads to clustering of Miro1 and subsequent mitochondrial calcium overload that facilitates mitochondrial dysfunction and apoptosis. Additionally, impaired Miro1 function leads to disruption of cellular calcium homeostasis by alterations of mitochondrial calcium buffering. This figure was created using elements from Servier Medical Art, licensed under a Creative Common Attribution 3.0 Generic License (www.smart.servier.com).

Our findings imply that mutations in Miro1 cause an impairment of calcium homeostasis, resulting in decreased ATP production and increased calcium-dependent mitochondrial fragmentation, thereby contributing to the pathogenesis of PD.

MIRO1 AND ORGANELLAR MOVEMENT IN PARKINSON'S DISEASE

Mitochondrial Transport

Miro1 is a well-known adaptor for the mitochondrial transport machinery, forming a complex with the motor proteins dynein, kinesin, and myosin and thereby allowing mitochondrial movement along the cytoskeleton (2, 28, 37, 111, 112).

This function of Miro1 is especially crucial in neurons, as anterograde mitochondrial transport (from soma to synapses) is necessary to provide ATP and ensure calcium buffering at highly energy-demanding areas, such as synapses (113). An appropriate mitochondrial distribution is even more essential in dopaminergic neurons, because their pacemaking activity requires high-energy supply and makes them more vulnerable to excitotoxicity (113).

Retrograde mitochondrial movement is as well essential for the physiology of neurons *in vivo*, since lysosomal degradation of damaged mitochondria takes place mostly in the neuronal soma (113, 114).

Guo et al. first demonstrated the importance of dMiro for anterograde mitochondrial transport in neurons from *Drosophila* larvae (37). However, other studies reported that the expression of the null alleles B682 and SD32 within the first GTPase domain of dMiro, which cause the loss of the protein through its premature truncation, promoted a reduction in both anterograde and retrograde transport of mitochondria (111). Interestingly, the N-terminal GTPase domain of dMiro seems to be crucial for mitochondrial transport along axons and dendrites (38). In accordance, expression of the N-terminal GTPase loss-of-function mutation dMiroT25N led to premature death and aborted development of *Drosophila puparium*, a phenotype likely due to an accumulation of dysfunctional fragmented mitochondria in the soma of their sensory and motor neurons (38). Recently, inhibition of mitochondrial transport was linked to HDAC6-mediated deacetylation of the N-terminal GTPase domain of Miro1 in rodents (39). In addition, Miro1 knockout mice displayed a reduced number of mitochondria in distal dendrites, accompanied by a lower dendritic complexity and increased neuronal death (10). Of note, these mice are still expressing Miro2, suggesting that although both isoforms (Miro1 and Miro2) are involved in mitochondrial transport, they are not able to fully substitute each other (10).

From the molecular point of view, regulation of mitochondrial transport by mammalian Miro1 and Miro2 proteins occurs through the formation of a complex with the trafficking kinesin-binding proteins 1 and 2, so-called TRAK1 and TRAK2 (2, 115, 116). In particular, the building of the Miro/TRAK1/2 complex on the mitochondrial surface leads to the recruitment of the motor proteins kinesin and dynein for anterograde and retrograde transport, respectively (**Figure 6A**) (3, 117, 118).

However, the involvement of TRAK1 and TRAK2 differentially regulates mitochondrial transport. TRAK1 predominantly facilitates anterograde and retrograde movement in axons via interaction with kinesin or dynein, while TRAK2 is mostly found in dendrites binding to dynein and thus supporting retrograde movement (41, 119).

Mitochondrial transport is regulated by cytosolic calcium levels via the calcium sensor Miro1, and in 2009, two independent studies proposed different mechanisms of how calcium binding to Miro1 regulates mitochondrial transport. MacAskill et al. showed that Kif5 directly binds to Miro1 *in vitro* (93). Upon elevation of calcium levels, the EF-hand domains of Miro1 bind calcium, inducing a conformational shift and a decoupling of Miro1 and Kif5, as shown by co-immunoprecipitation in rat brain samples. Thus, the mitochondrial transport machinery is disassembled in order to derail mitochondria from the cytoskeleton (93).

In contrast, Wang and Schwarz found that kinesin is binding to Miro indirectly via Milton (*Drosophila* homolog of TRAK1/2) (3). Elevation of cytosolic calcium levels and the subsequent calcium binding to Miro allows a direct interaction of Kif5 with Miro, thereby detaching the whole transport machinery complex from the cytoskeleton and stopping mitochondrial transport in HEK cells and rat hippocampal cells. Hence, Kif5 was associated with the Miro/Milton complex on both moving and stationary mitochondria (3). This mechanism of calcium-dependent regulation of transport enables the fine-tuned arrest of mitochondria at sites of high-energy demand and cytosolic calcium levels, i.e., synapses (**Figure 6A**) (42, 103, 104).

Dysfunction of Miro1 causes alterations in mitochondrial transport. In rat hippocampal neurons, overexpression of Miro1 caused an increased recruitment of TRAK2 to the mitochondria, increasing the number of organelles transported to neuronal processes, while disruption of the Miro1-binding domain of TRAK2 led to mitochondrial transport arrest, showing a significant decrease in mitochondrial number in neuronal processes (93).

Miro1 is also known to interact with other PD-related proteins influencing mitochondrial transport in neurons. For example, wild-type LRRK2 and α-synuclein proteins were shown to bind to Miro1 on moving mitochondria, creating a complex

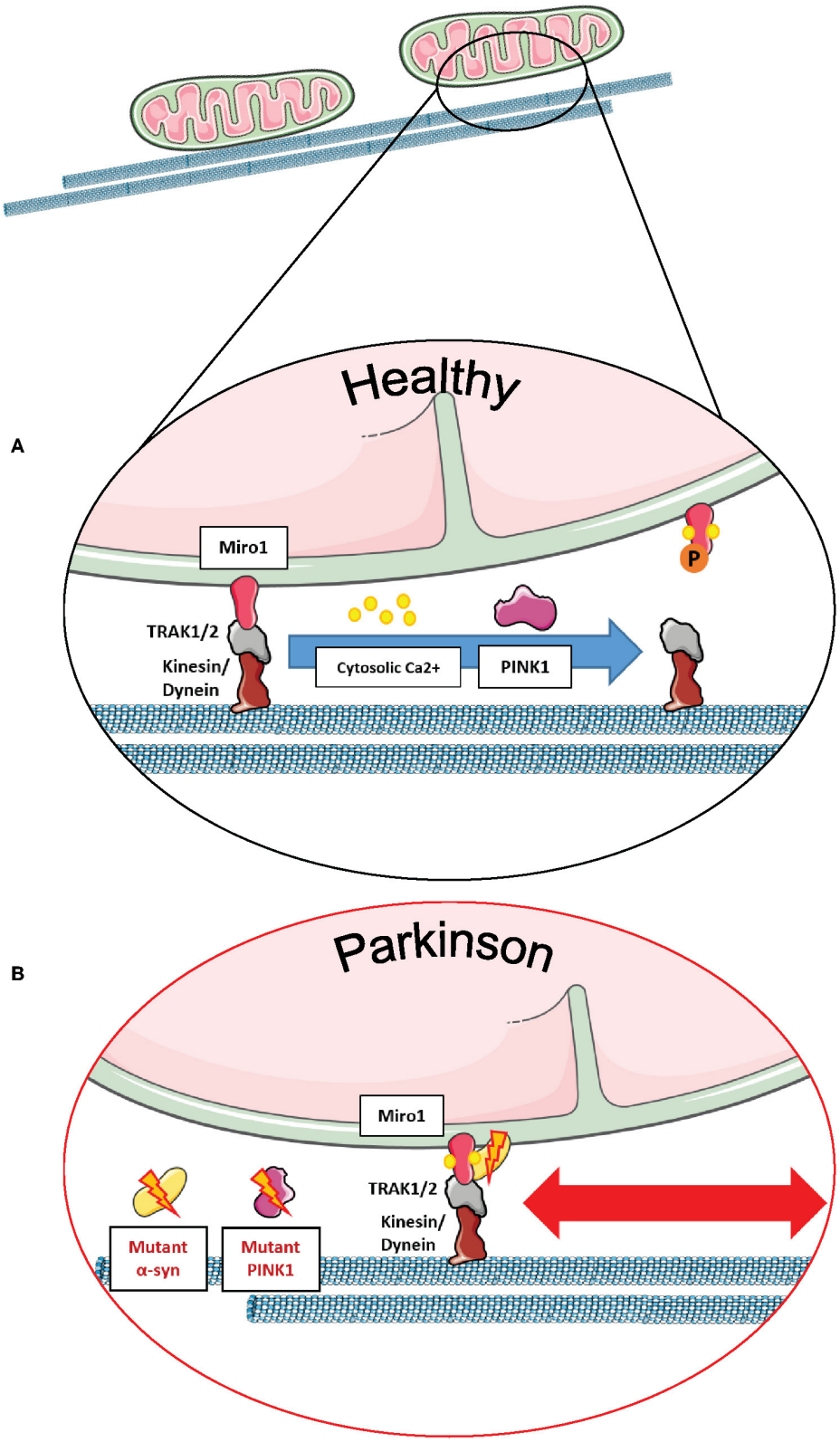

FIGURE 6 | Miro1 mediates calcium-dependent regulation of mitochondrial transport. **(A)** Miro1 is anchored to the outer mitochondrial membrane and links mitochondria to the motor proteins kinesin and dynein via interaction with TRAK1/2. Upon elevation of cytosolic calcium levels (i.e., at active synapses), calcium binds

(Continued)

FIGURE 6 | to the EF-hand domains of Miro1, leading to a conformational shift of Miro1 and a decoupling of mitochondria from the cytoskeleton. Thus, mitochondria are stopped at sites of high calcium levels, providing ATP and calcium buffering. PINK1/Parkin-mediated phosphorylation and ubiquitination of Miro1 and its subsequent proteasomal degradation also leads to arrest of mitochondrial transport, allowing lysosomal degradation of dysfunctional mitochondria. **(B)** Cells expressing PD-associated mutations of α-synuclein or PINK1 failed to remove Miro1 from the surface of impaired mitochondria, causing dysregulation of mitochondrial transport and delayed mitophagy. This figure was created using elements from Servier Medical Art, licensed under a Creative Common Attribution 3.0 Generic License (www.smart.servier.com).

that regulates the removal of Miro1 from the OMM and, therefore, promoting the detachment of mitochondria from the transport machinery (11, 12). Interestingly, the G2019S PD-associated mutation in LRRK2 disturbed this complex, inhibiting Miro1 removal from the transport machinery, thus delaying mitochondrial arrest in PD patient-derived fibroblasts and neurons (11). Moreover, the overexpression of wild-type α-synuclein and/or the PD-associated A53T mutation led to the stabilization of the α-synuclein-Miro1 complex in PD flies and human iPSC-derived neurons, preventing mitochondria to detach from the transport machinery and subsequently leading to a delayed mitochondrial arrest (**Figure 6B**) (12).

Furthermore, the PD-related protein PINK1 was also identified as an interaction partner of Miro1 in human neuroblastoma cells and primary fly neurons for the trafficking of mitochondria, and the loss of PINK1 led to aberrations in mitochondrial morphology and dynamics (7, 65). In addition, PD-associated PINK1 deletions promoted the movement of mitochondria via the stabilization of dMiro (**Figure 6B**), consequently leading to synaptic overgrowth and death of *Drosophila* dopaminergic neurons (21). Liu et al. showed in *Drosophila* muscle and dopaminergic neurons that downregulating dMiro could rescue mitochondrial transport and distribution defects observed in mutant PINK1 flies, whereas overexpressing dMiro alone led to mitochondrial enlargement and dopaminergic neuronal death (9).

Intercellular Mitochondrial Transfer

Converging evidence supports the notion that mitochondria can be transferred between mammalian cells, in order to replace damaged organelles and prevent death of the recipient cell. There are different approaches to analyze the transfer of mitochondria between cells in co-cultures. One way is to label mitochondria of donor cells and recipient cells in red or green, respectively, allowing the detection of cells with mixed mitochondria after co-culture (120). Another approach is to label only the mitochondria from the donor cells in order to detect their transfer into recipient cells labeled with GFP, phalloidin, or cell tracker dyes (121–124).

Since the first observation of this phenomenon in human stem cells (125), intercellular transfer of mitochondria was also noticed between healthy and cancer cells (126–128) and, more relevant to neurodegeneration, between astrocytes and neurons. In particular, by using co-culture experiments, Hayakawa et al. demonstrated that transfer of mitochondria from astrocytes to neurons improved mitochondrial function of the latter, resulting in increased neuronal recovery and survival after stroke (129). The molecular mechanisms ensuring intercellular mitochondrial transfer between neuronal cell types have not been fully elucidated yet; either the selective formation of tunneling nanotubes (TNT), the establishment of gap junctions, or the release of extracellular microvesicles containing mitochondria have been observed in different non-neuronal models (126, 128, 130, 131).

Despite the fact that the last stage of the transfer is still being debated, it is widely accepted that intercellular mitochondria donation requires a fully functional mitochondrial transport machinery. In light of its fundamental role in regulating mitochondrial movement along microtubules, a strong body of evidence indicates that Miro1 also plays a key role in mitochondrial transfer between different cell types, including non-neuronal cells (120–123). For instance, inhibition of mitochondrial complex I activity by rotenone treatment significantly decreased Miro1 protein levels in mesenchymal stem cells (MSCs), leading to impaired transfer of mRFP-labeled mitochondria to recipient primary mouse epithelial cells containing mGFP-labeled mitochondria. Consequently, Miro1-depleted MSCs displayed reduced donor activity compared to control cells, a phenotype specifically linked to impaired mitochondrial movement along microtubules (120).

Importantly, Gao et al. recently demonstrated that Miro1, as well as Miro2, participates in the transfer of mitochondria between brain cells, as displayed by a reduced mitochondrial transfer efficiency from neurons expressing mito-DsRed to GFP-labeled astrocytes upon shRNA-mediated Miro1 or Miro2 downregulation. Conversely, mitochondrial transfer increased when Miro1 or Miro2 were ectopically expressed (124).

Since mitochondrial transfer is activated by loss of respiratory function in recipient cells, the presence of functional Miro1 in donor cells is crucial to enhance mitochondrial transfer capacity and rescue mitochondrial dysfunction in injured cells. This mechanism is extremely important for many neurodegenerative diseases including PD, as it may represent a key neuroprotective approach in stem cell-based regenerative medicine. At the same time, the transfer of damaged mitochondria between different cell types may also trigger the spread of PD pathology to other brain regions and therefore needs to be taken into account for the design of targeted therapies (132).

Peroxisomal Transport

Until recently, Miro1 was described as an entirely mitochondrial protein (27, 28, 133). However, in 2017 Costello et al. revealed that Miro1 was also localized to peroxisomes in COS-7 cells (22). The peroxisomal receptor/chaperone PEX19 was found to be necessary for the integration of Miro1 into the peroxisomal membrane (23). Recent findings suggest that the N-terminal GTPase domain regulates the direct interaction of the transmembrane domain of Miro with Pex19 (134).

In 2018, Okumoto et al. showed that the localization of Miro1 to mitochondria or peroxisomes depends on the alternative splicing of exons 19 and 20. The resulting different insertions between the C-terminal GTPase domain and the transmembrane domain determine the organelle-targeting specificity of Miro1. Variant-1 of Miro1 does not contain either the exon 19 or the exon 20 and localizes exclusively to mitochondria. Variant-3 contains exon 20 and is likewise found only on mitochondria. In contrast, variant-2 contains exon 19 and localizes partially to peroxisomes, whereas variant-4 containing both exons 19 and 20 is localized mostly to peroxisomes and to a minor extent to mitochondria (24).

In human cancer cells, Miro1 variants−1 and−2 were predominantly expressed, while variants−3 and−4 showed low expression levels of 10% compared to variants−1 and−2 (24). However, in contrast to this study, Covill-Cooke et al. recently showed that Miro1 variants lacking exon 19 as well as Miro2 are able to localize to peroxisomes in MEFs (134).

Initially, the study of Castro et al. suggested the main function of Miro1 in the regulation of peroxisomal transport and transport-dependent peroxisomal proliferation in fibroblasts (23). Nevertheless, the role of Miro in peroxisomal movement was questioned later. The knockout of Miro1 or Miro2 or a double knockout of both proteins did not reveal any effect on long-range microtubule-dependent peroxisome transport in MEFs (134). Interestingly, knockout of Miro2 revealed a significant reduction in median net displacement of peroxisomes in MEFs. This short-range peroxisomal movement was independent of the integrity of the actin and microtubule cytoskeleton but followed the oscillating movements of the ER, suggesting that Miro might regulate short-range peroxisome transport via the interaction with the ER (134).

While the results of the study by Covill-Cooke suggest that the main function of Miro at peroxisomes is independent of transport, their study demonstrated a major impact of Miro on peroxisome size and number. Double knockout of Miro1 and Miro2 in MEFs caused a significant reduction in peroxisome size, accompanied by increase in peroxisome number (134). This phenotype is likely caused by an increased interaction of the fission proteins Drp1 and Fis1 at peroxisomes, indicating that Miro proteins regulate Fis1-/Drp1-dependent fission not only of mitochondria (135) but also of peroxisomes (134).

Of note, the single knockout of Miro1 or Miro2 had no effect on peroxisome size or number, while overexpression of Miro1, but not Miro2, caused an increase in peroxisome size. This result suggests that peroxisome morphology is mainly regulated by Miro1, and Miro2 has the ability to compensate for Miro1 impairment in peroxisomes (134). This is interesting because other studies demonstrated that Miro2 was not able to compensate for the lack of Miro1 on mitochondrial level in murine brains (10, 136). Future investigations will be necessary to uncover the differential functions of Miro1 and Miro2 in mitochondria and peroxisomes and their impact in neurodegeneration. Peroxisomes are critically involved in lipid metabolism and defense against ROS (137, 138). The physical link to mitochondria and the ER is important for peroxisomal proliferation and function (139, 140). Given the crucial roles of Miro1 at mitochondria and MERCs, further investigations are needed to elucidate Miro1 functions outside of mitochondria.

To date, peroxisomal dysfunction in the pathogenesis of neurodegenerative diseases like PD is not well understood. A previous study showed a reduction in plasmalogen levels in blood plasma of PD patients (25). Plasmalogens are phospholipids synthesized in peroxisomes, which are involved in the defense against ROS. Interestingly, mice deficient in the peroxisomal proteins Pex2, Pex5, or Pex13 showed an elevation of α-synuclein oligomers and α-synuclein phosphorylation in brain tissue. The observed α-synuclein aggregation correlated with changes of peroxisomal lipid synthesis instead of being associated with mitochondrial dysfunction or oxidative stress (26).

The calcium handling function of peroxisomes is largely unknown. Previous studies showed that increased cytosolic calcium concentrations lead to an elevation of peroxisome calcium levels, suggesting that peroxisomes might play a role in calcium homeostasis (141). The newly identified role of Miro1 as adaptor for peroxisomal transport, together with the known function of Miro1 in calcium homeostasis, raises the question whether Miro1 is also involved in peroxisomal calcium handling. Furthermore, it remains to be investigated how calcium transients regulate Miro1-mediated peroxisomal transport and distribution and how this would influence peroxisomal function in the healthy state and in the context of PD.

OUTLOOK

The emerging role of Miro GTPases in brain health and disease provides unique opportunities for a better understanding of neuronal homeostasis and indicates these proteins as potential therapeutic targets and entry-points for precision medicine. Especially from the perspective of neurodegeneration, the roles of Miro1 as an adaptor for mitochondrial transport and as a PINK1/Parkin-mediated mitophagy substrate are of high relevance in the context of brain disorders, in particular for PD. In this review, we showed that Miro1 is not only a crucial component of the mitochondrial transport machinery and mitochondrial quality control, but it is also an important regulator of mitochondrial and cytosolic calcium homeostasis, mitochondria and ER interface, and peroxisomal dynamics. Based on a variety of *in vitro*, *ex vivo*, and *in vivo* studies performed in yeast, animal, and human models, Miro GTPases stand no longer as exclusive mitochondrial proteins, but their recently discovered key functions further extend their physiological role to other organelles and cellular compartments.

Based on genetic studies, a direct link of Miro1 to neurodegeneration in PD was established. Together with the fact that Miro1 physically and functionally interacts with a number of PD-related proteins, Miro1 has recently been proposed both as a molecular signature in PD and as a therapeutic target, which could be used as a biomarker for the diagnosis and treatment of PD (66). Hsieh et al. were able to rescue impaired mitophagy and neuronal cell death by pharmacologically removing excess Miro1. Treatment with the compound called "Miro1 reducer" in combination with CCCP lead to Miro1 degradation and

induction of mitophagy in fibroblasts derived from PD patients. Additionally, iPSC-derived neurons from PD patients displayed significant death after induction of oxidative stress via antimycin, while control neurons did not show cell death under these conditions. Remarkably, treatment with the "Miro1 reducer" rescued iPSC-derived neurons from PD patients under antimycin stress, thereby demonstrating that the removal of excess Miro1 is neuroprotective (66).

Another possible approach for pharmacological intervention was demonstrated by Lee et al. in 2016. This study revealed that the recruitment of Miro1 to MERCs depends on the phosphorylation of the N-terminal GTPase domain by Polo kinase, thereby critically regulating mitochondrial calcium uptake and mitochondrial energy production (84). Specific inhibition of Polo kinase with BI2536 reduced the localization of Miro1 to MERCs and also caused a destabilization of MERCs (84). This finding is especially interesting in the light of increased numbers of MERCs and enhanced localization of Miro1 to MERCs observed in iPSC-derived Miro1-R272Q neurons (67). Thus, pharmacologically targeting regulators of Miro1 function such as Polo kinase offers another promising approach for personalized medicine but also bears the risk of unwanted side effects.

Future studies should focus on the impact of Miro1 on neuronal homeostasis, and the establishment of screening campaigns on cellular phenotypes in patient-based cellular models should be performed to rescue impaired Miro1 function. Identified compounds may be applicable to patients beyond monogenic PD, as impaired Miro1 function was also identified in sporadic PD (11, 12, 66). Further applications beyond PD may be also considered, as functional associations between Miro1 and key proteins causative of other neurodegenerative diseases, such as Alzheimer's disease (142, 143), amyotrophic lateral sclerosis (144, 145), and Charcot–Marie–Tooth disease (146), were discovered during the past years.

AUTHOR CONTRIBUTIONS

DG and RK designed and organized the structure of the review. DG, CB-E, AC, and GA developed the writing of the original review draft. DG, CB-E, GA, and RK performed the revision and editing of the original draft. DG, CB-E, AC, and GA developed all the literature research for the writing of this review. Finally, CB-E performed the figures contained in the review.

FUNDING

The current work was supported by the Fonds National de Recherche (FNR) within the PEARL Excellence Programme [FNR/P13/6682797] to RK, the PARK-QC DTU (PRIDE17/12244779/PARK-QC), and the MiRisk project (C17/BM/11676395).

ACKNOWLEDGMENTS

Work of RK was supported by the following projects: MotaSYN (12719684), MAMaSyn, the Michael J. Fox Foundation, and the European Union's Horizon2020 research and innovation program (WIDESPREAD; CENTRE-PD; grant agreement no. 692320).

REFERENCES

1. Wolff AM, Petersen JG, Nilsson-Tillgren T, Din N. The open reading frame YAL048c affects the secretion of proteinase A in *S. cerevisiae*. *Yeast*. (1999) 15:427–34. doi: 10.1002/(SICI)1097-0061(19990330)15:5<427:AID-YEA362>3.0.CO;2-5
2. MacAskill AF, Brickley K, Stephenson FA, Kittler JT. GTPase dependent recruitment of Grif-1 by Miro1 regulates mitochondrial trafficking in hippocampal neurons. *Mol Cell Neurosci*. (2009) 40:301–12. doi: 10.1016/j.mcn.2008.10.016
3. Wang X, Schwarz TL. The mechanism of Ca2+-dependent regulation of kinesin-mediated mitochondrial motility. *Cell*. (2009) 136:163–74. doi: 10.1016/j.cell.2008.11.046
4. Chang KT, Niescier RF, Min KT. Mitochondrial matrix Ca2+ as an intrinsic signal regulating mitochondrial motility in axons. *Proc Natl Acad Sci USA*. (2011) 108:15456–61. doi: 10.1073/pnas.1106862108
5. Narendra D, Tanaka A, Suen DF, Youle RJ. Parkin is recruited selectively to impaired mitochondria and promotes their autophagy. *J Cell Biol*. (2008) 183:795–803. doi: 10.1083/jcb.200809125
6. Narendra DP, Jin SM, Tanaka A, Suen DF, Gautier CA, Shen J, et al. PINK1 is selectively stabilized on impaired mitochondria to activate Parkin. *PLoS Biol*. (2010) 8:e1000298. doi: 10.1371/journal.pbio.1000298
7. Wang X, Winter D, Ashrafi G, Schlehe J, Wong YL, Selkoe D, et al. PINK1 and Parkin target miro for phosphorylation and degradation to arrest mitochondrial motility. *Cell*. (2011) 147:893–906. doi: 10.1016/j.cell.2011.10.018
8. Birsa N, Norkett R, Wauer T, Mevissen TET, Wu HC, Foltynie T, et al. Lysine 27 ubiquitination of the mitochondrial transport protein Miro is dependent on serine 65 of the Parkin ubiquitin ligase. *J Biol Chem*. (2014) 289:14569–82. doi: 10.1074/jbc.M114.563031
9. Liu S, Sawada T, Lee S, Yu W, Silverio G, Alapatt P, et al. Parkinson's disease-associated kinase PINK1 regulates miro protein level and axonal transport of mitochondria. *PLoS Genet*. (2012) 8:15–7. doi: 10.1371/journal.pgen.1002537
10. López-Doménech G, Higgs NF, Vaccaro V, Roš H, Arancibia-Cárcamo IL, MacAskill AF, et al. Loss of dendritic complexity precedes neurodegeneration in a mouse model with disrupted mitochondrial distribution in mature dendrites. *Cell Rep*. (2016) 17:317–27. doi: 10.1016/j.celrep.2016.09.004
11. Hsieh CH, Shaltouki A, Gonzalez AE, Bettencourt da Cruz A, Burbulla LF, St. Lawrence E, et al. Functional impairment in Miro degradation and mitophagy is a shared feature in familial and sporadic Parkinson's disease. *Cell Stem Cell*. (2016) 19:709–24. doi: 10.1016/j.stem.2016.08.002
12. Shaltouki A, Hsieh CH, Kim MJ, Wang X. Alpha-synuclein delays mitophagy and targeting Miro rescues neuron loss in Parkinson's models. *Acta Neuropathol*. (2018) 136:607–20. doi: 10.1007/s00401-018-1873-4
13. Grossmann D, Berenguer-Escuder C, Bellet ME, Scheibner D, Bohler J, Massart F, et al. Mutations in RHOT1 disrupt endoplasmic reticulum-mitochondria contact sites interfering with calcium homeostasis and mitochondrial dynamics in Parkinson's disease. *Antioxid Redox Signal*. (2019) 31:1213–34. doi: 10.1089/ars.2018.7718
14. Berenguer-Escuder C, Grossmann D, Massart F, Antony P, Burbulla LF, Glaab E, et al. Variants in Miro1 cause alterations of ER-mitochondria contact sites in fibroblasts from Parkinson's disease patients. *J Clin Med*. (2019) 8:E2226. doi: 10.3390/jcm8122226
15. Kornmann B, Osman C, Walter P. The conserved GTPase Gem1 regulates endoplasmic reticulum-mitochondria connections. *Proc Natl Acad Sci USA*. (2011) 10:14151–6. doi: 10.1073/pnas.1111314108

16. Kornmann B, Currie E, Collins SR, Schuldiner M, Nunnari J, Weissman JS, et al. An ER-mitochondria tethering complex revealed by a synthetic biology screen. *Science.* (2009) 325:477–81. doi: 10.1126/science.1175088
17. Lee KS, Huh S, Lee S, Wu Z, Kim AK, Kang HY, et al. Altered ER–mitochondria contact impacts mitochondria calcium homeostasis and contributes to neurodegeneration in vivo in disease models. *Proc Natl Acad Sci USA.* (2018) 115:E8844–E8853. doi: 10.1073/pnas.1721136115
18. Cal,ì T, Ottolini D, Negro A, Brini M. Enhanced parkin levels favor ER-mitochondria cross talk and guarantee Ca(2+) transfer to sustain cell bioenergetics. *Biochim Biophys Acta.* (2013) 1832:495–508. doi: 10.1016/j.bbadis.2013.01.004
19. Basso V, Marchesan E, Peggion C, Chakraborty J, von Stockum S, Giacomello M, et al. Regulation of ER-mitochondria contacts by Parkin via Mfn2. *Pharmacol Res.* (2018) 138:43–56. doi: 10.1016/j.phrs.2018.09.006
20. Cal,ì T, Ottolini D, Vicario M, Catoni C, Vallese F, Cieri D, et al. splitGFP technology reveals dose-dependent ER-mitochondria interface modulation by α-Synuclein A53T and A30P mutants. *Cells.* (2019) 8:E1072. doi: 10.3390/cells8091072
21. Tsai PI, Course MM, Lovas JR, Hsieh CH, Babic M, Zinsmaier KE, et al. PINK1-mediated phosphorylation of Miro inhibits synaptic growth and protects dopaminergic neurons in Drosophila. *Sci Rep.* (2014) 4:6962. doi: 10.1038/srep06962
22. Costello JL, Castro IG, Camões F, Schrader TA, McNeall D, Yang J, et al. Predicting the targeting of tail-anchored proteins to subcellular compartments in mammalian cells. *J Cell Sci.* (2017) 130:1675–87. doi: 10.1242/jcs.200204
23. Castro IG, Richards DM, Metz J, Costello JL, Passmore JB, Schrader TA, et al. A role for Mitochondrial Rho GTPase 1. (MIRO1). in motility and membrane dynamics of peroxisomes. *Traffic.* (2018) 19:229–42. doi: 10.1111/tra.12549
24. Okumoto K, Ono T, Toyama R, Shimomura A, Nagata A, Fujiki Y. New splicing variants of mitochondrial Rho GTPase-1. (Miro1). transport peroxisomes. *J Cell Biol.* (2018) 217:619–33. doi: 10.1083/jcb.201708122
25. Dragonas C, Bertsch T, Sieber CC, Brosche T. Plasmalogens as a marker of elevated systemic oxidative stress in Parkinson's disease. *Clin Chem Lab Med.* (2009) 47:894–7. doi: 10.1515/CCLM.2009.205
26. Yakunin E, Moser A, Loeb V, Saada A, Faust P, Crane DI, et al. Alpha-synuclein abnormalities in mouse models of peroxisome biogenesis disorders. *J Neurosci Res.* (2010) 88:1–19. doi: 10.1002/jnr.22246
27. Fransson A, Ruusala A, Aspenström P. Atypical Rho GTPases have roles in mitochondrial homeostasis and apoptosis. *J Biol Chem.* (2003) 278:6495–502. doi: 10.1074/jbc.M208609200
28. Fransson S, Ruusala A, Aspenström P. The atypical Rho GTPases Miro-1 and Miro-2 have essential roles in mitochondrial trafficking. *Biochem Biophys Res Commun.* (2006) 344:500–10. doi: 10.1016/j.bbrc.2006.03.163
29. Wennerberg K. The Ras superfamily at a glance. *J Cell Sci.* (2005) 118:843–6. doi: 10.1242/jcs.01660
30. Vlahou G, Eli,áš M, von Kleist-Retzow JC, Wiesner RJ, Rivero F. The Ras related GTPase Miro is not required for mitochondrial transport in Dictyostelium discoideum. *Eur J Cell Biol.* (2010) 90:342–55. doi: 10.1016/j.ejcb.2010.10.012
31. Colicelli J. Human RAS superfamily proteins and related GTPases. *Sci STKE.* (2004) 2004:RE13. doi: 10.1126/stke.2502004re13
32. Boureux A, Vignal E, Faure S, Fort P. Evolution of the rho family of ras-like GTPases in eukaryotes. *Mol Biol Evol.* (2007) 24:203–16. doi: 10.1093/molbev/msl145
33. Koshiba T, Holman HA, Kubara K, Yasukawa K, Kawabata S, Okamoto K, et al. Structure-function analysis of the yeast mitochondrial Rho GTPase, Gem1p: implications for mitochondrial inheritance. *J Biol Chem.* (2011) 286:354–62. doi: 10.1074/jbc.M110.180034
34. Smith KP, Focia PJ, Chakravarthy S, Landahl EC, Klosowiak JL, Rice SE, et al. Structural assembly of the human Miro1/2 GTPases based on the crystal structure of the N-Terminal GTPase domain. *bioRxiv.* (2019) doi: 10.1101/729251
35. Klosowiak JL, Focia PJ, Chakravarthy S, Landahl EC, Freymann DM, Rice SE. Structural coupling of the EF hand and C-Terminal GTPase domains in the mitochondrial protein Miro. *EMBO Rep.* (2013) 14:968–74. doi: 10.1038/embor.2013.151
36. Klosowiak JL, Park S, Smith KP, French ME, Focia PJ, Freymann DM, et al. Structural insights into Parkin substrate lysine targeting from minimal Miro substrates. *Sci Rep.* (2016) 6:1–13. doi: 10.1038/srep33019
37. Guo X, Macleod GT, Wellington A, Hu F, Panchumarthi S, Schoenfield M, et al. The GTPase dMiro is required for axonal transport of mitochondria to Drosophila synapses. *Neuron.* (2005) 47:379–93. doi: 10.1016/j.neuron.2005.06.027
38. Babic M, Russo GJ, Wellington AJ, Sangston RM, Gonzalez M, Zinsmaier KE. Miro's N-Terminal GTPase domain is required for transport of mitochondria into axons and dendrites. *J Neurosci.* (2015) 35:5754–71. doi: 10.1523/JNEUROSCI.1035-14.2015
39. Kalinski AL, Kar AN, Craver J, Tosolini AP, Sleigh JN, Lee SJ, et al. Deacetylation of Miro1 by HDAC6 blocks mitochondrial transport and mediates axon growth inhibition. *J Cell Biol.* (2019) 218:1871–90. doi: 10.1083/jcb.201702187
40. Peters D, Kay L, Eswaran J, Lakey J, Soundararajan M. Human Miro proteins act as NTP hydrolases through a novel, non-canonical catalytic mechanism. *Int J Mol Sci.* (2018) 19:3839. doi: 10.3390/ijms19123839
41. Kay L, Pienaar IS, Cooray R, Black G, Soundararajan M. Understanding miro GTPases: implications in the treatment of neurodegenerative disorders. *Mol Neurobiol.* (2018) 55:7352–65. doi: 10.1007/s12035-018-0927-x
42. Saotome M, Safiulina D, Szabadkai G, Das S, Fransson A, Aspenstrom P, et al. Bidirectional Ca2+-dependent control of mitochondrial dynamics by the Miro GTPase. *Proc Natl Acad Sci USA.* (2008) 105:20728–33. doi: 10.1073/pnas.0808953105
43. Hoeflich KP, Ikura M. Calmodulin in action: diversity in target recognition and activation mechanisms. *Cell.* (2002) 108:739–42. doi: 10.1016/S0092-8674(02)0682-7
44. Gifford JL, Walsh MP, Vogel HJ. Structures and metal-ion-binding properties of the Ca2+-binding helix–loop–helix EF-hand motifs. *Biochem J.* (2007) 405:199–221. doi: 10.1042/BJ20070255
45. Karbowski M, Youle RJ. Dynamics of mitochondrial morphology in healthy cells and during apoptosis. *Cell Death Differ.* (2003) 10:870–80. doi: 10.1038/sj.cdd.4401260
46. Franco-Iborra S, Vila M, Perier C. The Parkinson disease mitochondrial hypothesis: where are we at? *Neuroscientist.* (2016) 22:266–77. doi: 10.1177/1073858415574600
47. Saxton WM, Hollenbeck PJ. The axonal transport of mitochondria. *J Cell Sci.* (2005) 118:5411–9. doi: 10.1242/jcs.053850
48. Yellen G. Fueling thought: management of glycolysis and oxidative phosphorylation in neuronal metabolism. *J Cell Biol.* (2018) 217:2235–46. doi: 10.1083/jcb.201803152
49. Van Laar VS, Berman SB. Mitochondrial dynamics in Parkinson's disease. *Exp Neurol.* (2009) 218:247–56. doi: 10.1016/j.expneurol.2009.03.019
50. Larsen SB, Hanss Z, Krüger R. The genetic architecture of mitochondrial dysfunction in Parkinson's disease. *Cell Tissue Res.* (2018) 373:21–37. doi: 10.1007/s00441-017-2768-8
51. Grünewald A, Kumar KR, Sue CM. New insights into the complex role of mitochondria in Parkinson's disease. *Prog Neurobiol.* (2019) 177:73–93. doi: 10.1016/j.pneurobio.2018.09.003
52. van der Merwe C, Jalali Sefid Dashti Z, Christoffels A, Loos B, Bardien S. Evidence for a common biological pathway linking three Parkinson's disease-causing genes: parkin, PINK1 and DJ-1. *Eur J Neurosci.* (2015) 41:1113–25. doi: 10.1111/ejn.12872
53. Kane LA, Youle RJ. PINK1 and Parkin flag miro to direct mitochondrial traffic. *Cell.* (2011) 147:721–723. doi: 10.1016/j.cell.2011.10.028
54. Anvret A, Ran C, Westerlund M, Sydow O, Willows T, Olson L, et al. Genetic screening of the mitochondrial Rho GTPases MIRO1 and MIRO2 in Parkinson's disease. *Open Neurol J.* (2012) 6:1–5. doi: 10.2174/1874205X01206010001
55. Blauwendraat C, Heilbron K, Vallerga CL, Bandres-Ciga S, von Coelln R, Pihlstrøm L, et al. Parkinson's disease age at onset genome-wide association study: Defining heritability, genetic loci, and α-synuclein mechanisms. *Mov Disord.* (2019) 34:866–75. doi: 10.1002/mds.27659
56. Nalls MA, Blauwendraat C, Vallerga CL, Heilbron K, Bandres-Ciga S, Chang D, et al. Identification of novel risk loci, causal insights, and heritable risk for Parkinson's disease: a meta-analysis of genome-wide association

studies. *Lancet Neurol.* (2019) 18:1091–102. doi: 10.1016/S1474-4422(19)30320-5
57. Saeed M. Genomic convergence of locus-based GWAS meta-analysis identifies AXIN1 as a novel Parkinson's gene. *Immunogenetics.* (2018) 70:563–70. doi: 10.1007/s00251-018-1068-0
58. Twig G, Hyde B, Shirihai OS. Mitochondrial fusion, fission and autophagy as a quality control axis: the bioenergetic view. *Biochim Biophys Acta.* (2008) 1777:1092–7. doi: 10.1016/j.bbabio.2008.05.001
59. Mishra P, Chan DC. Mitochondrial dynamics and inheritance during cell division, development and disease. *Nat Rev Mol Cell Biol.* (2014) 15:634–46. doi: 10.1038/nrm3877
60. Van Laar VS, Berman SB. The interplay of neuronal mitochondrial dynamics and bioenergetics: Implications for Parkinson's disease. *Neurobiol Dis.* (2013) 51:43–55. doi: 10.1016/j.nbd.2012.05.015
61. Kocaturk NM, Gozuacik D. Cross talk between mammalian autophagy and the ubiquitin-proteasome system. *Front Cell Dev Biol.* (2018) 6:1–27. doi: 10.3389/fcell.2018.00128
62. Bayne AN, Trempe JF. Mechanisms of PINK1, ubiquitin and Parkin interactions in mitochondrial quality control and beyond. *Cell Mol Life Sci.* (2019) 76:4589–611. doi: 10.1007/s00018-019-03203-4
63. Sarraf SA, Raman M, Guarani-Pereira V, Sowa ME, Huttlin EL, Gygi SP, et al. Landscape of the PARKIN-dependent ubiquitylome in response to mitochondrial depolarization. *Nature.* (2013) 496:372–6. doi: 10.1038/nature12043
64. Kazlauskaite A, Kelly V, Johnson C, Baillie C, Hastie CJ, Peggie M, et al. Phosphorylation of Parkin at serine65 is essential for activation: elaboration of a Miro1 substrate-based assay of Parkin E3 ligase activity. *Open Biol.* (2014) 4:130213. doi: 10.1098/rsob.130213
65. Weihofen A, Thomas KJ, Ostaszewski BL, Cookson MR, Selkoe DJ. Pink1 forms a multiprotein complex with Miro and Milton, linking Pink1 function to mitochondrial trafficking. *Biochemistry.* (2009) 10:2045–52. doi: 10.1021/bi8019178
66. Hsieh CH, Li L, Vanhauwaert R, Nguyen KT, Davis MD, Bu G, et al. Miro1 marks Parkinson's disease subset and Miro1 reducer rescues neuron loss in Parkinson's models. *Cell Metab.* (2019) 30:1131–40. doi: 10.1016/j.cmet.2019.08.023
67. Berenguer-Escuder C, Grossmann D, Antony P, Arena G, Wasner K, Massart F, et al. Impaired mitochondrial-endoplasmic reticulum interaction and mitophagy in Miro1-mutant neurons in Parkinson's Disease. *Hum Mol Genet.* (2020) ddaa066. doi: 10.1093/hmg/ddaa066
68. Cieri D, Vicario M, Giacomello M, Vallese F, Filadi R, Wagner T, et al. SPLICS: a split green fluorescent protein-based contact site sensor for narrow and wide heterotypic organelle juxtaposition. *Cell Death Differ.* (2017) 25:1131–45. doi: 10.1038/s41418-017-0033-z
69. McLelland GL, Goiran T, Yi W, Dorval G, Chen CX, Lauinger ND, et al. Mfn2 ubiquitination by PINK1/parkin gates the p97-dependent release of ER from mitochondria to drive mitophagy. *Elife.* (2018) 7:e32866. doi: 10.7554/eLife.32866
70. Helle SC, Kanfer G, Kolar K, Lang A, Michel AH, Kornmann B. Organization and function of membrane contact sites. *Biochim Biophys Acta.* (2013) 1833:2526–41. doi: 10.1016/j.bbamcr.2013.01.028
71. Lee S, Min KT. The interface between ER and mitochondria: molecular compositions and functions. *Mol Cells.* (2018) 41:1000–7. doi: 10.14348/molcells.2018.0438
72. Petrungaro C, Kornmann B. Lipid exchange at ER-mitochondria contact sites: a puzzle falling into place with quite a few pieces missing. *Curr Opin Cell Biol.* (2019) 57:71–6. doi: 10.1016/j.ceb.2018.11.005
73. Krols M, van Isterdael G, Asselbergh B, Kremer A, Lippens S, Timmerman V, et al. Mitochondria-associated membranes as hubs for neurodegeneration. *Acta Neuropathol.* (2016) 131:505–23. doi: 10.1007/s00401-015-1528-7
74. Moltedo O, Remondelli P, Amodio G. The mitochondria-endoplasmic reticulum contacts and their critical role in aging and age-associated diseases. *Front Cell Dev Biol.* (2019) 7:172. doi: 10.3389/fcell.2019.00172
75. Gómez-Suaga P, Bravo-San Pedro JM, González-Polo RA, Fuentes JM, Niso-Santano M. ER-mitochondria signaling in Parkinson's disease. *Cell Death Dis.* (2018) 9:337. doi: 10.1038/s41419-017-0079-3
76. Cal,ì T, Ottolini D, Negro A, Brini M. α-Synuclein controls mitochondrial calcium homeostasis by enhancing endoplasmic reticulum-mitochondria interactions. *J Biol Chem.* (2012) 287:17914–29. doi: 10.1074/jbc.M111.302794
77. Toyofuku T, Okamoto Y, Ishikawa T, Sasawatari S, Kumanogoh A. LRRK2 regulates endoplasmic reticulum-mitochondrial tethering through the PERK-mediated ubiquitination pathway. *EMBO J.* (2019) 10:e100875. doi: 10.15252/embj.2018100875
78. Guardia-Laguarta C, Area-Gomez E, Rüb C, Liu Y, Magrané J, Becker D, et al. α-Synuclein is localized to mitochondria-associated ER membranes. *J Neurosci.* (2014) 34:249–59. doi: 10.1523/JNEUROSCI.2507-13.2014
79. Guardia-Laguarta C, Liu Y, Lauritzen KH, Erdjument-Bromage H, Martin B, Swayne TC, et al. PINK1 Content in Mitochondria is Regulated by ER-Associated Degradation. *J Neurosci.* (2019) 39:7074–85. doi: 10.1523/JNEUROSCI.1691-18.2019
80. Stroud DA, Oeljeklaus S, Wiese S, Bohnert M, Lewandrowski U, Sickmann A, et al. Composition and topology of the endoplasmic reticulum-mitochondria encounter structure. *J Mol Biol.* (2011) 413:743–50. doi: 10.1016/j.jmb.2011.09.012
81. Nguyen TT, Lewandowska A, Choi JY, Markgraf DF, Junker M, Bilgin M, et al. Gem1 and ERMES do not directly affect phosphatidylserine transport from ER to mitochondria or mitochondrial inheritance. *Traffic.* (2013) 13:880–90. doi: 10.1111/j.1600-0854.2012.01352.x
82. Murley A, Lackner LL, Osman C, West M, Voeltz GK, Walter P, et al. ER-associated mitochondrial division links the distribution of mitochondria and mitochondrial DNA in yeast. *Elife.* (2013) 2:e00422. doi: 10.7554/eLife.00422
83. Koch B, Tucey TM, Lo TL, Novakovic S, Boag P, Traven A. The mitochondrial GTPase Gem1 contributes to the cell wall stress response and invasive growth of Candida albicans. *Front Microbiol.* (2017) 8:2555. doi: 10.3389/fmicb.2017.02555
84. Lee S, Lee KS, Huh S, Liu S, Lee DY, Hong SH, et al. Polo kinase phosphorylates Miro to control ER-mitochondria contact sites and mitochondrial Ca(2+) homeostasis in neural stem cell development. *Dev Cell.* (2016) 37:174–89. doi: 10.1016/j.devcel.2016.03.023
85. Modi S, López-Doménech G, Halff EF, Covill-Cooke C, Ivankovic D, Melandri D, et al. Miro clusters regulate ER-mitochondria contact sites and link cristae organization to the mitochondrial transport machinery. *Nat Commun.* (2019) 10:4399. doi: 10.1038/s41467-019-12382-4
86. Roberts R, Ktistakis NT. Omegasomes: PI3P platforms that manufacture autophagosomes. *Essays Biochem.* (2013) 55:17–27. doi: 10.1042/bse0550017
87. Ktistakis NT. ER platforms mediating autophagosome generation. *Biochim Biophys Acta Mol Cell Biol Lipids.* (2020) 1865:158433. doi: 10.1016/j.bbalip.2019.03.005
88. Valadas JS, Esposito G, Vandekerkhove D, Miskiewicz K, Deaulmerie L, Raitano S, et al. ER lipid defects in neuropeptidergic neurons impair sleep patterns in Parkinson's disease. *Neuron.* (2018) 98:1155–69.e6. http://doi.org/10.1016/j.neuron.2018.05.022
89. Tanaka A, Cleland MM, Xu S, Narendra DP, Suen DF, Karbowski M, et al. Proteasome and p97 mediate mitophagy and degradation of mitofusins induced by Parkin. *J Cell Biol.* (2010) 191:1367–80. doi: 10.1083/jcb.201007013
90. Geisler S, Holmström KM, Skujat D, Fiesel FC, Rothfuss OC, Kahle PJ, et al. PINK1/Parkin-mediated mitophagy is dependent on VDAC1 and p62/SQSTM1. *Nat Cell Biol.* (2010) 12:119–31. doi: 10.1038/ncb2012
91. Shlevkov E, Kramer T, Schapansky J, LaVoie MJ, Schwarz TL. Miro phosphorylation sites regulate Parkin recruitment and mitochondrial motility. *Proc Natl Acad Sci USA.* (2016) 113:E6097–106. doi: 10.1073/pnas.1612283113
92. Starkov AA. The molecular identity of the mitochondrial Ca2+ sequestration system. *FEBS J.* (2010) 277:3652–63. doi: 10.1111/j.1742-4658.2010.07756.x
93. MacAskill AF, Rinholm JE, Twelvetrees AE, Arancibia-Carcamo IL, Muir J, Fransson A, et al. Miro1 is a calcium sensor for glutamate receptor-dependent localization of mitochondria at synapses. *Neuron.* (2009) 61:541–55. doi: 10.1016/j.neuron.2009.01.030

94. Nemani N, Carvalho E, Tomar D, Dong Z, Ketschek A, Breves SL, et al. MIRO-1 determines mitochondrial shape transition upon GPCR activation and Ca2+ stress. *Cell Rep.* (2018) 23:1005–19. doi: 10.1016/j.celrep.2018.03.098
95. Niescier RF, Hong K, Park D, Min KT. MCU interacts with Miro1 to modulate mitochondrial functions in neurons. *J Neurosci.* (2018) 38:4666–77. doi: 10.1523/JNEUROSCI.0504-18.2018
96. McCormack JG, Halestrap AP, Denton RM. Role of calcium ions in regulation of mammalian intramitochondrial metabolism. *Physiol Rev.* (1990) 70:391–425. doi: 10.1152/physrev.1990.70.2.391
97. Jouaville LS, Pinton P, Bastianutto C, Rutter GA, Rizzuto R. Regulation of mitochondrial ATP synthesis by calcium: evidence for a long-term metabolic priming. *Proc Natl Acad Sci USA.* (1999) 96:13807–12. doi: 10.1073/pnas.96.24.13807
98. Cárdenas C, Miller RA, Smith I, Bui T, Molgó J, Müller M, et al. Essential regulation of cell bioenergetics by constitutive InsP3 receptor Ca2+ transfer to mitochondria. *Cell.* (2010) 142:270–83. doi: 10.1016/j.cell.2010.06.007
99. Treiman M, Caspersen C, Christensen SB. A tool coming of age: thapsigargin as an inhibitor of sarco-endoplasmic reticulum Ca(2+)-ATPases. *Trends Pharmacol Sci.* (1998) 19:131–5. doi: 10.1016/s0165-6147(98)01184-5
100. Parekh AB, Putney JW. Store-operated calcium channels. *Physiol Rev.* (2005) 85:757–810. doi: 10.1152/physrev.00057.2003
101. Kirichok Y, Krapivinsky G, Clapham DE. The mitochondrial calcium uniporter is a highly selective ion channel. *Nature.* (2004) 427:360–4. doi: 10.1038/nature02246
102. Vaccaro V, Devine MJ, Higgs NF, Kittler JT. Miro1-dependent mitochondrial positioning drives the rescaling of presynaptic Ca2+ signals during homeostatic plasticity. *EMBO Rep.* (2017) 18:231–40. doi: 10.15252/embr.201642710
103. Jackson JG, Robinson MB. Reciprocal regulation of mitochondrial dynamics and calcium signaling in astrocyte processes. *J Neurosci.* (2015) 35:15199–213. doi: 10.1523/JNEUROSCI.2049-15.2015
104. Stephen TL, Higgs NF, Sheehan DF, Al Awabdh S, López-Doménech G, Arancibia-Carcamo IL, et al. Miro1 regulates activity-driven positioning of mitochondria within astrocytic processes apposed to synapses to regulate intracellular calcium signaling. *J Neurosci.* (2015) 35:15996–6011. doi: 10.1523/JNEUROSCI.2068-15.2015
105. Verma M, Callio J, Otero PA, Sekler I, Wills ZP, Chu CT. Mitochondrial calcium dysregulation contributes to dendrite degeneration mediated by Parkinson's disease/Lewy Body disease-associated LRRK2 mutants. *J Neurosci.* (2017) 37:11151–65. doi: 10.1523/JNEUROSCI.3791-16.2017
106. Verma M, Wills Z, Chu CT. Excitatory dendritic mitochondrial calcium toxicity: implications for Parkinson's and other neurodegenerative diseases. *Front Neurosci.* (2018) 12:523. doi: 10.3389/fnins.2018.00523
107. Tabata Y, Imaizumi Y, Sugawara M, Andoh-Noda T, Banno S, Chai M, et al. T-type calcium channels determine the vulnerability of dopaminergic neurons to mitochondrial stress in familial Parkinson disease. *Stem Cell Rep.* (2018) 11:1171–84. doi: 10.1016/j.stemcr.2018.09.006
108. Wang H, Cheung F, Stoll AC, Rockwell P, Figueiredo-Pereira ME. Mitochondrial and calcium perturbations in rat CNS neurons induce calpain-cleavage of Parkin: phosphatase inhibition stabilizes pSer65Parkin reducing its calpain-cleavage. *Biochim Biophys Acta Mol Basis Dis.* (2019) 1865:1436–50. doi: 10.1016/j.bbadis.2019.02.016
109. Soman SK, Bazała M, Keatinge M, Bandmann O, Kuznicki J. Restriction of mitochondrial calcium overload by MCU inactivation renders a neuroprotective effect in zebrafish models of Parkinson's disease. *Biol Open.* (2019) 8:bio044347. doi: 10.1242/bio.044347
110. Leandrou E, Emmanouilidou E, Vekrellis K. Voltage-gated calcium channels and α-Synuclein: implications in Parkinson's disease. *Front Mol Neurosci.* (2019) 12:237. doi: 10.3389/fnmol.2019.00237
111. Russo GJ, Louie K, Wellington A, Macleod GT, Hu F, Panchumarthi S, et al. Drosophila miro is required for both anterograde and retrograde axonal mitochondrial transport. *J Neurosci.* (2009) 29:5443–55. doi: 10.1523/JNEUROSCI.5417-08.2009
112. Oeding SJ, Majstrowicz K, Hu X-P, Schwarz V, Freitag A, Honnert U, et al. Identification of Miro1 and Miro2 as mitochondrial receptors for myosin XIX. *J Cell Sci.* (2018) 131:jcs219469. doi: 10.1242/jcs.219469
113. Course MM, Wang X. Transporting mitochondria in neurons. *F1000Research.* (2016) 5:1735. doi: 10.12688/f1000research.7864.1
114. LaMonte BH, Wallace KE, Holloway BA, Shelly SS, Ascaño J, Tokito M, Van Winkle T, Howland DS, Holzbaur EL. Disruption of dynein/dynactin inhibits axonal transport in motor neurons causing late-onset progressive degeneration. *Neuron.* (2002) 34:715–27. doi: 10.1016/S0896-6273(02)00696-7
115. Beck M, Brickley K, Wilkinson HL, Sharma S, Smith M, Chazot PL, et al. Identification, molecular cloning, and characterization of a novel GABA a receptor-associated protein, GRIF-1. *J Biol Chem.* (2002) 277:30079–90. doi: 10.1074/jbc.M200438200
116. Iyer SPN, Akimoto Y, Hart GW. Identification and cloning of a novel family of coiled-coil domain proteins that interact with O -GlcNAc transferase. *J Biol Chem.* (2003) 278:5399–409. doi: 10.1074/jbc.M209384200
117. Hirokawa N, Noda Y, Okada Y. Kinesin and dynein superfamily proteins in organelle transport and cell division. *Curr Opin Cell Biol.* (1998) 10:60–73. doi: 10.1016/S0955-0674(98)80087-2
118. Morlino G, Barreiro O, Baixauli F, Robles-Valero J, Gonzalez-Granado JM, Villa-Bellosta R, et al. Miro-1 links mitochondria and microtubule dynein motors to control lymphocyte migration and polarity. *Mol Cell Biol.* (2014) 34:1412–26. doi: 10.1128/MCB.01177-13
119. van Spronsen M, Mikhaylova M, Lipka J, Schlager MA, van den Heuvel DJ, Kuijpers M, et al. TRAK/milton motor-adaptor proteins steer mitochondrial trafficking to axons and dendrites. *Neuron.* (2013) 77:485–502. doi: 10.1016/j.neuron.2012.11.027
120. Ahmad T, Mukherjee S, Pattnaik B, Kumar M, Singh S, Rehman R, et al. Miro1 regulates intercellular mitochondrial transport and enhances mesenchymal stem cell rescue efficacy. *EMBO J.* (2014) 33:994–1010. doi: 10.1002/embj.201386030
121. Zhang Y, Yu Z, Jiang D, Liang X, Liao S, Zhang Z, et al. iPSC-MSCs with high intrinsic MIRO1 and sensitivity to TNF-α yield efficacious mitochondrial transfer to rescue anthracycline-induced cardiomyopathy. *Stem Cell Rep.* (2016) 7:749–63. doi: 10.1016/j.stemcr.2016.08.009
122. Boukelmoune N, Chiu GS, Kavelaars A, Heijnen CJ. Mitochondrial transfer from mesenchymal stem cells to neural stem cells protects against the neurotoxic effects of cisplatin. *Acta Neuropath Commun.* (2018) 6:139. doi: 10.1186/s40478-018-0644-8
123. Babenko VA, Silachev DN, Popkov VA, Zorova LD, Pevzner IB, Plotnikov EY, et al. Miro1 enhances mitochondria transfer from multipotent mesenchymal stem cells (MMSC) to neural cells and improves the efficacy of cell recovery. *Molecules.* (2018) 23:1–14. doi: 10.3390/molecules23030687
124. Gao L, Zhang Z, Lu J, Pei G. Mitochondria are dynamically transferring between human neural cells and alexander disease-associated GFAP mutations impair the astrocytic transfer. *Front Cell Neurosci.* (2019) 13:1–16. doi: 10.3389/fncel.2019.00316
125. Spees JL, Olson SD, Whitney MJ, Prockop DJ. Mitochondrial transfer between cells can rescue aerobic respiration. *Proc Natl Acad Sci USA.* (2006) 103:1283–8. doi: 10.1073/pnas.0510511103
126. Islam MN, Das SR, Emin MT, Wei M, Sun L, Westphalen K, et al. Mitochondrial transfer from bone-marrow-derived stromal cells to pulmonary alveoli protects against acute lung injury. *Nat Med.* (2012) 18:759–65. doi: 10.1038/nm.2736
127. Tan AS, Baty JW, Dong LF, Bezawork-Geleta A, Endaya B, Goodwin J, et al. Mitochondrial genome acquisition restores respiratory function and tumorigenic potential of cancer cells without mitochondrial DNA. *Cell Metab.* (2015) 21:81–94. doi: 10.1016/j.cmet.2014.12.003
128. Torralba D, Baixauli F, Sánchez-Madrid F. Mitochondria know no boundaries: mechanisms and functions of intercellular mitochondrial transfer. *Front Cell Dev Biol.* (2016) 4:1–11. doi: 10.3389/fcell.2016.00107
129. Hayakawa K, Esposito E, Wang X, Terasaki Y, Liu Y, Xing C, et al. Transfer of mitochondria from astrocytes to neurons after stroke. *Nature.* (2016) 535:551–5. doi: 10.1038/nature18928
130. Vallabhaneni KC, Haller H, Dumler I. Vascular smooth muscle cells initiate proliferation of mesenchymal stem cells by mitochondrial

transfer via tunneling nanotubes. *Stem Cells Dev.* (2012) 21:3104–13. doi: 10.1089/scd.2011.0691
131. Jackson MV, Morrison TJ, Doherty DF, McAuley DF, Matthay MA, Kissenpfennig A, et al. Mitochondrial transfer via tunneling nanotubes is an important mechanism by which mesenchymal stem cells enhance macrophage phagocytosis in the in vitro and in vivo models of ARDS. *Stem Cells.* (2016) 34:2210–23. doi: 10.1002/stem.2372
132. Valdinocci D, Simões RF, Kovarova J, Cunha-Oliveira T, Neuzil J, Pountney DL. Intracellular and intercellular mitochondrial dynamics in Parkinson's disease. *Front Neurosci.* (2019) 13:1–8. doi: 10.3389/fnins.2019.00930
133. Frederick RL, McCaffery JM, Cunningham KW, Okamoto K, Shaw JM. Yeast Miro GTPase, Gem1p, regulates mitochondrial morphology via a novel pathway. *J Cell Biol.* (2004) 167:87–98. doi: 10.1083/jcb.200405100
134. Covill-Cooke C, Toncheva VS, Drew J, Birsa N, López-Doménech G, Kittler JT. Peroxisomal fission is modulated by the mitochondrial Rho-GTPases, Miro1 and Miro2. *EMBO Rep.* (2020) 2:e49865. doi: 10.15252/embr.201949865
135. Ding L, Lei Y, Han Y, Li Y, Ji X, Liu L. Vimar is a novel regulator of mitochondrial fission through Miro. *PLoS Genet.* (2016) 12:1–21. doi: 10.1371/journal.pgen.1006359
136. Nguyen TT, Oh SS, Weaver D, Lewandowska A, Maxfield D, Schuler MH, et al. Loss of Miro1-directed mitochondrial movement results in a novel murine model for neuron disease. *Proc Natl Acad Sci USA.* (2014) 111:E3631–40. doi: 10.1073/pnas.1402449111
137. Nordgren M, Fransen M. Peroxisomal metabolism and oxidative stress. *Biochimie.* (2014) 98:56–62. doi: 10.1016/j.biochi.2013.07.026
138. Waterham HR, Ferdinandusse S, Wanders RJA. Human disorders of peroxisome metabolism and biogenesis. *Biochim Biophys Acta.* (2016) 1863:922–33. doi: 10.1016/j.bbamcr.2015.11.015
139. Cohen Y, Klug YA, Dimitrov L, Erez Z, Chuartzman SG, Elinger D, et al. Peroxisomes are juxtaposed to strategic sites on mitochondria. *Mol BioSyst.* (2014) 10:1742–8. doi: 10.1039/c4mb00001c
140. Sugiura A, Mattie S, Prudent J, McBride HM. Newly born peroxisomes are a hybrid of mitochondrial and ER-derived pre-peroxisomes. *Nature.* (2017) 542:251–4. doi: 10.1038/nature21375
141. Drago I, Giacomello M, Pizzo P, Pozzan T. Calcium dynamics in the peroxisomal lumen of living cells. *J Biol Chem.* (2008) 283:14384–90. doi: 10.1074/jbc.M800600200
142. Iijima-Ando K, Hearn SA, Shenton C, Gatt A, Zhao L, Iijima K. Mitochondrial mislocalization underlies Abeta42-induced neuronal dysfunction in a Drosophila model of Alzheimer's disease. *PLoS ONE.* (2009) 4:e8310. doi: 10.1371/journal.pone.0008310
143. Iijima-Ando K, Sekiya M, Maruko-Otake A, Ohtake Y, Suzuki E, Lu B, Iijima KM. Loss of axonal mitochondria promotes tau-mediated neurodegeneration and Alzheimer's disease-related tau phosphorylation via PAR-1. *PLoS Genet.* (2012) 8. doi: 10.1371/journal.pgen.1002918
144. Zhang F, Wang W, Siedlak SL, Liu Y, Liu J, Jiang K, et al. Miro1 deficiency in amyotrophic lateral sclerosis. *Front Aging Neurosci.* (2015) 7:100. doi: 10.3389/fnagi.2015.00100
145. Moller A, Bauer CS, Cohen RN, Webster CP, De Vos KJ. Amyotrophic lateral sclerosis-associated mutant SOD1 inhibits anterograde axonal transport of mitochondria by reducing Miro1 levels. *Hum Mol Genet.* (2017) 26:4668–79. doi: 10.1093/hmg/ddx348
146. Misko A, Jiang S, Wegorzewska I, Milbrandt J, Baloh RH. Mitofusin 2 is necessary for transport of axonal mitochondria and interacts with the Miro/Milton complex. *J Neurosci.* (2010) 30:4232–40. doi: 10.1523/JNEUROSCI.6248-09.2010

Conflict of Interest: RK serves as Editorial Board Member of the European Journal of Clinical Investigation, the Journal of Parkinsonism and Related Disorders and the Journal of Neural Transmission. RK has received research grants from Fonds National de Recherche de Luxembourg (FNR) as Coordinator of the National Centre for Excellence in Research on Parkinson's disease (NCER-PD), Coordinator of the Study on COvid-19 National survey for assessing VIral spread by Non-affected CarriErs (CON-VINCE). RK received as well speaker's honoraria and/or travel grants from Abbvie, Zambon, and Medtronic and he participated as PI or site-PI for industry sponsored clinical trials without receiving honoraria.

The remaining authors declare that the research was conducted in the absence of any commercial or financial relationships that could be construed as a potential conflict of interest.

The handling editor declared a past collaboration with the authors.

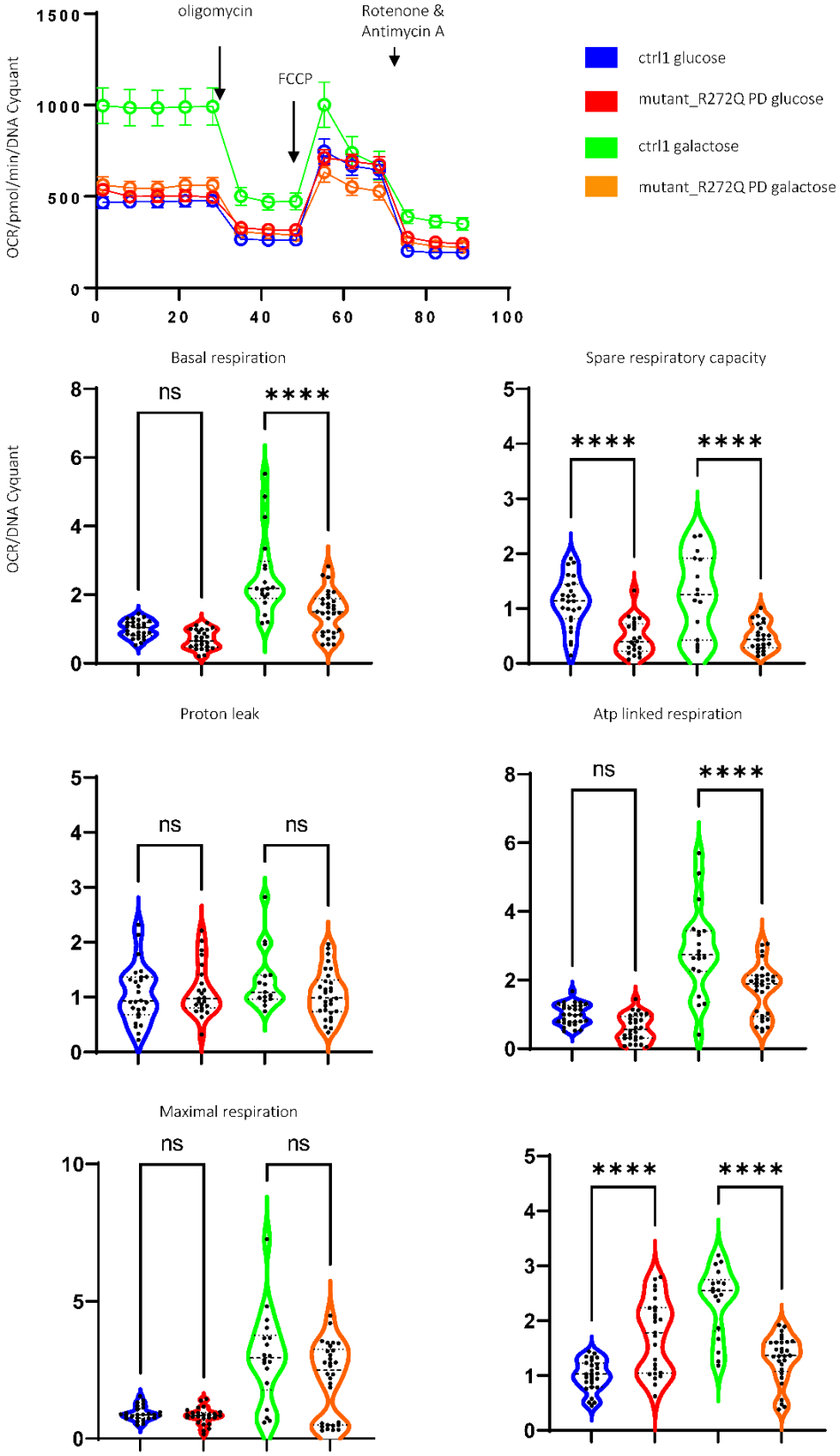

Appendix II: Impaired oxygen consumption rate in Miro1 p.R272Q mutant fibroblasts under galactose conditions

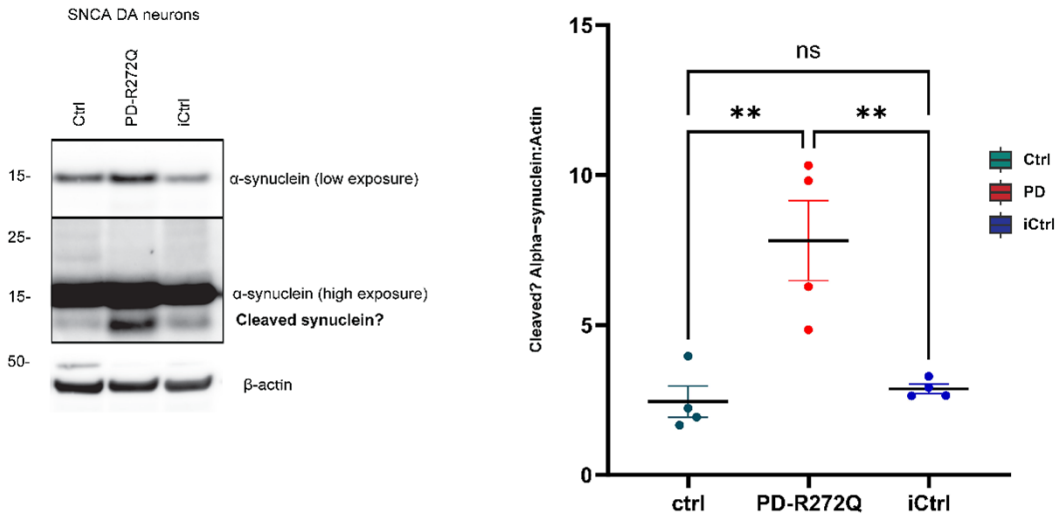

Appendix III: Higher protein levels of possibly cleaved α-synuclein levels in PD-R272Q Miro1 iPSC-derived neurons.

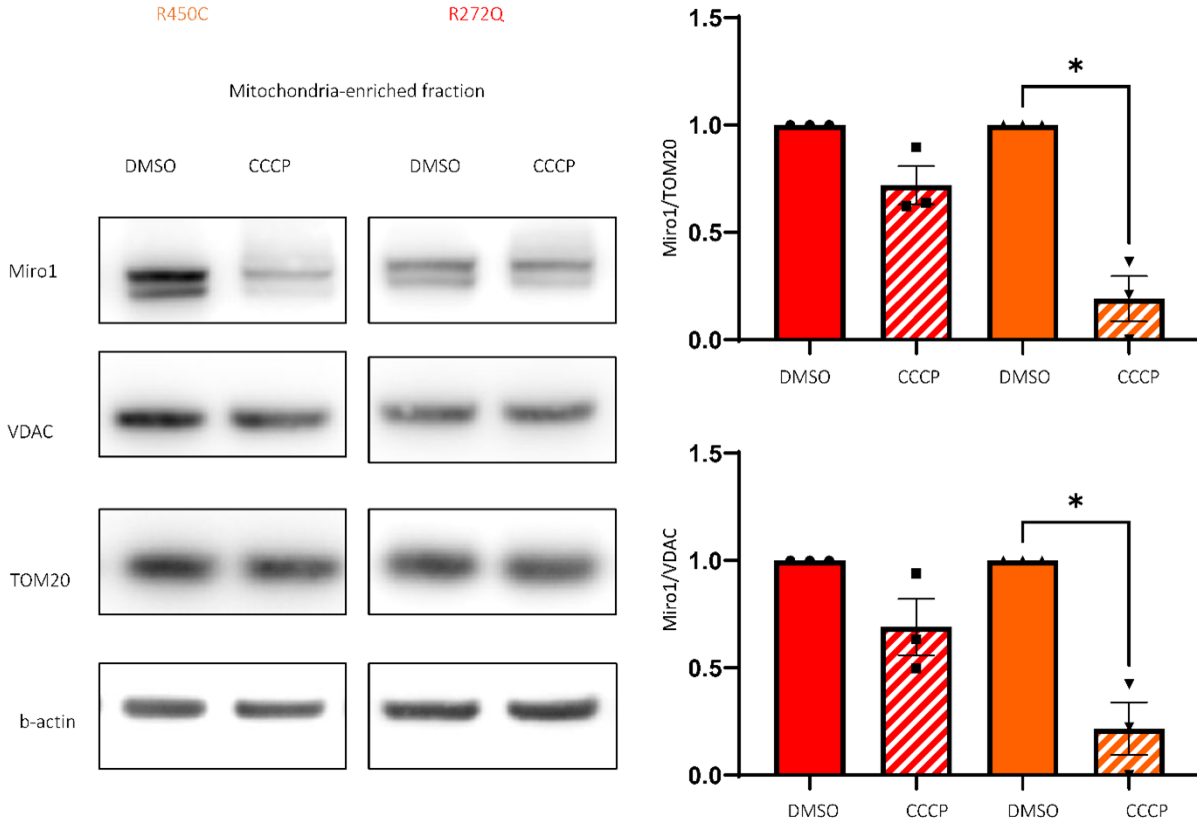

Appendix IV: Miro1 is not efficiently degraded in p.R272Q mutant fibroblasts compared to the p.R450C Miro1 mutant.

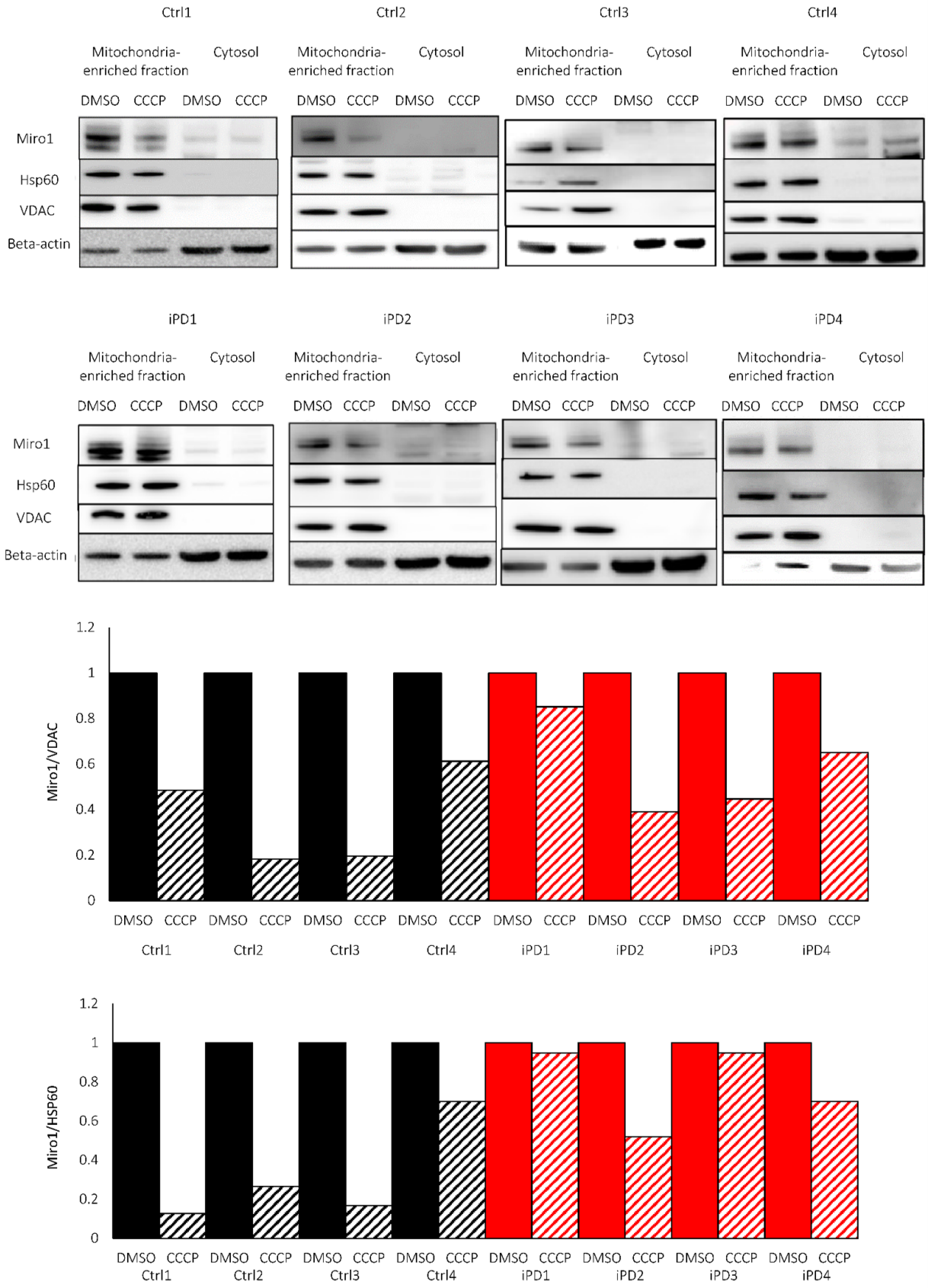

Appendix V: Miro1 is differentially degraded following CCCP treatment in control and idiopathic PD fibroblasts. (low-risk vs high-risk, n=4 for each group),

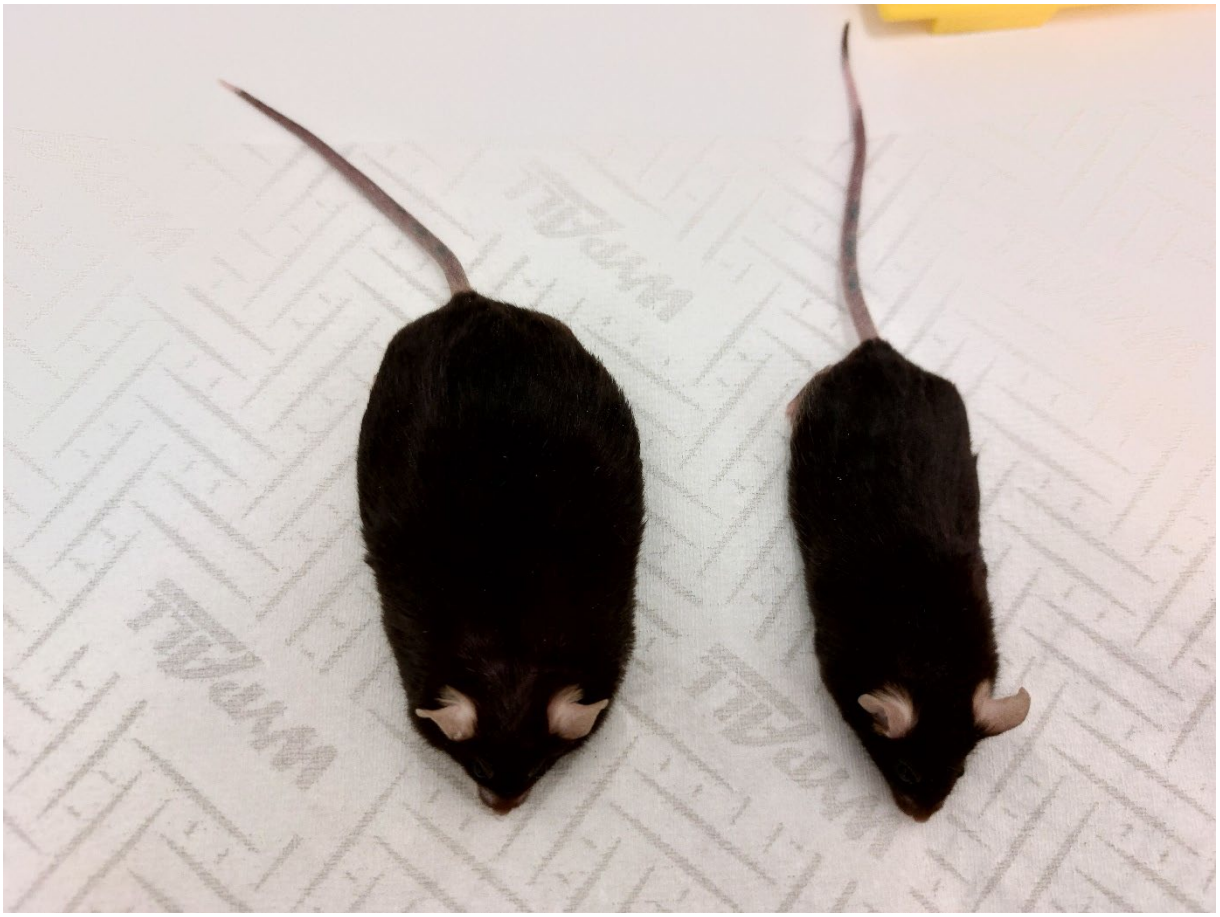

Appendix VI: Picture of Miro1 mice: homozygous KI (R285Q/R285Q), left, and WT, right.

VII Synopsis references

Acurex Biosciences to Present Early Clinical Results Supporting its Novel Parkinson's Disease Biomarkers at a Michael J. Fox Foundation Biomarkers Workshop [WWW Document], 2023. URL https://www.businesswire.com/news/home/20230515005012/en/Acurex-Biosciences-to-Present-Early-Clinical-Results-Supporting-its-Novel-Parkinson%E2%80%99s-Disease-Biomarkers-at-a-Michael-J.-Fox-Foundation-Biomarkers-Workshop (accessed 5.21.23).

Ahmad, T., Mukherjee, S., Pattnaik, B., Kumar, M., Singh, S., Kumar, M., Rehman, R., Tiwari, B.K., Jha, K.A., Barhanpurkar, A.P., Wani, M.R., Roy, S.S., Mabalirajan, U., Ghosh, B., Agrawal, A., 2014. Miro1 regulates intercellular mitochondrial transport & enhances mesenchymal stem cell rescue efficacy. EMBO J n/a-n/a. https://doi.org/10.1002/embj.201386030

Akita, H., Ogata, M., Jitsuki, S., Ogura, T., Oh-Nishi, A., Hoka, S., Saji, M., 2006. Nigral injection of antisense oligonucleotides to synaptotagmin I using HVJ–liposome vectors causes disruption of dopamine release in the striatum and impaired skill learning. Brain Research 1095, 178–189. https://doi.org/10.1016/j.brainres.2006.04.039

Anderson, J.P., Walker, D.E., Goldstein, J.M., Laat, R. de, Banducci, K., Caccavello, R.J., Barbour, R., Huang, J., Kling, K., Lee, M., Diep, L., Keim, P.S., Shen, X., Chataway, T., Schlossmacher, M.G., Seubert, P., Schenk, D., Sinha, S., Gai, W.P., Chilcote, T.J., 2006. Phosphorylation of Ser-129 Is the Dominant Pathological Modification of α-Synuclein in Familial and Sporadic Lewy Body Disease *. Journal of Biological Chemistry 281, 29739–29752. https://doi.org/10.1074/jbc.M600933200

Andrews, S., 2010. FASTQC. A quality control tool for high throughput sequence data.

Antony, Paul M. A., Diederich, N.J., Krüger, R., Balling, R., 2013. The hallmarks of Parkinson's disease. The FEBS Journal 280, 5981–5993. https://doi.org/10.1111/febs.12335

Antony, Paul M A, Diederich, N.J., Krüger, R., Balling, R., 2013. The hallmarks of Parkinson's disease. The FEBS journal 280, 5981–93. https://doi.org/10.1111/febs.12335

Arena, G., Landoulsi, Z., Grossmann, D., Vitali, A., Delcambre, S., Baron, A., Antony, P., Boussaad, I., Bobbili, D.R., Sreelatha, A.A.K., Pavelka, L., Klein, C., Seibler, P., Glaab, E., Sharma, M., Krüger, R., May, P., Grünewald, A., 2023. Polygenic risk scores validated in patient-derived cells stratify for mitochondrial subtypes of Parkinson's disease. https://doi.org/10.1101/2023.05.12.23289877

Arias-Fuenzalida, J., Jarazo, J., Walter, J., Gomez-Giro, G., Forster, J.I., Krueger, R., Antony, P.M.A., Schwamborn, J.C., 2019. Automated high-throughput high-content autophagy and mitophagy analysis platform. Sci Rep 9, 9455. https://doi.org/10.1038/s41598-019-45917-2

Ashrafi, A., Garcia, P., Kollmus, H., Schughart, K., Del Sol, A., Buttini, M., Glaab, E., 2017. Absence of regulator of G-protein signaling 4 does not protect against dopamine neuron dysfunction and injury in the mouse 6-hydroxydopamine lesion model of Parkinson's disease. Neurobiology of Aging 58, 30–33. https://doi.org/10.1016/j.neurobiolaging.2017.06.008

Ashrafi, G., Juan-Sanz, J. de, Farrell, R.J., Ryan, T.A., 2020. Molecular Tuning of the Axonal Mitochondrial Ca2+ Uniporter Ensures Metabolic Flexibility of Neurotransmission. Neuron 105, 678-687.e5. https://doi.org/10.1016/j.neuron.2019.11.020

Babenko, V., Silachev, D., Popkov, V., Zorova, L., Pevzner, I., Plotnikov, E., Sukhikh, G., Zorov, D., 2018. Miro1 Enhances Mitochondria Transfer from Multipotent Mesenchymal Stem Cells (MMSC) to Neural Cells and Improves the Efficacy of Cell Recovery. Molecules 23, 687. https://doi.org/10.3390/molecules23030687

Babic, M., Russo, G.J., Wellington, A.J., Sangston, R.M., Gonzalez, M., Zinsmaier, K.E., 2015. Miro's N-Terminal GTPase Domain Is Required for Transport of Mitochondria into Axons and Dendrites. Journal of Neuroscience 35, 5754–5771.

https://doi.org/10.1523/JNEUROSCI.1035-14.2015
Baev, A.Y., Vinokurov, A.Y., Novikova, I.N., Dremin, V. V, Potapova, E. V, Abramov, A.Y., 2022. Interaction of Mitochondrial Calcium and ROS in Neurodegeneration. Cells 11, 706. https://doi.org/10.3390/cells11040706
Balderas, E., Eberhardt, D.R., Lee, S., Pleinis, J.M., Sommakia, S., Balynas, A.M., Yin, X., Parker, M.C., Maguire, C.T., Cho, S., Szulik, M.W., Bakhtina, A., Bia, R.D., Friederich, M.W., Locke, T.M., Van Hove, J.L.K., Drakos, S.G., Sancak, Y., Tristani-Firouzi, M., Franklin, S., Rodan, A.R., Chaudhuri, D., 2022. Mitochondrial calcium uniporter stabilization preserves energetic homeostasis during Complex I impairment. Nat Commun 13, 2769. https://doi.org/10.1038/s41467-022-30236-4
Barasa, A., Wang, J., Dewey, R.B., 2021. Probable REM Sleep Behavior Disorder Is a Risk Factor for Symptom Progression in Parkinson Disease. Frontiers in Neurology 12.
Barbuti, P.A., Santos, B.FR., Antony, P.M., Massart, F., Cruciani, G., Dording, C.M., Pavelka, L., Kwon, Y.-J., Krüger, R., 2020. Gene-corrected Parkinson's disease neurons show the A30P alpha-synuclein point mutation leads to reduced neuronal branching and function (preprint). Neuroscience. https://doi.org/10.1101/2020.11.05.369389
Bayne, A.N., Trempe, J.-F., 2019. Mechanisms of PINK1, ubiquitin and Parkin interactions in mitochondrial quality control and beyond. Cell. Mol. Life Sci. 76, 4589–4611. https://doi.org/10.1007/s00018-019-03203-4
Becht, E., McInnes, L., Healy, J., Dutertre, C.-A., Kwok, I.W.H., Ng, L.G., Ginhoux, F., Newell, E.W., 2019. Dimensionality reduction for visualizing single-cell data using UMAP. Nature Biotechnology 37, 38–44. https://doi.org/10.1038/nbt.4314
Beckervordersandforth, R., Ebert, B., Schäffner, I., Moss, J., Fiebig, C., Shin, J., Moore, D.L., Ghosh, L., Trinchero, M.F., Stockburger, C., Friedland, K., Steib, K., von Wittgenstein, J., Keiner, S., Redecker, C., Hölter, S.M., Xiang, W., Wurst, W., Jagasia, R., Schinder, A.F., Ming, G.-L., Toni, N., Jessberger, S., Song, H., Lie, D.C., 2017. Role of Mitochondrial Metabolism in the Control of Early Lineage Progression and Aging Phenotypes in Adult Hippocampal Neurogenesis. Neuron 93, 560-573.e6. https://doi.org/10.1016/j.neuron.2016.12.017
Ben-Ari Fuchs, S., Lieder, I., Stelzer, G., Mazor, Y., Buzhor, E., Kaplan, S., Bogoch, Y., Plaschkes, I., Shitrit, A., Rappaport, N., Kohn, A., Edgar, R., Shenhav, L., Safran, M., Lancet, D., Guan-Golan, Y., Warshawsky, D., Shtrichman, R., 2016. GeneAnalytics: An Integrative Gene Set Analysis Tool for Next Generation Sequencing, RNAseq and Microarray Data. OMICS: A Journal of Integrative Biology 20, 139–151. https://doi.org/10.1089/omi.2015.0168
Benedetti, C., Haynes, C.M., Yang, Y., Harding, H.P., Ron, D., 2006. Ubiquitin-Like Protein 5 Positively Regulates Chaperone Gene Expression in the Mitochondrial Unfolded Protein Response. Genetics 174, 229–239. https://doi.org/10.1534/genetics.106.061580
Bentea, E., Verbruggen, L., Massie, A., 2017. The Proteasome Inhibition Model of Parkinson's Disease. J Parkinsons Dis 7, 31–63. https://doi.org/10.3233/JPD-160921
Berenguer-Escuder, C., Grossmann, D., Antony, P., Arena, G., Wasner, K., Massart, F., Jarazo, J., Walter, J., Schwamborn, J.C., Grünewald, A., Krüger, R., 2020a. Impaired mitochondrial–endoplasmic reticulum interaction and mitophagy in Miro1-mutant neurons in Parkinson's disease. Human Molecular Genetics ddaa066. https://doi.org/10.1093/hmg/ddaa066
Berenguer-Escuder, C., Grossmann, D., Antony, P., Arena, G., Wasner, K., Massart, F., Jarazo, J., Walter, J., Schwamborn, J.C., Grünewald, A., Krüger, R., 2020b. Impaired mitochondrial-endoplasmic reticulum interaction and mitophagy in Miro1-mutant neurons in Parkinson's disease. Human molecular genetics 29, 1353–1364. https://doi.org/10.1093/hmg/ddaa066
Berenguer-Escuder, C., Grossmann, D., Massart, F., Antony, P., Burbulla, L.F., Glaab, E., Imhoff, S., Trinh, J., Seibler, P., Grünewald, A., Krüger, R., 2019a. Variants in Miro1 Cause Alterations of ER-Mitochondria Contact Sites in Fibroblasts from Parkinson's Disease Patients. JCM 8, 2226. https://doi.org/10.3390/jcm8122226
Berenguer-Escuder, C., Grossmann, D., Massart, F., Antony, P., Burbulla, L.F., Glaab, E., Imhoff, S.,

Trinh, J., Seibler, P., Grünewald, A., Krüger, R., 2019b. Variants in Miro1 Cause Alterations of ER-Mitochondria Contact Sites in Fibroblasts from Parkinson's Disease Patients. Journal of Clinical Medicine 8, 2226. https://doi.org/10.3390/jcm8122226

Bharat, V., Hsieh, C.-H., Wang, X., 2021. Mitochondrial Defects in Fibroblasts of Pathogenic MAPT Patients. Front. Cell Dev. Biol. 9, 765408. https://doi.org/10.3389/fcell.2021.765408

Bharat, V., Vanhauwaert, R., Li, L., Muir, C.M., Durairaj, A.S., Chandra, S., Guen, Y. Le, Nandakishore, P., Hsieh, C.-H., Rensi, S.E., Altman, R.B., Greicius, M.D., Feng, L., Wang, X., 2022a. An Iron-Calcium-Miro Axis Influences Parkinson's Risk and Neurodegeneration. bioRxiv 2022.10.30.513580. https://doi.org/10.1101/2022.10.30.513580

Bharat, V., Vanhauwaert, R., Li, L., Muir, C.M., Durairaj, A.S., Chandra, S., Guen, Y.L., Nandakishore, P., Hsieh, C.-H., Rensi, S.E., Altman, R.B., Greicius, M.D., Feng, L., Wang, X., 2022b. An Iron-Calcium-Miro Axis Influences Parkinson's Risk and Neurodegeneration (preprint). Cell Biology. https://doi.org/10.1101/2022.10.30.513580

Bharat, V., Wang, X., 2020. Precision Neurology for Parkinson's Disease: Coupling Miro1-Based Diagnosis With Drug Discovery. Movement disorders : official journal of the Movement Disorder Society 35, 1502–1508. https://doi.org/10.1002/mds.28194

Blesa, J., Trigo-Damas, I., Quiroga-Varela, A., del Rey, N.L.-G., 2016a. Animal Models of Parkinson's Disease, in: Challenges in Parkinson's Disease. InTech. https://doi.org/10.5772/63328

Blesa, J., Trigo-Damas, I., Quiroga-Varela, A., Rey, N.L.-G. del, Blesa, J., Trigo-Damas, I., Quiroga-Varela, A., Rey, N.L.-G. del, 2016b. Animal Models of Parkinson's Disease, in: Challenges in Parkinson's Disease. IntechOpen. https://doi.org/10.5772/63328

Bohush, A., Niewiadomska, G., Filipek, A., 2018. Role of Mitogen Activated Protein Kinase Signaling in Parkinson's Disease. International Journal of Molecular Sciences 19, 2973. https://doi.org/10.3390/ijms19102973

Bolognin, S., Fossépré, M., Qing, X., Jarazo, J., Ščančar, J., Moreno, E.L., Nickels, S.L., Wasner, K., Ouzren, N., Walter, J., Grünewald, A., Glaab, E., Salamanca, L., Fleming, R.M.T., Antony, P.M.A., Schwamborn, J.C., 2019. 3D Cultures of Parkinson's Disease-Specific Dopaminergic Neurons for High Content Phenotyping and Drug Testing. Advanced Science 6, 1800927. https://doi.org/10.1002/advs.201800927

Boy, J., Schmidt, T., Wolburg, H., Mack, A., Nuber, S., Böttcher, M., Schmitt, I., Holzmann, C., Zimmermann, F., Servadio, A., Riess, O., 2009a. Reversibility of symptoms in a conditional mouse model of spinocerebellar ataxia type 3. Hum Mol Genet 18, 4282–4295. https://doi.org/10.1093/hmg/ddp381

Boy, J., Schmidt, T., Wolburg, H., Mack, A., Nuber, S., Böttcher, M., Schmitt, I., Holzmann, C., Zimmermann, F., Servadio, A., Riess, O., 2009b. Reversibility of symptoms in a conditional mouse model of spinocerebellar ataxia type 3. Human Molecular Genetics 18, 4282–4295. https://doi.org/10.1093/hmg/ddp381

Brakedal, B., Dölle, C., Riemer, F., Ma, Y., Nido, G.S., Skeie, G.O., Craven, A.R., Schwarzlmüller, T., Brekke, N., Diab, J., Sverkeli, L., Skjeie, V., Varhaug, K., Tysnes, O.-B., Peng, S., Haugarvoll, K., Ziegler, M., Grüner, R., Eidelberg, D., Tzoulis, C., 2022. The NADPARK study: A randomized phase I trial of nicotinamide riboside supplementation in Parkinson's disease. Cell Metabolism 34, 396-407.e6. https://doi.org/10.1016/j.cmet.2022.02.001

Brand, M.D., 2010. The sites and topology of mitochondrial superoxide production. Exp Gerontol 45, 466–472. https://doi.org/10.1016/j.exger.2010.01.003

Brembati, V., Faustini, G., Longhena, F., Bellucci, A., 2023. Alpha synuclein post translational modifications: potential targets for Parkinson's disease therapy? Front Mol Neurosci 16, 1197853. https://doi.org/10.3389/fnmol.2023.1197853

Burbulla, L.F., Song, P., Mazzulli, J.R., Zampese, E., Wong, Y.C., Jeon, S., Santos, D.P., Blanz, J., Obermaier, C.D., Strojny, C., Savas, J.N., Kiskinis, E., Zhuang, X., Krüger, R., Surmeier, D.J., Krainc, D., 2017. Dopamine oxidation mediates mitochondrial and lysosomal dysfunction in Parkinson's disease. Science 357, 1255–1261. https://doi.org/10.1126/science.aam9080

Bus, C., Zizmare, L., Feldkaemper, M., Geisler, S., Zarani, M., Schaedler, A., Klose, F., Admard, J., Mageean, C.J., Arena, G., Fallier-Becker, P., Ugun-Klusek, A., Maruszczak, K.K., Kapolou, K., Schmid, B., Rapaport, D., Ueffing, M., Casadei, N., Krüger, R., Gasser, T., Vogt Weisenhorn, D.M., Kahle, P.J., Trautwein, C., Gloeckner, C.J., Fitzgerald, J.C., 2020. Human Dopaminergic Neurons Lacking PINK1 Exhibit Disrupted Dopamine Metabolism Related to Vitamin B6 Co-Factors. iScience 23, 101797. https://doi.org/10.1016/j.isci.2020.101797

Byers, B., Cord, B., Nguyen, H.N., Schüle, B., Fenno, L., Lee, P.C., Deisseroth, K., Langston, J.W., Pera, R.R., Palmer, T.D., 2011. SNCA triplication Parkinson's patient's iPSC-derived DA neurons accumulate α-synuclein and are susceptible to oxidative stress. PLoS One 6, e26159. https://doi.org/10.1371/journal.pone.0026159

Cai, H., Liu, G., Sun, L., Ding, J., 2014. Aldehyde Dehydrogenase 1 making molecular inroads into the differential vulnerability of nigrostriatal dopaminergic neuron subtypes in Parkinson's disease. Transl Neurodegener 3, 27. https://doi.org/10.1186/2047-9158-3-27

Castellazzi, M., Patergnani, S., Donadio, M., Giorgi, C., Bonora, M., Fainardi, E., Casetta, I., Granieri, E., Pugliatti, M., Pinton, P., 2019. Correlation between auto/mitophagic processes and magnetic resonance imaging activity in multiple sclerosis patients. Journal of neuroinflammation 16, 131. https://doi.org/10.1186/s12974-019-1526-0

Castro, I.G., Richards, D.M., Metz, J., Costello, J.L., Passmore, J.B., Schrader, T.A., Gouveia, A., Ribeiro, D., Schrader, M., 2018. A role for Mitochondrial Rho GTPase 1 (MIRO1) in motility and membrane dynamics of peroxisomes. Traffic 19, 229–242. https://doi.org/10.1111/tra.12549

Castro, I.G., Schrader, M., 2018. Miro1 - the missing link to peroxisome motility. Commun Integr Biol 11, e1526573. https://doi.org/10.1080/19420889.2018.1526573

Chang, E.E.S., Ho, P.W.-L., Liu, H.-F., Pang, S.Y.-Y., Leung, C.-T., Malki, Y., Choi, Z.Y.-K., Ramsden, D.B., Ho, S.-L., 2022. LRRK2 mutant knock-in mouse models: therapeutic relevance in Parkinson's disease. Translational Neurodegeneration 11, 10. https://doi.org/10.1186/s40035-022-00285-2

Chang, K.T., Niescier, R.F., Min, K.-T., 2011. Mitochondrial matrix Ca2+ as an intrinsic signal regulating mitochondrial motility in axons. Proceedings of the National Academy of Sciences 108, 15456–15461. https://doi.org/10.1073/pnas.1106862108

Chaudhuri, K.R., Schapira, A.H.V., 2009. Non-motor symptoms of Parkinson's disease: dopaminergic pathophysiology and treatment. Lancet Neurol 8, 464–474. https://doi.org/10.1016/S1474-4422(09)70068-7

Chemla, A., Arena, G., Onal, G., Walter, J., Berenguer-Escuder, C., Grossmann, D., Grünewald, A., Schwamborn, J.C., Krüger, R., 2023. Generation of two induced pluripotent stem cell lines and the corresponding isogenic controls from Parkinson's disease patients carrying the heterozygous mutations c.815G{\textgreater}A (p.R272Q) or c.1348C{\textgreater}T (p.R450C) in the RHOT1 gene encod. Stem Cell Research 103145. https://doi.org/10.1016/j.scr.2023.103145

Chen, L., Liu, C., Gao, J., Xie, Z., Chan, L.W.C., Keating, D.J., Yang, Y., Sun, J., Zhou, F., Wei, Y., Men, X., Yang, S., 2017. Inhibition of Miro1 disturbs mitophagy and pancreatic β-cell function interfering insulin release via IRS-Akt-Foxo1 in diabetes. Oncotarget 8, 90693–90705. https://doi.org/10.18632/oncotarget.20963

Cherubini, M., Wade-Martins, R., 2018. Convergent pathways in Parkinson's disease. Cell and Tissue Research 373, 79–90. https://doi.org/10.1007/s00441-017-2700-2

Chesselet, M.-F., Fleming, S., Mortazavi, F., Meurers, B., 2008. Strengths and Limitations of Genetic Mouse Models of Parkinson's Disease. Parkinsonism Relat Disord 14, S84–S87. https://doi.org/10.1016/j.parkreldis.2008.04.004

Choi, M.L., Chappard, A., Singh, B.P., Maclachlan, C., Rodrigues, M., Fedotova, E.I., Berezhnov, A.V., De, S., Peddie, C.J., Athauda, D., Virdi, G.S., Zhang, W., Evans, J.R., Wernick, A.I., Zanjani, Z.S., Angelova, P.R., Esteras, N., Vinokurov, A.Y., Morris, K., Jeacock, K., Tosatto, L., Little, D., Gissen, P., Clarke, D.J., Kunath, T., Collinson, L., Klenerman, D., Abramov, A.Y., Horrocks,

M.H., Gandhi, S., 2022. Pathological structural conversion of α-synuclein at the mitochondria induces neuronal toxicity. Nat Neurosci 25, 1134–1148. https://doi.org/10.1038/s41593-022-01140-3
Chung, K.K.K., Dawson, V.L., Dawson, T.M., 2003. New insights into Parkinson's disease. J Neurol 250 Suppl 3, III15-24. https://doi.org/10.1007/s00415-003-1304-9
Chung, S.Y., Kishinevsky, S., Mazzulli, J.R., Graziotto, J., Mrejeru, A., Mosharov, E.V., Puspita, L., Valiulahi, P., Sulzer, D., Milner, T.A., Taldone, T., Krainc, D., Studer, L., Shim, J., 2016. Parkin and PINK1 Patient iPSC-Derived Midbrain Dopamine Neurons Exhibit Mitochondrial Dysfunction and α-Synuclein Accumulation. Stem Cell Reports 7, 664–677. https://doi.org/10.1016/j.stemcr.2016.08.012
Cieri, D., Vicario, M., Giacomello, M., Vallese, F., Filadi, R., Wagner, T., Pozzan, T., Pizzo, P., Scorrano, L., Brini, M., Calì, T., 2018. SPLICS: a split green fluorescent protein-based contact site sensor for narrow and wide heterotypic organelle juxtaposition. Cell Death Differ 25, 1131–1145. https://doi.org/10.1038/s41418-017-0033-z
Cmarko, L., Weiss, N., 2020. Selective inhibition of neuronal Cav3.3 T-type calcium channels by TAT-based channel peptide. Mol Brain 13, 95. https://doi.org/10.1186/s13041-020-00636-y
Colicelli, J., 2004. Human RAS Superfamily Proteins and Related GTPases. Science Signaling 2004, re13–re13. https://doi.org/10.1126/stke.2502004re13
Collatz, M.B., Rüdel, R., Brinkmeier, H., 1997. Intracellular calcium chelator BAPTA protects cells against toxic calcium overload but also alters physiological calcium responses. Cell Calcium 21, 453–459. https://doi.org/10.1016/S0143-4160(97)90056-7
Congdon, E.E., 2018. Sex Differences in Autophagy Contribute to Female Vulnerability in Alzheimer's Disease. Frontiers in Neuroscience 12.
Conner, M.R., Jang, D., Anderson, B.J., Kritzer, M.F., 2020. Biological Sex and Sex Hormone Impacts on Deficits in Episodic-Like Memory in a Rat Model of Early, Pre-motor Stages of Parkinson's Disease. Frontiers in Neurology 11.
Corsini, N.S., Knoblich, J.A., 2022. Human organoids: New strategies and methods for analyzing human development and disease. Cell 185, 2756–2769. https://doi.org/10.1016/j.cell.2022.06.051
Costello, J.L., Castro, I.G., Camões, F., Schrader, T.A., McNeall, D., Yang, J., Giannopoulou, E.-A., Gomes, S., Pogenberg, V., Bonekamp, N.A., Ribeiro, D., Wilmanns, M., Jedd, G., Islinger, M., Schrader, M., 2017. Predicting the targeting of tail-anchored proteins to subcellular compartments in mammalian cells. J Cell Sci 130, 1675–1687. https://doi.org/10.1242/jcs.200204
Course, M.M., Wang, X., 2016. Transporting mitochondria in neurons. F1000Res 5, 1735. https://doi.org/10.12688/f1000research.7864.1
Covill-Cooke, C., Toncheva, V.S., Drew, J., Birsa, N., López-Doménech, G., Kittler, J.T., 2020. Peroxisomal fission is modulated by the mitochondrial Rho-GTPases, Miro1 and Miro2. EMBO Rep 21. https://doi.org/10.15252/embr.201949865
Day, J.O., Mullin, S., 2021. The Genetics of Parkinson's Disease and Implications for Clinical Practice. Genes 12, 1006. https://doi.org/10.3390/genes12071006
de Lau, L.M.L., Breteler, M.M.B., 2006. Epidemiology of Parkinson's disease. Lancet Neurol 5, 525–535. https://doi.org/10.1016/S1474-4422(06)70471-9
Dias, V., Junn, E., Mouradian, M.M., 2013. The role of oxidative stress in Parkinson's disease. J Parkinsons Dis 3, 461–491. https://doi.org/10.3233/JPD-130230
Diepenbroek, M., Casadei, N., Esmer, H., Saido, T.C., Takano, J., Kahle, P.J., Nixon, R.A., Rao, M.V., Melki, R., Pieri, L., Helling, S., Marcus, K., Krueger, R., Masliah, E., Riess, O., Nuber, S., 2014. Overexpression of the calpain-specific inhibitor calpastatin reduces human alpha-Synuclein processing, aggregation and synaptic impairment in [A30P]αSyn transgenic mice. Hum Mol Genet 23, 3975–3989. https://doi.org/10.1093/hmg/ddu112
Dixit, E., Boulant, S., Zhang, Y., Lee, A.S.Y., Odendall, C., Shum, B., Hacohen, N., Chen, Z.J., Whelan,

S.P., Fransen, M., Nibert, M.L., Superti-Furga, G., Kagan, J.C., 2010. Peroxisomes are signaling platforms for antiviral innate immunity. Cell 141, 668–681. https://doi.org/10.1016/j.cell.2010.04.018

Dobin, A., Davis, C.A., Schlesinger, F., Drenkow, J., Zaleski, C., Jha, S., Batut, P., Chaisson, M., Gingeras, T.R., 2013. STAR: ultrafast universal RNA-seq aligner. Bioinformatics 29, 15–21. https://doi.org/10.1093/bioinformatics/bts635

Dodson, P.D., Dreyer, J.K., Jennings, K.A., Syed, E.C.J., Wade-Martins, R., Cragg, S.J., Bolam, J.P., Magill, P.J., 2016. Representation of spontaneous movement by dopaminergic neurons is cell-type selective and disrupted in parkinsonism. Proceedings of the National Academy of Sciences of the United States of America 113, E2180-8. https://doi.org/10.1073/pnas.1515941113

Dorsey, E.R., Elbaz, A., Nichols, E., Abd-Allah, F., Abdelalim, A., Adsuar, J.C., Ansha, M.G., Brayne, C., Choi, J.-Y.J., Collado-Mateo, D., Dahodwala, N., Do, H.P., Edessa, D., Endres, M., Fereshtehnejad, S.-M., Foreman, K.J., Gankpe, F.G., Gupta, R., Hankey, G.J., Hay, S.I., Hegazy, M.I., Hibstu, D.T., Kasaeian, A., Khader, Y., Khalil, I., Khang, Y.-H., Kim, Y.J., Kokubo, Y., Logroscino, G., Massano, J., Ibrahim, N.M., Mohammed, M.A., Mohammadi, A., Moradi-Lakeh, M., Naghavi, M., Nguyen, B.T., Nirayo, Y.L., Ogbo, F.A., Owolabi, M.O., Pereira, D.M., Postma, M.J., Qorbani, M., Rahman, M.A., Roba, K.T., Safari, H., Safiri, S., Satpathy, M., Sawhney, M., Shafieesabet, A., Shiferaw, M.S., Smith, M., Szoeke, C.E.I., Tabarés-Seisdedos, R., Truong, N.T., Ukwaja, K.N., Venketasubramanian, N., Villafaina, S., Weldegwergs, K. gidey, Westerman, R., Wijeratne, T., Winkler, A.S., Xuan, B.T., Yonemoto, N., Feigin, V.L., Vos, T., Murray, C.J.L., 2018a. Global, regional, and national burden of Parkinson's disease, 1990–2016: a systematic analysis for the Global Burden of Disease Study 2016. The Lancet Neurology 17, 939–953. https://doi.org/10.1016/S1474-4422(18)30295-3

Dorsey, E.R., Sherer, T., Okun, M.S., Bloem, B.R., 2018b. The Emerging Evidence of the Parkinson Pandemic. JPD 8, S3–S8. https://doi.org/10.3233/JPD-181474

Dufty, B.M., Warner, L.R., Hou, S.T., Jiang, S.X., Gomez-Isla, T., Leenhouts, K.M., Oxford, J.T., Feany, M.B., Masliah, E., Rohn, T.T., 2007. Calpain-cleavage of alpha-synuclein: connecting proteolytic processing to disease-linked aggregation. Am J Pathol 170, 1725–1738. https://doi.org/10.2353/ajpath.2007.061232

Ebrahimi-Fakhari, D., Wahlster, L., McLean, P.J., 2012. PROTEIN DEGRADATION PATHWAYS IN PARKINSON'S DISEASE – CURSE OR BLESSING. Acta Neuropathol 124, 153–172. https://doi.org/10.1007/s00401-012-1004-6

Emmanouilidou, E., Melachroinou, K., Roumeliotis, T., Garbis, S.D., Ntzouni, M., Margaritis, L.H., Stefanis, L., Vekrellis, K., 2010. Cell-Produced α-Synuclein Is Secreted in a Calcium-Dependent Manner by Exosomes and Impacts Neuronal Survival. J Neurosci 30, 6838–6851. https://doi.org/10.1523/JNEUROSCI.5699-09.2010

English, K., Shepherd, A., Uzor, N.-E., Trinh, R., Kavelaars, A., Heijnen, C.J., 2020. Astrocytes rescue neuronal health after cisplatin treatment through mitochondrial transfer. acta neuropathol commun 8, 36. https://doi.org/10.1186/s40478-020-00897-7

Fahed, A.C., Wang, M., Homburger, J.R., Patel, A.P., Bick, A.G., Neben, C.L., Lai, C., Brockman, D., Philippakis, A., Ellinor, P.T., Cassa, C.A., Lebo, M., Ng, K., Lander, E.S., Zhou, A.Y., Kathiresan, S., Khera, A. V, 2020. Polygenic background modifies penetrance of monogenic variants for tier 1 genomic conditions. Nature communications 11, 3635. https://doi.org/10.1038/s41467-020-17374-3

Fang, C., Hernandez, P., Liow, K., Damiano, E., Zetterberg, H., Blennow, K., Feng, D., Chen, M., Maccecchini, M., 2023. Buntanetap, a Novel Translational Inhibitor of Multiple Neurotoxic Proteins, Proves to Be Safe and Promising in Both Alzheimer's and Parkinson's Patients. J Prev Alzheimers Dis 10, 25–33. https://doi.org/10.14283/jpad.2022.84

Feigin, V.L., Abajobir, A.A., Abate, K.H., Abd-Allah, F., Abdulle, A.M., Abera, S.F., Abyu, G.Y., Ahmed, M.B., Aichour, A.N., Aichour, I., Aichour, M.T.E., Akinyemi, R.O., Alabed, S., Al-Raddadi, R.,

Alvis-Guzman, N., Amare, A.T., Ansari, H., Anwari, P., Ärnlöv, J., Asayesh, H., Asgedom, S.W., Atey, T.M., Avila-Burgos, L., Frinel, E., Avokpaho, G.A., Azarpazhooh, M.R., Barac, A., Barboza, M., Barker-Collo, S.L., Bärnighausen, T., Bedi, N., Beghi, E., Bennett, D.A., Bensenor, I.M., Berhane, A., Betsu, B.D., Bhaumik, S., Birlik, S.M., Biryukov, S., Boneya, D.J., Bulto, L.N.B., Carabin, H., Casey, D., Castañeda-Orjuela, C.A., Catalá-López, F., Chen, H., Chitheer, A.A., Chowdhury, R., Christensen, H., Dandona, L., Dandona, R., de Veber, G.A., Dharmaratne, S.D., Do, H.P., Dokova, K., Dorsey, E.R., Ellenbogen, R.G., Eskandarieh, S., Farvid, M.S., Fereshtehnejad, S.-M., Fischer, F., Foreman, K.J., Geleijnse, J.M., Gillum, R.F., Giussani, G., Goldberg, E.M., Gona, P.N., Goulart, A.C., Gugnani, H.C., Gupta, Rahul, Hachinski, V., Gupta, Rajeev, Hamadeh, R.R., Hambisa, M., Hankey, G.J., Hareri, H.A., Havmoeller, R., Hay, S.I., Heydarpour, P., Hotez, P.J., Jakovljevic, M. (Michael) B., Javanbakht, M., Jeemon, P., Jonas, J.B., Kalkonde, Y., Kandel, A., Karch, A., Kasaeian, A., Kastor, A., Keiyoro, P.N., Khader, Y.S., Khalil, I.A., Khan, E.A., Khang, Y.-H., Tawfih, A., Khoja, A., Khubchandani, J., Kulkarni, C., Kim, D., Kim, Y.J., Kivimaki, M., Kokubo, Y., Kosen, S., Kravchenko, M., Krishnamurthi, R.V., Defo, B.K., Kumar, G.A., Kumar, R., Kyu, H.H., Larsson, A., Lavados, P.M., Li, Y., Liang, X., Liben, M.L., Lo, W.D., Logroscino, G., Lotufo, P.A., Loy, C.T., Mackay, M.T., El Razek, H.M.A., El Razek, M.M.A., Majeed, A., Malekzadeh, R., Manhertz, T., Mantovani, L.G., Massano, J., Mazidi, M., McAlinden, C., Mehata, S., Mehndiratta, M.M., Memish, Z.A., Mendoza, W., Mengistie, M.A., Mensah, G.A., Meretoja, A., Mezgebe, H.B., Miller, T.R., Mishra, S.R., Ibrahim, N.M., Mohammadi, A., Mohammed, K.E., Mohammed, S., Mokdad, A.H., Moradi-Lakeh, M., Velasquez, I.M., Musa, K.I., Naghavi, M., Ngunjiri, J.W., Nguyen, C.T., Nguyen, G., Le Nguyen, Q., Nguyen, T.H., Nichols, E., Ningrum, D.N.A., Nong, V.M., Norrving, B., Noubiap, J.J.N., Ogbo, F.A., Owolabi, M.O., Pandian, J.D., Parmar, P.G., Pereira, D.M., Petzold, M., Phillips, M.R., Piradov, M.A., Poulton, R.G., Pourmalek, F., Qorbani, M., Rafay, A., Rahman, M., Rahman, M.H., Rai, R.K., Rajsic, S., Ranta, A., Rawaf, S., Renzaho, A.M.N., Rezai, M.S., Roth, G.A., Roshandel, G., Rubagotti, E., Sachdev, P., Safiri, S., Sahathevan, R., Sahraian, M.A., Samy, A.M., Santalucia, P., Santos, I.S., Sartorius, B., Satpathy, M., Sawhney, M., Saylan, M.I., Sepanlou, S.G., Shaikh, M.A., Shakir, R., Shamsizadeh, M., Sheth, K.N., Shigematsu, M., Shoman, H., Silva, D.A.S., Smith, M., Sobngwi, E., Sposato, L.A., Stanaway, J.D., Stein, D.J., Steiner, T.J., Stovner, L.J., Abdulkader, R.S., El Szoeke, C., Tabarés-Seisdedos, R., Tanne, D., Theadom, A.M., Thrift, A.G., Tirschwell, D.L., Topor-Madry, R., Tran, B.X., Truelsen, T., Tuem, K.B., Ukwaja, K.N., Uthman, O.A., Varakin, Y.Y., Vasankari, T., Venketasubramanian, N., Vlassov, V.V., Wadilo, F., Wakayo, T., Wallin, M.T., Weiderpass, E., Westerman, R., Wijeratne, T., Wiysonge, C.S., Woldu, M.A., Wolfe, C.D.A., Xavier, D., Xu, G., Yano, Y., Yimam, H.H., Yonemoto, N., Yu, C., Zaidi, Z., El Sayed Zaki, M., Zunt, J.R., Murray, C.J.L., Vos, T., 2017. Global, regional, and national burden of neurological disorders during 1990–2015: a systematic analysis for the Global Burden of Disease Study 2015. The Lancet Neurology 16, 877–897. https://doi.org/10.1016/S1474-4422(17)30299-5

Fernie, A.R., Carrari, F., Sweetlove, L.J., 2004. Respiratory metabolism: glycolysis, the TCA cycle and mitochondrial electron transport. Curr Opin Plant Biol 7, 254–261. https://doi.org/10.1016/j.pbi.2004.03.007

Ferrero, H., Larrayoz, I.M., Martisova, E., Solas, M., Howlett, D.R., Francis, P.T., Gil-Bea, F.J., Martínez, A., Ramírez, M.J., 2018. Increased Levels of Brain Adrenomedullin in the Neuropathology of Alzheimer's Disease. Molecular Neurobiology 55, 5177–5183. https://doi.org/10.1007/s12035-017-0700-6

Franco-Iborra, S., Vila, M., Perier, C., 2016. The Parkinson Disease Mitochondrial Hypothesis: Where Are We at? Neuroscientist 22, 266–277. https://doi.org/10.1177/1073858415574600

Fransson, Å., Ruusala, A., Aspenström, P., 2003. Atypical Rho GTPases Have Roles in Mitochondrial Homeostasis and Apoptosis. Journal of Biological Chemistry 278, 6495–6502. https://doi.org/10.1074/jbc.M208609200

Friedman, J.R., Nunnari, J., 2014. Mitochondrial form and function. Nature 505, 335–343.

https://doi.org/10.1038/nature12985
Frith, C.D., Bloxham, C.A., Carpenter, K.N., 1986a. Impairments in the learning and performance of a new manual skill in patients with Parkinson's disease. Journal of Neurology, Neurosurgery & Psychiatry 49, 661–668. https://doi.org/10.1136/jnnp.49.6.661
Frith, C.D., Bloxham, C.A., Carpenter, K.N., 1986b. Impairments in the learning and performance of a new manual skill in patients with Parkinson's disease. Journal of neurology, neurosurgery, and psychiatry 49, 661–8. https://doi.org/10.1136/jnnp.49.6.661
Fu, H., Zhou, H., Yu, X., Xu, J., Zhou, J., Meng, X., Zhao, J., Zhou, Y., Chisholm, A.D., Xu, S., 2020. Wounding triggers MIRO-1 dependent mitochondrial fragmentation that accelerates epidermal wound closure through oxidative signaling. Nat Commun 11, 1050. https://doi.org/10.1038/s41467-020-14885-x
Fujiwara, H., Hasegawa, M., Dohmae, N., Kawashima, A., Masliah, E., Goldberg, M.S., Shen, J., Takio, K., Iwatsubo, T., 2002a. alpha-Synuclein is phosphorylated in synucleinopathy lesions. Nat Cell Biol 4, 160–164. https://doi.org/10.1038/ncb748
Fujiwara, H., Hasegawa, M., Dohmae, N., Kawashima, A., Masliah, E., Goldberg, M.S., Shen, J., Takio, K., Iwatsubo, T., 2002b. alpha-Synuclein is phosphorylated in synucleinopathy lesions. Nature cell biology 4, 160–4. https://doi.org/10.1038/ncb748
Furnish, M., Boulton, D.P., Genther, V., Grofova, D., Ellinwood, M.L., Romero, L., Lucia, M.S., Cramer, S.D., Caino, M.C., 2022. MIRO2 Regulates Prostate Cancer Cell Growth via GCN1-Dependent Stress Signaling. Mol Cancer Res 20, 607–621. https://doi.org/10.1158/1541-7786.MCR-21-0374
Gaig, C., Martí, M.J., Ezquerra, M., Cardozo, A., Rey, M.J., Tolosa, E., 2009. G2019S LRRK2 mutation causing Parkinson's disease without Lewy bodies. BMJ Case Rep 2009, bcr08.2008.0632. https://doi.org/10.1136/bcr.08.2008.0632
Gao, J., Sang, M., Zhang, X., Zheng, T., Pan, J., Dai, M., Zhou, L., Yang, S., 2015. Miro1-mediated mitochondrial dysfunction under high nutrient stress is linked to NOD-like receptor 3 (NLRP3)-dependent inflammatory responses in rat pancreatic beta cells. Free Radical Biology and Medicine 89, 322–332. https://doi.org/10.1016/j.freeradbiomed.2015.09.002
GBD 2015 Disease and Injury Incidence and Prevalence Collaborators, 2016. Global, regional, and national incidence, prevalence, and years lived with disability for 310 diseases and injuries, 1990-2015: a systematic analysis for the Global Burden of Disease Study 2015. Lancet 388, 1545–1602. https://doi.org/10.1016/S0140-6736(16)31678-6
Germer, E.L., Imhoff, S., Vilariño-Güell, C., Kasten, M., Seibler, P., Brüggemann, N., Klein, C., Trinh, J., 2019. The Role of Rare Coding Variants in Parkinson's Disease GWAS Loci. Frontiers in Neurology 10, 1284. https://doi.org/10.3389/fneur.2019.01284
Gialluisi, A., Reccia, M.G., Modugno, N., Nutile, T., Lombardi, A., Di Giovannantonio, L.G., Pietracupa, S., Ruggiero, D., Scala, S., Gambardella, S., Iacoviello, L., Gianfrancesco, F., Acampora, D., D'Esposito, M., Simeone, A., Ciullo, M., Esposito, T., 2021. Identification of sixteen novel candidate genes for late onset Parkinson's disease. Mol Neurodegener 16, 35. https://doi.org/10.1186/s13024-021-00455-2
Gispert, S., Ricciardi, F., Kurz, A., Azizov, M., Hoepken, H.-H., Becker, D., Voos, W., Leuner, K., Müller, W.E., Kudin, A.P., Kunz, W.S., Zimmermann, A., Roeper, J., Wenzel, D., Jendrach, M., García-Arencíbia, M., Fernández-Ruiz, J., Huber, L., Rohrer, H., Barrera, M., Reichert, A.S., Rüb, U., Chen, A., Nussbaum, R.L., Auburger, G., 2009. Parkinson phenotype in aged PINK1-deficient mice is accompanied by progressive mitochondrial dysfunction in absence of neurodegeneration. PLoS One 4, e5777. https://doi.org/10.1371/journal.pone.0005777
Glaab, E., Schneider, R., 2015. Comparative pathway and network analysis of brain transcriptome changes during adult aging and in Parkinson's disease. Neurobiology of Disease 74, 1–13. https://doi.org/10.1016/j.nbd.2014.11.002
Goldberg, Matthew S., Fleming, S.M., Palacino, J.J., Cepeda, C., Lam, H.A., Bhatnagar, A., Meloni, E.G., Wu, N., Ackerson, L.C., Klapstein, G.J., Gajendiran, M., Roth, B.L., Chesselet, M.-F., Maidment,

N.T., Levine, M.S., Shen, J., 2003. Parkin-deficient Mice Exhibit Nigrostriatal Deficits but Not Loss of Dopaminergic Neurons *. Journal of Biological Chemistry 278, 43628–43635. https://doi.org/10.1074/jbc.M308947200

Goldberg, Matthew S, Fleming, S.M., Palacino, J.J., Cepeda, C., Lam, H.A., Bhatnagar, A., Meloni, E.G., Wu, N., Ackerson, L.C., Klapstein, G.J., Gajendiran, M., Roth, B.L., Chesselet, M.-F., Maidment, N.T., Levine, M.S., Shen, J., 2003. Parkin-deficient Mice Exhibit Nigrostriatal Deficits but Not Loss of Dopaminergic Neurons. Journal of Biological Chemistry 278, 43628–43635. https://doi.org/10.1074/jbc.M308947200

Goldman, S.M., Marek, K., Ottman, R., Meng, C., Comyns, K., Chan, P., Ma, J., Marras, C., Langston, J.W., Ross, G.W., Tanner, C.M., 2019. Concordance for Parkinson's disease in twins: A 20-year update. Ann Neurol 85, 600–605. https://doi.org/10.1002/ana.25441

Grossmann, D., Berenguer-Escuder, C., Bellet, M.E., Scheibner, D., Bohler, J., Massart, F., Rapaport, D., Skupin, A., Fouquier d'Hérouël, A., Sharma, M., Ghelfi, J., Raković, A., Lichtner, P., Antony, P., Glaab, E., May, P., Dimmer, K.S., Fitzgerald, J.C., Grünewald, A., Krüger, R., 2019a. Mutations in *RHOT1* Disrupt Endoplasmic Reticulum–Mitochondria Contact Sites Interfering with Calcium Homeostasis and Mitochondrial Dynamics in Parkinson's Disease. Antioxidants & Redox Signaling 31, 1213–1234. https://doi.org/10.1089/ars.2018.7718

Grossmann, D., Berenguer-Escuder, C., Bellet, M.E., Scheibner, D., Bohler, J., Massart, F., Rapaport, D., Skupin, A., Fouquier d'Hérouël, A., Sharma, M., Ghelfi, J., Raković, A., Lichtner, P., Antony, P., Glaab, E., May, P., Dimmer, K.S., Fitzgerald, J.C., Grünewald, A., Krüger, R., 2019b. Mutations in RHOT1 Disrupt Endoplasmic Reticulum–Mitochondria Contact Sites Interfering with Calcium Homeostasis and Mitochondrial Dynamics in Parkinson's Disease. Antioxidants & Redox Signaling 31, 1213–1234. https://doi.org/10.1089/ars.2018.7718

Grossmann, D., Berenguer-Escuder, C., Chemla, A., Arena, G., Krüger, R., 2020a. The Emerging Role of RHOT1/Miro1 in the Pathogenesis of Parkinson's Disease. Front. Neurol. 11, 587. https://doi.org/10.3389/fneur.2020.00587

Grossmann, D., Berenguer-Escuder, C., Chemla, A., Arena, G., Krüger, R., 2020b. The Emerging Role of RHOT1/Miro1 in the Pathogenesis of Parkinson's Disease. Frontiers in neurology 11, 587. https://doi.org/10.3389/fneur.2020.00587

Grossmann, D., Krüger, R., 2020. The Emerging Role of RHOT1/Miro1 in the Pathogenesis of Parkinson's Disease. Frontiers in Neurology 11, 20.

Groten, C.J., MacVicar, B.A., 2022. Mitochondrial Ca2+ uptake by the MCU facilitates pyramidal neuron excitability and metabolism during action potential firing. Commun Biol 5, 1–15. https://doi.org/10.1038/s42003-022-03848-1

Grünewald, A., Kumar, K.R., Sue, C.M., 2019. New insights into the complex role of mitochondria in Parkinson's disease. Prog Neurobiol 177, 73–93. https://doi.org/10.1016/j.pneurobio.2018.09.003

Grünewald, A., Rygiel, K.A., Hepplewhite, P.D., Morris, C.M., Picard, M., Turnbull, D.M., 2016. Mitochondrial DNA Depletion in Respiratory Chain-Deficient Parkinson Disease Neurons. Ann Neurol 79, 366–378. https://doi.org/10.1002/ana.24571

Guardia-Laguarta, C., Area-Gomez, E., Rüb, C., Liu, Y., Magrané, J., Becker, D., Voos, W., Schon, E.A., Przedborski, S., 2014. α-Synuclein Is Localized to Mitochondria-Associated ER Membranes. J. Neurosci. 34, 249–259. https://doi.org/10.1523/JNEUROSCI.2507-13.2014

Guo, X., Macleod, G.T., Wellington, A., Hu, F., Panchumarthi, S., Schoenfield, M., Marin, L., Charlton, M.P., Atwood, H.L., Zinsmaier, K.E., 2005. The GTPase dMiro Is Required for Axonal Transport of Mitochondria to Drosophila Synapses. Neuron 47, 379–393. https://doi.org/10.1016/j.neuron.2005.06.027

Haddad, D., Nakamura, K., 2016. Understanding the susceptibility of dopamine neurons to mitochondrial stressors in Parkinson's disease 28.

Haenseler, W., Sansom, S.N., Buchrieser, J., Newey, S.E., Moore, C.S., Nicholls, F.J., Chintawar, S., Schnell, C., Antel, J.P., Allen, N.D., Cader, M.Z., Wade-Martins, R., James, W.S., Cowley, S.A.,

2017. A Highly Efficient Human Pluripotent Stem Cell Microglia Model Displays a Neuronal-Co-culture-Specific Expression Profile and Inflammatory Response. Stem Cell Reports 8, 1727–1742. https://doi.org/10.1016/j.stemcr.2017.05.017

Han, J.Y., Choi, T.S., Kim, H.I., 2018a. Molecular Role of Ca2+ and Hard Divalent Metal Cations on Accelerated Fibrillation and Interfibrillar Aggregation of α-Synuclein. Sci Rep 8, 1895. https://doi.org/10.1038/s41598-018-20320-5

Han, J.Y., Choi, T.S., Kim, H.I., 2018b. Molecular Role of Ca2+ and Hard Divalent Metal Cations on Accelerated Fibrillation and Interfibrillar Aggregation of α-Synuclein. Scientific Reports 8, 1895. https://doi.org/10.1038/s41598-018-20320-5

Hawkes, C.H., 2008. The prodromal phase of sporadic Parkinson's disease: does it exist and if so how long is it? Mov Disord 23, 1799–1807. https://doi.org/10.1002/mds.22242

Hely, M.A., Morris, J.G.L., Reid, W.G.J., Trafficante, R., 2005. Sydney Multicenter Study of Parkinson's disease: non-L-dopa-responsive problems dominate at 15 years. Mov Disord 20, 190–199. https://doi.org/10.1002/mds.20324

Hiller, K., Hangebrauk, J., Jäger, C., Spura, J., Schreiber, K., Schomburg, D., 2009. MetaboliteDetector: comprehensive analysis tool for targeted and nontargeted GC/MS based metabolome analysis. Analytical chemistry 81, 3429–39. https://doi.org/10.1021/ac802689c

Hinkle, K.M., Yue, M., Behrouz, B., Dächsel, J.C., Lincoln, S.J., Bowles, E.E., Beevers, J.E., Dugger, B., Winner, B., Prots, I., Kent, C.B., Nishioka, K., Lin, W.-L., Dickson, D.W., Janus, C.J., Farrer, M.J., Melrose, H.L., 2012. LRRK2 knockout mice have an intact dopaminergic system but display alterations in exploratory and motor co-ordination behaviors. Mol Neurodegener 7, 25. https://doi.org/10.1186/1750-1326-7-25

Hirokawa, N., Noda, Y., Okada, Y., 1998. Kinesin and dynein superfamily proteins in organelle transport and cell division. Current Opinion in Cell Biology 10, 60–73. https://doi.org/10.1016/S0955-0674(98)80087-2

Howlett, E.H., Jensen, N., Belmonte, F., Zafar, F., Hu, X., Kluss, J., Schüle, B., Kaufman, B.A., Greenamyre, J.T., Sanders, L.H., 2017. LRRK2 G2019S-induced mitochondrial DNA damage is LRRK2 kinase dependent and inhibition restores mtDNA integrity in Parkinson's disease. Hum Mol Genet 26, 4340–4351. https://doi.org/10.1093/hmg/ddx320

Hsieh, C.-H., Li, L., Vanhauwaert, R., Nguyen, K.T., Davis, M.D., Bu, G., Wszolek, Z.K., Wang, X., 2019a. Miro1 Marks Parkinson's Disease Subset and Miro1 Reducer Rescues Neuron Loss in Parkinson's Models. Cell Metabolism 30, 1131-1140.e7. https://doi.org/10.1016/j.cmet.2019.08.023

Hsieh, C.-H., Li, L., Vanhauwaert, R., Nguyen, K.T., Davis, M.D., Bu, G., Wszolek, Z.K., Wang, X., 2019b. Miro1 Marks Parkinson's Disease Subset and Miro1 Reducer Rescues Neuron Loss in Parkinson's Models. Cell metabolism 30, 1131-1140.e7. https://doi.org/10.1016/j.cmet.2019.08.023

Hsieh, C.-H., Shaltouki, A., Gonzalez, A.E., Bettencourt da Cruz, A., Burbulla, L.F., St. Lawrence, E., Schüle, B., Krainc, D., Palmer, T.D., Wang, X., 2016a. Functional Impairment in Miro Degradation and Mitophagy Is a Shared Feature in Familial and Sporadic Parkinson's Disease. Cell Stem Cell 19, 709–724. https://doi.org/10.1016/j.stem.2016.08.002

Hsieh, C.-H., Shaltouki, A., Gonzalez, A.E., Bettencourt da Cruz, A., Burbulla, L.F., St. Lawrence, E., Schüle, B., Krainc, D., Palmer, T.D., Wang, X., 2016b. Functional Impairment in Miro Degradation and Mitophagy Is a Shared Feature in Familial and Sporadic Parkinson's Disease. Cell Stem Cell 19, 709–724. https://doi.org/10.1016/j.stem.2016.08.002

Jackson, J.G., Robinson, M.B., 2015. Reciprocal Regulation of Mitochondrial Dynamics and Calcium Signaling in Astrocyte Processes. Journal of Neuroscience 35, 15199–15213. https://doi.org/10.1523/JNEUROSCI.2049-15.2015

Jaeger, C., Glaab, E., Michelucci, A., Binz, T.M., Koeglsberger, S., Garcia, P., Trezzi, J.-P., Ghelfi, J., Balling, R., Buttini, M., 2015. The mouse brain metabolome: region-specific signatures and response to excitotoxic neuronal injury. The American journal of pathology 185, 1699–712.

https://doi.org/10.1016/j.ajpath.2015.02.016
Jäger, C., Hiller, K., Buttini, M., 2016. Metabolic Profiling and Quantification of Neurotransmitters in Mouse Brain by Gas Chromatography-Mass Spectrometry. Current protocols in mouse biology 6, 333–342. https://doi.org/10.1002/cpmo.15
Jakkamsetti, V., Scudder, W., Kathote, G., Ma, Q., Angulo, G., Dobariya, A., Rosenberg, R.N., Beutler, B., Pascual, J.M., 2021. Quantification of early learning and movement sub-structure predictive of motor performance. Scientific Reports 11, 14405. https://doi.org/10.1038/s41598-021-93944-9
Jankovic, J., 2008. Parkinson's disease: clinical features and diagnosis. J Neurol Neurosurg Psychiatry 79, 368–376. https://doi.org/10.1136/jnnp.2007.131045
Jo, D.S., Park, N.Y., Cho, D.-H., 2020. Peroxisome quality control and dysregulated lipid metabolism in neurodegenerative diseases. Exp Mol Med 52, 1486–1495. https://doi.org/10.1038/s12276-020-00503-9
Johansen, K.K., Torp, S.H., Farrer, M.J., Gustavsson, E.K., Aasly, J.O., 2018. A Case of Parkinson's Disease with No Lewy Body Pathology due to a Homozygous Exon Deletion in Parkin. Case Rep Neurol Med 2018, 6838965. https://doi.org/10.1155/2018/6838965
Johnson, B., 2022. Parkinson's disease drug hunters think outside the α-synuclein box. Nature Biotechnology 40, 1705–1707. https://doi.org/10.1038/s41587-022-01610-w
Joksimovic, S.Lj., Joksimovic, S.M., Tesic, V., García-Caballero, A., Feseha, S., Zamponi, G.W., Jevtovic-Todorovic, V., Todorovic, S.M., 2018. Selective inhibition of Cav3.2 channels reverses hyperexcitability of peripheral nociceptors and alleviates post-surgical pain. Sci Signal 11, eaao4425. https://doi.org/10.1126/scisignal.aao4425
Jouaville, L.S., Pinton, P., Bastianutto, C., Rutter, G.A., Rizzuto, R., 1999. Regulation of mitochondrial ATP synthesis by calcium: Evidence for a long-term metabolic priming. Proc. Natl. Acad. Sci. U.S.A. 96, 13807–13812. https://doi.org/10.1073/pnas.96.24.13807
Kalia, L.V., Lang, A.E., 2015. Parkinson's disease. Lancet 386, 896–912. https://doi.org/10.1016/S0140-6736(14)61393-3
Kalinski, A.L., Kar, A.N., Craver, J., Tosolini, A.P., Sleigh, J.N., Lee, S.J., Hawthorne, A., Brito-Vargas, P., Miller-Randolph, S., Passino, R., Shi, L., Wong, V.S.C., Picci, C., Smith, D.S., Willis, D.E., Havton, L.A., Schiavo, G., Giger, R.J., Langley, B., Twiss, J.L., 2019. Deacetylation of Miro1 by HDAC6 blocks mitochondrial transport and mediates axon growth inhibition. J. Cell Biol. 218, 1871–1890. https://doi.org/10.1083/jcb.201702187
Kang, K., Kim, J., Ryu, B., Lee, S.-G., Oh, M.-S., Baek, J., Ren, X., Canavero, S., Kim, C.-Y., Chung, H.M., 2021. BAPTA, a calcium chelator, neuroprotects injured neurons in vitro and promotes motor recovery after spinal cord transection in vivo. CNS Neuroscience & Therapeutics 27, 919–929. https://doi.org/10.1111/cns.13651
Karampetsou, M., Ardah, M.T., Semitekolou, M., Polissidis, A., Samiotaki, M., Kalomoiri, M., Majbour, N., Xanthou, G., El-Agnaf, O.M.A., Vekrellis, K., 2017. Phosphorylated exogenous alpha-synuclein fibrils exacerbate pathology and induce neuronal dysfunction in mice. Sci Rep 7, 16533. https://doi.org/10.1038/s41598-017-15813-8
Karbowski, M., Youle, R.J., 2003. Dynamics of mitochondrial morphology in healthy cells and during apoptosis. Cell Death Differ 10, 870–880. https://doi.org/10.1038/sj.cdd.4401260
Kay, L., Pienaar, I.S., Cooray, R., Black, G., Soundararajan, M., 2018. Understanding Miro GTPases: Implications in the Treatment of Neurodegenerative Disorders. Mol Neurobiol 55, 7352–7365. https://doi.org/10.1007/s12035-018-0927-x
Keller, M.F., Saad, M., Bras, J., Bettella, F., Nicolaou, N., Simón-Sánchez, J., Mittag, F., Büchel, F., Sharma, M., Gibbs, J.R., Schulte, C., Moskvina, V., Durr, A., Holmans, P., Kilarski, L.L., Guerreiro, R., Hernandez, D.G., Brice, A., Ylikotila, P., Stefánsson, H., Majamaa, K., Morris, H.R., Williams, N., Gasser, T., Heutink, P., Wood, N.W., Hardy, J., Martinez, M., Singleton, A.B., Nalls, M.A., International Parkinson's Disease Genomics Consortium (IPDGC), Wellcome Trust Case Control Consortium 2 (WTCCC2), 2012. Using genome-wide complex trait analysis

to quantify “missing heritability” in Parkinson’s disease. Hum Mol Genet 21, 4996–5009. https://doi.org/10.1093/hmg/dds335

Kia, D.A., Zhang, D., Guelfi, S., Manzoni, C., Hubbard, L., Reynolds, R.H., Botía, J., Ryten, M., Ferrari, R., Lewis, P.A., Williams, N., Trabzuni, D., Hardy, J., Wood, N.W., United Kingdom Brain Expression Consortium (UKBEC) and the International Parkinson’s Disease Genomics Consortium (IPDGC), Noyce, A.J., Kaiyrzhanov, R., Middlehurst, B., Kia, D.A., Tan, M., Houlden, H., Morris, H.R., Plun-Favreau, H., Holmans, P., Hardy, J., Trabzuni, D., Bras, J., PhD, J.Q., Mok, K.Y., Kinghorn, K.J., Billingsley, K., Wood, N.W., Lewis, P., Schreglmann, S., Guerreiro, R., Lovering, R., R’Bibo, L., Manzoni, C., Rizig, M., Ryten, M., Guelfi, S., Escott-Price, V., Chelban, V., Foltynie, T., Williams, N., Brice, A., Danjou, F., Lesage, S., Corvol, J.-C., Martinez, M., Schulte, C., Brockmann, K., Simón-Sánchez, J., Heutink, P., Rizzu, P., Sharma, M., Gasser, T., Nicolas, A., Cookson, M.R., Bandres-Ciga, S., Blauwendraat, C., Craig, D.W., Faghri, F., Gibbs, J.R., Hernandez, D.G., Van Keuren-Jensen, K., Shulman, J.M., Leonard, H.L., Nalls, M.A., Robak, L., Lubbe, S., Finkbeiner, S., Mencacci, N.E., Lungu, C., Singleton, A.B., Scholz, S.W., Reed, X., Alcalay, R.N., Gan-Or, Z., Rouleau, G.A., Krohn, L., van Hilten, J.J., Marinus, J., Adarmes-Gómez, A.D., Aguilar, M., Alvarez, I., Alvarez, V., Javier Barrero, F., Bergareche Yarza, J.A., Bernal-Bernal, I., Blazquez, M., Bonilla-Toribio, M., Botía, J.A., Boungiorno, M.T., Buiza-Rueda, D., Càmara, A., Carrillo, F., Carrión-Claro, M., Cerdan, D., Clarimón, J., Compta, Y., Diez-Fairen, M., Dols-Icardo, O., Duarte, J., Duran, R., Escamilla-Sevilla, F., Ezquerra, M., Feliz, C., Fernàndez, M., Fernàndez-Santiago, R., Garcia, C., García-Ruiz, P., Gómez-Garre, P., Gomez Heredia, M.J., Gonzalez-Aramburu, I., Pagola, A.G., Hoenicka, J., Infante, J., Jimenez-Escrig, A., Kulisevsky, J., Labrador-Espinosa, M.A., Lopez-Sendon, J.L., Arregui, A.L. de M., Macias, D., Torres, I.M., Marín, J., Marti, M.J., Martínez-Castrillo, J.C., Mèndez-del-Barrio, C., González, M.M., Adolfo Mínguez, M.M., Mir, P., Rezola, E.M., Muñoz, E., Pagonabarraga, J., Pastor, P., Errazquin, F.P., Perinán-Tocino, T., Ruiz-Martínez, J., Ruz, C., Rodriguez, A.S., Sierra, M., Suarez-Sanmartin, E., Tabernero, C., Tartari, J.P., Tejera-Parrado, C., Tolosa, E., Valldeoriola, F., Vargas-González, L., Vela, L., Vives, F., Zimprich, A., Pihlstrom, L., Toft, M., Koks, S., Taba, P., Hassin-Baer, S., Weale, M., Ramasamy, A., Smith, C., Guelfi, M.S., D’sa, K., Forabosco, P., Botiá, J.A., 2021. Identification of Candidate Parkinson Disease Genes by Integrating Genome-Wide Association Study, Expression, and Epigenetic Data Sets. JAMA Neurol. https://doi.org/10.1001/jamaneurol.2020.5257

Kim, C., Alcalay, R., 2017. Genetic Forms of Parkinson’s Disease. Seminars in Neurology 37, 135–146. https://doi.org/10.1055/s-0037-1601567

Kitada, T., Tong, Y., Gautier, C.A., Shen, J., 2009. Absence of nigral degeneration in aged parkin/DJ-1/PINK1 triple knockout mice. Journal of Neurochemistry 111, 696–702. https://doi.org/10.1111/j.1471-4159.2009.06350.x

Klosowiak, J.L., Focia, P.J., Chakravarthy, S., Landahl, E.C., Freymann, D.M., Rice, S.E., 2013. Structural coupling of the EF hand and C-terminal GTPase domains in the mitochondrial protein Miro. EMBO Rep 14, 968–974. https://doi.org/10.1038/embor.2013.151

Klosowiak, J.L., Park, S., Smith, K.P., French, M.E., Focia, P.J., Freymann, D.M., Rice, S.E., 2016a. Structural insights into Parkin substrate lysine targeting from minimal Miro substrates. Sci Rep 6, 33019. https://doi.org/10.1038/srep33019

Klosowiak, J.L., Park, S., Smith, K.P., French, M.E., Focia, P.J., Freymann, D.M., Rice, S.E., 2016b. Structural insights into Parkin substrate lysine targeting from minimal Miro substrates. Scientific reports 6, 33019. https://doi.org/10.1038/srep33019

König, T., Nolte, H., Aaltonen, M.J., Tatsuta, T., Krols, M., Stroh, T., Langer, T., McBride, H.M., 2021. MIROs and DRP1 drive mitochondrial-derived vesicle biogenesis and promote quality control. Nat Cell Biol 23, 1271–1286. https://doi.org/10.1038/s41556-021-00798-4

Koshiba, T., Holman, H.A., Kubara, K., Yasukawa, K., Kawabata, S., Okamoto, K., Macfarlane, J., Shaw, J.M., 2011. Structure-Function Analysis of the Yeast Mitochondrial Rho GTPase, Gem1p: IMPLICATIONS FOR MITOCHONDRIAL INHERITANCE. J. Biol. Chem. 286, 354–362.

https://doi.org/10.1074/jbc.M110.180034
Krüger, R., Kuhn, W., Müller, T., Woitalla, D., Graeber, M., Kösel, S., Przuntek, H., Epplen, J.T., Schöls, L., Riess, O., 1998. Ala30Pro mutation in the gene encoding alpha-synuclein in Parkinson's disease. Nat Genet 18, 106–108. https://doi.org/10.1038/ng0298-106
Kruman, I.I., Mattson, M.P., 1999. Pivotal role of mitochondrial calcium uptake in neural cell apoptosis and necrosis. J Neurochem 72, 529–540. https://doi.org/10.1046/j.1471-4159.1999.0720529.x
Kumar, A., Kopra, J., Varendi, K., Porokuokka, L.L., Panhelainen, A., Kuure, S., Marshall, P., Karalija, N., Härma, M.-A., Vilenius, C., Lilleväli, K., Tekko, T., Mijatovic, J., Pulkkinen, N., Jakobson, Madis, Jakobson, Maili, Ola, R., Palm, E., Lindahl, M., Strömberg, I., Võikar, V., Piepponen, T.P., Saarma, M., Andressoo, J.-O., 2015. GDNF Overexpression from the Native Locus Reveals its Role in the Nigrostriatal Dopaminergic System Function. PLOS Genetics 11, e1005710. https://doi.org/10.1371/journal.pgen.1005710
La Manno, G., Gyllborg, D., Codeluppi, S., Nishimura, K., Salto, C., Zeisel, A., Borm, L.E., Stott, S.R.W., Toledo, E.M., Villaescusa, J.C., Lönnerberg, P., Ryge, J., Barker, R.A., Arenas, E., Linnarsson, S., 2016. Molecular Diversity of Midbrain Development in Mouse, Human, and Stem Cells. Cell 167, 566-580.e19. https://doi.org/10.1016/j.cell.2016.09.027
LaMonte, B.H., Wallace, K.E., Holloway, B.A., Shelly, S.S., Ascaño, J., Tokito, M., Van Winkle, T., Howland, D.S., Holzbaur, E.L.F., 2002. Disruption of Dynein/Dynactin Inhibits Axonal Transport in Motor Neurons Causing Late-Onset Progressive Degeneration. Neuron 34, 715–727. https://doi.org/10.1016/S0896-6273(02)00696-7
Langston, J.W., 2006. The Parkinson's complex: parkinsonism is just the tip of the iceberg. Ann Neurol 59, 591–596. https://doi.org/10.1002/ana.20834
Langston, J.W., Ballard, P., Tetrud, J.W., Irwin, I., 1983. Chronic Parkinsonism in humans due to a product of meperidine-analog synthesis. Science 219, 979–980. https://doi.org/10.1126/science.6823561
Langston, J.W., Forno, L.S., Rebert, C.S., Irwin, I., 1984. Selective nigral toxicity after systemic administration of 1-methyl-4-phenyl-1,2,5,6-tetrahydropyrine (MPTP) in the squirrel monkey. Brain Res 292, 390–394. https://doi.org/10.1016/0006-8993(84)90777-7
Larráyoz, I.M., Martínez, A., 2012. Proadrenomedullin N-terminal 20 peptide increases kinesin's velocity both in vitro and in vivo. Endocrinology 153, 1734–42. https://doi.org/10.1210/en.2011-1685
Larsen, S.B., Hanss, Z., Krüger, R., 2018. The genetic architecture of mitochondrial dysfunction in Parkinson's disease. Cell Tissue Res 373, 21–37. https://doi.org/10.1007/s00441-017-2768-8
Lautenschläger, J., Stephens, A.D., Fusco, G., Ströhl, F., Curry, N., Zacharopoulou, M., Michel, C.H., Laine, R., Nespovitaya, N., Fantham, M., Pinotsi, D., Zago, W., Fraser, P., Tandon, A., St George-Hyslop, P., Rees, E., Phillips, J.J., De Simone, A., Kaminski, C.F., Schierle, G.S.K., 2018. C-terminal calcium binding of α-synuclein modulates synaptic vesicle interaction. Nat Commun 9, 712. https://doi.org/10.1038/s41467-018-03111-4
Lautrup, S., Sinclair, D.A., Mattson, M.P., Fang, E.F., 2019. NAD+ in Brain Aging and Neurodegenerative Disorders. Cell Metabolism 30, 630–655. https://doi.org/10.1016/j.cmet.2019.09.001
Leandrou, E., Emmanouilidou, E., Vekrellis, K., 2019a. Voltage-Gated Calcium Channels and α-Synuclein: Implications in Parkinson's Disease. Front. Mol. Neurosci. 12, 237. https://doi.org/10.3389/fnmol.2019.00237
Leandrou, E., Emmanouilidou, E., Vekrellis, K., 2019b. Voltage-Gated Calcium Channels and α-Synuclein: Implications in Parkinson's Disease. Frontiers in Molecular Neuroscience 12, 237. https://doi.org/10.3389/fnmol.2019.00237
Lee, K.-S., Huh, S., Lee, S., Wu, Z., Kim, A.-K., Kang, H.-Y., Lu, B., 2018. Altered ER–mitochondria contact impacts mitochondria calcium homeostasis and contributes to neurodegeneration in vivo in disease models. Proc Natl Acad Sci U S A 115, E8844–E8853.

https://doi.org/10.1073/pnas.1721136115
Lee, K.-W., Chen, W., Junn, E., Im, J.-Y., Grosso, H., Sonsalla, P.K., Feng, X., Ray, N., Fernandez, J.R., Chao, Y., Masliah, E., Voronkov, M., Braithwaite, S.P., Stock, J.B., Mouradian, M.M., 2011a. Enhanced Phosphatase Activity Attenuates α-Synucleinopathy in a Mouse Model. J. Neurosci. 31, 6963–6971. https://doi.org/10.1523/JNEUROSCI.6513-10.2011
Lee, K.-W., Chen, W., Junn, E., Im, J.-Y., Grosso, H., Sonsalla, P.K., Feng, X., Ray, N., Fernandez, J.R., Chao, Y., Masliah, E., Voronkov, M., Braithwaite, S.P., Stock, J.B., Mouradian, M.M., 2011b. Enhanced phosphatase activity attenuates α-synucleinopathy in a mouse model. The Journal of neuroscience : the official journal of the Society for Neuroscience 31, 6963–71. https://doi.org/10.1523/JNEUROSCI.6513-10.2011
Lee, S., Lee, K.-S., Huh, S., Liu, S., Lee, D.-Y., Hong, S.H., Yu, K., Lu, B., 2016. Polo Kinase Phosphorylates Miro to Control ER-Mitochondria Contact Sites and Mitochondrial Ca2+ Homeostasis in Neural Stem Cell Development. Developmental Cell 37, 174–189. https://doi.org/10.1016/j.devcel.2016.03.023
Li, B., Guo, Y.-S., Sun, M.-M., Dong, H., Wu, S.-Y., Wu, D.-X., Li, C.-Y., 2008. The NADPH oxidase is involved in lipopolysaccharide-mediated motor neuron injury. Brain Research 1226, 199–208. https://doi.org/10.1016/j.brainres.2008.06.024
Li, B., Zhang, Y., Li, H., Shen, H., Wang, Y., Li, X., Cui, G., Chen, G., 2021. Miro1 Regulates Neuronal Mitochondrial Transport and Distribution to Alleviate Neuronal Damage in Secondary Brain Injury After Intracerebral Hemorrhage in Rats. Cell Mol Neurobiol 41, 795–812. https://doi.org/10.1007/s10571-020-00887-2
Li, J.-M., Li, X., Chan, L.W.C., Hu, R., Zheng, T., Li, H., Yang, S., 2023. Lipotoxicity-polarised macrophage-derived exosomes regulate mitochondrial fitness through Miro1-mediated mitophagy inhibition and contribute to type 2 diabetes development in mice. Diabetologia 66, 2368–2386. https://doi.org/10.1007/s00125-023-05992-7
Li, L., Conradson, D.M., Bharat, V., Kim, M.J., Hsieh, C.-H., Minhas, P.S., Papakyrikos, A.M., Durairaj, A.S., Ludlam, A., Andreasson, K.I., Partridge, L., Cianfrocco, M.A., Wang, X., 2021a. A mitochondrial membrane-bridging machinery mediates signal transduction of intramitochondrial oxidation. Nat Metab 3, 1242–1258. https://doi.org/10.1038/s42255-021-00443-2
Li, L., Conradson, D.M., Bharat, V., Kim, M.J., Hsieh, C.-H., Minhas, P.S., Papakyrikos, A.M., Durairaj, A.S., Ludlam, A., Andreasson, K.I., Partridge, L., Cianfrocco, M.A., Wang, X., 2021b. A mitochondrial membrane-bridging machinery mediates signal transduction of intramitochondrial oxidation. Nature Metabolism 3, 1242–1258. https://doi.org/10.1038/s42255-021-00443-2
Li, L., Conradson, D.M., Bharat, V., Kim, M.J., Hsieh, C.-H., Minhas, P.S., Papakyrikos, A.M., Durairaj, A.S., Ludlam, A., Andreasson, K.I., Partridge, L., Cianfrocco, M.A., Wang, X., 2021c. A mitochondrial membrane-bridging machinery mediates signal transduction of intramitochondrial oxidation. Nature metabolism 3, 1242–1258. https://doi.org/10.1038/s42255-021-00443-2
Li, X., Tao, Yezheng, Bradley, R., Du, Z., Tao, Yunlong, Kong, L., Dong, Y., Jones, J., Yan, Y., Harder, C.R.K., Friedman, L.M., Bilal, M., Hoffmann, B., Zhang, S.-C., 2018. Fast Generation of Functional Subtype Astrocytes from Human Pluripotent Stem Cells. Stem Cell Reports 11, 998–1008. https://doi.org/10.1016/j.stemcr.2018.08.019
Li, Xujun, Chan, L.W.C., Li, Xianyu, Liu, C., Yang, G., Gao, J., Dai, M., Wang, Y., Xie, Z., Liu, J., Zhou, F., Zheng, T., Feng, D., Guo, S., Li, H., Sun, K., Yang, S., 2020. Obesity-Induced Regulator of Calcineurin 1 Overexpression Leads to β-Cell Failure Through Mitophagy Pathway Inhibition. Antioxidants & Redox Signaling 32, 413–428. https://doi.org/10.1089/ars.2019.7806
Liao, Y., Smyth, G.K., Shi, W., 2019. The R package Rsubread is easier, faster, cheaper and better for alignment and quantification of RNA sequencing reads. Nucleic Acids Research 47, e47–e47. https://doi.org/10.1093/nar/gkz114

Liu, G., Yu, J., Ding, J., Xie, C., Sun, L., Rudenko, I., Zheng, W., Sastry, N., Luo, J., Rudow, G., Troncoso, J.C., Cai, H., 2014. Aldehyde dehydrogenase 1 defines and protects a nigrostriatal dopaminergic neuron subpopulation. J Clin Invest 124, 3032–3046. https://doi.org/10.1172/JCI72176

Liu, S., Sawada, T., Lee, S., Yu, W., Silverio, G., Alapatt, P., Millan, I., Shen, A., Saxton, W., Kanao, T., Takahashi, R., Hattori, N., Imai, Y., Lu, B., 2012. Parkinson's Disease–Associated Kinase PINK1 Regulates Miro Protein Level and Axonal Transport of Mitochondria. PLoS Genet 8, e1002537. https://doi.org/10.1371/journal.pgen.1002537

López-Doménech, G., Higgs, N.F., Vaccaro, V., Roš, H., Arancibia-Cárcamo, I.L., MacAskill, A.F., Kittler, J.T., 2016a. Loss of Dendritic Complexity Precedes Neurodegeneration in a Mouse Model with Disrupted Mitochondrial Distribution in Mature Dendrites. Cell Reports 17, 317–327. https://doi.org/10.1016/j.celrep.2016.09.004

López-Doménech, G., Higgs, N.F., Vaccaro, V., Roš, H., Arancibia-Cárcamo, I.L., MacAskill, A.F., Kittler, J.T., 2016b. Loss of Dendritic Complexity Precedes Neurodegeneration in a Mouse Model with Disrupted Mitochondrial Distribution in Mature Dendrites. Cell reports 17, 317–327. https://doi.org/10.1016/j.celrep.2016.09.004

López-Doménech, G., Howden, J.H., Covill-Cooke, C., Morfill, C., Patel, J.V., Bürli, R., Crowther, D., Birsa, N., Brandon, N.J., Kittler, J.T., 2021. Loss of neuronal Miro1 disrupts mitophagy and induces hyperactivation of the integrated stress response. The EMBO Journal 40, e100715. https://doi.org/10.15252/embj.2018100715

López-Doménech, G., Howden, J.H., Covill-Cooke, C., Morfill, C., Patel, J. V, Bürli, R., Crowther, D., Birsa, N., Brandon, N.J., Kittler, J.T., 2021. Loss of neuronal Miro1 disrupts mitophagy and induces hyperactivation of the integrated stress response. The EMBO Journal 40, e100715. https://doi.org/10.15252/embj.2018100715

Love, M.I., Huber, W., Anders, S., 2014. Moderated estimation of fold change and dispersion for RNA-seq data with DESeq2. Genome Biology 15, 550. https://doi.org/10.1186/s13059-014-0550-8

Luo, Y., Hoffer, A., Hoffer, B., Qi, X., 2015. Mitochondria: A Therapeutic Target for Parkinson's Disease? Int J Mol Sci 16, 20704–20730. https://doi.org/10.3390/ijms160920704

MacAskill, A.F., Brickley, K., Stephenson, F.A., Kittler, J.T., 2009a. GTPase dependent recruitment of Grif-1 by Miro1 regulates mitochondrial trafficking in hippocampal neurons. Molecular and Cellular Neuroscience 40, 301–312. https://doi.org/10.1016/j.mcn.2008.10.016

MacAskill, A.F., Rinholm, J.E., Twelvetrees, A.E., Arancibia-Carcamo, I.L., Muir, J., Fransson, A., Aspenstrom, P., Attwell, D., Kittler, J.T., 2009b. Miro1 Is a Calcium Sensor for Glutamate Receptor-Dependent Localization of Mitochondria at Synapses. Neuron 61, 541–555. https://doi.org/10.1016/j.neuron.2009.01.030

Mahmoodazdeh, A., Shafiee, S.M., Sisakht, M., Khoshdel, Z., Takhshid, M.A., 2020. Adrenomedullin protects rat dorsal root ganglion neurons against doxorubicin-induced toxicity by ameliorating oxidative stress. Iranian journal of basic medical sciences 23, 1197–1206. https://doi.org/10.22038/ijbms.2020.45134.10514

Makarious, M.B., Lake, J., Pitz, V., Fu, A.Y., Guidubaldi, J.L., Solsberg, C.W., Bandres-Ciga, S., Leonard, H.L., Kim, J.J., Billingsley, K.J., Grenn, F.P., Jerez, P.A., Alvarado, C.X., Iwaki, H., Ta, M., Vitale, D., Hernandez, D., Torkamani, A., Ryten, M., Hardy, J., Scholz, S.W., Traynor, B.J., Dalgard, C.L., Ehrlich, D.J., Tanaka, T., Ferrucci, L., Beach, T.G., Serrano, G.E., Real, R., Morris, H.R., Ding, J., Gibbs, J.R., Singleton, A.B., Nalls, M.A., Bhangale, T., Blauwendraat, C., 2023. Large-scale rare variant burden testing in Parkinson's disease. Brain awad214. https://doi.org/10.1093/brain/awad214

Marchitti, S.A., Deitrich, R.A., Vasiliou, V., 2007. Neurotoxicity and metabolism of the catecholamine-derived 3,4-dihydroxyphenylacetaldehyde and 3,4-dihydroxyphenylglycolaldehyde: the role of aldehyde dehydrogenase. Pharmacol Rev 59, 125–150. https://doi.org/10.1124/pr.59.2.1

Marras, C., Lang, A., van de Warrenburg, B.P., Sue, C.M., Tabrizi, S.J., Bertram, L., Mercimek-Mahmutoglu, S., Ebrahimi-Fakhari, D., Warner, T.T., Durr, A., Assmann, B., Lohmann, K.,

Kostic, V., Klein, C., 2016. Nomenclature of genetic movement disorders: Recommendations of the international Parkinson and movement disorder society task force. Mov Disord 31, 436–457. https://doi.org/10.1002/mds.26527
Mätlik, K., Võikar, V., Vilenius, C., Kulesskaya, N., Andressoo, J.-O., 2018. Two-fold elevation of endogenous GDNF levels in mice improves motor coordination without causing side-effects. Sci Rep 8, 11861. https://doi.org/10.1038/s41598-018-29988-1
Matsuda, W., Furuta, T., Nakamura, K.C., Hioki, H., Fujiyama, F., Arai, R., Kaneko, T., 2009. Single Nigrostriatal Dopaminergic Neurons Form Widely Spread and Highly Dense Axonal Arborizations in the Neostriatum. J Neurosci 29, 444–453. https://doi.org/10.1523/JNEUROSCI.4029-08.2009
McBride, H.M., Neuspiel, M., Wasiak, S., 2006. Mitochondria: more than just a powerhouse. Curr Biol 16, R551-560. https://doi.org/10.1016/j.cub.2006.06.054
McCormack, J.G., Halestrap, A.P., Denton, R.M., 1990. Role of calcium ions in regulation of mammalian intramitochondrial metabolism. Physiological Reviews 70, 391–425. https://doi.org/10.1152/physrev.1990.70.2.391
McLelland, G.-L., Goiran, T., Yi, W., Dorval, G., Chen, C.X., Lauinger, N.D., Krahn, A.I., Valimehr, S., Rakovic, A., Rouiller, I., Durcan, T.M., Trempe, J.-F., Fon, E.A., 2018. Mfn2 ubiquitination by PINK1/parkin gates the p97-dependent release of ER from mitochondria to drive mitophagy. eLife 7, e32866. https://doi.org/10.7554/eLife.32866
McLelland, G.-L., Soubannier, V., Chen, C.X., McBride, H.M., Fon, E.A., 2014. Parkin and PINK1 function in a vesicular trafficking pathway regulating mitochondrial quality control. The EMBO Journal 33, 282–295. https://doi.org/10.1002/embj.201385902
Mhyre, T.R., Boyd, J.T., Hamill, R.W., Maguire-Zeiss, K.A., 2012. Parkinson's disease. Subcell Biochem 65, 389–455. https://doi.org/10.1007/978-94-007-5416-4_16
Moller, A., Bauer, C.S., Cohen, R.N., Webster, C.P., De Vos, K.J., 2017. Amyotrophic lateral sclerosis-associated mutant SOD1 inhibits anterograde axonal transport of mitochondria by reducing Miro1 levels. Human Molecular Genetics 26, 4668–4679. https://doi.org/10.1093/hmg/ddx348
Monzel, A.S., Hemmer, K., Kaoma, T., Smits, L.M., Bolognin, S., Lucarelli, P., Rosety, I., Zagare, A., Antony, P., Nickels, S.L., Krueger, R., Azuaje, F., Schwamborn, J.C., 2020. Machine learning-assisted neurotoxicity prediction in human midbrain organoids. Parkinsonism & Related Disorders 75, 105–109. https://doi.org/10.1016/j.parkreldis.2020.05.011
Monzel, A.S., Smits, L.M., Hemmer, K., Hachi, S., Moreno, E.L., van Wuellen, T., Jarazo, J., Walter, J., Brüggemann, I., Boussaad, I., Berger, E., Fleming, R.M.T., Bolognin, S., Schwamborn, J.C., 2017a. Derivation of Human Midbrain-Specific Organoids from Neuroepithelial Stem Cells. Stem Cell Reports 8, 1144–1154. https://doi.org/10.1016/j.stemcr.2017.03.010
Monzel, A.S., Smits, L.M., Hemmer, K., Hachi, S., Moreno, E.L., van Wuellen, T., Jarazo, J., Walter, J., Brüggemann, I., Boussaad, I., Berger, E., Fleming, R.M.T., Bolognin, S., Schwamborn, J.C., 2017b. Derivation of Human Midbrain-Specific Organoids from Neuroepithelial Stem Cells. Stem Cell Reports 8, 1144–1154. https://doi.org/10.1016/j.stemcr.2017.03.010
Moretto, E., Stuart, S., Surana, S., Vargas, J.N.S., Schiavo, G., 2022. The Role of Extracellular Matrix Components in the Spreading of Pathological Protein Aggregates. Frontiers in cellular neuroscience 16, 844211. https://doi.org/10.3389/fncel.2022.844211
Morlino, G., Barreiro, O., Baixauli, F., Robles-Valero, J., Gonzalez-Granado, J.M., Villa-Bellosta, R., Cuenca, J., Sanchez-Sorzano, C.O., Veiga, E., Martin-Cofreces, N.B., Sanchez-Madrid, F., 2014. Miro-1 Links Mitochondria and Microtubule Dynein Motors To Control Lymphocyte Migration and Polarity. Molecular and Cellular Biology 34, 1412–1426. https://doi.org/10.1128/MCB.01177-13
Nalls, M.A., Blauwendraat, C., Vallerga, C.L., Heilbron, K., Bandres-Ciga, S., Chang, D., Tan, M., Kia, D.A., Noyce, A.J., Xue, A., Bras, J., Young, E., von Coelln, R., Simón-Sánchez, J., Schulte, C., Sharma, M., Krohn, L., Pihlstrøm, L., Siitonen, A., Iwaki, H., Leonard, H., Faghri, F., Gibbs, J.R.,

Hernandez, D.G., Scholz, S.W., Botia, J.A., Martinez, M., Corvol, J.-C., Lesage, S., Jankovic, J., Shulman, L.M., Sutherland, M., Tienari, P., Majamaa, K., Toft, M., Andreassen, O.A., Bangale, T., Brice, A., Yang, J., Gan-Or, Z., Gasser, T., Heutink, P., Shulman, J.M., Wood, N.W., Hinds, D.A., Hardy, J.A., Morris, H.R., Gratten, J., Visscher, P.M., Graham, R.R., Singleton, A.B., 23andMe Research Team, System Genomics of Parkinson's Disease Consortium, International Parkinson's Disease Genomics Consortium, 2019. Identification of novel risk loci, causal insights, and heritable risk for Parkinson's disease: a meta-analysis of genome-wide association studies. Lancet Neurol 18, 1091–1102. https://doi.org/10.1016/S1474-4422(19)30320-5

Nath, S., Goodwin, J., Engelborghs, Y., Pountney, D.L., 2011. Raised calcium promotes α-synuclein aggregate formation. Molecular and Cellular Neuroscience 46, 516–526. https://doi.org/10.1016/j.mcn.2010.12.004

Nemani, N., Carvalho, E., Tomar, D., Dong, Z., Ketschek, A., Breves, S.L., Jaña, F., Worth, A.M., Heffler, J., Palaniappan, P., Tripathi, A., Subbiah, R., Riitano, M.F., Seelam, A., Manfred, T., Itoh, K., Meng, S., Sesaki, H., Craigen, W.J., Rajan, S., Shanmughapriya, S., Caplan, J., Prosser, B.L., Gill, D.L., Stathopulos, P.B., Gallo, G., Chan, D.C., Mishra, P., Madesh, M., 2018. MIRO-1 Determines Mitochondrial Shape Transition upon GPCR Activation and Ca2+ Stress. Cell Reports 23, 1005–1019. https://doi.org/10.1016/j.celrep.2018.03.098

Nguyen, D., Bharat, V., Conradson, D.M., Nandakishore, P., Wang, X., 2021a. Miro1 Impairment in a Parkinson's At-Risk Cohort. Frontiers in Molecular Neuroscience 14.

Nguyen, D., Bharat, V., Conradson, D.M., Nandakishore, P., Wang, X., 2021b. Miro1 Impairment in a Parkinson's At-Risk Cohort. Frontiers in Molecular Neuroscience 14, 734273. https://doi.org/10.3389/fnmol.2021.734273

Nguyen, T.T., Oh, S.S., Weaver, D., Lewandowska, A., Maxfield, D., Schuler, M.-H., Smith, N.K., Macfarlane, J., Saunders, G., Palmer, C.A., Debattisti, V., Koshiba, T., Pulst, S., Feldman, E.L., Hajnoczky, G., Shaw, J.M., 2014. Loss of Miro1-directed mitochondrial movement results in a novel murine model for neuron disease. Proceedings of the National Academy of Sciences 111, E3631–E3640. https://doi.org/10.1073/pnas.1402449111

Nickels, S.L., Modamio, J., Mendes-Pinheiro, B., Monzel, A.S., Betsou, F., Schwamborn, J.C., 2020. Reproducible generation of human midbrain organoids for in vitro modeling of Parkinson's disease. Stem Cell Res 46, 101870. https://doi.org/10.1016/j.scr.2020.101870

Nicoletti, V., Palermo, G., Del Prete, E., Mancuso, M., Ceravolo, R., 2021. Understanding the Multiple Role of Mitochondria in Parkinson's Disease and Related Disorders: Lesson From Genetics and Protein–Interaction Network. Frontiers in Cell and Developmental Biology 9, 636506. https://doi.org/10.3389/fcell.2021.636506

Niescier, R.F., Chang, K.T., Min, K.-T., 2013. Miro, MCU, and calcium: bridging our understanding of mitochondrial movement in axons. Front. Cell. Neurosci. 7. https://doi.org/10.3389/fncel.2013.00148

Niescier, R.F., Hong, K., Park, D., Min, K.-T., 2018. MCU Interacts with Miro1 to Modulate Mitochondrial Functions in Neurons. J. Neurosci. 38, 4666–4677. https://doi.org/10.1523/JNEUROSCI.0504-18.2018

Nolfi-Donegan, D., Braganza, A., Shiva, S., 2020. Mitochondrial electron transport chain: Oxidative phosphorylation, oxidant production, and methods of measurement. Redox Biology 37, 101674. https://doi.org/10.1016/j.redox.2020.101674

Novello, S., Arcuri, L., Dovero, S., Dutheil, N., Shimshek, D.R., Bezard, E., Morari, M., 2018. G2019S LRRK2 mutation facilitates α-synuclein neuropathology in aged mice. Neurobiology of Disease 120, 21–33. https://doi.org/10.1016/j.nbd.2018.08.018

Nuber, S., Selkoe, D.J., 2023. The Parkinson-Associated Toxin Paraquat Shifts Physiological α-Synuclein Tetramers toward Monomers That Can Be Calpain-Truncated and Form Oligomers. Am J Pathol 193, 520–531. https://doi.org/10.1016/j.ajpath.2023.01.010

Okuzumi, A., Hatano, T., Matsumoto, G., Nojiri, S., Ueno, S.-I., Imamichi-Tatano, Y., Kimura, H.,

Kakuta, S., Kondo, A., Fukuhara, T., Li, Y., Funayama, M., Saiki, S., Taniguchi, D., Tsunemi, T., McIntyre, D., Gérardy, J.-J., Mittelbronn, M., Kruger, R., Uchiyama, Y., Nukina, N., Hattori, N., 2023. Propagative α-synuclein seeds as serum biomarkers for synucleinopathies. Nat Med. https://doi.org/10.1038/s41591-023-02358-9

Ortner, N.J., 2021. Voltage-Gated Ca2+ Channels in Dopaminergic Substantia Nigra Neurons: Therapeutic Targets for Neuroprotection in Parkinson's Disease? Frontiers in Synaptic Neuroscience 13.

Ou, Z., Pan, J., Tang, S., Duan, D., Yu, D., Nong, H., Wang, Z., 2021. Global Trends in the Incidence, Prevalence, and Years Lived With Disability of Parkinson's Disease in 204 Countries/Territories From 1990 to 2019. Frontiers in Public Health 9, 776847. https://doi.org/10.3389/fpubh.2021.776847

Pagano, G., Taylor, K.I., Anzures-Cabrera, J., Marchesi, M., Simuni, T., Marek, K., Postuma, R.B., Pavese, N., Stocchi, F., Azulay, J.-P., Mollenhauer, B., López-Manzanares, L., Russell, D.S., Boyd, J.T., Nicholas, A.P., Luquin, M.R., Hauser, R.A., Gasser, T., Poewe, W., Ricci, B., Boulay, A., Vogt, A., Boess, F.G., Dukart, J., D'Urso, G., Finch, R., Zanigni, S., Monnet, A., Pross, N., Hahn, A., Svoboda, H., Britschgi, M., Lipsmeier, F., Volkova-Volkmar, E., Lindemann, M., Dziadek, S., Holiga, Š., Rukina, D., Kustermann, T., Kerchner, G.A., Fontoura, P., Umbricht, D., Doody, R., Nikolcheva, T., Bonni, A., 2022. Trial of Prasinezumab in Early-Stage Parkinson's Disease. New England Journal of Medicine 387, 421–432. https://doi.org/10.1056/NEJMoa2202867

Panchal, K., Tiwari, A.K., 2021. Miro (Mitochondrial Rho GTPase), a key player of mitochondrial axonal transport and mitochondrial dynamics in neurodegenerative diseases. Mitochondrion 56, 118–135. https://doi.org/10.1016/j.mito.2020.10.005

Pekkurnaz, G., Wang, X., 2022. Mitochondrial heterogeneity and homeostasis through the lens of a neuron. Nat Metab 4, 802–812. https://doi.org/10.1038/s42255-022-00594-w

Pérez, M.J., Baden, P., Deleidi, M., 2021. Progresses in both basic research and clinical trials of NAD+ in Parkinson's disease. Mechanisms of Ageing and Development 197, 111499. https://doi.org/10.1016/j.mad.2021.111499

Periñán, M.T., Gómez-Garre, P., Blauwendraat, C., Mir, P., Bandres-Ciga, S., 2020. The role of RHOT1 and RHOT2 genetic variation on Parkinson disease risk and onset. Neurobiology of Aging S0197458020302190. https://doi.org/10.1016/j.neurobiolaging.2020.07.003

Polymeropoulos, M.H., Lavedan, C., Leroy, E., Ide, S.E., Dehejia, A., Dutra, A., Pike, B., Root, H., Rubenstein, J., Boyer, R., Stenroos, E.S., Chandrasekharappa, S., Athanassiadou, A., Papapetropoulos, T., Johnson, W.G., Lazzarini, A.M., Duvoisin, R.C., Di Iorio, G., Golbe, L.I., Nussbaum, R.L., 1997. Mutation in the alpha-synuclein gene identified in families with Parkinson's disease. Science 276, 2045–2047. https://doi.org/10.1126/science.276.5321.2045

Poppe, M., Reimertz, C., Düssmann, H., Krohn, A.J., Luetjens, C.M., Böckelmann, D., Nieminen, A.L., Kögel, D., Prehn, J.H., 2001. Dissipation of potassium and proton gradients inhibits mitochondrial hyperpolarization and cytochrome c release during neural apoptosis. J Neurosci 21, 4551–4563. https://doi.org/10.1523/JNEUROSCI.21-13-04551.2001

Pulido, C., Ryan, T.A., 2021. Synaptic vesicle pools are a major hidden resting metabolic burden of nerve terminals. Sci Adv 7, eabi9027. https://doi.org/10.1126/sciadv.abi9027

Raff, M.C., Whitmore, A. V, Finn, J.T., 2002. Axonal Self-Destruction and Neurodegeneration. Science 296, 868–871. https://doi.org/10.1126/science.1068613

Ramsay, R.R., Kowal, A.T., Johnson, M.K., Salach, J.I., Singer, T.P., 1987. The inhibition site of MPP+, the neurotoxic bioactivation product of 1-methyl-4-phenyl-1,2,3,6-tetrahydropyridine is near the Q-binding site of NADH dehydrogenase. Arch Biochem Biophys 259, 645–649. https://doi.org/10.1016/0003-9861(87)90531-5

Ramsay, R.R., Salach, J.I., Singer, T.P., 1986. Uptake of the neurotoxin 1-methyl-4-phenylpyridine (MPP+) by mitochondria and its relation to the inhibition of the mitochondrial oxidation of

NAD+-linked substrates by MPP+. Biochem Biophys Res Commun 134, 743–748. https://doi.org/10.1016/s0006-291x(86)80483-1
Reeve, A., Simcox, E., Turnbull, D., 2014. Ageing and Parkinson's disease: why is advancing age the biggest risk factor? Ageing Res Rev 14, 19–30. https://doi.org/10.1016/j.arr.2014.01.004
Reinhardt, P., Glatza, M., Hemmer, K., Tsytsyura, Y., Thiel, C.S., Höing, S., Moritz, S., Parga, J.A., Wagner, L., Bruder, J.M., Wu, G., Schmid, B., Röpke, A., Klingauf, J., Schwamborn, J.C., Gasser, T., Schöler, H.R., Sterneckert, J., 2013. Derivation and Expansion Using Only Small Molecules of Human Neural Progenitors for Neurodegenerative Disease Modeling. PLoS ONE 8, e59252. https://doi.org/10.1371/journal.pone.0059252
Richard, M., Kaufmann, P., Kornberger, R., Dingemanse, J., 2019. First-in-man study of ACT-709478, a novel selective triple T-type calcium channel blocker. Epilepsia 60, 968–978. https://doi.org/10.1111/epi.14732
Richard, M., Kaufmann, P., Ort, M., Kornberger, R., Dingemanse, J., 2020. Multiple-Ascending Dose Study in Healthy Subjects to Assess the Pharmacokinetics, Tolerability, and CYP3A4 Interaction Potential of the T-Type Calcium Channel Blocker ACT-709478, A Potential New Antiepileptic Drug. CNS Drugs 34, 311–323. https://doi.org/10.1007/s40263-019-00697-1
Riederer, P., Berg, D., Casadei, N., Cheng, F., Classen, J., Dresel, C., Jost, W., Krüger, R., Müller, T., Reichmann, H., Rieß, O., Storch, A., Strobel, S., van Eimeren, T., Völker, H.-U., Winkler, J., Winklhofer, K.F., Wüllner, U., Zunke, F., Monoranu, C.-M., 2019. α-Synuclein in Parkinson's disease: causal or bystander? J Neural Transm 126, 815–840. https://doi.org/10.1007/s00702-019-02025-9
Rizzuto, R., De Stefani, D., Raffaello, A., Mammucari, C., 2012. Mitochondria as sensors and regulators of calcium signalling. Nat Rev Mol Cell Biol 13, 566–578. https://doi.org/10.1038/nrm3412
Rousseaux, M.W.C., Marcogliese, P.C., Qu, D., Hewitt, S.J., Seang, S., Kim, R.H., Slack, R.S., Schlossmacher, M.G., Lagace, D.C., Mak, T.W., Park, D.S., 2012. Progressive dopaminergic cell loss with unilateral-to-bilateral progression in a genetic model of Parkinson disease. Proceedings of the National Academy of Sciences 109, 15918–15923. https://doi.org/10.1073/pnas.1205102109
Russo, G.J., Louie, K., Wellington, A., Macleod, G.T., Hu, F., Panchumarthi, S., Zinsmaier, K.E., 2009. Drosophila Miro Is Required for Both Anterograde and Retrograde Axonal Mitochondrial Transport. Journal of Neuroscience 29, 5443–5455. https://doi.org/10.1523/JNEUROSCI.5417-08.2009
Ryan, S.D., Dolatabadi, N., Chan, S.F., Zhang, X., Akhtar, M.W., Parker, J., Soldner, F., Sunico, C.R., Nagar, S., Talantova, M., Lee, B., Lopez, K., Nutter, A., Shan, B., Molokanova, E., Zhang, Y., Han, X., Nakamura, T., Masliah, E., Yates, J.R., Nakanishi, N., Andreyev, A.Y., Okamoto, S., Jaenisch, R., Ambasudhan, R., Lipton, S.A., 2013. Isogenic human iPSC Parkinson's model shows nitrosative stress-induced dysfunction in MEF2-PGC1α transcription. Cell 155, 1351–1364. https://doi.org/10.1016/j.cell.2013.11.009
Ryan, T., Bamm, V.V., Stykel, M.G., Coackley, C.L., Humphries, K.M., Jamieson-Williams, R., Ambasudhan, R., Mosser, D.D., Lipton, S.A., Harauz, G., Ryan, S.D., 2018. Cardiolipin exposure on the outer mitochondrial membrane modulates α-synuclein. Nat Commun 9, 817. https://doi.org/10.1038/s41467-018-03241-9
Sabari, S.S., Balasubramani, K., Iyer, M., Sureshbabu, H.W., Venkatesan, D., Gopalakrishnan, A.V., Narayanaswamy, A., Senthil Kumar, N., Vellingiri, B., 2023. Type 2 Diabetes (T2DM) and Parkinson's Disease (PD): a Mechanistic Approach. Mol Neurobiol 1–27. https://doi.org/10.1007/s12035-023-03359-y
Saeed, M., 2018. Genomic convergence of locus-based GWAS meta-analysis identifies AXIN1 as a novel Parkinson's gene. Immunogenetics 70, 563–570. https://doi.org/10.1007/s00251-018-1068-0
Sanchez, G., Varaschin, R.K., Büeler, H., Marcogliese, P.C., Park, D.S., Trudeau, L.-E., 2014. Unaltered Striatal Dopamine Release Levels in Young Parkin Knockout, Pink1 Knockout, DJ-1 Knockout

and LRRK2 R1441G Transgenic Mice. PLoS ONE 9, e94826. https://doi.org/10.1371/journal.pone.0094826
Sanders, L.H., Laganière, J., Cooper, O., Mak, S.K., Vu, B.J., Huang, Y.A., Paschon, D.E., Vangipuram, M., Sundararajan, R., Urnov, F.D., Langston, J.W., Gregory, P.D., Zhang, H.S., Greenamyre, J.T., Isacson, O., Schüle, B., 2014. LRRK2 mutations cause mitochondrial DNA damage in iPSC-derived neural cells from Parkinson's disease patients: reversal by gene correction. Neurobiol Dis 62, 381–386. https://doi.org/10.1016/j.nbd.2013.10.013
Santiago, J.A., Potashkin, J.A., 2013. Shared dysregulated pathways lead to Parkinson's disease and diabetes. Trends in Molecular Medicine 19, 176–186. https://doi.org/10.1016/j.molmed.2013.01.002
Saotome, M., Safiulina, D., Szabadkai, G., Das, S., Fransson, A., Aspenstrom, P., Rizzuto, R., Hajnoczky, G., 2008. Bidirectional Ca2+-dependent control of mitochondrial dynamics by the Miro GTPase. Proceedings of the National Academy of Sciences 105, 20728–20733. https://doi.org/10.1073/pnas.0808953105
Saxton, W.M., Hollenbeck, P.J., 2012. The axonal transport of mitochondria. Journal of Cell Science 125, 2095–2104. https://doi.org/10.1242/jcs.053850
Scheiblich, H., Dansokho, C., Mercan, D., Schmidt, S.V., Bousset, L., Wischhof, L., Eikens, F., Odainic, A., Spitzer, J., Griep, A., Schwartz, S., Bano, D., Latz, E., Melki, R., Heneka, M.T., 2021. Microglia jointly degrade fibrillar alpha-synuclein cargo by distribution through tunneling nanotubes. Cell 184, 5089-5106.e21. https://doi.org/10.1016/j.cell.2021.09.007
Schneider, T., Dibué, M., Hescheler, J., 2013. How "Pharmacoresistant" is Cav2.3, the Major Component of Voltage-Gated R-type Ca2+ Channels? Pharmaceuticals (Basel) 6, 759–776. https://doi.org/10.3390/ph6060759
Schöndorf, D.C., Aureli, M., McAllister, F.E., Hindley, C.J., Mayer, F., Schmid, B., Sardi, S.P., Valsecchi, M., Hoffmann, S., Schwarz, L.K., Hedrich, U., Berg, D., Shihabuddin, L.S., Hu, J., Pruszak, J., Gygi, S.P., Sonnino, S., Gasser, T., Deleidi, M., 2014. iPSC-derived neurons from GBA1-associated Parkinson's disease patients show autophagic defects and impaired calcium homeostasis. Nat Commun 5, 4028. https://doi.org/10.1038/ncomms5028
Schubert, M., Lindgreen, S., Orlando, L., 2016. AdapterRemoval v2: rapid adapter trimming, identification, and read merging. BMC Research Notes 9, 88. https://doi.org/10.1186/s13104-016-1900-2
Schwab, A.J., Sison, S.L., Meade, M.R., Broniowska, K.A., Corbett, J.A., Ebert, A.D., 2017. Decreased Sirtuin Deacetylase Activity in LRRK2 G2019S iPSC-Derived Dopaminergic Neurons. Stem Cell Reports 9, 1839–1852. https://doi.org/10.1016/j.stemcr.2017.10.010
Schwarz, L., Fitzgerald, J.C., 2022. Steady-State Levels of Miro1 Linked to Phosphorylation at Serine 156 and Mitochondrial Respiration in Dopaminergic Neurons. Cells 11, 1269. https://doi.org/10.3390/cells11081269
Schwarz, L., Sharma, K., Dodi, L.D., Rieder, L.-S., Fallier-Becker, P., Casadei, N., Fitzgerald, J.C., 2022a. Miro1 R272Q disrupts mitochondrial calcium handling and neurotransmitter uptake in dopaminergic neurons. Front. Mol. Neurosci. 15, 966209. https://doi.org/10.3389/fnmol.2022.966209
Schwarz, L., Sharma, K., Dodi, L.D., Rieder, L.-S., Fallier-Becker, P., Casadei, N., Fitzgerald, J.C., 2022b. Miro1 R272Q disrupts mitochondrial calcium handling and neurotransmitter uptake in dopaminergic neurons. Frontiers in Molecular Neuroscience 15, 966209. https://doi.org/10.3389/fnmol.2022.966209
Scialò, F., Fernández-Ayala, D.J., Sanz, A., 2017. Role of Mitochondrial Reverse Electron Transport in ROS Signaling: Potential Roles in Health and Disease. Frontiers in Physiology 8.
Segura-Aguilar, J., Paris, I., Muñoz, P., Ferrari, E., Zecca, L., Zucca, F.A., 2014. Protective and toxic roles of dopamine in Parkinson's disease. J Neurochem 129, 898–915. https://doi.org/10.1111/jnc.12686
Shahmoradian, S.H., Lewis, A.J., Genoud, C., Hench, J., Moors, T.E., Navarro, P.P., Castaño-Díez, D.,

Schweighauser, G., Graff-Meyer, A., Goldie, K.N., Sütterlin, R., Huisman, E., Ingrassia, A., Gier, Y. de, Rozemuller, A.J.M., Wang, J., Paepe, A.D., Erny, J., Staempfli, A., Hoernschemeyer, J., Großerüschkamp, F., Niedieker, D., El-Mashtoly, S.F., Quadri, M., Van IJcken, W.F.J., Bonifati, V., Gerwert, K., Bohrmann, B., Frank, S., Britschgi, M., Stahlberg, H., Van de Berg, W.D.J., Lauer, M.E., 2019. Lewy pathology in Parkinson's disease consists of crowded organelles and lipid membranes. Nat Neurosci 22, 1099–1109. https://doi.org/10.1038/s41593-019-0423-2

Shaltouki, A., Hsieh, C.-H., Kim, M.J., Wang, X., 2018a. Alpha-synuclein delays mitophagy and targeting Miro rescues neuron loss in Parkinson's models. Acta Neuropathol 136, 607–620. https://doi.org/10.1007/s00401-018-1873-4

Shaltouki, A., Hsieh, C.-H., Kim, M.J., Wang, X., 2018b. Alpha-synuclein delays mitophagy and targeting Miro rescues neuron loss in Parkinson's models. Acta neuropathologica 136, 607–620. https://doi.org/10.1007/s00401-018-1873-4

Shulman, J.M., De Jager, P.L., Feany, M.B., 2011. Parkinson's Disease: Genetics and Pathogenesis. Annu. Rev. Pathol. Mech. Dis. 6, 193–222. https://doi.org/10.1146/annurev-pathol-011110-130242

Siegert, Richard J., Taylor, K.D., Weatherall, M., Abernethy, D.A., 2006. Is implicit sequence learning impaired in Parkinson's disease? A meta-analysis. Neuropsychology 20, 490–495. https://doi.org/10.1037/0894-4105.20.4.490

Siegert, Richard J, Taylor, K.D., Weatherall, M., Abernethy, D.A., 2006. Is implicit sequence learning impaired in Parkinson's disease? A meta-analysis. Neuropsychology 20, 490–495. https://doi.org/10.1037/0894-4105.20.4.490

Smith, K.P., Focia, P.J., Chakravarthy, S., Landahl, E.C., Klosowiak, J.L., Rice, S.E., Freymann, D.M., 2019. Structural assembly of the human Miro1/2 GTPases based on the crystal structure of the N-terminal GTPase domain (preprint). Cell Biology. https://doi.org/10.1101/729251

Song, P., Trajkovic, K., Tsunemi, T., Krainc, D., 2016. Parkin Modulates Endosomal Organization and Function of the Endo-Lysosomal Pathway. J. Neurosci. 36, 2425–2437. https://doi.org/10.1523/JNEUROSCI.2569-15.2016

Sonustun, B., Altay, M.F., Strand, C., Ebanks, K., Hondhamuni, G., Warner, T.T., Lashuel, H.A., Bandopadhyay, R., 2022. Pathological Relevance of Post-Translationally Modified Alpha-Synuclein (pSer87, pSer129, nTyr39) in Idiopathic Parkinson's Disease and Multiple System Atrophy. Cells 11, 906. https://doi.org/10.3390/cells11050906

Sorrentino, Z.A., Giasson, B.I., 2020. The emerging role of α-synuclein truncation in aggregation and disease. Journal of Biological Chemistry 295, 10224–10244. https://doi.org/10.1074/jbc.REV120.011743

Spillantini, M.G., Schmidt, M.L., Lee, V.M., Trojanowski, J.Q., Jakes, R., Goedert, M., 1997. Alpha-synuclein in Lewy bodies. Nature 388, 839–840. https://doi.org/10.1038/42166

Stephen, T.-L., Higgs, N.F., Sheehan, D.F., Al Awabdh, S., Lopez-Domenech, G., Arancibia-Carcamo, I.L., Kittler, J.T., 2015. Miro1 Regulates Activity-Driven Positioning of Mitochondria within Astrocytic Processes Apposed to Synapses to Regulate Intracellular Calcium Signaling. Journal of Neuroscience 35, 15996–16011. https://doi.org/10.1523/JNEUROSCI.2068-15.2015

Stock, D., Leslie, A.G., Walker, J.E., 1999. Molecular architecture of the rotary motor in ATP synthase. Science 286, 1700–1705. https://doi.org/10.1126/science.286.5445.1700

Stuart, T., Butler, A., Hoffman, P., Hafemeister, C., Papalexi, E., Mauck, W.M., Hao, Y., Stoeckius, M., Smibert, P., Satija, R., 2019. Comprehensive Integration of Single-Cell Data. Cell 177, 1888-1902.e21. https://doi.org/10.1016/j.cell.2019.05.031

Sugiura, A., McLelland, G.-L., Fon, E.A., McBride, H.M., 2014. A new pathway for mitochondrial quality control: mitochondrial-derived vesicles. EMBO J 33, 2142–2156. https://doi.org/10.15252/embj.201488104

Surmeier, D.J., Schumacker, P.T., 2013. Calcium, bioenergetics, and neuronal vulnerability in Parkinson's disease. J Biol Chem 288, 10736–10741. https://doi.org/10.1074/jbc.R112.410530

Tabata, Y., Imaizumi, Y., Sugawara, M., Andoh-Noda, T., Banno, S., Chai, M., Sone, T., Yamazaki, K., Ito, M., Tsukahara, K., Saya, H., Hattori, N., Kohyama, J., Okano, H., 2018. T-type Calcium Channels Determine the Vulnerability of Dopaminergic Neurons to Mitochondrial Stress in Familial Parkinson Disease. Stem Cell Reports 11, 1171–1184. https://doi.org/10.1016/j.stemcr.2018.09.006

Takahashi, K., Tanabe, K., Ohnuki, M., Narita, M., Ichisaka, T., Tomoda, K., Yamanaka, S., 2007. Induction of pluripotent stem cells from adult human fibroblasts by defined factors. Cell 131, 861–872. https://doi.org/10.1016/j.cell.2007.11.019

Takahashi, K., Yamanaka, S., 2006. Induction of pluripotent stem cells from mouse embryonic and adult fibroblast cultures by defined factors. Cell 126, 663–676. https://doi.org/10.1016/j.cell.2006.07.024

Thorne, N.J., Tumbarello, D.A., 2022. The relationship of alpha-synuclein to mitochondrial dynamics and quality control. Frontiers in Molecular Neuroscience 15, 947191. https://doi.org/10.3389/fnmol.2022.947191

Tran, J., Anastacio, H., Bardy, C., 2020. Genetic predispositions of Parkinson's disease revealed in patient-derived brain cells. npj Parkinsons Dis. 6, 1–18. https://doi.org/10.1038/s41531-020-0110-8

Tsai, P.-I., Course, M.M., Lovas, J.R., Hsieh, C.-H., Babic, M., Zinsmaier, K.E., Wang, X., 2014a. PINK1-mediated Phosphorylation of Miro Inhibits Synaptic Growth and Protects Dopaminergic Neurons in Drosophila. Sci Rep 4, 6962. https://doi.org/10.1038/srep06962

Tsai, P.-I., Course, M.M., Lovas, J.R., Hsieh, C.-H., Babic, M., Zinsmaier, K.E., Wang, X., 2014b. PINK1-mediated Phosphorylation of Miro Inhibits Synaptic Growth and Protects Dopaminergic Neurons in Drosophila. Scientific Reports 4, 6962. https://doi.org/10.1038/srep06962

Tseng, N., Lambie, S.C., Huynh, C.Q., Sanford, B., Patel, M., Herson, P.S., Ormond, D.R., 2021. Mitochondrial transfer from mesenchymal stem cells improves neuronal metabolism after oxidant injury in vitro: The role of Miro1. J Cereb Blood Flow Metab 41, 761–770. https://doi.org/10.1177/0271678X20928147

Turconi, G., Kopra, J., Võikar, V., Kulesskaya, N., Vilenius, C., Piepponen, T.P., Andressoo, J.-O., 2020. Chronic 2-Fold Elevation of Endogenous GDNF Levels Is Safe and Enhances Motor and Dopaminergic Function in Aged Mice. Molecular Therapy - Methods & Clinical Development 17, 831–842. https://doi.org/10.1016/j.omtm.2020.04.003

Van Laar, V.S., Berman, S.B., 2009. Mitochondrial dynamics in Parkinson's disease. Exp Neurol 218, 247–256. https://doi.org/10.1016/j.expneurol.2009.03.019

Vander Heiden, M.G., Chandel, N.S., Williamson, E.K., Schumacker, P.T., Thompson, C.B., 1997. Bcl-xL regulates the membrane potential and volume homeostasis of mitochondria. Cell 91, 627–637. https://doi.org/10.1016/s0092-8674(00)80450-x

van Spronsen, M., Mikhaylova, M., Lipka, J., Schlager, M.A., van den Heuvel, D.J., Kuijpers, M., Wulf, P.S., Keijzer, N., Demmers, J., Kapitein, L.C., Jaarsma, D., Gerritsen, H.C., Akhmanova, A., Hoogenraad, C.C., 2013. TRAK/Milton Motor-Adaptor Proteins Steer Mitochondrial Trafficking to Axons and Dendrites. Neuron 77, 485–502. https://doi.org/10.1016/j.neuron.2012.11.027

Vlahou, G., Eliáš, M., von Kleist-Retzow, J.-C., Wiesner, R.J., Rivero, F., 2011. The Ras related GTPase Miro is not required for mitochondrial transport in Dictyostelium discoideum. European Journal of Cell Biology 90, 342–355. https://doi.org/10.1016/j.ejcb.2010.10.012

Wang, X., Schwarz, T.L., 2009. The Mechanism of Ca2+-Dependent Regulation of Kinesin-Mediated Mitochondrial Motility. Cell 136, 163–174. https://doi.org/10.1016/j.cell.2008.11.046

Wang, X., Winter, D., Ashrafi, G., Schlehe, J., Wong, Y.L., Selkoe, D., Rice, S., Steen, J., LaVoie, M.J., Schwarz, T.L., 2011. PINK1 and Parkin Target Miro for Phosphorylation and Degradation to Arrest Mitochondrial Motility. Cell 147, 893–906. https://doi.org/10.1016/j.cell.2011.10.018

Wasilewski, M., Chacinska, A., 2021a. MIC60 relays oxidation to block mitophagy. Nat Metab 3, 1146–1147. https://doi.org/10.1038/s42255-021-00460-1

Wasilewski, M., Chacinska, A., 2021b. MIC60 relays oxidation to block mitophagy. Nature Metabolism 3, 1146–1147. https://doi.org/10.1038/s42255-021-00460-1
Wong, H.-S., Dighe, P.A., Mezera, V., Monternier, P.-A., Brand, M.D., 2017. Production of superoxide and hydrogen peroxide from specific mitochondrial sites under different bioenergetic conditions. J Biol Chem 292, 16804–16809. https://doi.org/10.1074/jbc.R117.789271
Wu, J., Kung, J., Dong, J., Chang, L., Xie, C., Habib, A., Hawes, S., Yang, N., Chen, V., Liu, Z., Evans, R., Liang, B., Sun, L., Ding, J., Yu, J., Saez-Atienzar, S., Tang, B., Khaliq, Z., Lin, D.-T., Le, W., Cai, H., 2019. Distinct Connectivity and Functionality of Aldehyde Dehydrogenase 1a1-Positive Nigrostriatal Dopaminergic Neurons in Motor Learning. Cell Rep 28, 1167-1181.e7. https://doi.org/10.1016/j.celrep.2019.06.095
Wüllner, U., Borghammer, P., Choe, C., Csoti, I., Falkenburger, B., Gasser, T., Lingor, P., Riederer, P., 2023. The heterogeneity of Parkinson's disease. Journal of Neural Transmission 130, 827–838. https://doi.org/10.1007/s00702-023-02635-4
Xiao, W., Wang, R.-S., Handy, D.E., Loscalzo, J., 2018. NAD(H) and NADP(H) Redox Couples and Cellular Energy Metabolism. Antioxidants & Redox Signaling 28, 251–272. https://doi.org/10.1089/ars.2017.7216
Yellen, G., 2018. Fueling thought: Management of glycolysis and oxidative phosphorylation in neuronal metabolism. J Cell Biol 217, 2235–2246. https://doi.org/10.1083/jcb.201803152
Yoon, Y.-S., You, J.S., Kim, T.-K., Ahn, W.J., Kim, M.J., Son, K.H., Ricarte, D., Ortiz, D., Lee, S.-J., Lee, H.-J., 2022. Senescence and impaired DNA damage responses in alpha-synucleinopathy models. Exp Mol Med 54, 115–128. https://doi.org/10.1038/s12276-022-00727-x
Zagare, A., Barmpa, K., Smajic, S., Smits, L.M., Grzyb, K., Grünewald, A., Skupin, A., Nickels, S.L., Schwamborn, J.C., 2022. Midbrain organoids mimic early embryonic neurodevelopment and recapitulate LRRK2-p.Gly2019Ser-associated gene expression. American journal of human genetics 109, 311–327. https://doi.org/10.1016/j.ajhg.2021.12.009
Zagare, A., Gobin, M., Monzel, A.S., Schwamborn, J.C., 2021a. A robust protocol for the generation of human midbrain organoids. STAR Protoc 2, 100524. https://doi.org/10.1016/j.xpro.2021.100524
Zagare, A., Gobin, M., Monzel, A.S., Schwamborn, J.C., 2021b. A robust protocol for the generation of human midbrain organoids. STAR Protocols 2, 100524. https://doi.org/10.1016/j.xpro.2021.100524
Zagare, A., Preciat, G., Nickels, Sarah.L., Luo, X., Monzel, A.S., Gomez-Giro, G., Robertson, G., Jaeger, C., Sharif, J., Koseki, H., Diederich, N.J., Glaab, E., Fleming, R.M.T., Schwamborn, J.C., n.d. Omics data integration allows the dentification of an idiopathic Parkinson's disease signature. under revision Nature Communications. https://doi.org/10.17881/v8jg-pw83
Zhang, N., Yu, X., Xie, J., Xu, H., 2021. New Insights into the Role of Ferritin in Iron Homeostasis and Neurodegenerative Diseases. Molecular Neurobiology 58, 2812–2823. https://doi.org/10.1007/s12035-020-02277-7
Zhang, Y., Yu, Z., Jiang, D., Liang, X., Liao, S., Zhang, Z., Yue, W., Li, X., Chiu, S.-M., Chai, Y.-H., Liang, Y., Chow, Y., Han, S., Xu, A., Tse, H.-F., Lian, Q., 2016. iPSC-MSCs with High Intrinsic MIRO1 and Sensitivity to TNF-α Yield Efficacious Mitochondrial Transfer to Rescue Anthracycline-Induced Cardiomyopathy. Stem Cell Reports 7, 749–763. https://doi.org/10.1016/j.stemcr.2016.08.009
Zhao, R.-Z., Jiang, S., Zhang, L., Yu, Z.-B., 2019. Mitochondrial electron transport chain, ROS generation and uncoupling (Review). Int J Mol Med 44, 3–15. https://doi.org/10.3892/ijmm.2019.4188
Zhu, A., Ibrahim, J.G., Love, M.I., 2019. Heavy-tailed prior distributions for sequence count data: removing the noise and preserving large differences. Bioinformatics 35, 2084–2092. https://doi.org/10.1093/bioinformatics/bty895
Zhuang, Aojia, Zhuang, Aobo, Chen, Y., Qin, Z., Zhu, D., Ren, L., Wei, Y., Zhou, P., Yue, X., He, F., Xu, J., Ding, C., 2023. Proteomic characteristics reveal the signatures and the risks of T1 colorectal

cancer metastasis to lymph nodes. eLife 12, e82959. https://doi.org/10.7554/eLife.82959
Zigmond, M.J., Hastings, T.G., Perez, R.G., 2002. Increased dopamine turnover after partial loss of dopaminergic neurons: compensation or toxicity?q 5.